SOUND PROPAGATION IN URBAN SPACES

by

Paul R. Donavan

B.S. University of California at Berkeley
(1971)

S.M., Massachusetts Institute of Technology
(1973)

SUBMITTED IN PARTIAL FULFILLMENT
OF THE REQUIREMENTS FOR THE
DEGREE OF

DOCTOR OF SCIENCE

at the

MASSACHUSETTS INSTITUTE OF TECHNOLOGY

January, 1976

Signature of Author.....
Department of Mechanical Engineering, January 15, 1976

Certified by.....
Thesis Supervisor

Accepted by.....
Chairman, Department Committee on Graduate Students

SOUND PROPAGATION IN URBAN SPACES

by

Paul R. Donavan

Submitted to the Department of Mechanical Engineering on January 15, 1976 in partial fulfillment of the requirements for the Degree of Doctor of Science.

ABSTRACT

Basic acoustical imaging theory is examined for its utility in assessing sound propagation in urban areas. Imaging theory assuming smooth-wall, specular reflection is determined not to be appropriate for urban propagation simulation. Because of building surface irregularities, the sound field in a city street is found to be significantly modified relative to a smooth-wall channel.

To account partially for surface irregularities, a first order model of scattered reflection is developed. This model incorporates the added absorption effect produced by scattering from irregularities into acoustical imaging theory. The propagation model is shown to be valid only when there is direct line of sight between source and receiver.

In order to develop a more widely applicable urban noise propagation model, the scattered field produced by typical building surface irregularities is examined in detail with acoustical model studies. With the results of these studies, a second order model of scattered reflection is developed. The applicability of this scattering model and a further modified form of specular imaging theory to general urban sound propagation is verified with field and acoustical model data.

Using the second order scattering model and imaging theory, computed attenuation values are presented for a number of typical urban geometries. The computed values are applicable to point and line sources and to traffic flows. Additional factors affecting urban sound propagation are discussed.

Thesis Supervisor: Dr. Richard H. Lyon
Title: Professor of Mechanical Engineering

ACKNOWLEDGEMENTS

Not only for his guidance and advice in the work represented by this thesis, but also for his interest in urban sound propagation and environmental noise, I would like to thank very much Professor Richard H. Lyon. I am also appreciative of the advice, assistance and interest of Professor D. Graham Holmes. My appreciation is also due to the members of the MIT Acoustics and Vibrations Laboratory for their intellectual as well as manual assistance in this work. I would like to particularly thank Richard DeJong for his help in instrumentation, in gathering field data and in precipitating ideas through discussion. For her help in the physical preparation of this thesis, I am very appreciative of the effort given by Mary Toscano. I would further like to especially thank my wife, Bonnie, for her help, patience, and encouragement in the completion of this work.

TABLE OF CONTENTS

TABLE OF CONTENTS (CONTINUED)

TABLE OF CONTENTS (CONTINUED)

LIST OF FIGURES

LIST OF FIGURES

LIST OF FIGURES (CONTINUED)

LIST OF FIGURES (CONTINUED)

LIST OF FIGURES (CONTINUED)

LIST OF FIGURES (CONTINUED)

I. INTRODUCTION

With increasing public concern over noise as an environmental pollutant, considerable attention has recently been given to sound propagation outdoors. One particular topic of concern is propagation in semi-confined or urban spaces. The understanding of this particular propagation case is desirable for a number of practical reasons aside from the purely physical questions involved. One such practical reason is the need for impact assessment of new facilities prior to their construction. Within this category is the obvious concern over permanent, direct noise impact due to such facilities as above ground rapid transit systems, highways, heliports and STOL ports. A more subtle impact is the effect such facilities may have on existing traffic patterns and their associated noise. Another less obvious impact is the temporary impact created by increased heavy truck traffic, jack hammers, pile drivers, etc., and by traffic rerouting during construction of the facility.

A second practical reason for understanding urban sound propagation is assessing the effectiveness of noise abatement procedures. This would involve such measures as traffic rerouting, elimination of truck traffic, reducing traffic volume, or implementing source noise standards. Another use of such understanding is the area of site selection and urban planning. For planning purposes, it would be quite desirable to have predicted noise levels as an input at the planning stage for urban redevelopment and new development. Also at the planning stage, predicted noise

level information would be useful for site selection of noise sensitive buildings such as hospitals, schools and theaters. This would be a particularly valuable input when the building itself would significantly modify existing propagation characteristics or when field data at the site is not available. A final reason for understanding urban sound propagation is the possibility that such knowledge may infer methods of noise intrusion reduction. From the physical viewpoint, urban sound propagation is of interest because it combines many aspects of outdoor sound propagation which in open propagation are somewhat separable. These aspects include local reverberation, diffraction, scattering, and near grazing reflection.

Previous work in outdoor sound propagation has been largely restricted to open and semi-open spaces. One topic which has been considered quite extensively is that of noise and noise propagation from freely flowing traffic in various topographical settings. Other areas of work have been propagation over acoustically "soft" ground, barrier theory and performance, and the attenuative and scattering characteristics of trees.

On the topic of noise level determination in semi-confined and urban areas, there have been several studies which consider prediction of steady state or background noise levels. Olson and Shaw [1] originated the work on this topic with a theoretical prediction model using source densities within a region. A barrier or propagation factor was then empirically determined and applied as a correction to the

theoretical result. With the use of a cellular model which considers reverberation and barrier effects, Lyon and Davies [2] extended and refined steady state noise level prediction. Work of a similar nature has been reported by Malchaire and Horstman [3] who consider the contribution of area, line and point sources to the steady state level. Like the Olson and Shaw work, this study also relies on empirical methods to determine propagation correction factors.

In addition to the work on background level determination in semi-confined spaces, there have been a number of studies dealing specifically with sound propagation. These have typically involved the use of acoustical imaging theory with the two simplifying assumptions of a high frequency optical limit and totally specular wall reflection. The first of these studies was made by Schlatter [4] who considered propagation in a channel. Sound propagation into a city street from overhead sources, particularly helicopters, was studied in some detail by Pande [5], Kinney [6] and Donavan [7]. Using these same two assumptions, propagation from intersections into side streets and around corners has also been investigated [8]. In a similar study, Lee [9] developed a nomogram for propagation around a corner and for propagation through multiple intersections.

Using an approach quite different from those mentioned above, Holmes [10] has developed a method of sound level determination in semi-confined spaces which does not necessitate detailed knowledge of the propagation. This method is embodied in a computer program which

follows and counts acoustic "packets" randomly emitted from a point source into a specified semi-confined, two-dimensional space. Although this approach utilizes the optical limit assumption, it does permit non-specular reflection, assuming the parameters of the scattered reflection are known.

Field data available for urban sound propagation assessment is quite limited and typically quite specialized. One such study published by Jones [11] reports data for siren noise propagation from a building top in New York City. One interesting aspect of this study was the determination of a building shielding factor equal to that of Olson and Shaw. A second study which is more applicable to propagation assessment is that reported by Wiener, Malme and Gogos [12]. This work concerns loudspeaker noise propagation and presents attenuations down a street and around a corner from the source. Another applicable study is that prepared by Delaney, Copeland and Payne [13]. This report presents extensive and detailed data of noise levels produced in side street from traffic flows in arterial streets. In a field experiment designed specifically to study sound propagation, Kinney [6] obtained comparative helicopter fly-over data for both an open field and a city street. Although this study is useful for studying propagation, it is limited to a very specialized case.

Comparison of the above discussed field data to results predicted by specular imaging theory generally indicate a lack of correspondence between the two. The only case in which adequate agreement is achieved

is that of the low reverberation, aircraft fly-over case. Good correspondence between the field data and imaging has been demonstrated by both Kinney [6] and Donavan [7]. For sources located in the street channel, the reverberation associated with propagation is considerable. In this case the correspondence between specular imaging and field data is quite poor. The probable cause of this discrepancy lies not in imaging theory assumptions, but rather in the totally specular reflection assumption. Evidence of building surface scattering has recently been demonstrated in acoustic model studies [8]. It was shown in this study that the addition of periodic rectangular roughness elements representing building facade structure quite markedly effected the sound distribution in a street. The attenuation rates achieved in this model study were found to correspond much better to those of the published field data. The scattering phenomenon associated with rectangular periodic irregularities has been studied by Deriugin [14] and Wagner [15]. Unfortunately, in the former work, the solutions obtained are too specialized, while the latter work considers only the high and low frequency limits.

The ultimate purpose of the work presented here is to develop methods of predicting sound levels in urban areas for the range of typical sources and geometries found in such areas. In the development of this subject there are a number of sub-issues addressed. The first of these is the determination of the utility and limitations of specular imaging theory. The second issue is the quantitative assess-

ment of scattering from rectangularly irregular surfaces for the geometries and frequencies of interest in urban propagation. The third task is the development of a practical model of the scattering phenomenon which can be incorporated into a modified form of imaging theory. The final and previously neglected step is the validation of propagation theory with field as well as acoustic model data.

II. BASIC ACOUSTICAL IMAGING THEORY

2.1 Theoretical Background

The basis for acoustical imaging theory is derived from the examination of the sound field produced by an ideal point source near an infinite, rigid plane. The geometry of this situation is given in Figure 2.1. The boundary conditions imposed on the field are that the normal fluid velocity and hence the normal gradient of pressure be zero at the surface. From potential flow theory, it is known that these conditions can be met by replacing the reflecting surface with an image of the source [16]. This image is located on the line normal to the plane passing through the source at a distance twice that between the original source and reflecting plane. In the case of a rigid surface, the pressure field is given by Morse and Ingard [17] to be

$$p = A \left(\frac{1}{4\pi r_1} e^{ikr_1} + \frac{1}{4\pi r_2} e^{ikr_2}\right) e^{-i\omega t}$$

where A is in general a complex amplitude and k is the acoustic wavenumber, $k = 2\pi/\lambda$. For the more realistic case of a non-rigid surface, Morse and Ingard use an approximate Green's function solution. With the assumption that the measurement point is at least a half wavelength away from the surface, the following expression for the pressure field is obtained:

$$P = A \left(\frac{1}{4\pi r_1} e^{ikr_1} + \left[\frac{\cos\phi-\beta}{\cos\phi+\beta}\right] \frac{1}{4\pi r_2} e^{ikr_2}\right) e^{-i\omega t}$$

where β is the acoustic admittance of the surface and is generally complex.

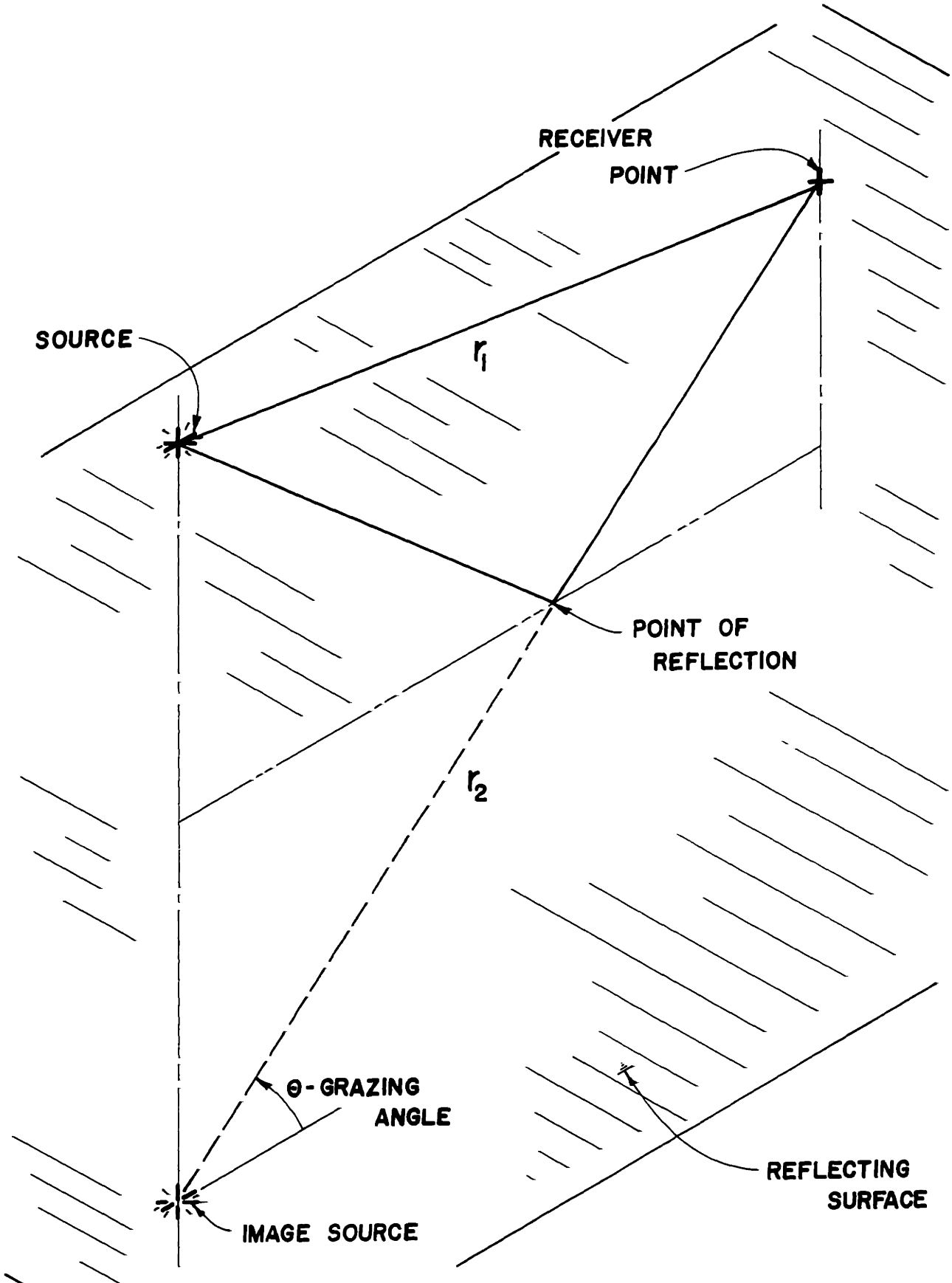

FIGURE 2.1: Geometry of Point Source Reflection from an Infinite, Rigid Surface

To begin simplifying the expression for the pressure field, the first assumption to make is that of real admittance. This assumption means that there is no or very little phase shift upon reflection. For urban propagation, the surfaces encountered are typically non-porous and nearly perfectly rigid for the wavelengths involved, thus making this assumption a reasonable one. Another practical reason for this assumption is that while admittance magnitude can be measured for a surface, it is extremely difficult to determine phase shift as a function of incident angle. Thus it is assumed that the bracketed quantity corresponds to a real reflection coefficient which depends on the incident angle, ϕ, and the real value of surface admittance.

Further simplification of the pressure field expression can be made by forming a ratio of direct and reflected energy. Using the above assumption, taking the real part of the pressure, squaring it, and dividing by the direct pressure, yields the following expression:

$$P_r^2 \simeq 1 + \frac{A_2^2 r_1^2}{A_1^2 (r_1+c\Delta t)} + \frac{1}{\Delta f} \cdot \frac{2A_2 r_1}{A_1 (r_1+c\Delta t)} \left[\frac{1}{2\pi\Delta t} \cdot \sin 2\pi\Delta t f \right.$$

$$\left. + \frac{c}{2\pi(r_1+c\Delta t)} \sin \frac{2\pi}{c} (2r_1+c\Delta t) f \right]_{f_1}^{f_2}$$

Assuming that Δt is small, the first two terms add to a sum of two or less. For the third term, the multiplicative amplitude factor

$$2A_2 r_1 / A_1 (r_1+c\Delta t)$$

is of the order 1. Thus if

$$\Delta f >> 1/2\pi\Delta t$$

then the third term is negligible compared to the first two terms. The sum of the first two terms is between 1 and 2. This leads to the "energy addition" of pressure signals which for the maximum case gives a 3 dB increase in sound level. Imaging theory as it is applied to street propagation uses exclusively this energy addition principle to sum image strengths. Also it is assumed that the reflection coefficient is independent of incident angle.

2.2 Application to Channel Propagation

The simplest application of specular imaging theory is the assessment of propagation down a straight channel with no openings. The geometry of this propagation case is presented in Figure 2.2. Shown in the figure are several multiply-reflected paths in which sound propagates to the receiver. To represent these paths, image streets can be constructed such that image wall W_R' represents the image of wall W_R as reflected by wall W_L. Similarly, image wall W_L'' represents the image of wall W_L as reflected by walls W_R and W_L. In this manner, the entire image space is constructed. As indicated in Figure 2.2, reflected paths between source and receiver can be replaced by straight lines connecting the source with image receivers which pass through the street walls. It should be noted that each passage through a wall or image wall corresponds to one reflection. If carried to its limits, an array of images infinite in extent is produced which runs perpendicular to the channel and represents all

FIGURE 2.2: Channel Propagation - Replacement of Multiply Reflected Paths with Images

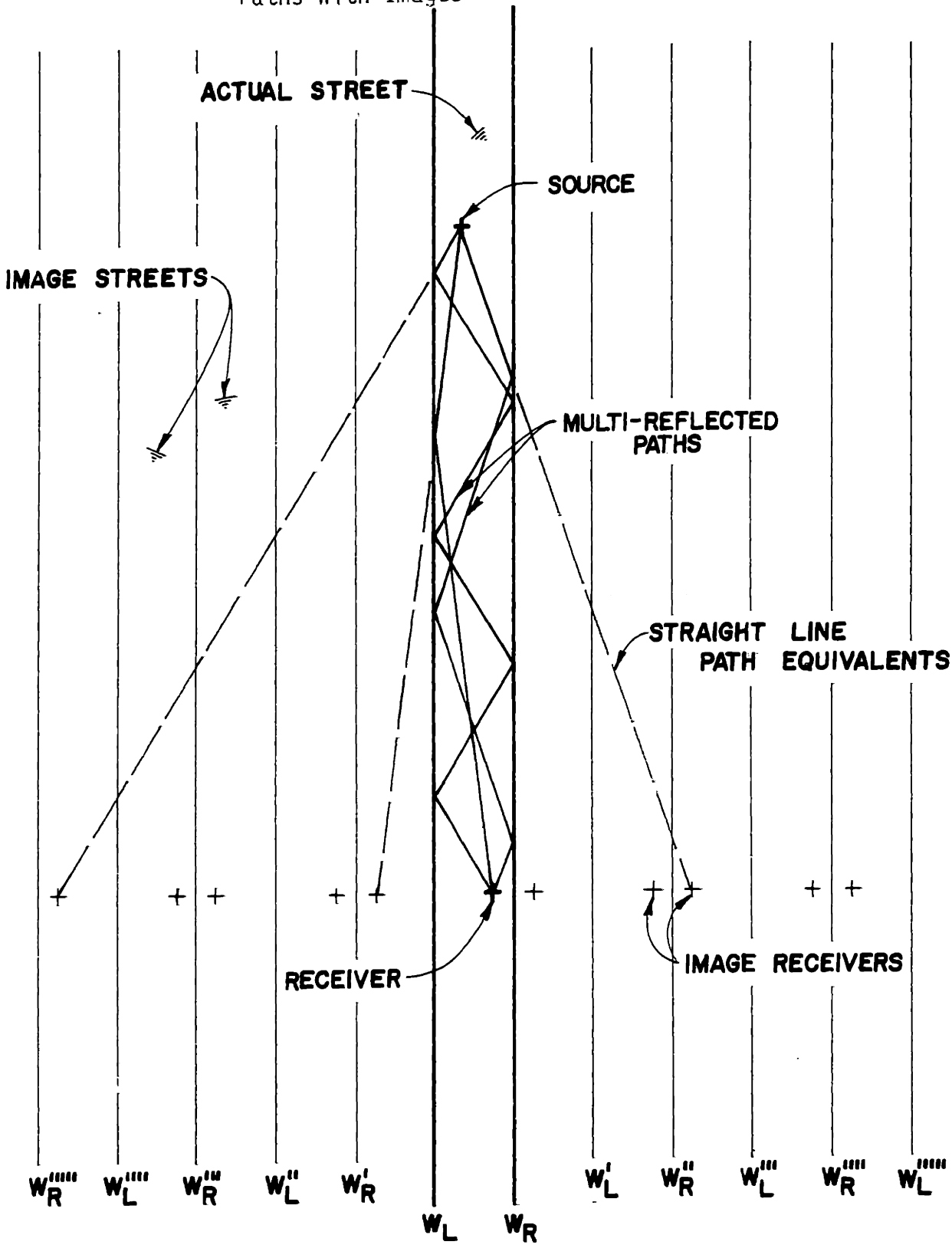

possible paths. If the walls are not perfectly reflecting, a reflection ratio can be defined which is the ratio of reflected energy to incident. This ratio must be applied for every reflection, thus the strength of the i^{th} image is

$$A_i^2 = (R)^i \cdot A^2$$

where R is the reflection ratio and A the pressure amplitude of the source. The array is now composed of images which exponentially decay in strength with distance from the actual channel. It should be noted that the reciprocity theorem of acoustics implies the use of image sources is equivalent to the use of image receivers.

A slightly more complicated case is that of propagation around a corner at a four-way channel intersection. The geometry of this configuration is presented in Figure 2.3. As in the previous case, several multiply-reflected paths are shown along with their image space equivalent. For this configuration reflections in the source street are replaced by image sources, while reflections in the receiver street are represented by image receivers. It should be noted that only those reflected paths which finally reflect from the far side of the source street can ever enter the receiver street. This condition leads to a semi-infinite array of images in the source street as opposed to infinite. Similarly, since incoming rays in the receiver street must reflect on the far side of that street, only a semi-infinite array is produced in the receiver street. As in the straight channel case, the image strengths decay exponentially

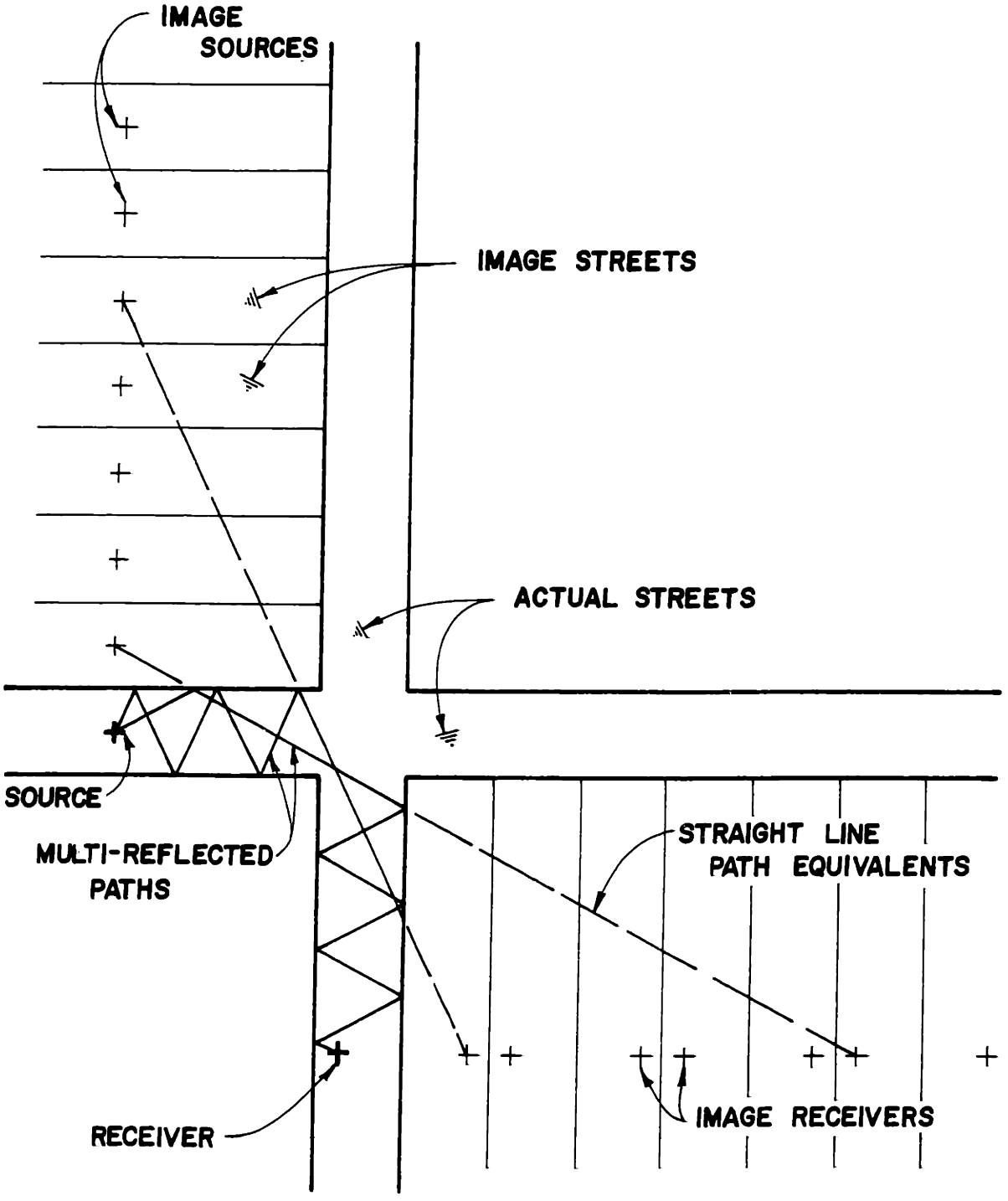

FIGURE 2.3: Propagation Around a Corner - Replacement of Multiply Reflected Paths with Images

with distance from the actual street for R < 1.

In order to determine a sound level at the receiver point, two techniques have commonly been employed. The first of these is the discrete summation of the energy of all the images which are found to contribute to the level. This is done with proper attention to image strength and path length divergence, as indicated in the previous section. The second method utilizes the approximation of the image array by a line source of exponentially decaying strength. The array chosen may be either the source image array as used by Schlatter [4] or receiver image array as used by Lee [9]. With this line source approximation, the incremental sound intensity at the receiver is given by [7]

$$dI = \frac{\alpha W e^{-\mu|x|} dx}{2\pi L (r)^2}$$

where

W = acoustic power of source

L = street width

X = variable distance from actual street centerline to the increment dx

$\mu = -\frac{1}{L} \ln R$, R = reflection coefficient

$\alpha = \frac{\sqrt{R} \ln R}{R-1}$

r = distance from increment dx to receiver.

To obtain the total intensity, this expression is then integrated over those portions of the line source which contribute. If the actual

street is included in this portion, a point source of strength

$$I = \frac{W}{2\pi r^2} \quad \frac{(1-\sqrt{R})}{(1+\sqrt{R})}$$

must be added to the integral value. For the case of straight channel propagation, integration of the incremental intensity can be done analytically as the limits of integration are from 0 to ∞. For finite limits, however, numerical integration must be resorted to.

To apply either the discrete summation or line source methods, the extent of the image array must be determined for all cases other than straight channels with no openings. As an example of determining limits, consider again the around a corner propagation depicted in Figure 2.3. Examination of this figure indicates that there are two criterion for propagation to the receiver. The first is that the ray path pass through the opening of the receiver street. The other is that multiply reflected paths in the source street, those paths from image sources, must reflect off, that is pass through, the far wall of the source street. These two criterion establish the influence limits for each of the image sources as shown in Figure 2.4. Indicated in this figure are the two methods of level determination. For the discrete method, the "cone of influence" of each image source includes those image receivers which contribute to the total level. For the line source method, the intersection of the cone with the line of the array determines the limits of the intensity integration. It should be noted that the intensity integral value must be multiplied by a factor of $(R)^i$ for the i^{th} image source.

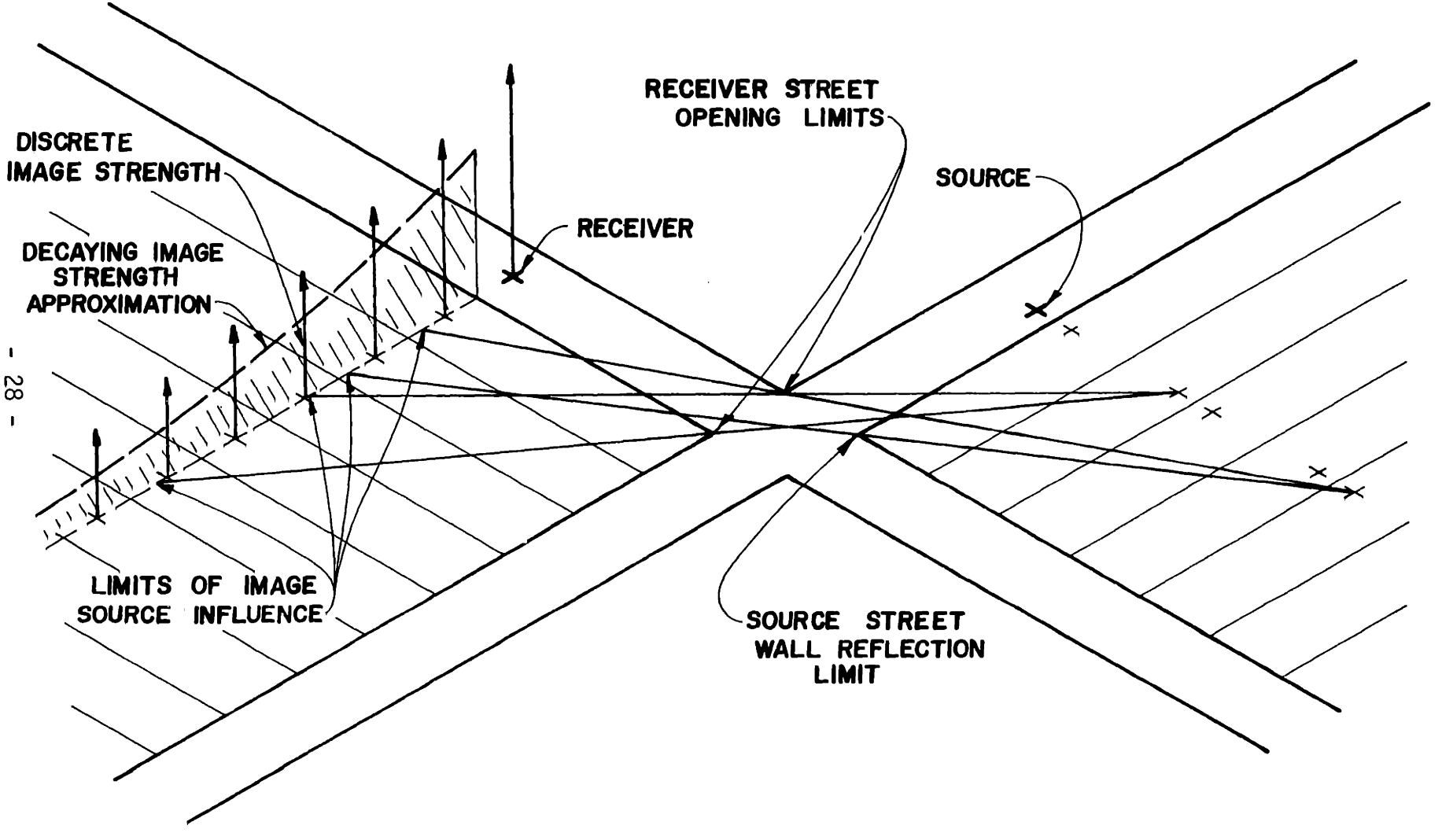

FIGURE 2.4: Discrete Image Summation and Line Source Approximation Applied to Propagation Around a Corner

As a final example of imaging applied to channel propagation, consider propagation around a corner, down a channel, and through an intersection. The geometry of this configuration is given in Figure 2.5. As before, the multiply reflected paths are shown along with their straight line equivalents. It will be observed that the two paths meet the criterion described previously for around a corner propagation, that is, reflection from the far source street wall and passage through the receiver street opening. Further, it should be observed that straight-line path equivalents can be connected to image receivers. However, if the ray paths themselves are followed, it is seen that the paths do not go to the receiver, but rather are lost to the side street. Thus, there is an additional condition on the straight line equivalents from image source to image receiver. This condition is that the line equivalent does not pass through the side street opening or any of its images. Thus, for this propagation case, the cones of influence of each image source are modified as depicted in Figure 2.6.

2.3 Results Predicted by Specular Imaging Theory

2.3.1 Comparison of Application Methods

Generally the results computed from the discrete summation and line source methods of imaging compare quite well to each other. Some variation is expected as the line source method is an average sound level over the receiver street while discrete image summation applies to one point in the receiver street. One example of comparison of these two methods is afforded in Figure 2.7. This figure plots attenuation down a channel relative to the source free field sound level at one street width.

FIGURE 2.5: Propagation Around a Corner and Through an Intersection - Replacement of Multiply Reflected Paths by Images

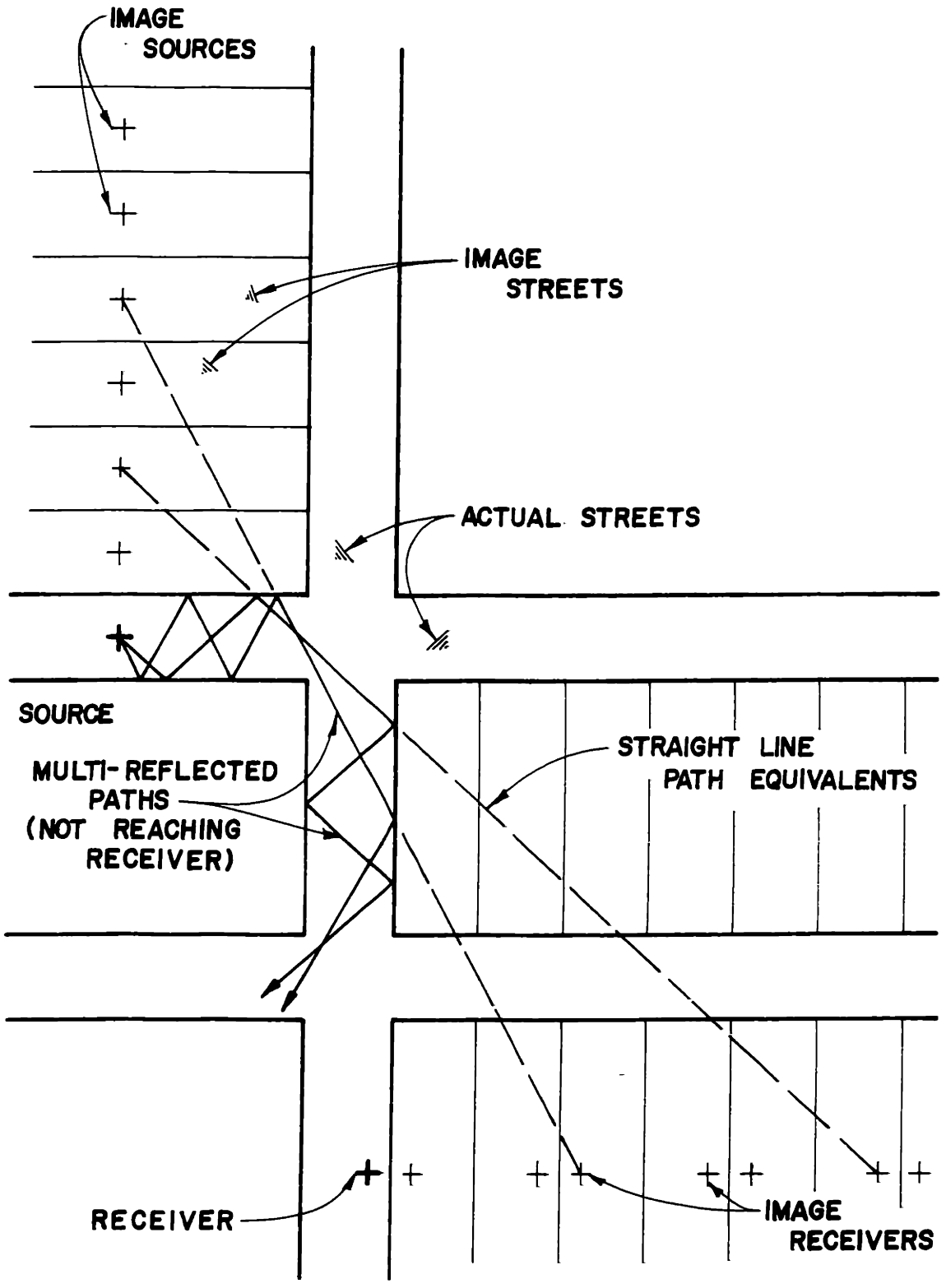

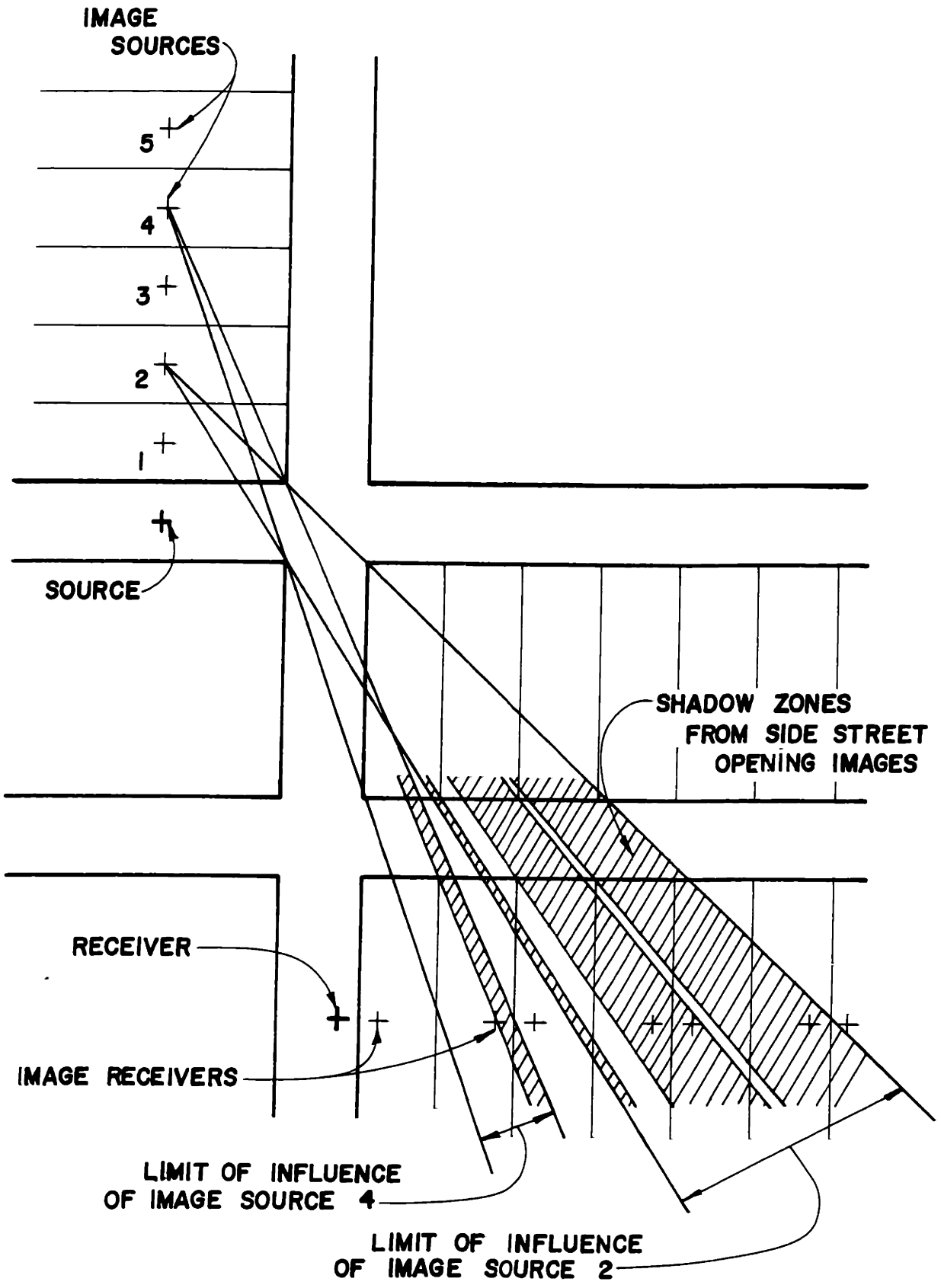

FIGURE 2.6: Application of Imaging to Propagation Around a Corner and Through an Intersection

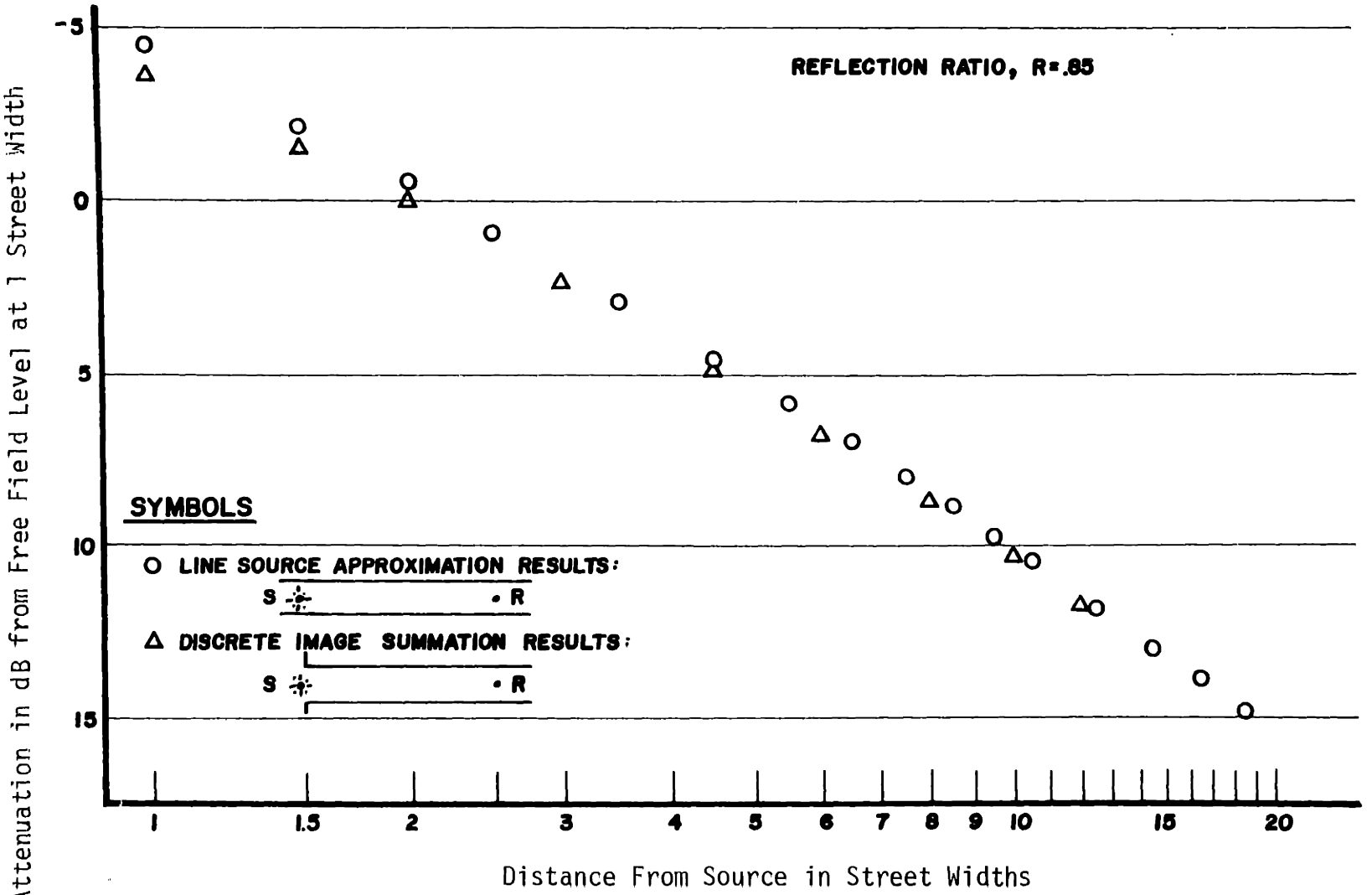

FIGURE 2.7: Line Source Approximation and Discrete Image Summation Results for Channel Propagation

The line source approximation values are those reported by Schlatter [4] for a straight channel. The discrete summation values are for a slightly different configuration, that of propagation into a channel with the source slightly outside the channel. Owing primarily to the slight difference in configuration, the discrete values are .8 to .5 dB lower near the source. Much better correspondence is achieved after 3 street widths distance from the source.

Another comparison of discrete image summation and line source approximation results is presented in Figure 2.8. The configuration for this comparison is propagation around a corner. Line source results are those of Lee [9]. It will be noted that the line source results are consistently 1 to 1.5 dB higher than those for discrete summation. One possible reason for this discrepancy may lie in the approximations required by Lee in empirically producing normalized curves for the line source case. Another possible cause of the discrepancy is that for propagation around a corner, the sound level in the receiver street is quite dependent on receiver location across the street. Variation can be as much as 3 or 4 dB. Thus, it is not surprising to see small differences between the discrete case in which the receiver is located on the street centerline and the street averaged line source case.

A final compared case which is indicative of sound level variation across the receiver street is presented in Figure 2.9. The configuration considered is again propagation around a corner, however, for a tee intersection as opposed to four-way. Compared in this figure are results

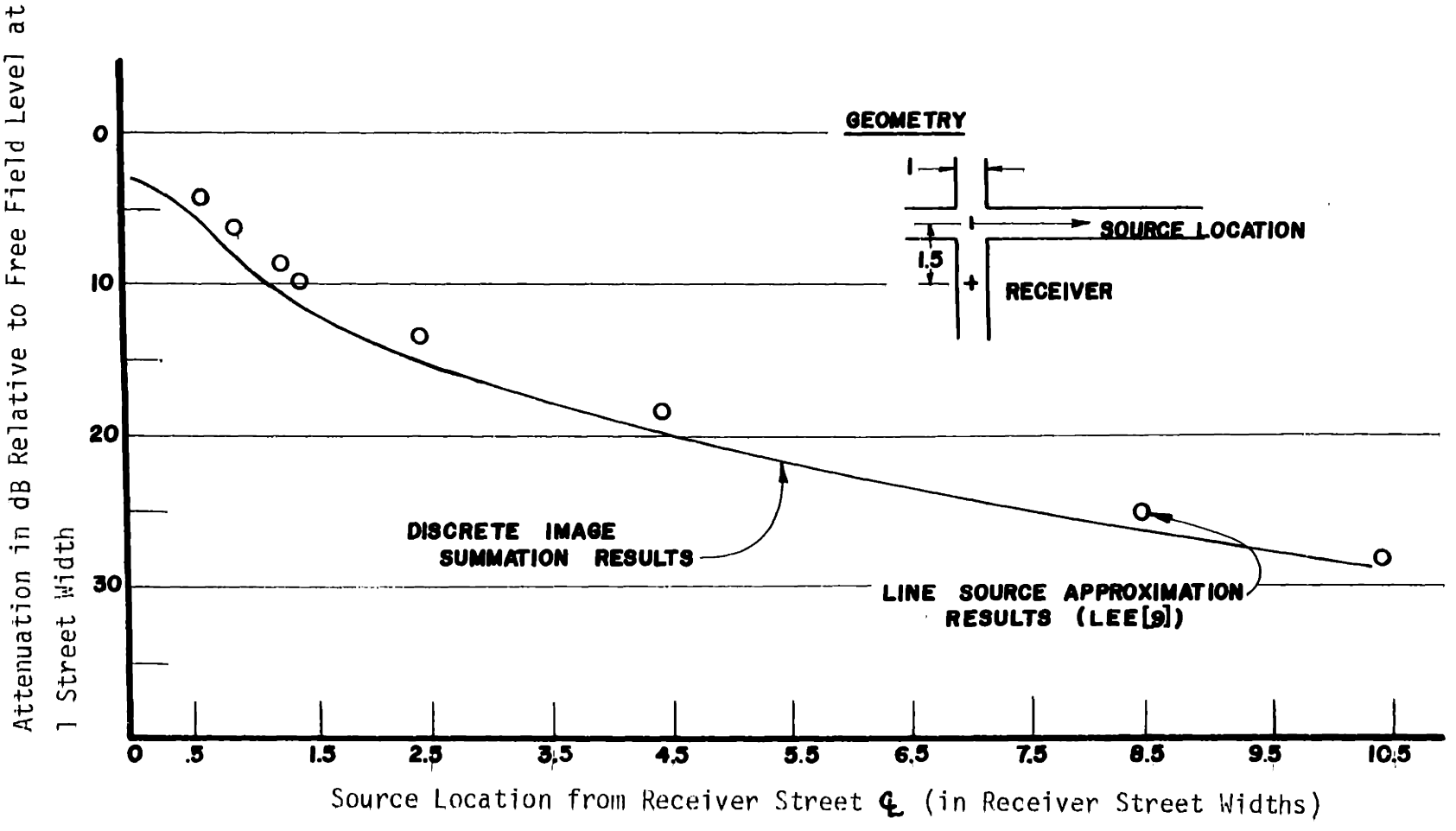

FIGURE 2.8: Line Source Approximation and Discrete Image Summation Results for Propagation Around a Corner

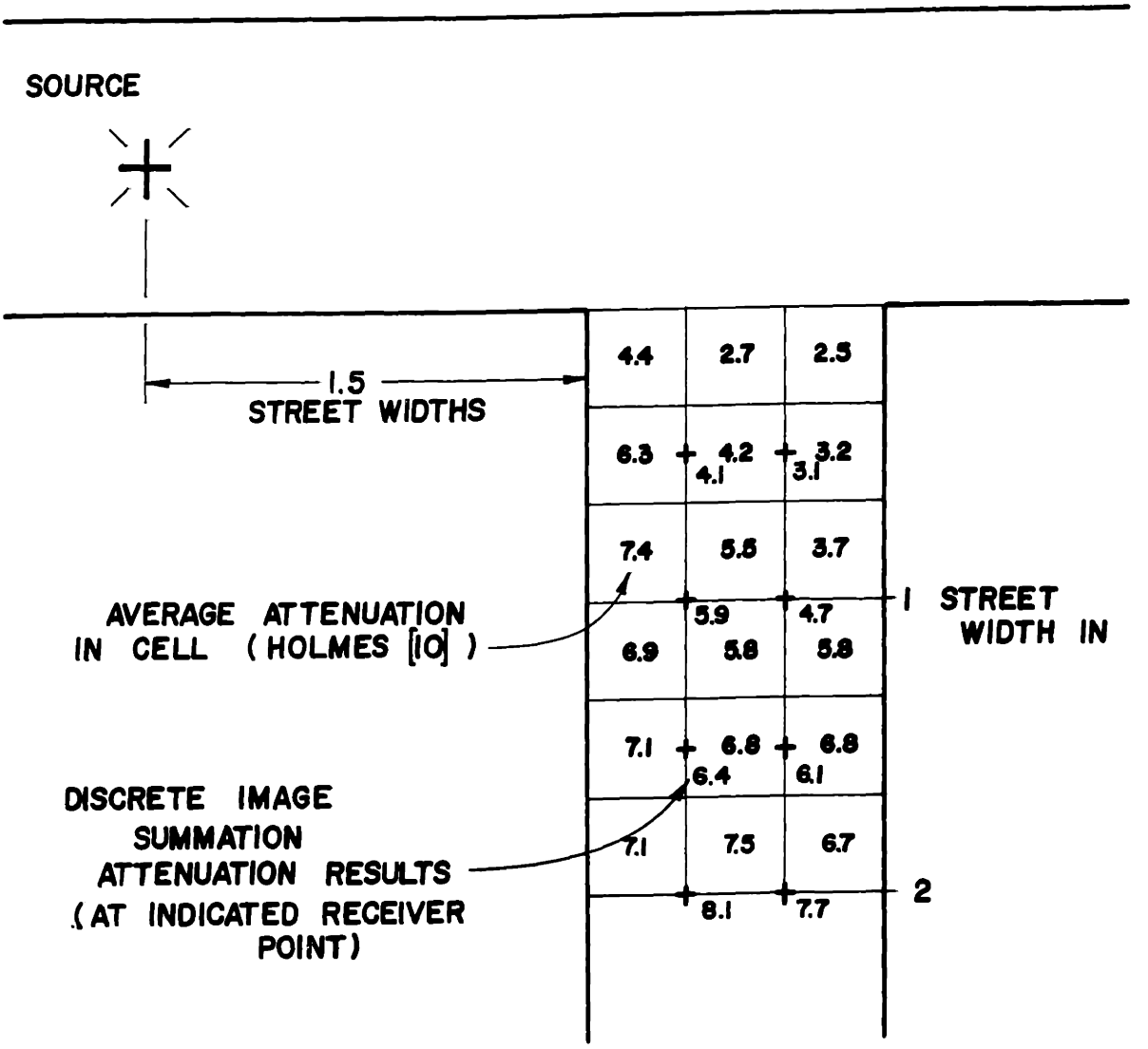

FIGURE 2.9: Numerical Simulation and Discrete Image Summation Results for Propagation Around a Corner

obtained from the propagation simulation computer program of Holmes [10] and the results predicted by discrete image summation. In considering the two sets of results, it should be noted the computer simulation results are averaged over a square with dimensions of 1/3 street width, thus some interpolation is required in comparing these to the point receiver locations. However, with this interpolation it will be seen that there is quite good agreement between these two sets of results.

2.3.2 Sound Level Fall-Off Rates with Distance

With the results obtained from specular imaging theory, one can quite readily obtain sound level fall-off rates for the various types of propagation configurations. For the straight channel case [4], if the value of the reflection coefficient, R, is high, the upper limit fall-off rate is 3 dB/dd. For R less than 1.0, the lower limiting rate is 6 dB/dd. It should be noted that these two fall-off rates correspond to the free field rates of a line source and point source, respectively. For immediate values of R, the fall-off rate lies somewhere between the extremes. For all values of R which are less than 1.0 and greater than 0.0, the fall-off rate itself is a function of distance down the street. Very near the source, the actual source dominates the image sources and fall-off is 6 dB/dd. At a distance on the order of a street width, the fall-off rate becomes close to 3 dB/dd for large R. At much further distances from the source, there is a transition back to the 6 dB/dd rate. This transition is governed by the amount of wall absorption present. For propagation in a street channel, typical absorption coefficients for the buildings (concrete, glass, brick, etc.) give values of R equal to

about .9 to .95 [18]. These values of R give fall-off rates in the middle distance region of about 3.5 dB/dd. Transition to 6 dB/dd occurs well beyond 20 street widths from the source.

Sound level fall-off rates for propagation around a corner have also been determined [8]. For values of R corresponding to urban building materials, if the source is near the intersection, a fall-off rate of 3.5 dB/dd initially is observed with a transition to 6.0 dB/dd within four to five street widths. Thus the effect of the corner appears to be to hasten the transition observed for the straight channel case. This behavior is indicated in Figure 2.10(a) for both acoustical model data and its imaging theory simulation. When the source is farther from the intersection as shown in Figure 2.10(b), the fall-off in receiver street is a constant 6 dB/dd. For both of these two cases, the level does not fall below the free field level of the source as indicated in the figures. This behavior is also indicated for source positions up to 10 street widths into the source street. However, if the distance of source from the intersection is moderate, three street widths, and if more absorption is applied to the building walls, free field attenuation will be exceeded. This behavior is indicated in Figure 2.10(c). The results in this figure are for R = .65. A fall-off rate of 14.5 dB/dd is attained, a rate which is much higher than that attainable in a straight street.

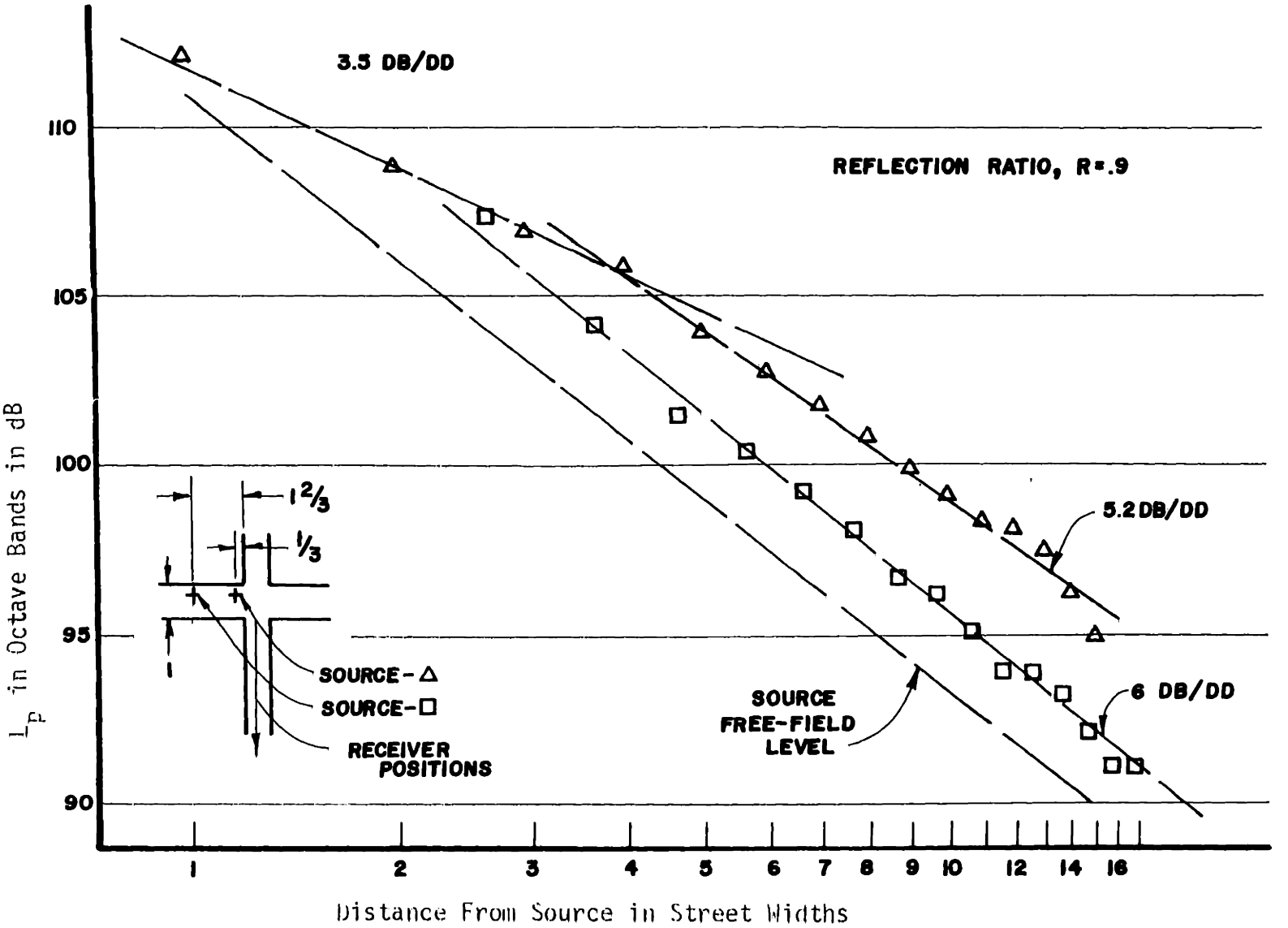

FIGURE 2.10: Sound Propagation Around a Corner at a Four-way Intersection

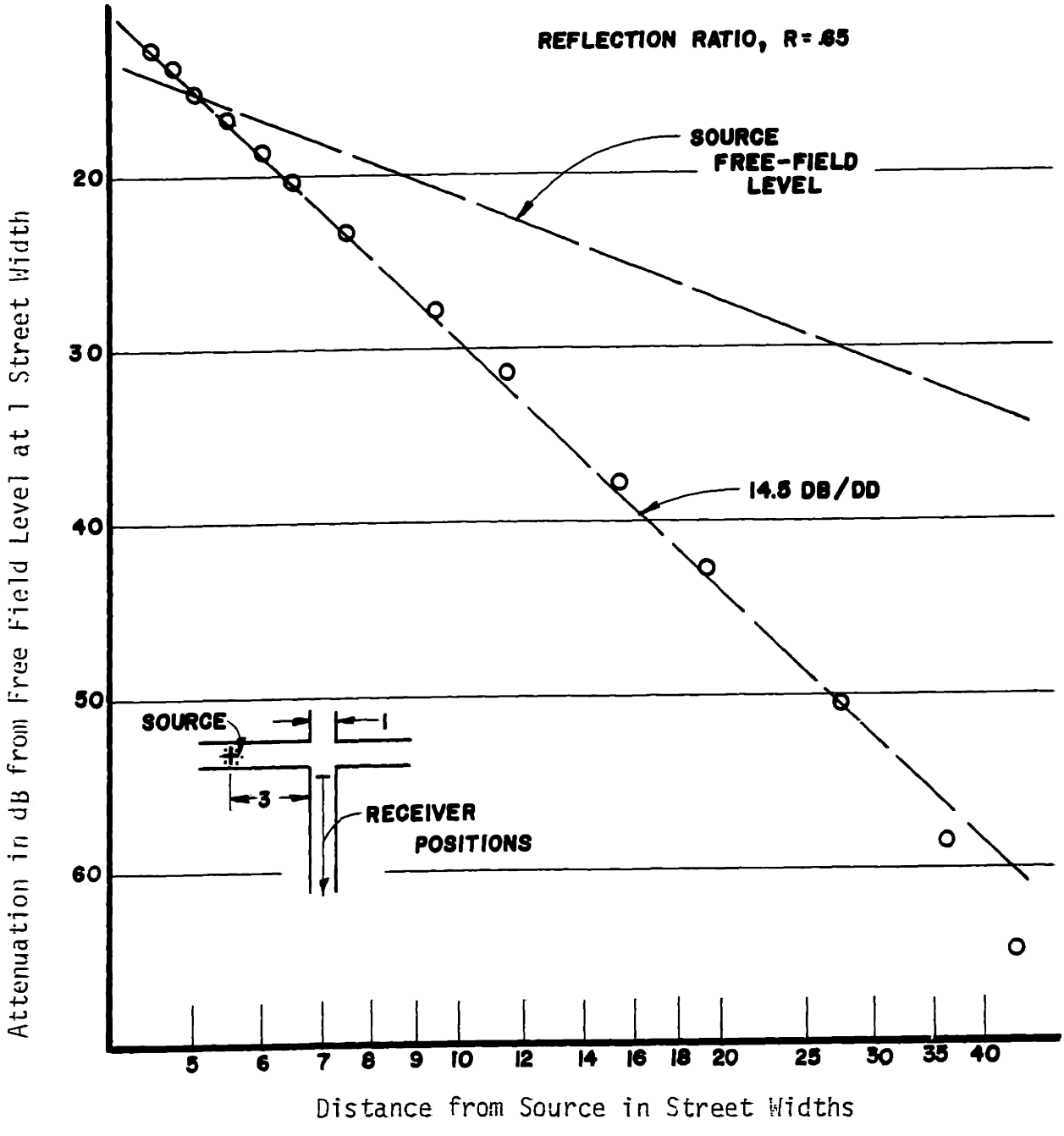

FIGURE 2.10 Sound Propagation Around a Corner at a Four-way Intersection

III. APPLICATION OF IMAGING THEORY TO CITY STREETS

3.1 Published Field Data and Specular Imaging Theory Results

As discussed in a previous section, there is very little published urban noise field data which can be used directly for propagation assessment. A typical problem with the available data is that the source is specialized, that is, either directive or narrow-band, or it is of unknown acoustic specification. However, from what data does exist, there is good indication that specular imaging theory alone does not compare well to actual street propagation. One indicator of this discrepancy is from the work of Wiener, Malme and Gogos [12]. This study reports excess attenuation (attenuation beyond spherical spreading) near 0 or greater for propagation down a city street. Assuming a reflection coefficient consistent with typical building materials, specular imaging gives an excess attenuation of -2.0 to -2.5 dB/dd. The source used in this field study was a loudspeaker and thus directivity effects are to be expected. It is not, however, at all clear that this would account for the significant difference between the two rates of fall-off.

Another source of comparison of field data and specular imaging theory is the work reported by Delaney, Copeland and Payne [13]. The reported data is in the form of L_{10}, L_{50}, and L_{90} sound levels for receiver positions down an urban side street away from an arterial street containing freely flowing traffic. Because of the nature of the source, absolute levels down the side street cannot be compared to imaging results.

However, it is possible to compare the fall-off rates down the side street if an assumption is made. Since the traffic density is such that on the average, fewer than one vehicle is in the intersection at an instant, it may be assumed the L_{10} levels fall-off down the street as if there were just one source and it were located in the intersection. Using this assumption, comparative results using the L_{10} values and specular imaging theory for a point source located an appropriate distance outside a channel are presented in Figure 3.1. The field data displays two fall-off rates, about 4 dB/dd near the source and about 9 dB/dd farther from the source. The imaging theory gives a constant rate with distance of about 3.5 to 4.0 dB/dd. Although the assumptions made in this comparison are somewhat questionable, the difference is substantial enough to indicate the disparity between specular imaging and propagation in actual streets.

The lack of agreement observed between specular imaging theory and published field data could be attributed to several things. One problem area could be in meeting the imaging theory criterion which leads to energy addition of images. Violation of this criterion would occur if the source or the measurement bands were too narrow in frequency or if the difference in path length for adjacent images was extremely small. The nature of the field data, however, makes this possibility unlikely. The Delaney, Copeland, Payne data is reported in A-weighted sound level and since vehicular noise sources are typically broad band [19], the energy addition criterion is easily met. The Wiener, Malme and Gogos data is obtained for 1/3 octave bands of white noise which is also sufficiently

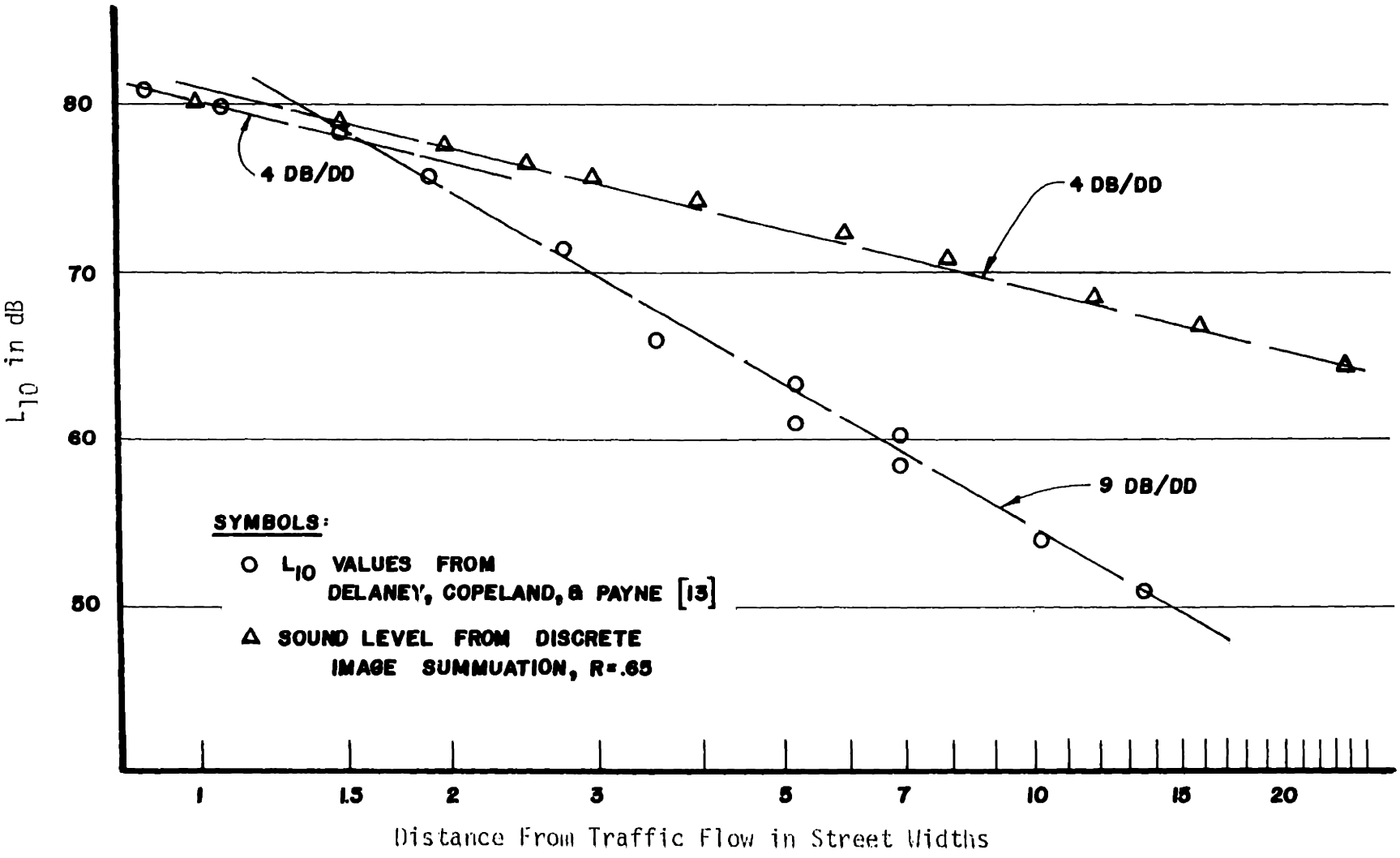

FIGURE 3.1: Comparison of Delany, Copeland and Payne Date to Specular Imaging Theory Results

broad. This possibility is also discounted by the generally good agreement obtained between specular imaging and smooth wall, acoustical model data [4,8].

Another possible cause of disagreement between specular imaging and field data is the effect of meteorological conditions in the field data. This was shown by Wiener, Malme and Gogos, however, not to be important for urban propagation.

A third possible reason for the discrepancy between field data and specular imaging is diffraction. This problem only arises for propagation around a corner and thus cannot explain the differences observed for sound level fall-off down a street. For propagation around a corner, diffraction effects will very definitely be present. The question of the magnitude of this effect is then of importance. Because of the $1/\lambda$ dependence of the diffracted field [20], diffraction is not expected to be important in urban propagation except possibly for only the lowest frequencies of interest. When diffraction effects are observable, they will tend to increase levels when there is no direct line of sight to the receiver, and decrease levels slightly when there is.

A much more probable cause of the poor correspondence between specular imaging theory and field data is the scattering of sound upon reflection from building surfaces. The specular reflection assumption commonly employed idealizes building surfaces as acoustically smooth, constant impedance walls. Considering the similarity of the acoustic

properties of materials commonly used in construction, the constant surface impedance assumption appears to be valid. The assumption of acoustical smooth surfaces, however, is quite weak. Typically, building surfaces have considerable irregularity due to window recesses, decorative facade structures, doorways, etc. Furthermore, these rectangular irregularities typically have dimensions on the order of an acoustic wavelength for the frequencies of importance in urban noise propagation. These frequencies include the octave bands centered at 250, 500, 1000, and 2000 Hz as determined from typical, A-weighted urban noise spectra [19]. Examples of building surfaces displaying such surface irregularity are shown in Figure 3.2. Typically, surface irregularities can be considered as rectangular, periodic protrusions in the building surface which very often are most pronounced in the vertical direction. Evidence that the presence of such protrusions affect the sound level in a channel relative to smooth walls was reported in an earlier paper [8] and will again be demonstrated with additional data. It was shown in this earlier paper that the protrusions produce sound level fall-offs in a channel similar to those seen in the published field data.

3.2 Experimental Investigations of Street Propagation

3.2.1 Field Experiments

Due to the limited amount of published data, it was necessary to undertake field measurements in a typical urban setting. The experiment was designed explicitly for propagation assessment. A source of known

FIGURE 3.2: Building Surface Irregularities

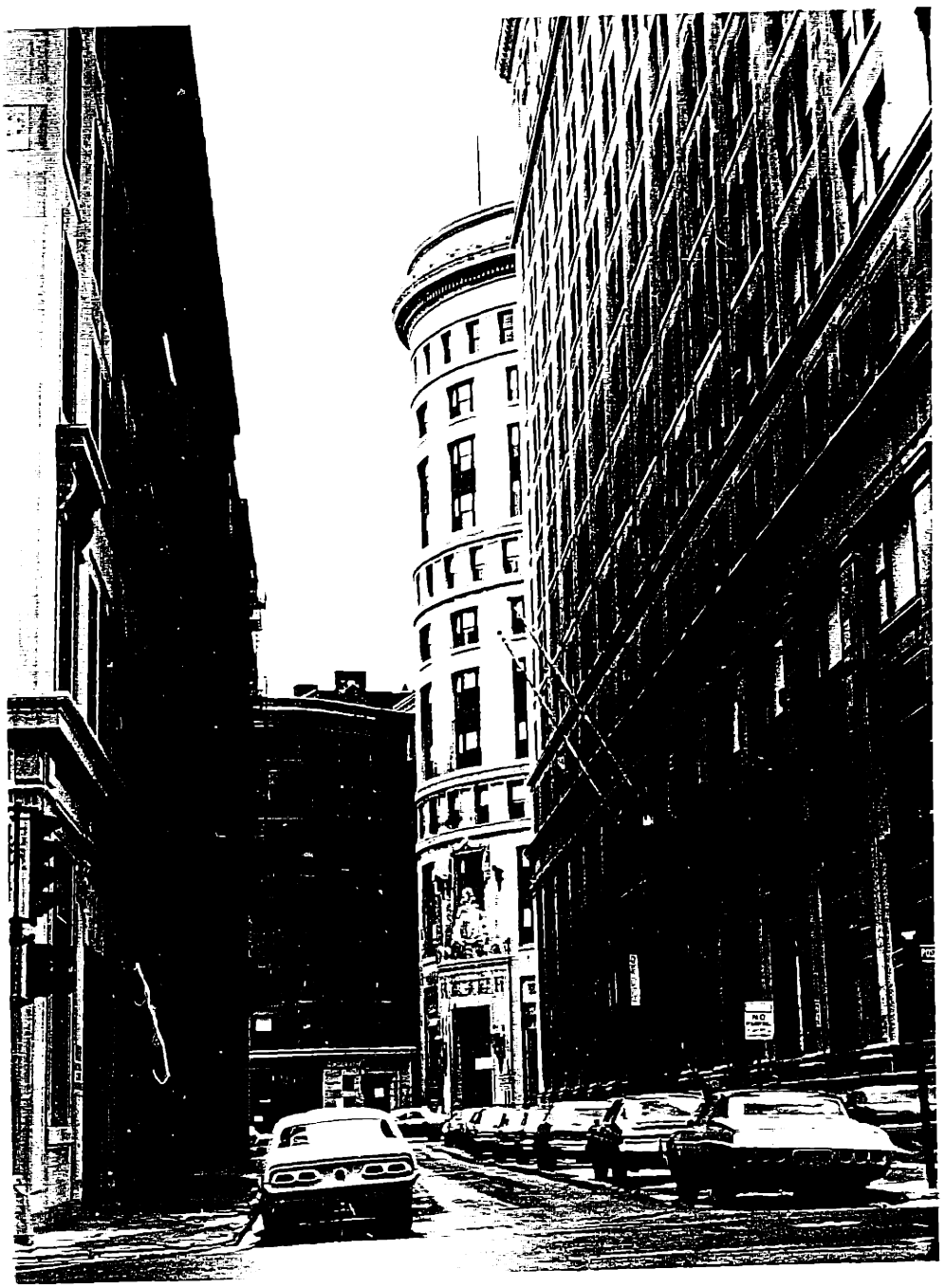

FIGURE 3.2: Building Surface Irregularities

acoustical properties was used and variables such as meteorological effects and background noise were minimized. The data was taken in a format which would readily allow comparison to both acoustical model and imaging theory results.

The site for this study was selected to meet several criteria. One criterion was that the buildings in the area have a facade structure that is typical of most urban buildings. Another criterion was that the site contain a variety of propagation cases in a relatively small area so that a proper signal to noise ratio could be maintained. An additional criterion was that vehicular traffic could be eliminated during the test. A plan of the site is presented in Figure 3.3. Several photographs of the site are presented in Figure 3.4.

The noise source used in the field test was a .32 caliber starter's pistol. This source was used because it is highly portable, non-directive, broad band, and has a high energy level. The 1/3 octave band relative energy spectrum of the pressure pulse produced by this source is presented in Figure 3.5. From this figure it will be noted that the maximum energy occurs in the 1/3 octave band centered at 1,600 Hz. Also, it will be noted that sufficient energy is available in octave bands of experimental interest, those centered at 250, 500 and 1000 Hz. Although the absolute level is not presented in Figure 3.5. it was determined that the peak sound pressure level at 12 ft in the 1600 Hz 1/3 octave band was 115.2 dB Re .0002 microbars. The measured directivity of the starter's pistol is presented in Figure 3.6. It will

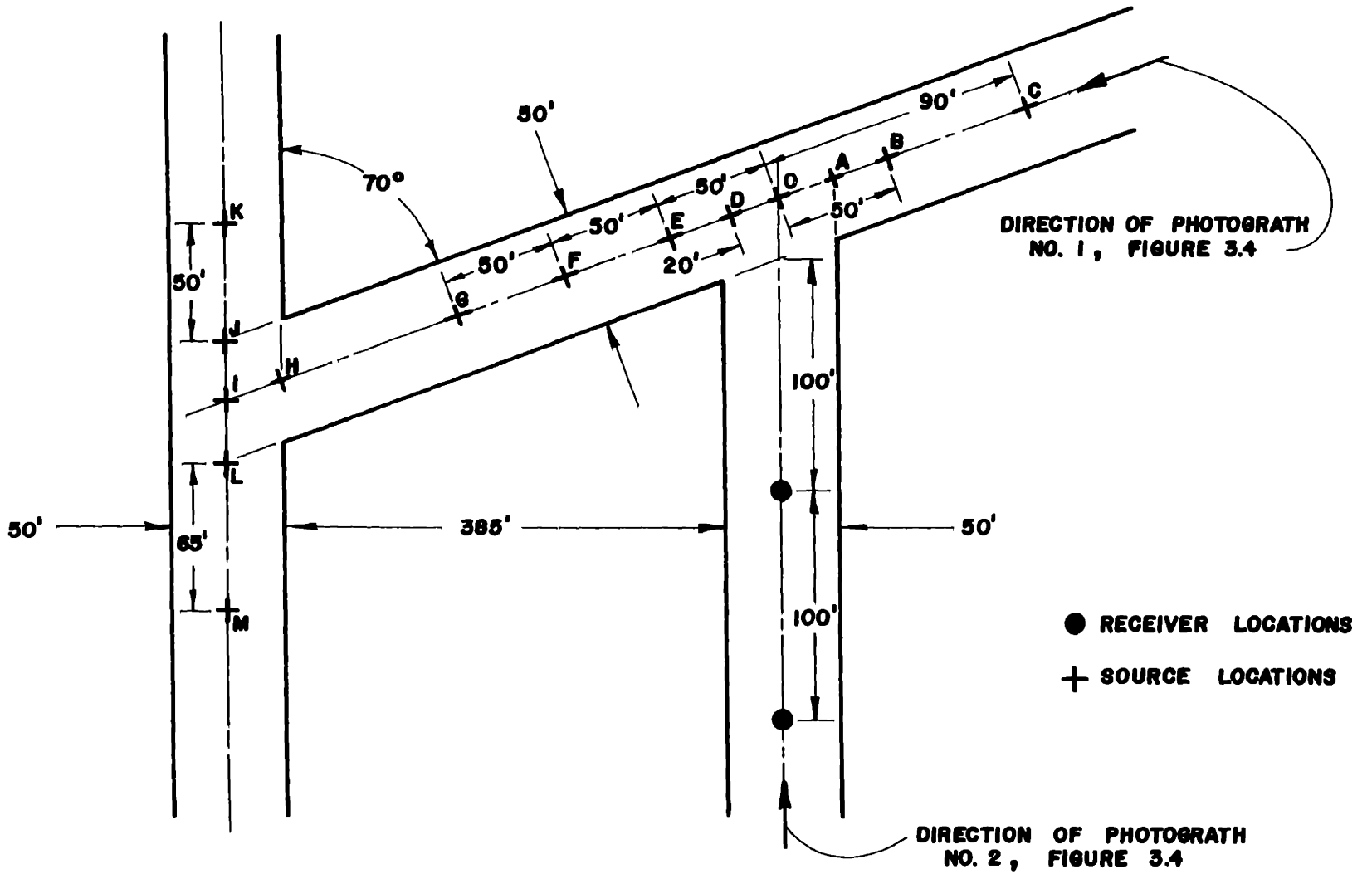

FIGURE 3.3: Street Plan of Field Experiment Site

FIGURE 3.4: Site of Field Experiments

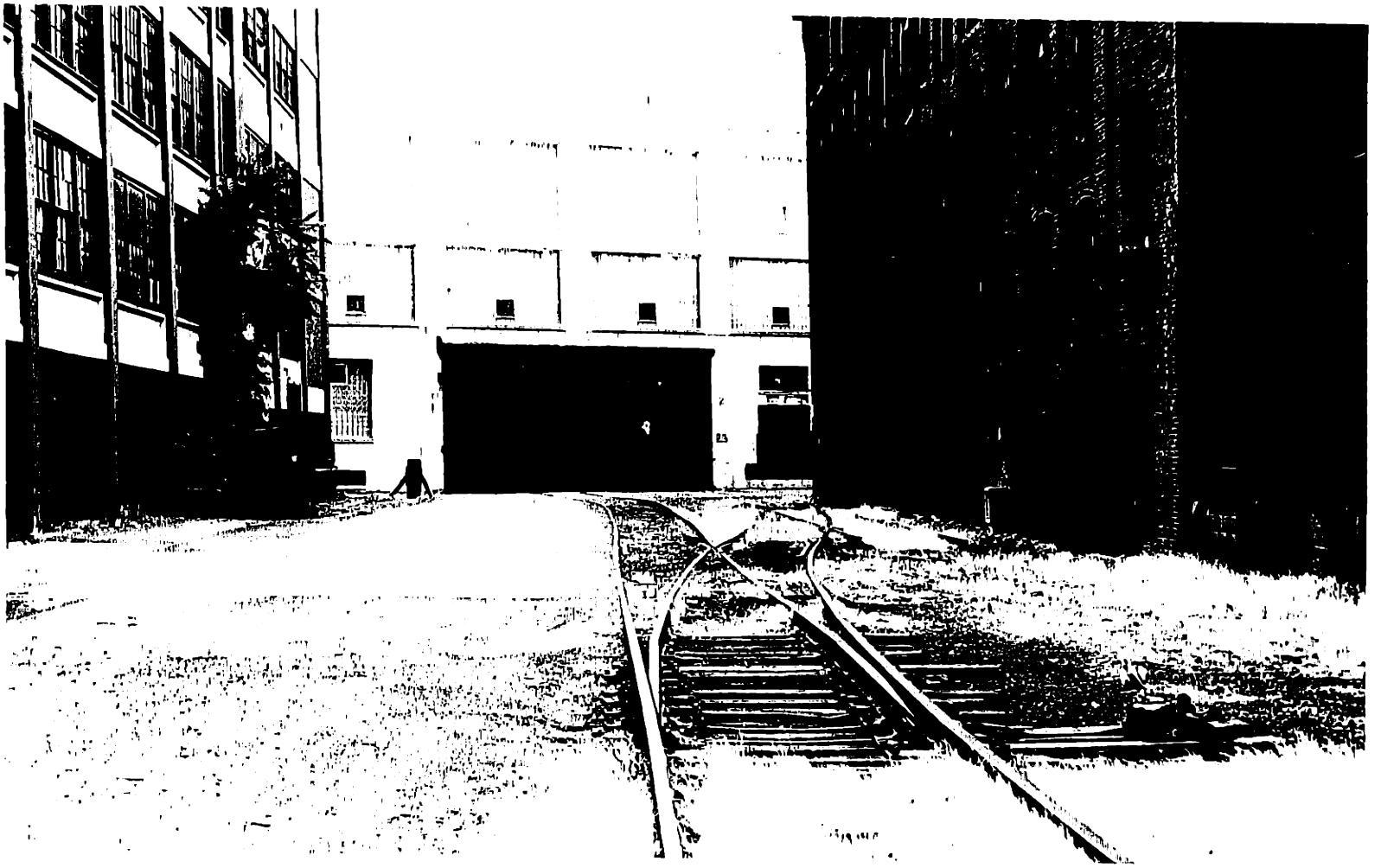

FIGURE 3.4: Site of Field Experiments

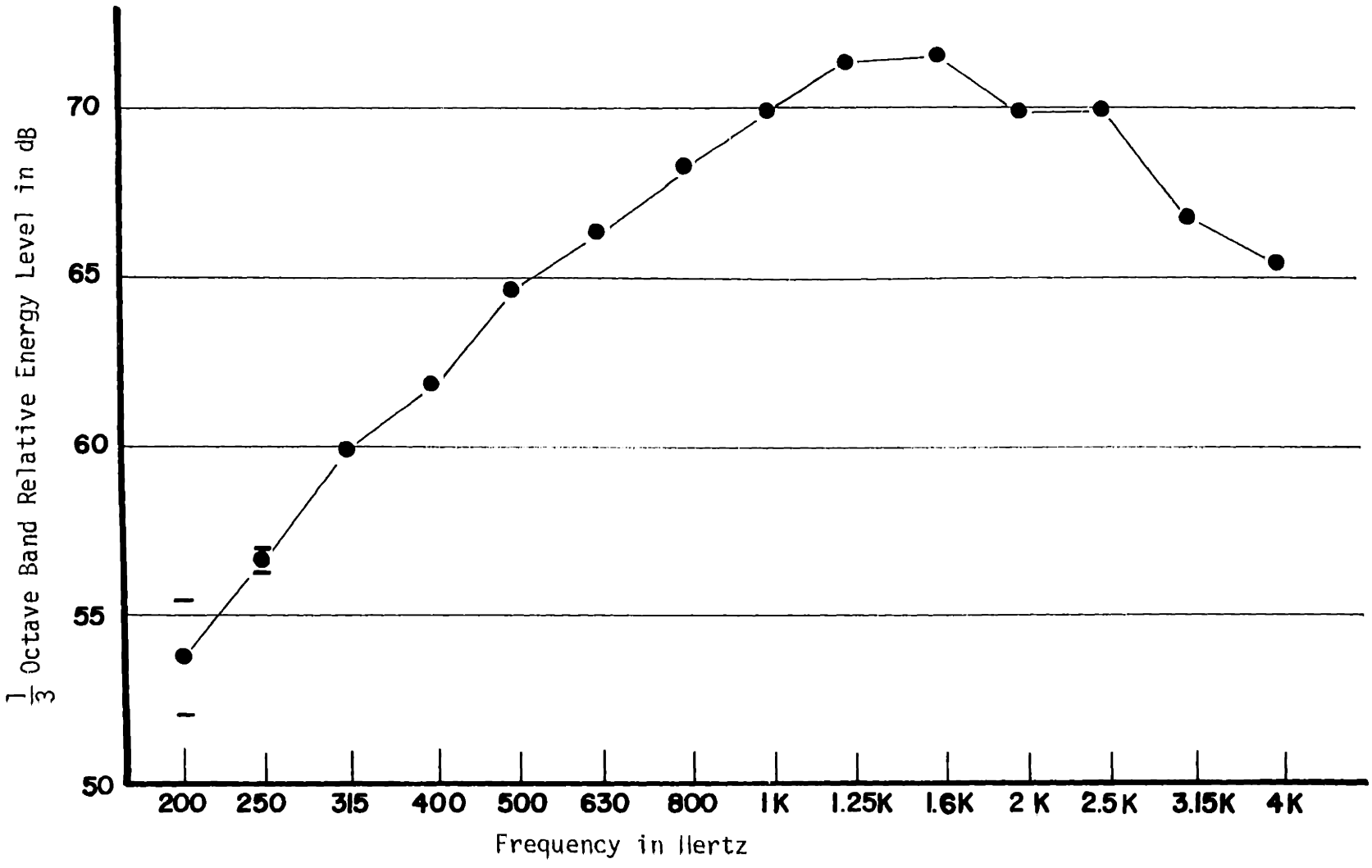

FIGURE 3.5: Energy Spectrum of Starter's Pistol Noise Source at 12 Feet

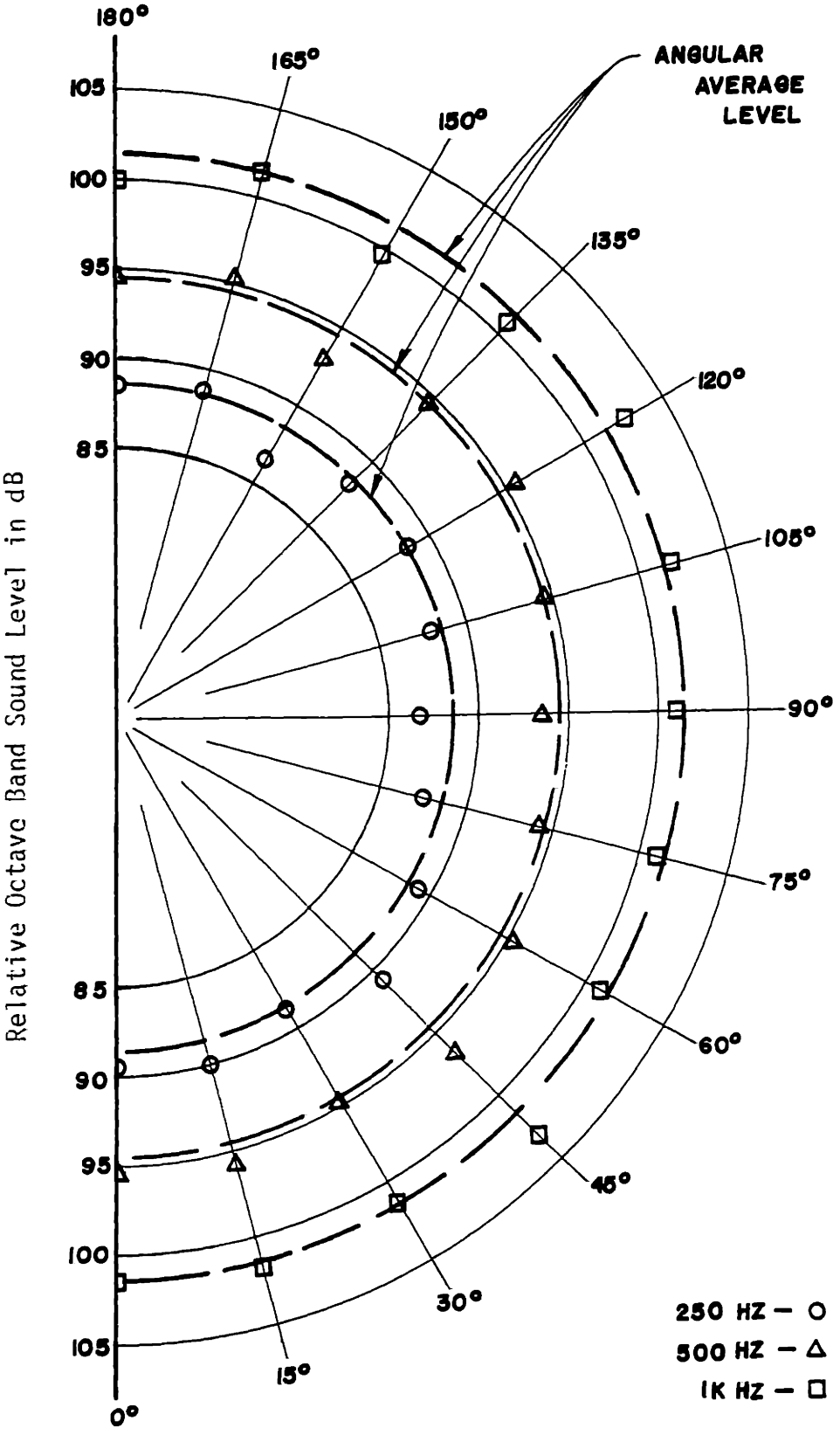

FIGURE 3.6: Starter's Pistol Directivity

be noted from this figure that the noise source is basically omni-directional with the greatest deviations from the idealized source occurring in the 250 Hz octave band. In this band, deviations from the angularly averaged level is a maximum of 2 dB. As an indicator of experimental variation, standard deviations for each measured point are .5 to 3 dB. Three shots were averaged to obtain each point.

The experiment consisted of recording the pressure signal time histories of the pistol shots for a number of different source and receiver locations. These locations are specified in Figure 3.3. The data was recorded with a 1" B&K condensor microphone which fed into a three-track Nagra tape recorder. The data was then analyzed later in the laboratory. For the measurements, the microphone was placed at a height of six feet and oriented with its axis parallel to the street centerline. The source was hand-held, firer in a kneeling position with arm extended upward giving a source height of about five feet. For each source and receiver geometry, five pistol shots were recorded. The data was taken on a Sunday morning in order that background noise and traffic be minimal. As a very necessary precaution, a policeman was hired to be at the site during the experiment.

The data analysis instrumentation chain is presented in Figure 3.7. The pressure signal was played back through the same tape recorder, filtered into octave bands, amplified, recorded digitally and transferred to a mini-computer. The settings of the various instruments are also indicated in Figure 3.7. The data was filtered into octave bands

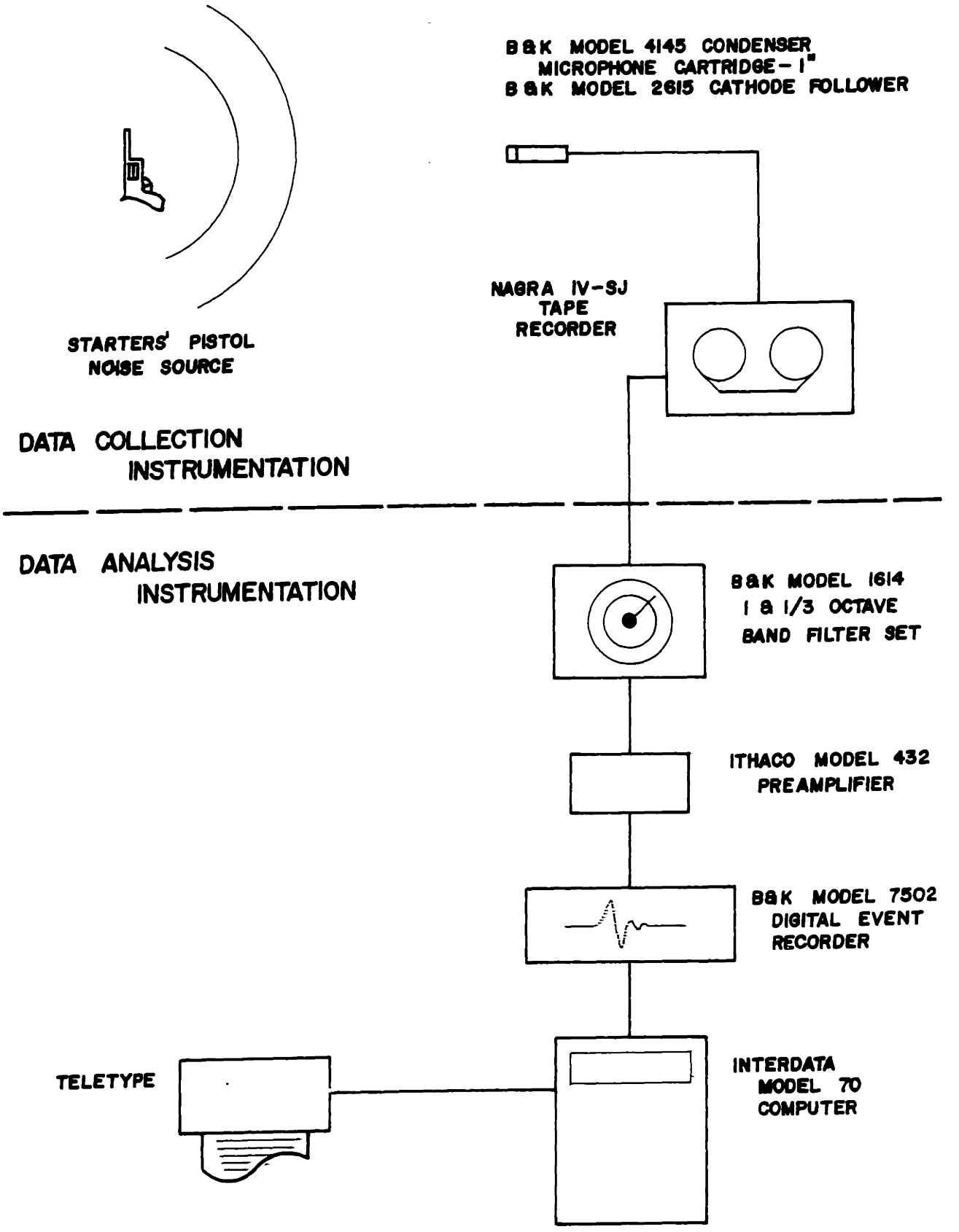

FIGURE 3.7: Field Experiment Instrumentation System

centered at 250, 500 and 1000 Hz. The data, once in the computer, was processed in the digital equivalent of the analog processing used by Masiak [21] and DeJong [22] to obtain the energy of a spark transient signal. This digital processing consisted of squaring the signal, taking the sum of the value at each sample point, and taking the logarithm of that sum. The level obtained corresponds to the energy of the pressure signal as observed at the receiver position. The level is correlated to the steady state sound level which would be measured at the receiver point for an equivalent steady state source [23]. As only relative attenuation values were of concern, no attempt was made to determine the absolute sound pressure levels.

The results of the field experiment were reduced to attenuations relative to the level obtained for the closest source-receiver distance with direct line of sight. The attenuations are shown in Figure 3.8 and Table 3.1. Presented are the values for the 250, 500 and 1000 Hz octave bands as well as the average of the level in these three bands. These results will be discussed and compared in later sections.

3.2.2 Acoustical Model Experiments

In order to establish a data base for comparison to theoretical results and to the above field data, a set of acoustical model experiments was performed. These experiments were designed explicitly to simulate propagation in urban street channels. The choice of model experiments was made due to relative ease in which data can be taken and parameters varied. Of particular interest was the effects produced on sound

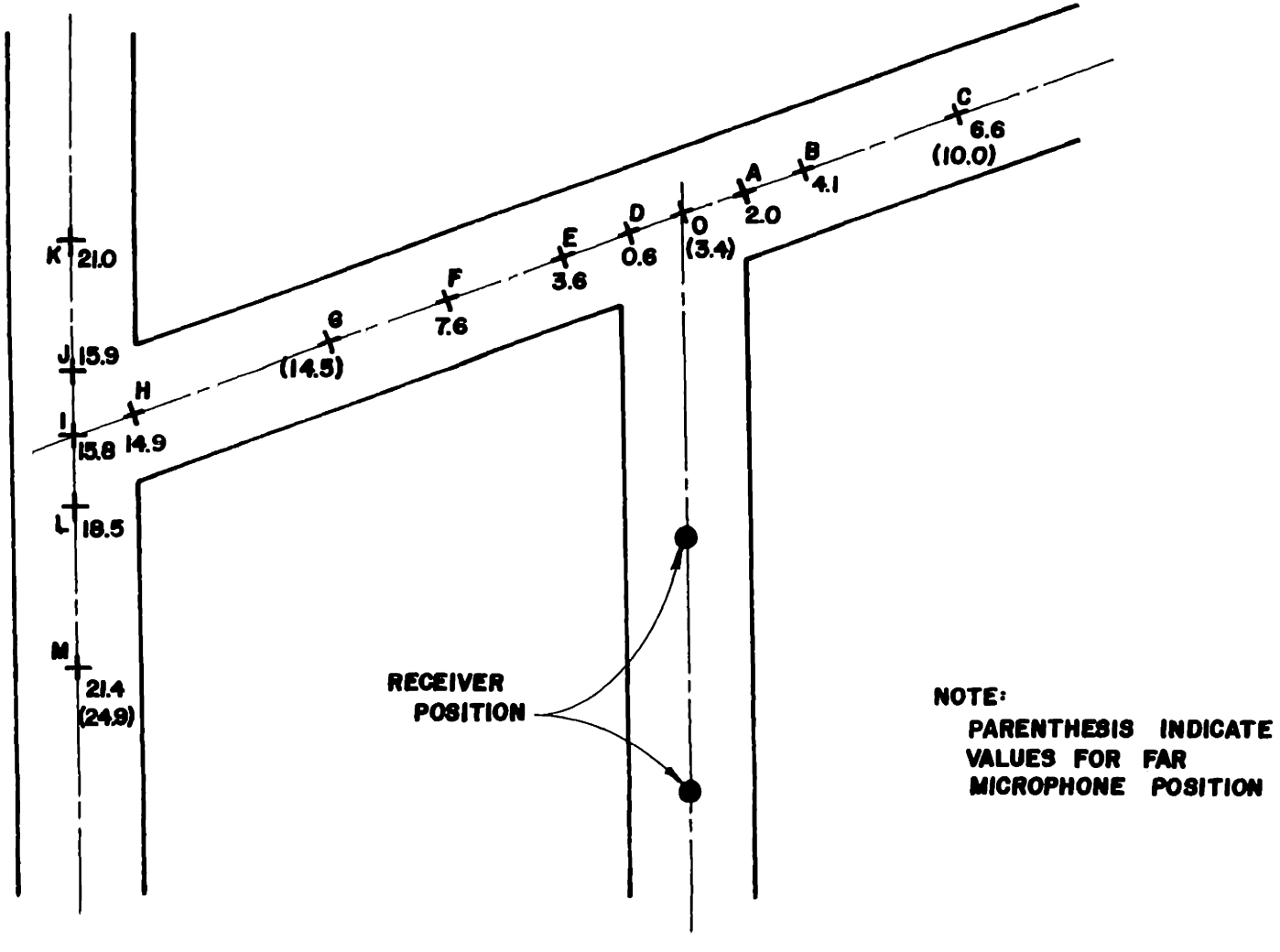

FIGURE 3.8: Field Measurements: Relative Attenuations in Decibels (Averaged in Frequency)

TABLE 3.1 FIELD MEASUREMENTS: RELATIVE ATTENUATION IN DECIBELS

Source Position	Receiver Position	Octave Band Center Frequency 250 Hz	500 Hz	1000 Hz
O	Near	0	0	0
A	Near	.8	1.9	3.1
B	Near	3.1	4.0	5.0
C	Near	7.6	5.9	6.2
D	Near	.9	.3	.7
E	Near	4.4	3.5	2.7
F	Near	8.5	7.2	7.0
H	Near	15.5	14.6	14.4
I	Near	15.9	15.9	15.7
J	Near	16.7	15.6	15.2
K	Near	21.1	21.3	20.4
L	Near	19.0	18.2	18.2
M	Near	20.7	22.1	21.3
O	Far	3.5	3.3	3.5
C	Far	11.0	9.4	9.4
G	Far	15.6	14.1	13.6
M	Far	21.5	25.3	26.6

propagation by variation of simulated building facade structures. The configurations tested are shown in Figure 3.9. Tee intersection measurements were made for smooth-walled buildings as well as for buildings with periodic, rectangular surface protrusions in three different geometries. For one of the protrusion geometries, data was also obtained for a four-way intersection, a four-way interesection with a cross street between the source street and receiver and for the second cross street. The model scale used was 1:32.

The noise source used in the model experiments was specially designed to be used in studies in which the source is very near the ground. The source consists of an air jet impinging a surface of multiple cavities of various diameter. The source is contained in a canister approximately 1" in diameter and 2" in length. The source is pictured in Figure 3.10. It was designed to have a relatively flat spectrum with sufficient power to be useful up to the modeling frequency bands of 31.5 and 63 kHz corresponding to those important in urban noise propagation. High source level is necessary to overcome air absorption effects and microphone limitations at these high frequencies. The narrow band sound level spectrum of the source at 2 ft is presented in Figure 3.11. The corresponding octave band levels are given along with source directivity in the plane perpendicular to the canister axis in Figure 3.12(a). Source directivity in the plane through the axis is given in Figure 3.12(b). The air pressure supplied to the source was at 90 psig. As flow is choked in the jet nozzle [24], the volume flow rate of the source is 0.8 ft^3/min for air at 90 psig and 72°F.

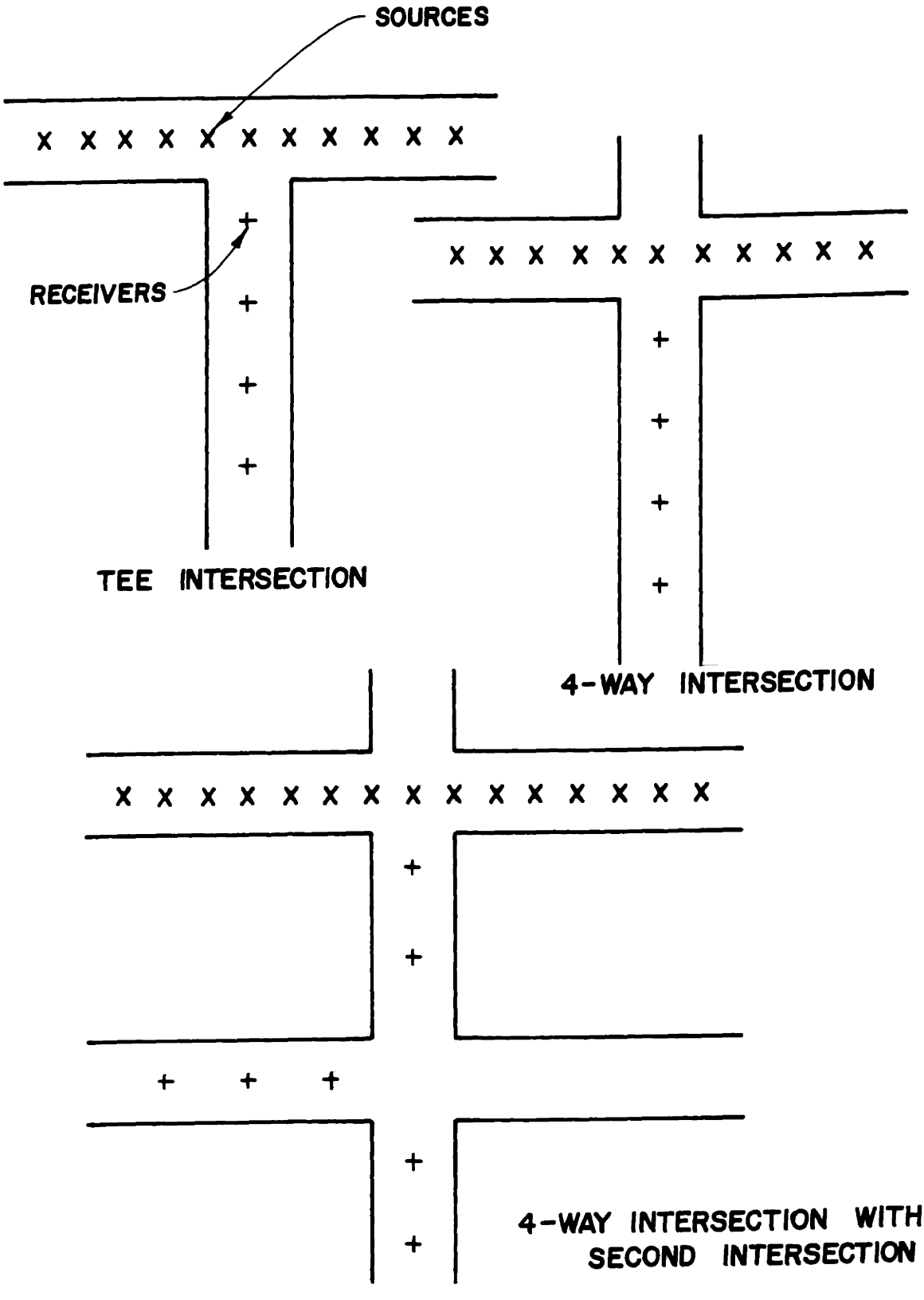

FIGURE 3.9: Configurations of Acoustical Model Experiments

FIGURE 3.10: Air Jet Noise Source

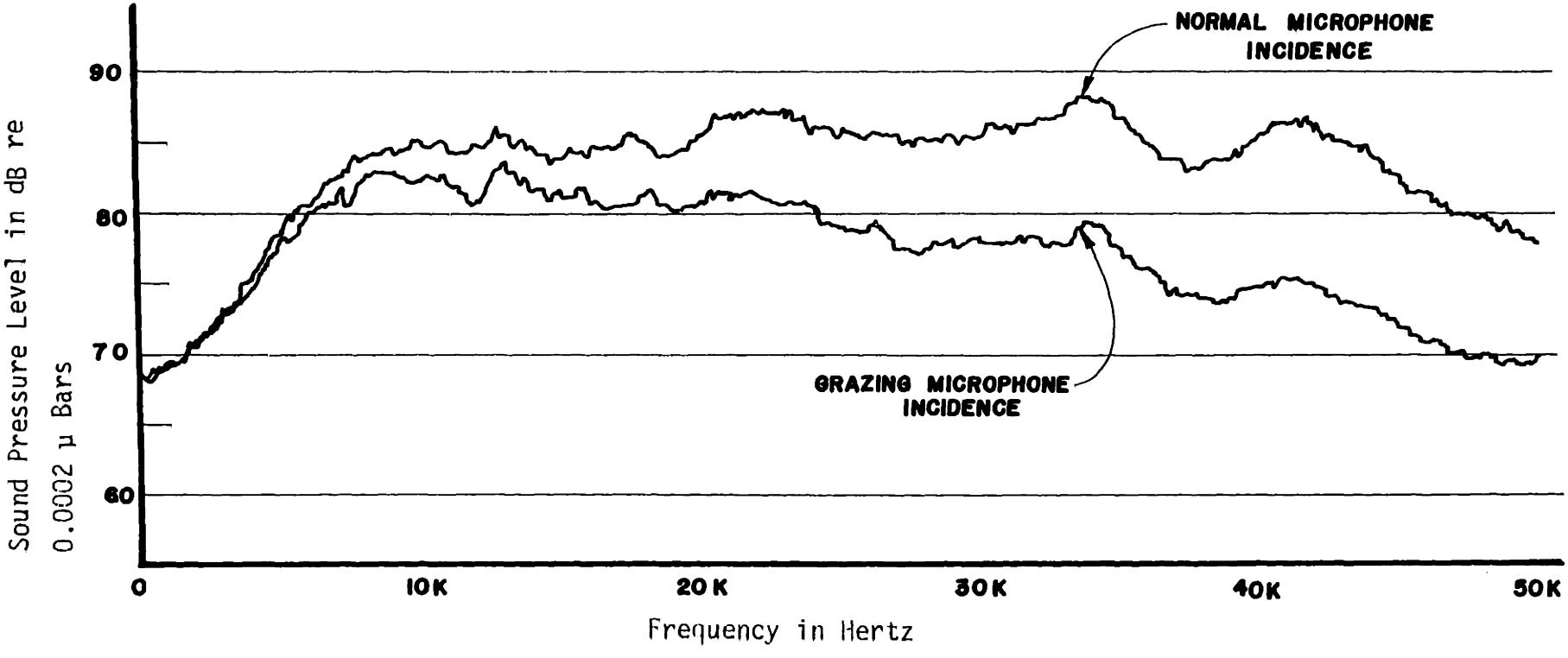

FIGURE 3.11: Air Jet Source, Narrow-band Spectrum

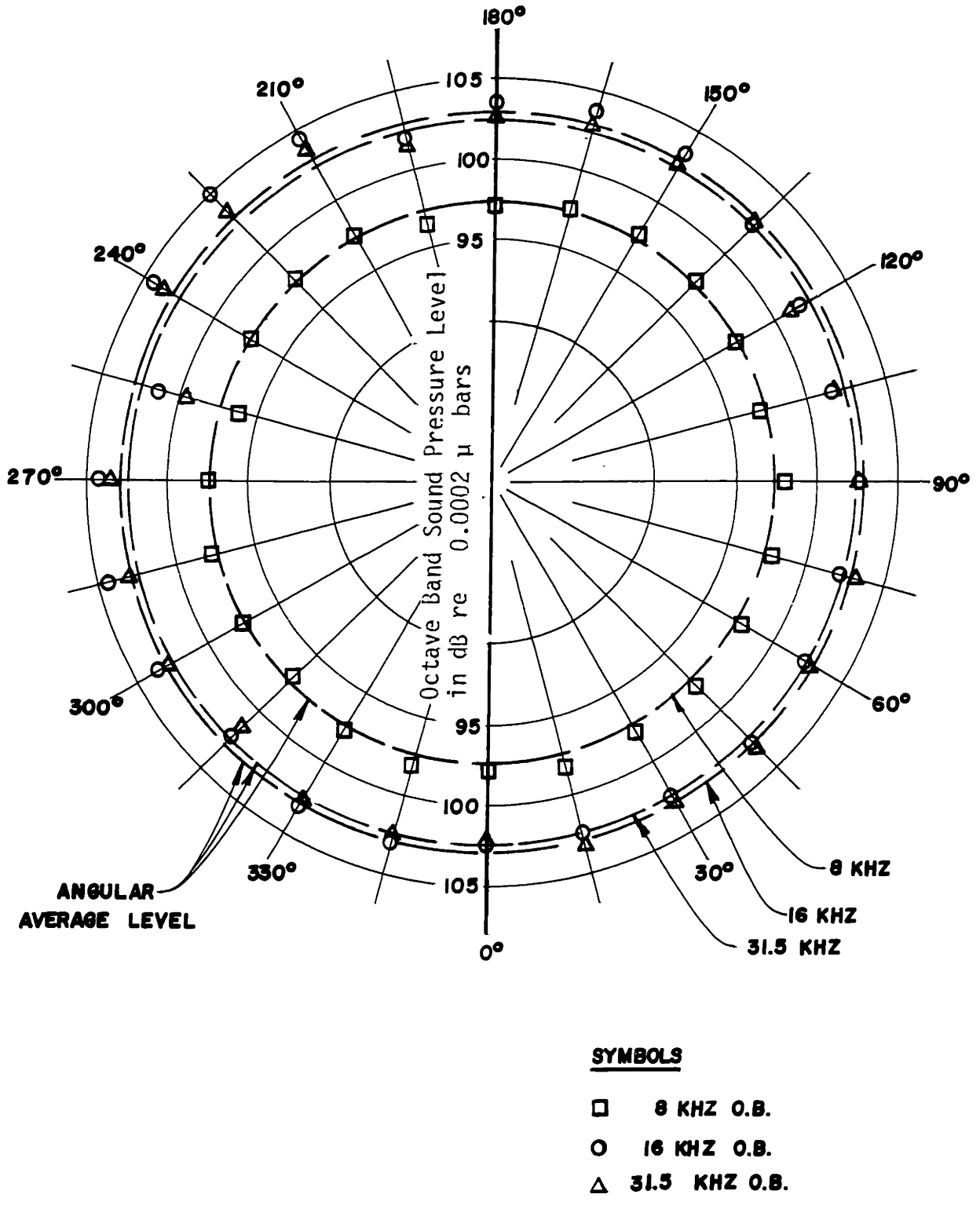

FIGURE 3.12: Air Jet Source Directivity - Perpendicular to Source Axis

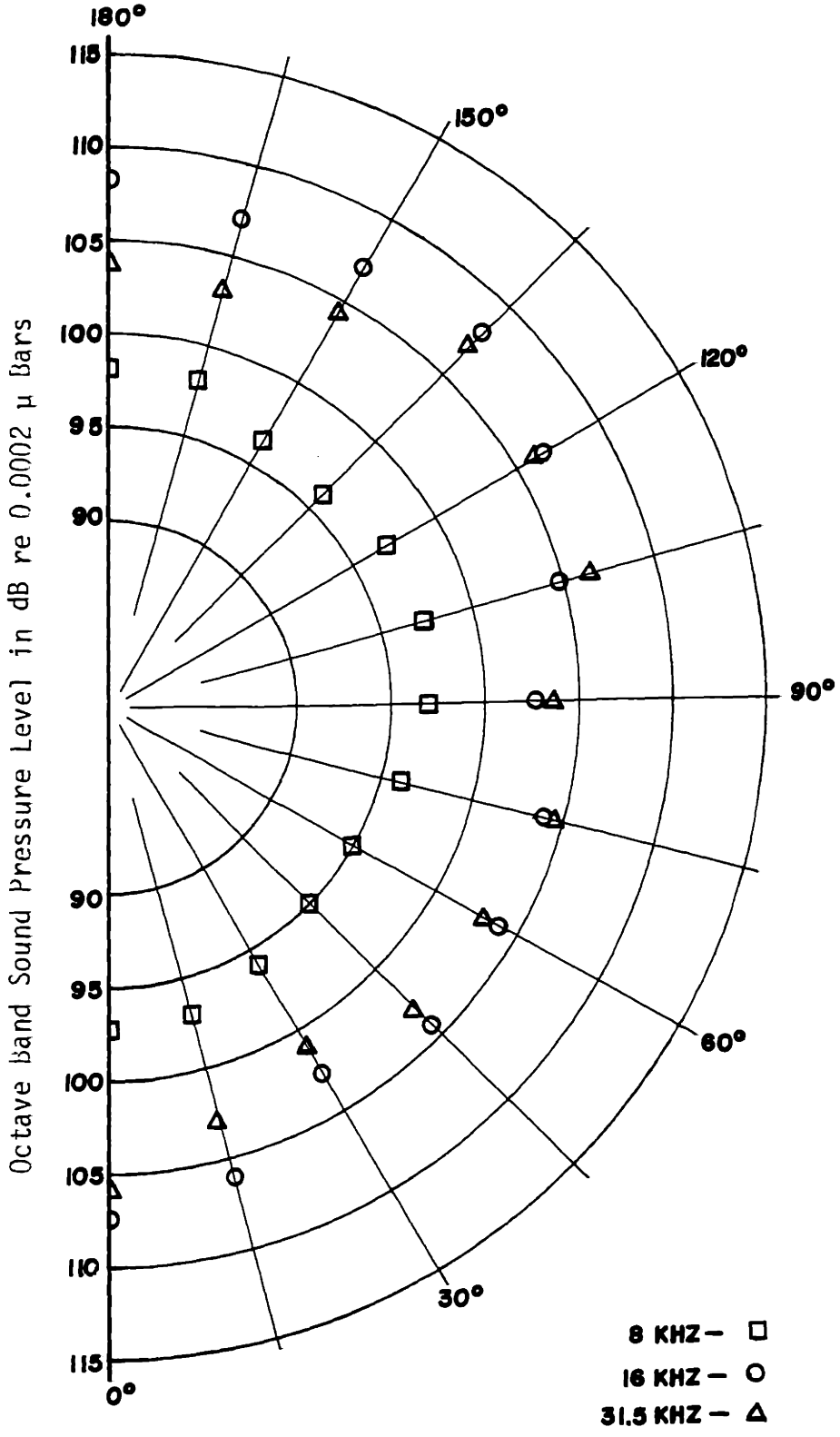

FIGURE 3.12b: Air Jet Source Directivity - Parallel to Source Axis

The instrumentation chain used in these steady state model experiments is presented in Figure 3.13. The transducer used was a 1/4" B&K condensor microphone chosen for its sensitivity of -48.4 dB/volt. This sensitivity is 12.9 dB higher than a 1/8" B&K microphone and 45.1 dB higher than a 1/10" BBN microphone. However, to obtain sensitivity, directivity must be compromised. The measured microphone directivity is given in Figure 3.14. In order to minimize effects of directivity on the experiment, the microphone was oriented with its axis perpendicular to the plane of propagation. The effect that this orientation has on the source spectrum is shown in Figure 3.11(b). It will be noted from this figure that there is a superimposed high frequency roll-off, but that the source-microphone combination still produces a broad band spectrum. Motion of the source was provided with a small cart running on an I-beam suspended over the source and street. The cart was pulled by an electric motor and long bicycle chain. The motion of the cart was used to trigger instantaneous sound level sampling at 3" intervals along the beam. Triggering was accomplished with a contact switch on the cart. The cart, beam, source and switch are pictured in Figure 3.15.

The geometry of the street configurations tested in the experiment is presented in Figure 3.16. Also indicated in this figure are the source and receiver locations. The geometries of the vertical protrusions used to simulate facade structures are detailed in Figure 3.17. The experiments consisted of moving the source along the source street and monitoring the sound level at the different receiver points.

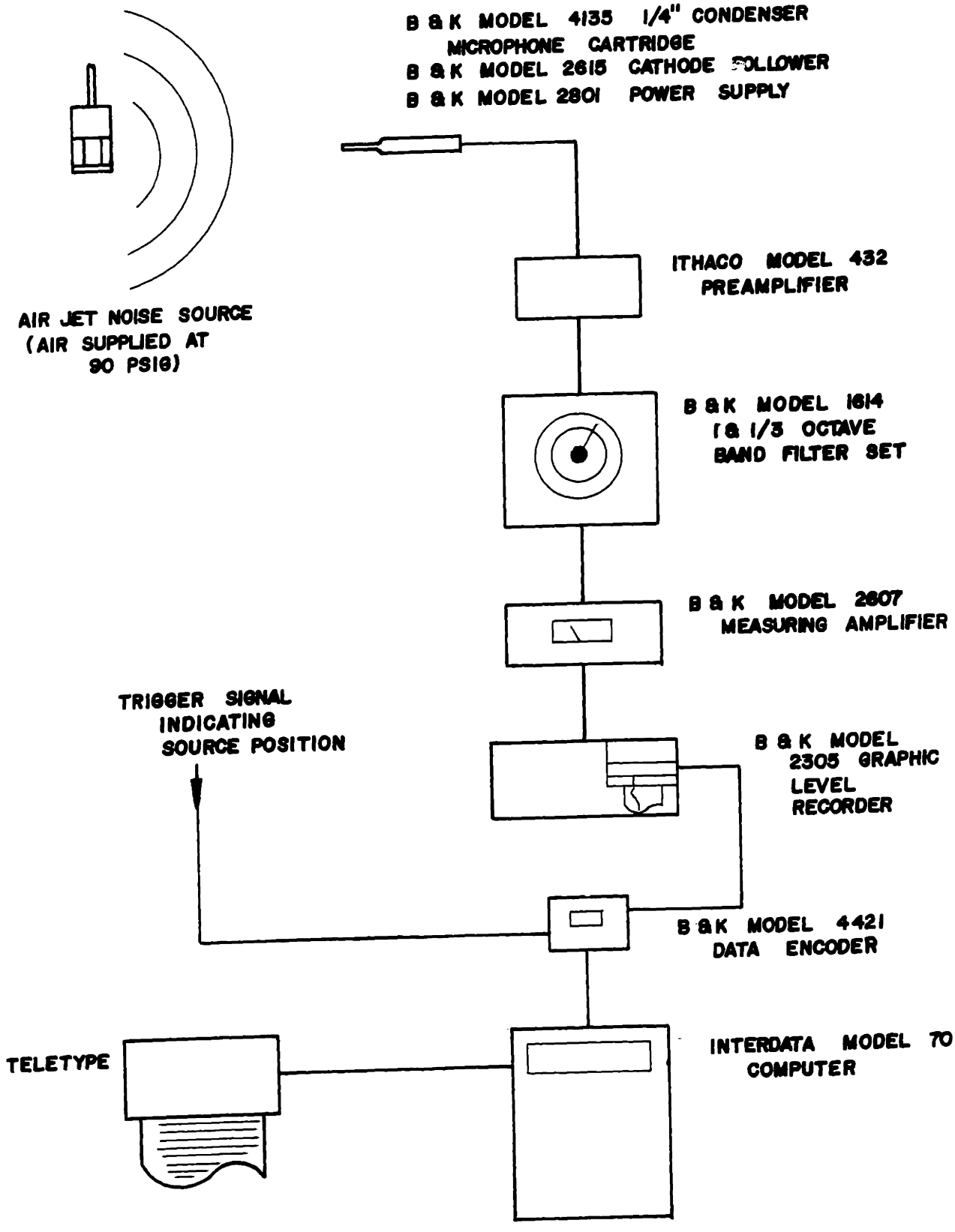

FIGURE 3.13: Acoustical Model Experiment Instrumentation System - Steady State

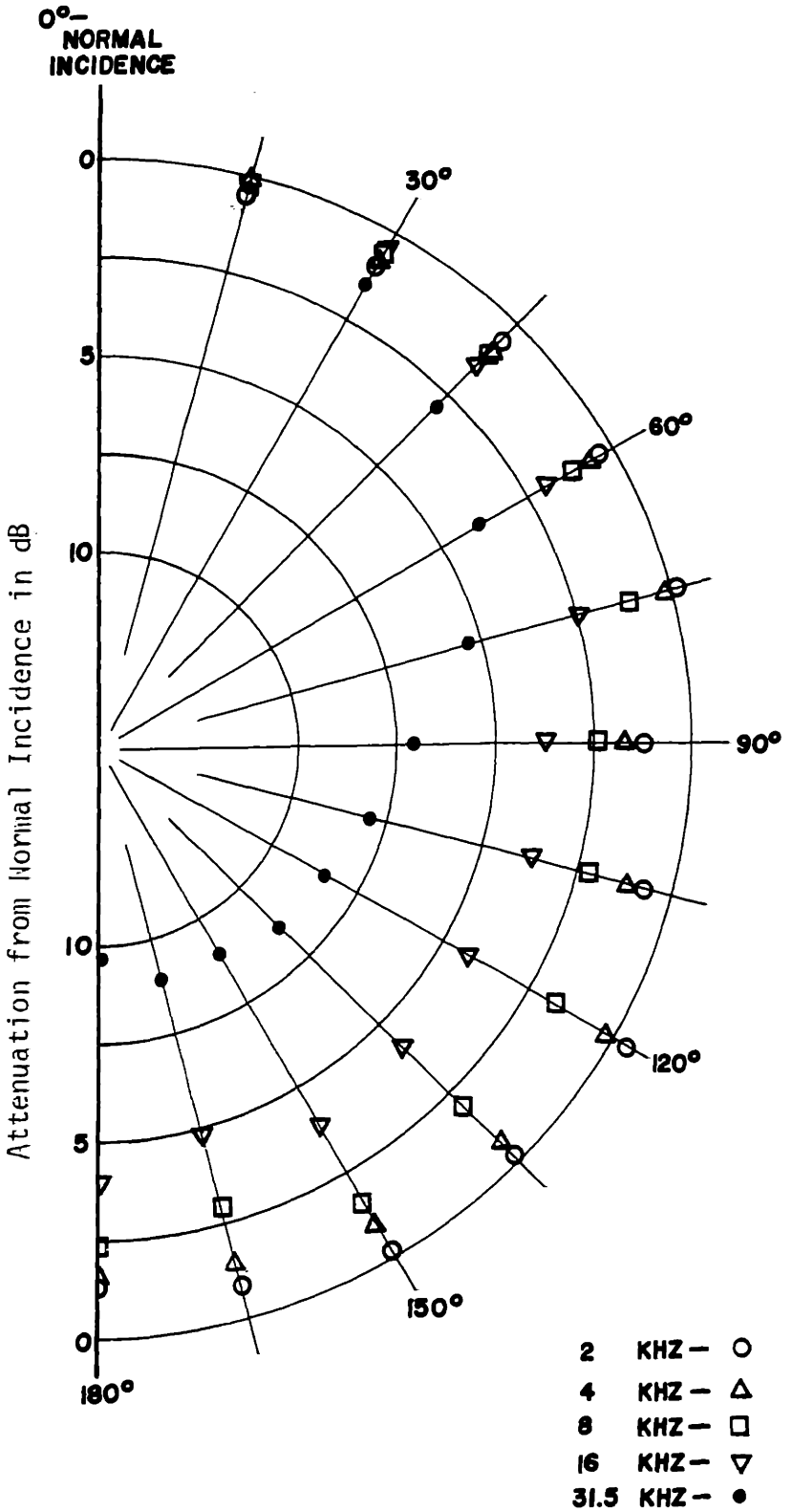

FIGURE 3.14: $\frac{1}{4}$" B and K Microphone Axial Directivity

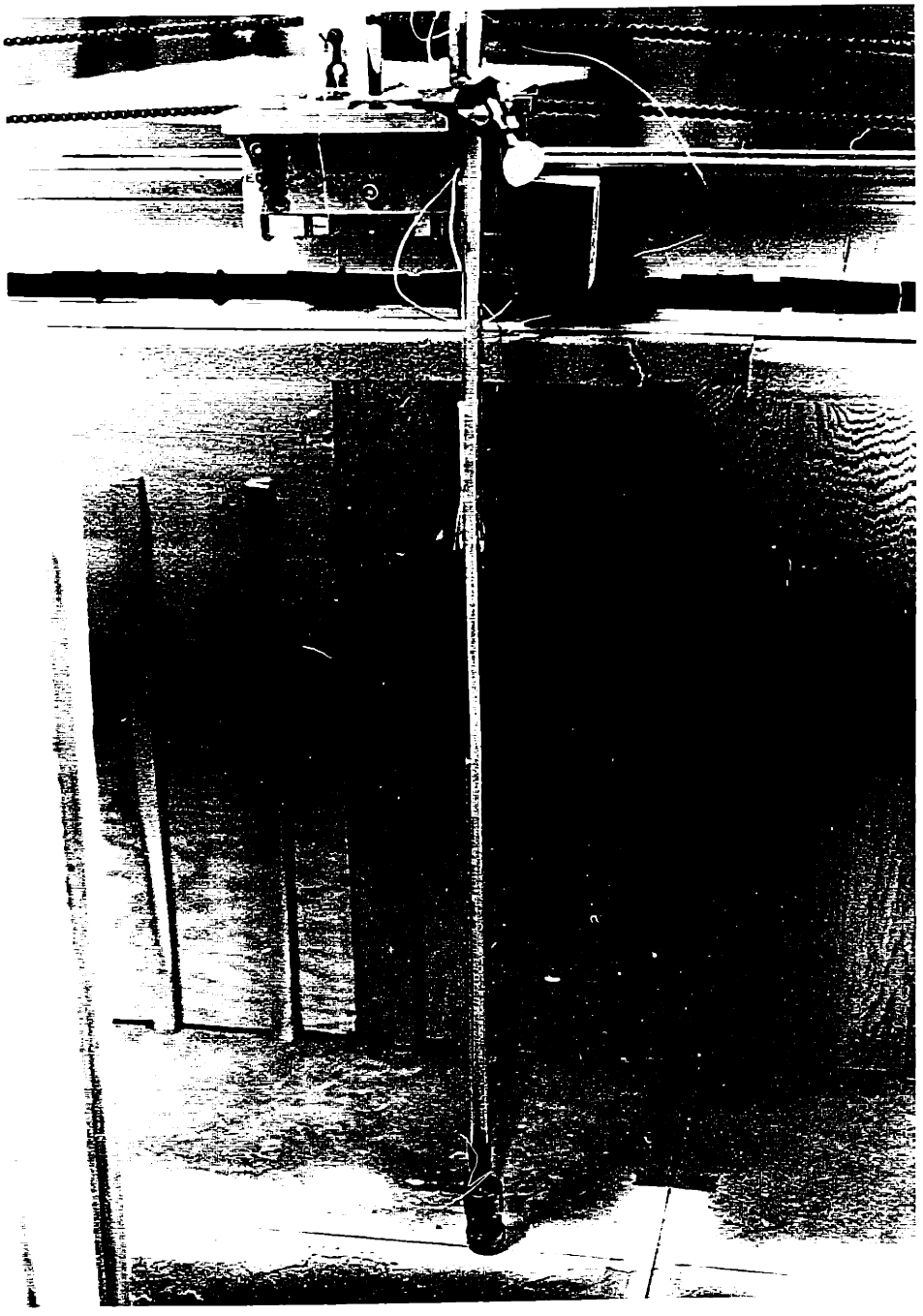

FIGURE 3.15: Air Jet Noise Source and Source Positioning System

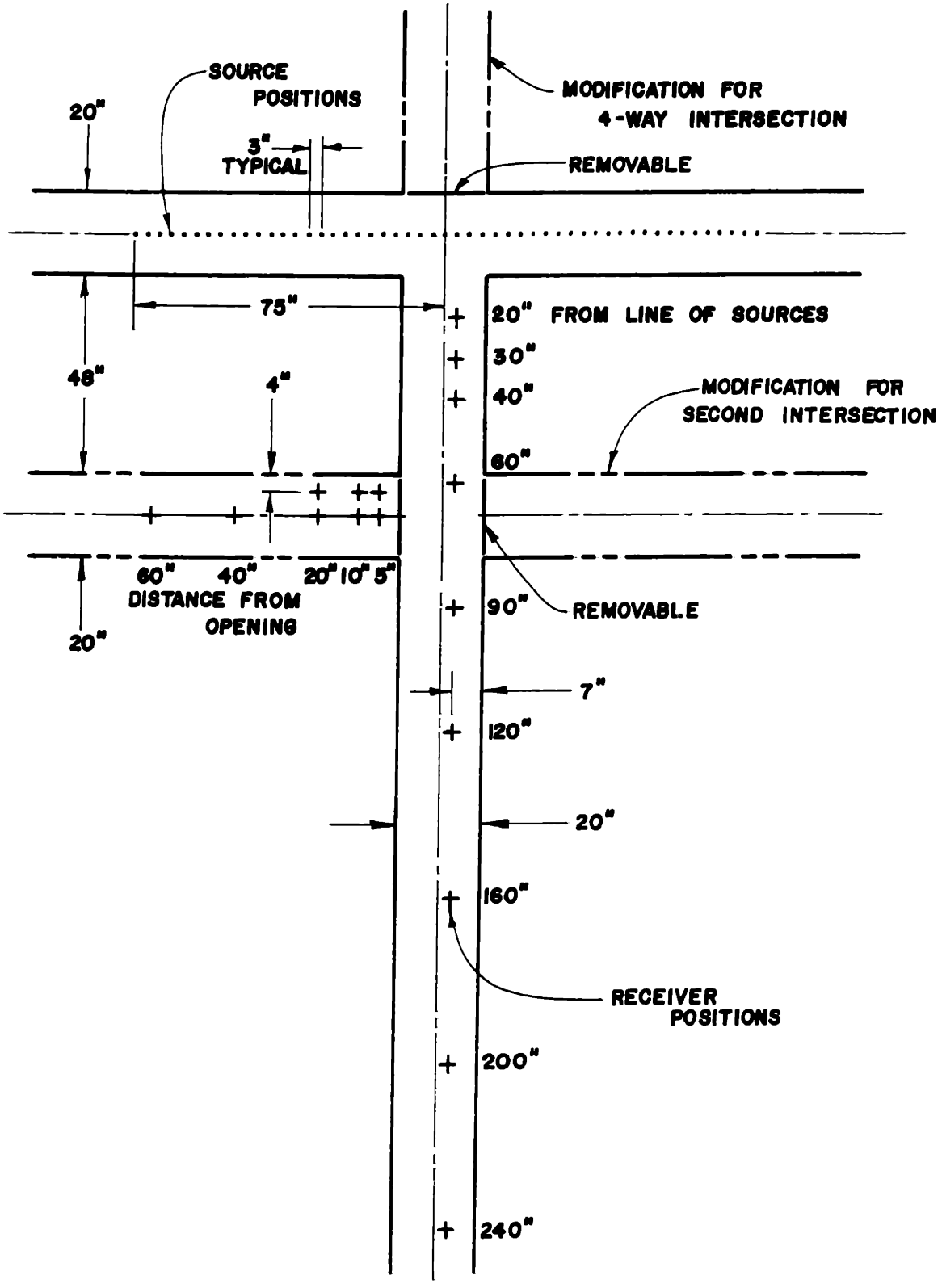

FIGURE 3.16: Street Plan for Acoustical Model Experiments

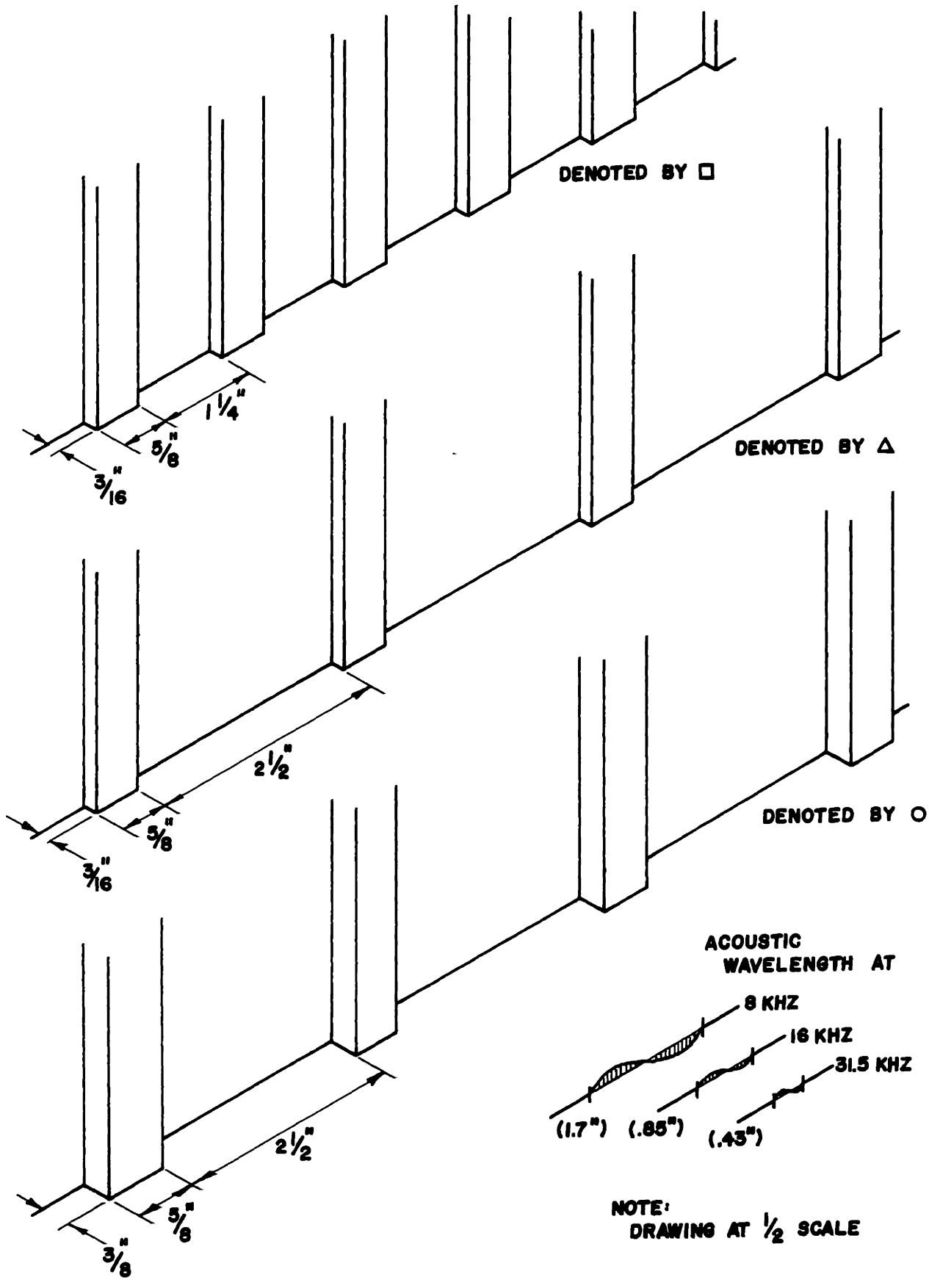

FIGURE 3.17: Simulated Facade Structures for Acoustical Model Experiments

Instantaneous sound level was recorded in the computer for each of 51 sample points spaced 3" apart. Thus a digitized time history of sound level was produced at each receiver point for the 8, 16 and 31.5 kHz. octave bands. In order to minimize ground reflection effects, source and microphone positions were as near to the floor as practical. The source was propelled along the source street centerline at a height of 1/4" from the concrete floor. The microphone was suspended from the building tops to a height of 1" from the floor, thus producing a vertical orientation of its axis. A photograph showing the source and microphone orientations as well as the street configuration is presented in Figure 3.18. During the experiments, the channel was isolated from the reverberant field of the test room with open cell foam backed with cardboard. This arrangement provided both an anechoic "sky" above the channel and transmission loss for sound from the reverberant field entering the channel. Using this isolation, background levels in the street channel were determined by blocking the entrance to the receiver street with 3" of fiberglass. Background level was found to be almost independent of source and receiver position. Since the distant source and receiver positions were most sensitive to background noise, these extreme positions were used for the measurement. The background level was then corrected for when necessary by the computer.

Some of the data obtained for the smooth wall tee intersection is presented in Figure 3.19. The data shown corresponds to the sound level received at the microphone for the three indicated positions as the source passed through the intersection. Also plotted with the data are specular

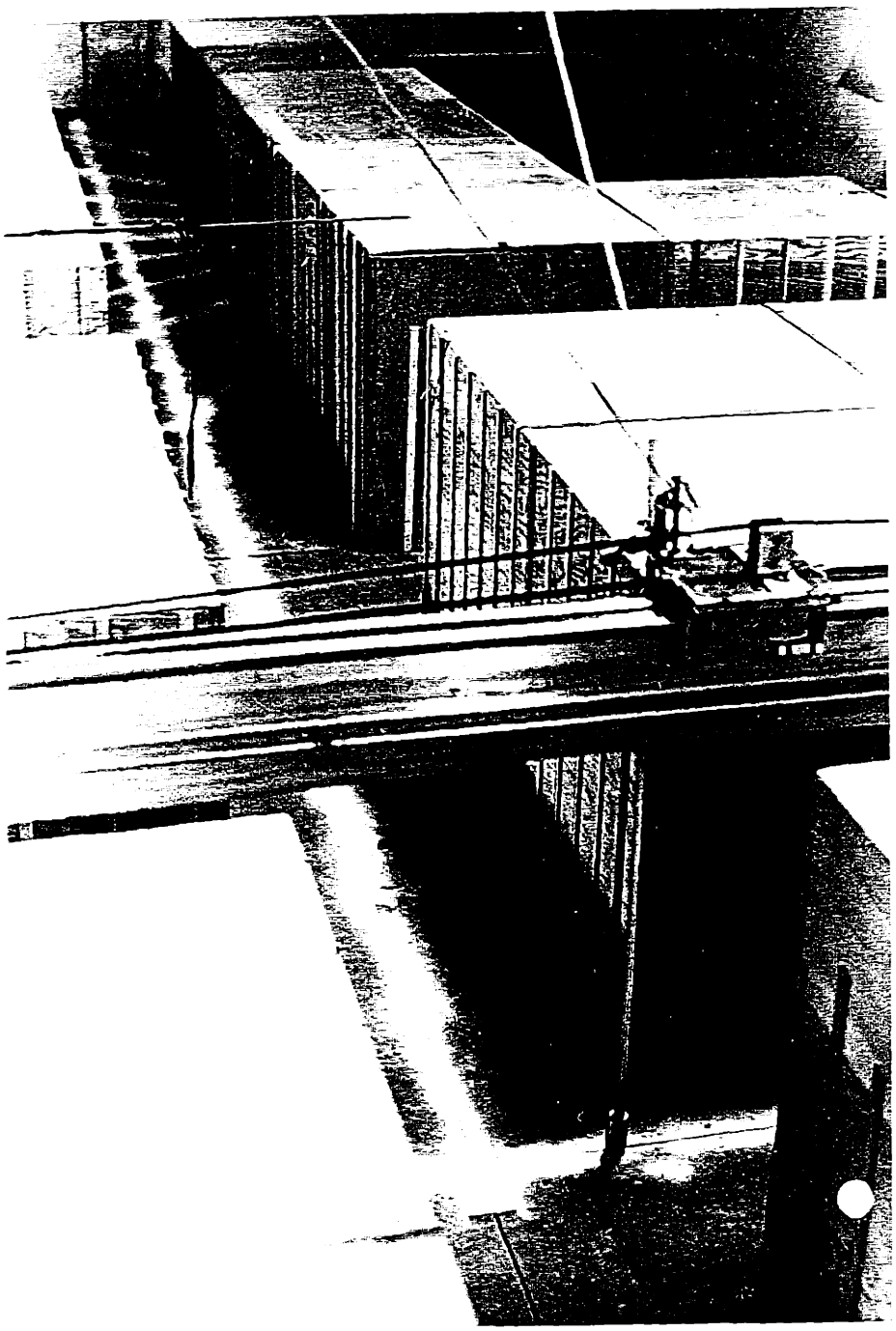

FIGURE 3.18: The Acoustical Model

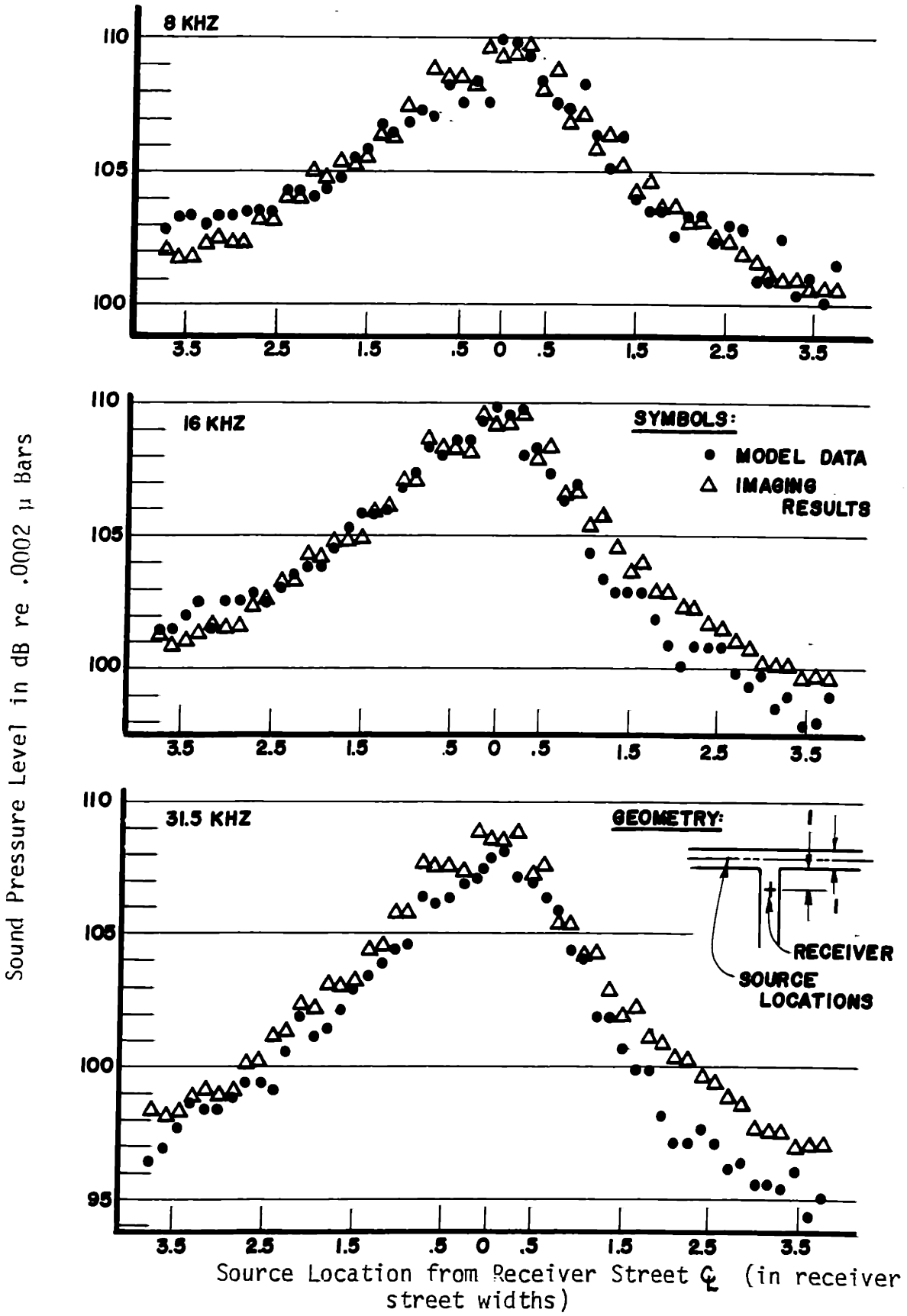

FIGURE 3.19: Smooth Wall Acoustical Model Pass-by Data and Specular Imaging Theory Simulation

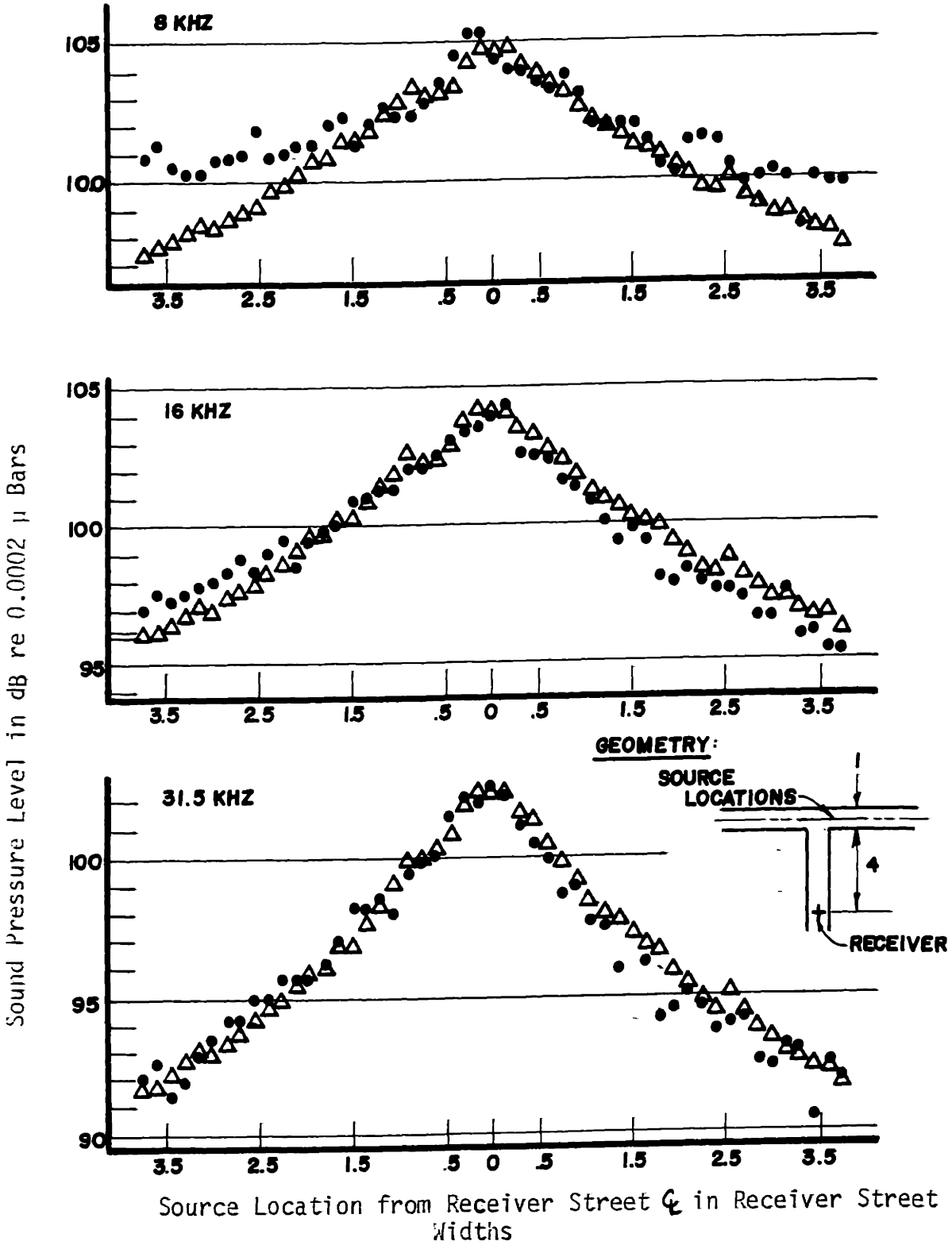

FIGURE 3.19: Smooth-wall Acoustical Model Pass-by Data and Specular Imaging Theory Simulation

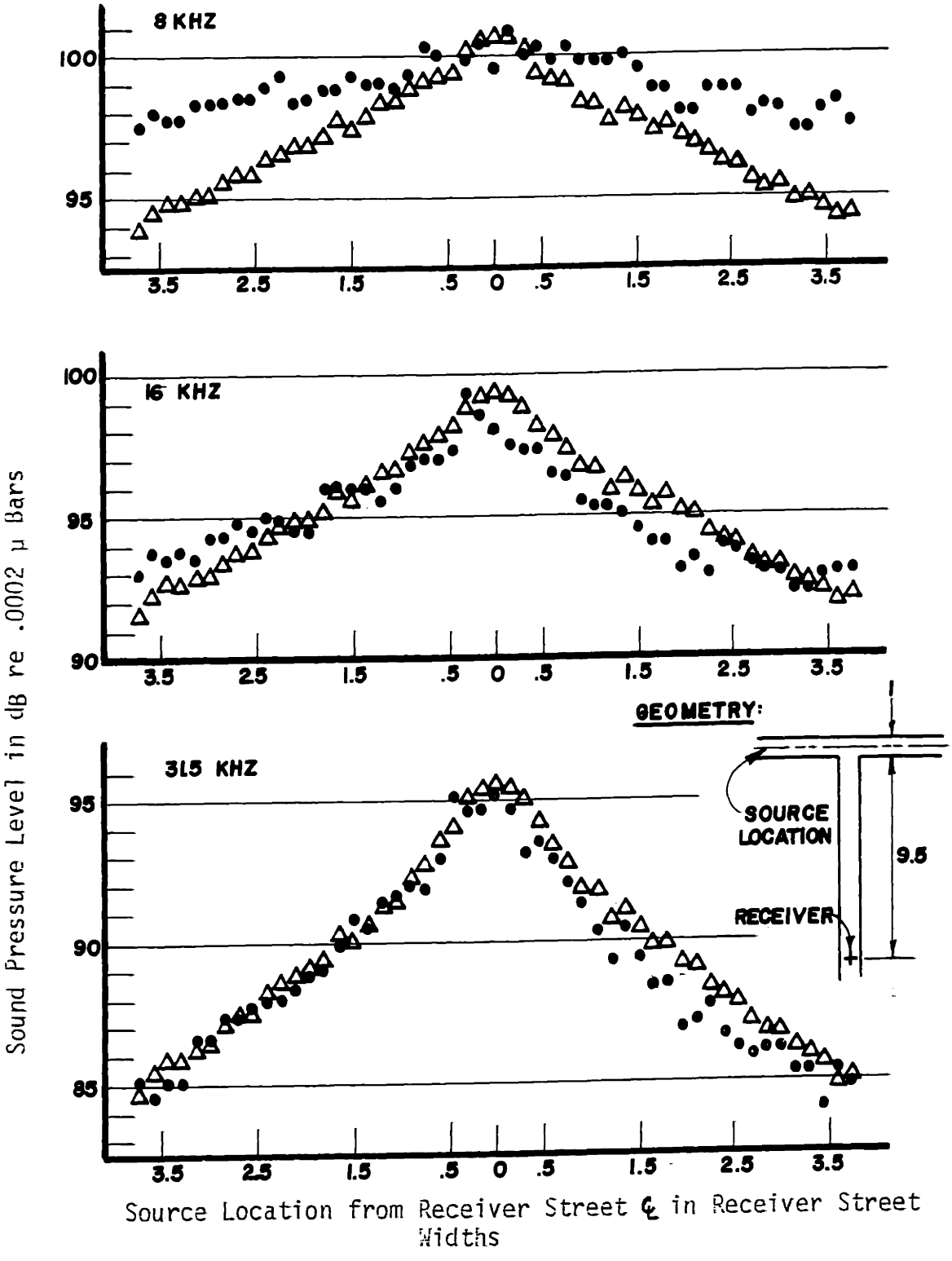

FIGURE 3.19: Smooth Wall Acoustical Model Data and Specular Imaging Theory Simulation

imaging values calculated for each of the source and receiver locations. Because of the high amount of air absorption at the modeling frequencies, the imaging values are corrected for air absorption directly in the computer simulation. The correction factors used were .028 dB/ft, .102 dB/ft and .315 dB/ft for the 8, 16 and 31.5 kHz octave bands, respectively. These factors were obtained from the theoretical work of Evans, Bass and Sutherland [25]. Comparison of the model and imaging results in Figure 3.19 indicate generally good agreement between theory and experiment. While the source is in the intersection, the difference between the results is at most 1 dB for all cases. Correspondence when the source is around the corner from the receiver is not quite so consistent. For all three receiver positions, the model and theoretical results show differences on the order of 1 dB or less for the 31.5 kHz octave band. For the 16 kHz band, the model data tends to be slightly higher than the theoretical results up to a maximum difference of 2 dB. The 8 kHz band data displays a similar tendency with a maximum difference of about 4 dB at the receiver position furthest from the intersection. Due to the frequency dependence of the variation between model and imaging results, the good agreement achieved for the source in the intersection, and the lack of sensitivity of the 8 kHz octave band to air absorption, it is concluded that the differences observed are due primarily to diffraction around the corner. Such a conclusion is also quite consistent with the quite good correspondence seen for the 31.5 kHz band for which contribution from diffraction will be considerably less than 8 kHz, approximately 4 dB less for Fresnel numbers between 0 and 1.0 [20].

The sound levels measured for each source pass-by can be logarithmically summed to give a level which corresponds to having a line source in the source street. For each frequency band, the decay of this line source level can be plotted versus distance using the values at each receiver position. Data presented in this manner for the smooth wall tee intersection is given in Figure 3.20. Also indicated in this figure are similar results obtained with imaging theory. Again there is evidence of diffraction as the model values exceed the imaging values by about 2 dB for positions furthest from the source in the 8 kHz octave band. The values for 16 and 31.5 kHz octave bands, however, correspond extremely well with differences less than 1 dB. It will be noted that near the source, the model data is slightly lower than the imaging values. For the imaging values, ground reflection was accounted for by pressure addition of direct and reflected signals. This adds 6 dB to the level obtained with no ground reflecting surface. Basically, this assumption requires that the path length difference between the direct and ground reflected paths be less than 1/4 wavelength. Near the source, this criterion is not met by the 31.5 kHz band and thus the model shows something less than the additional 6 dB from ground reflection. Ground reflection will be discussed in more detail in a succeeding section.

For comparison to the smooth wall results, some of the tee intersection pass-by data obtained with periodic rectangular protrusions on the model is presented in Figure 3.21. It should be noted that considering the substantial changes in protrusion geometry for the three types considered, there is remarkably little variation in the sound

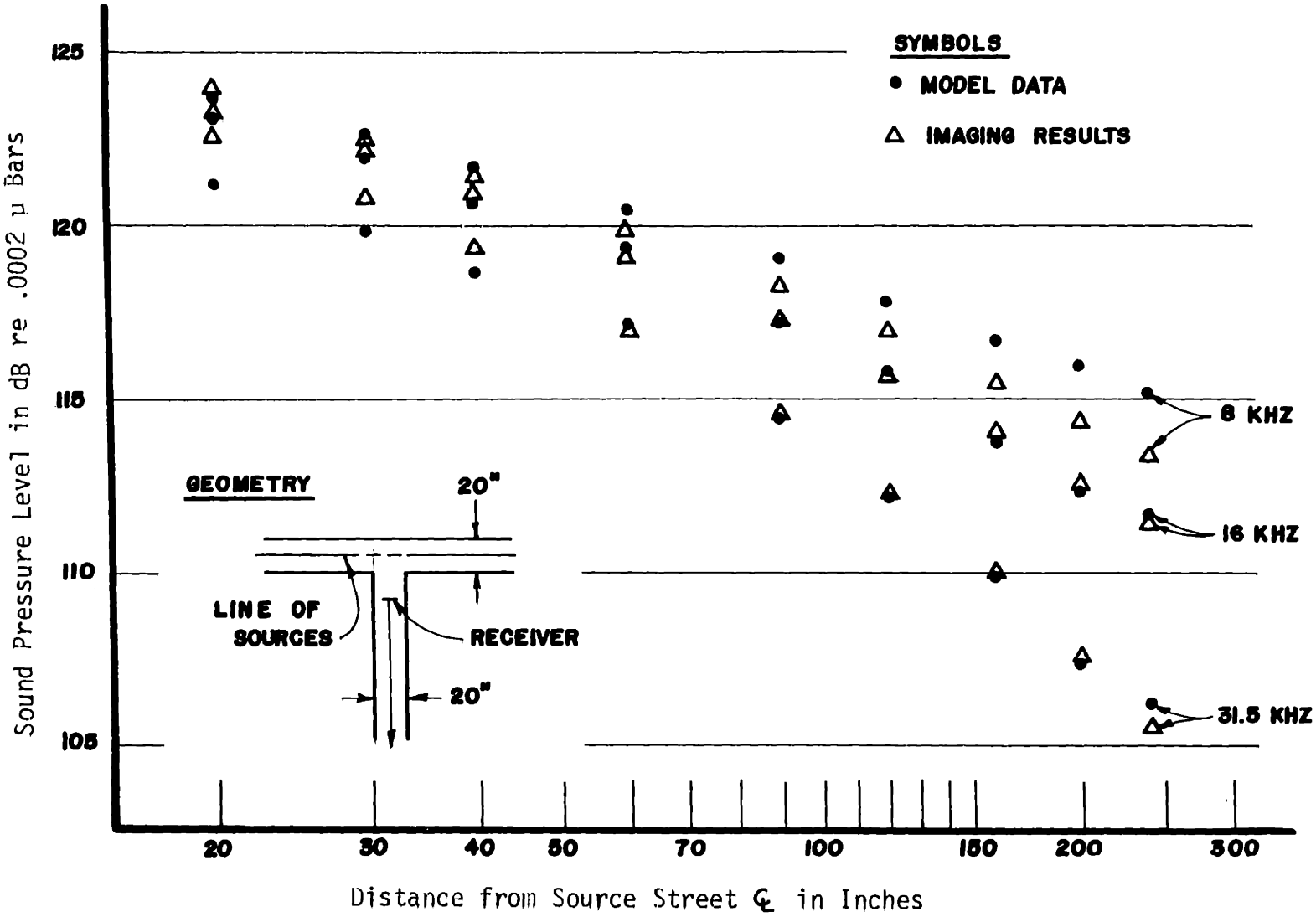

FIGURE 3.20: Smooth-wall Acoustical Model Line Source Levels and Specular Imaging Theory Simulation

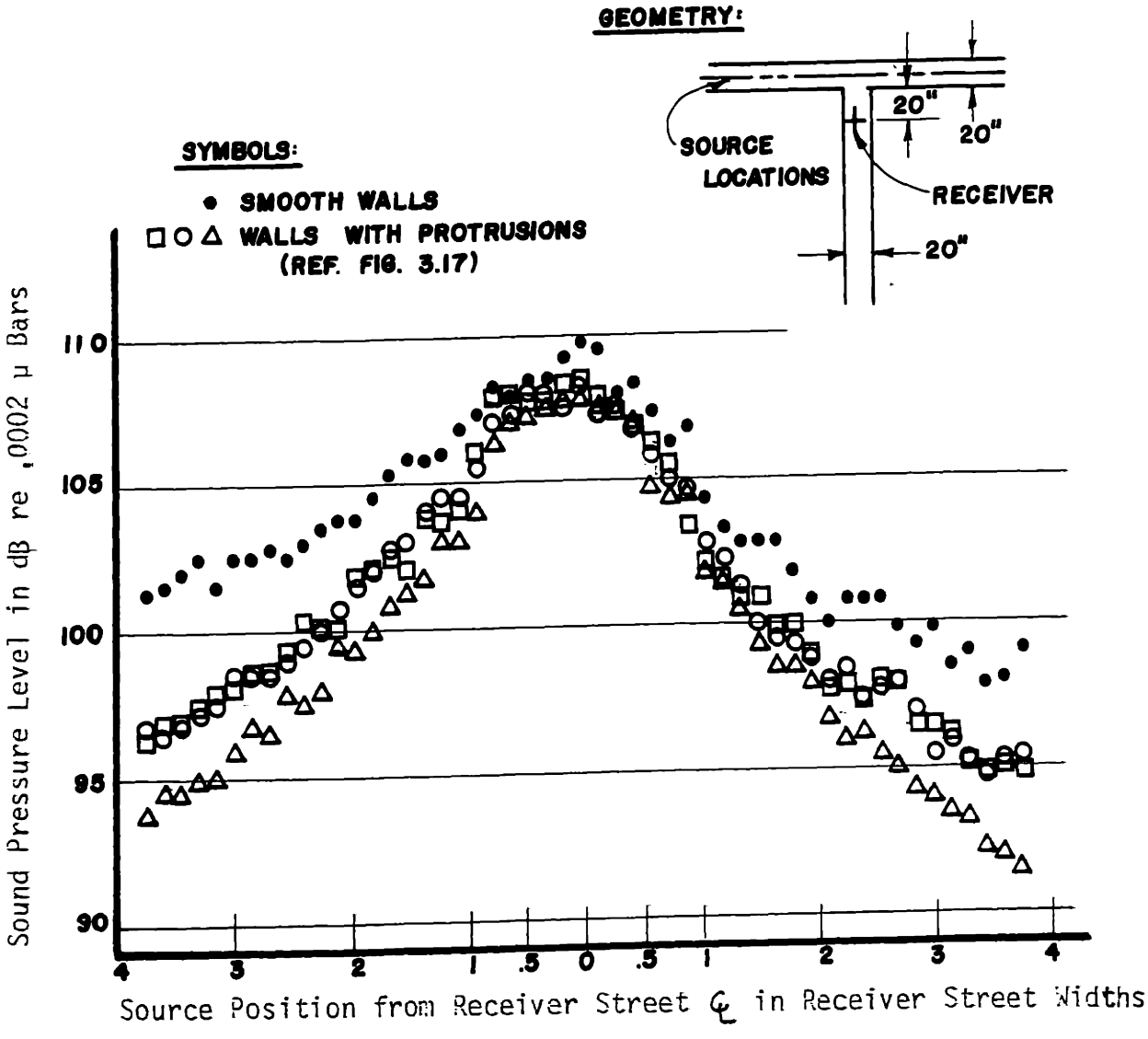

FIGURE 3.21: Acoustical Model Pass-by Data With and Without Wall Protrusions at 16 K Hertz

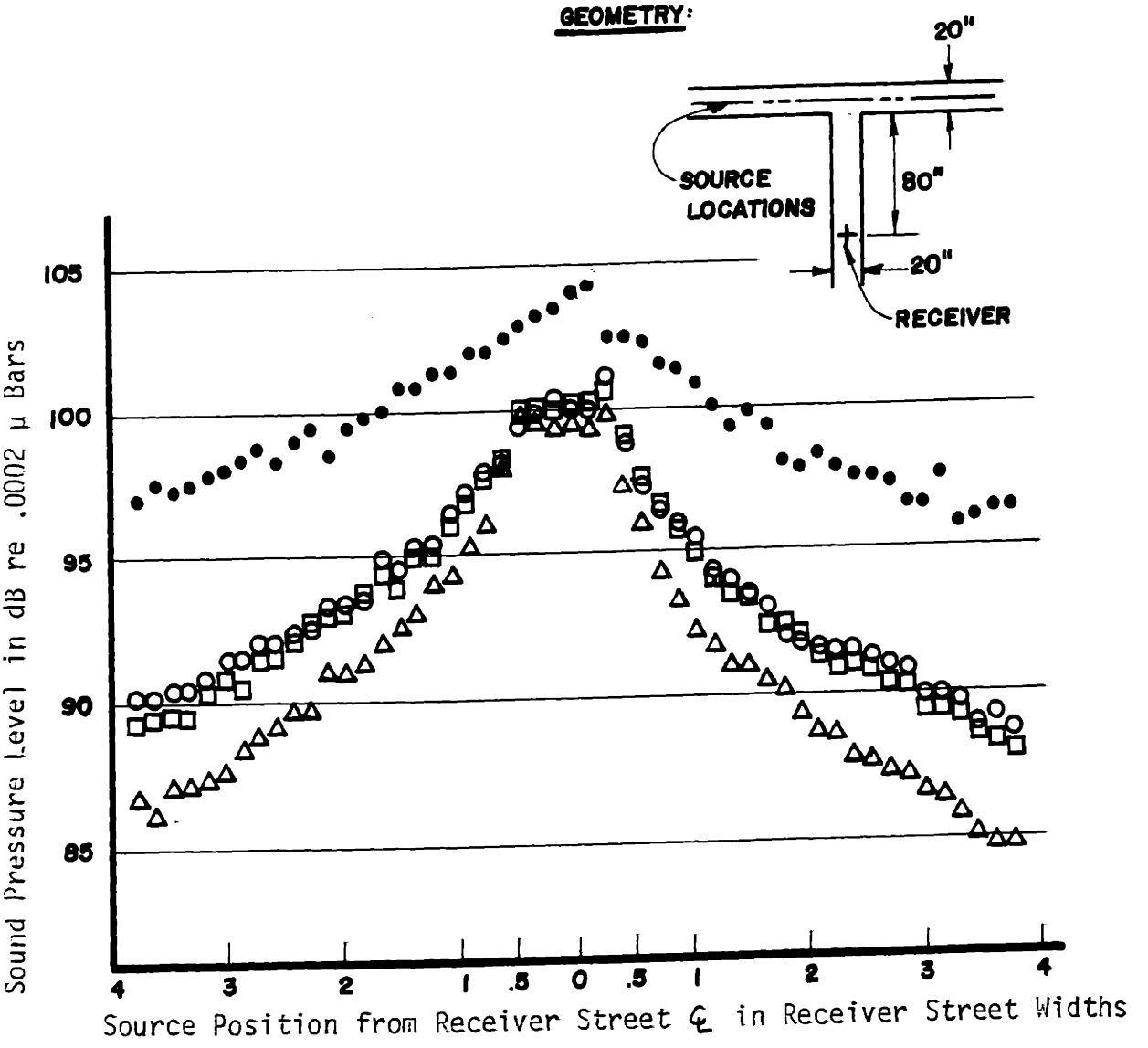

FIGURE 3.21: Acoustical Model Pass-by Data With and Without Protrusions at 16 K Hertz

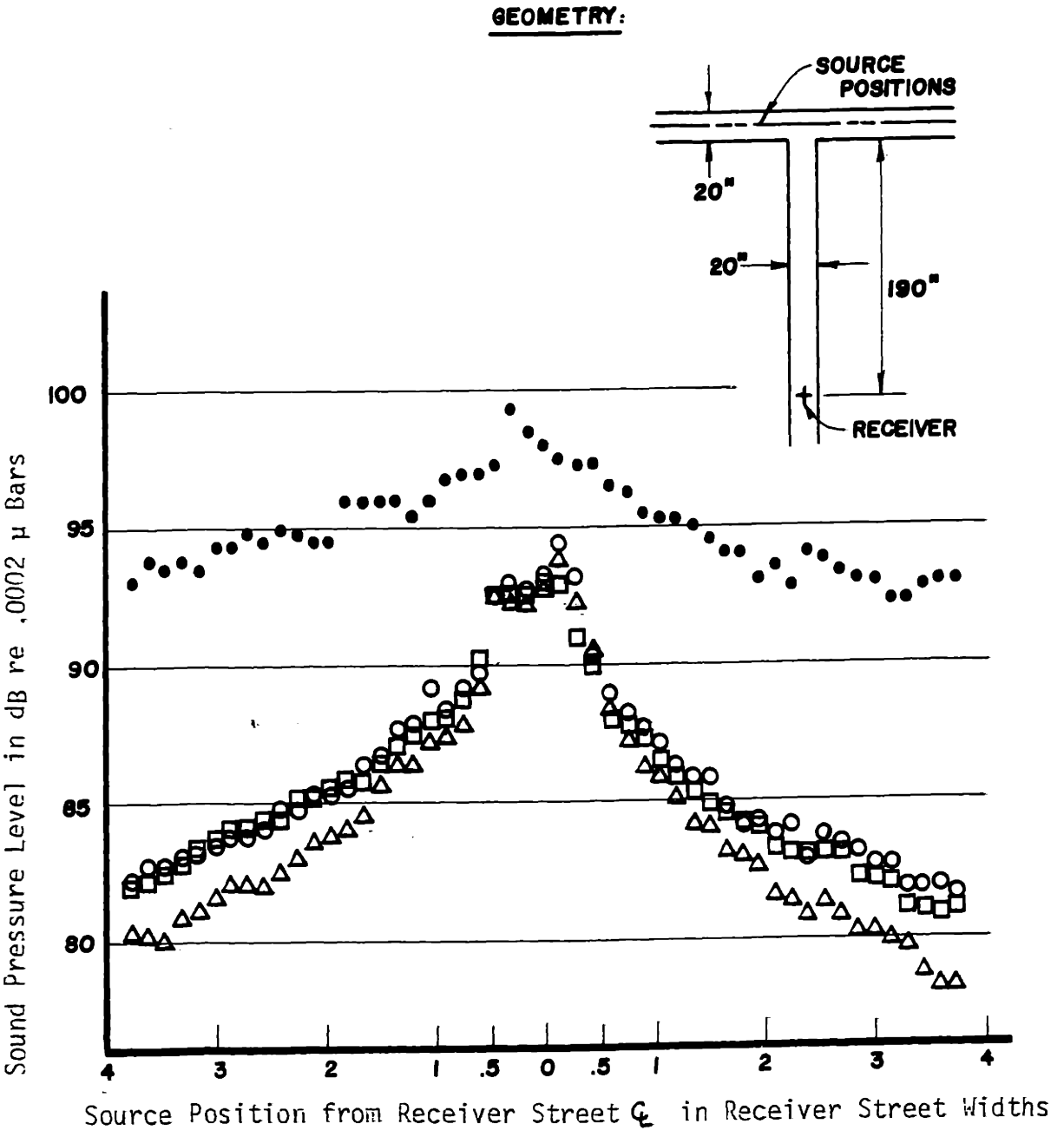

FIGURE 3.21: Acoustical Model Pass-by Data With and Without Protrusions at 16 KHertz

level produced in the street. This result was found to hold for all receiver positions and all three octave bands. Typically the differences observed are a maximum of 2 to 3 dB with much smaller differences when the source is in the intersection. In comparing the smooth wall data to that with the protrusions, substantial differences are observed. Near the source, the smooth wall values are slightly higher, a maximum of 1 dB for the source in the intersection, and about 3 to 7 dB higher for the source around the corner. For farther distances from the source street, differences become even more pronounced. At ten street widths from the source path, the smooth wall level exceeds the level for protrusions by 3 to 6 dB when the source is in the intersection and by about 10 to 12 dB when it is around the corner. More data from the model experiment will be presented in Section IV.

For further comparison, line source levels for the model with periodic protrusions have also been determined. These are presented in Figure 3.22 along with the smooth wall results. Again, it will be noted that the levels produced with the smooth walls are substantially higher. For distances away from the source, this difference is typically 8 to 9 dB for all frequencies.

Comparison can also be made between the model results for both smooth walls and walls with protrusions to the data obtained in the field experiment. For this comparison, model data obtained at three street widths from the source line for the 8 kHz octave band is used.

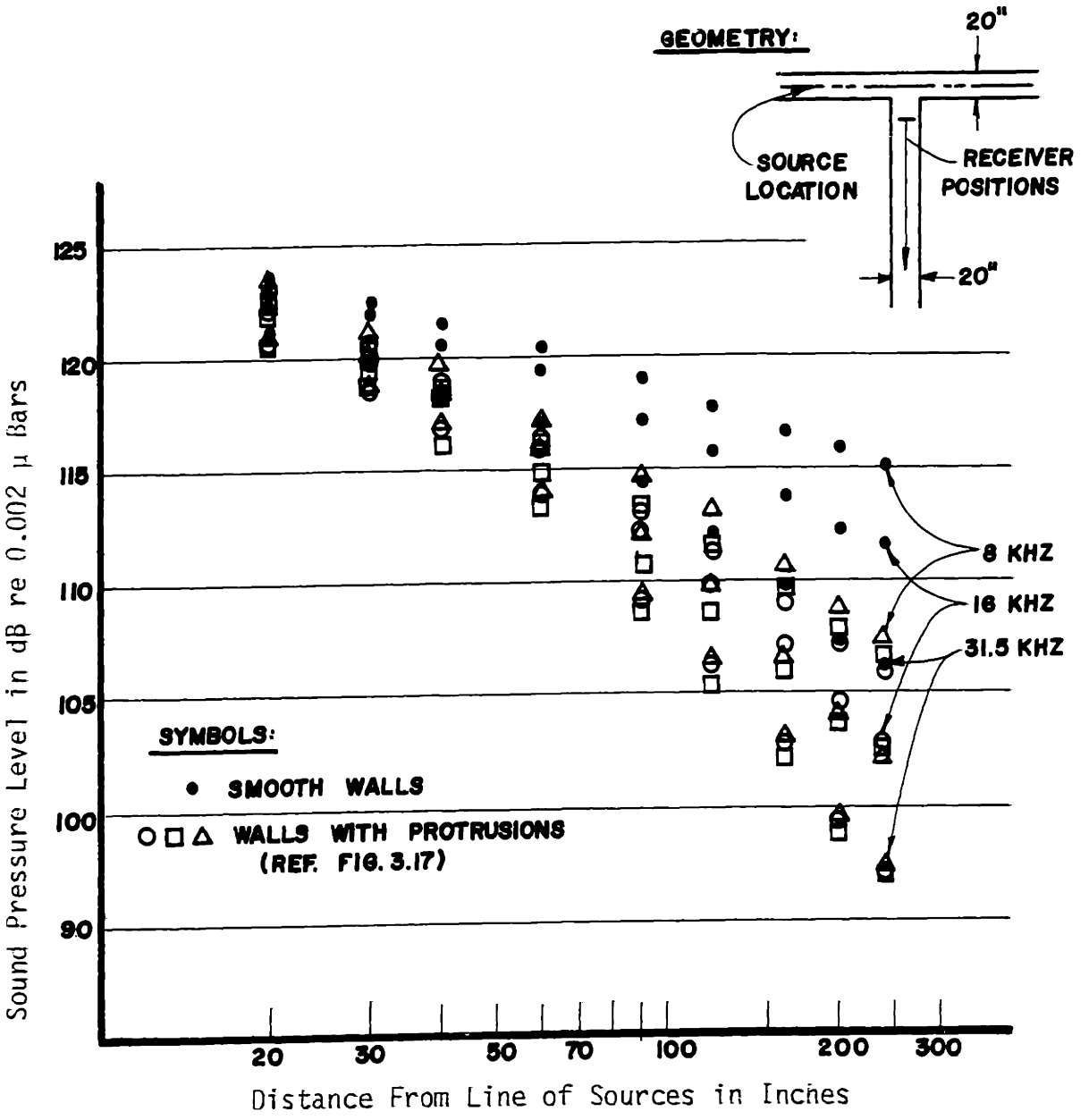

FIGURE 3.22: Acoustical Model Line Source Levels With and Without Protrusions

Eight kilohertz was chosen in order that air absorption effects be minimal. The field data are the frequency averaged attenuation of Figure 3.8. The comparison of the various data is presented in Figure 3.23. Using the attenuation for the source at the intersection centerline for normalization, the smooth wall results tend to be higher than the field data. When the source is near the intersection, differences between the two results are slight. Further from the intersection, the difference reaches to about 2 to 3 dB. For the field data point furthest from the intersection, although there is no model data for this point, there is an indication that the difference may be quite substantial, 7 dB or more. The results for the simulated facade model compare more favorable to the field data. Also, for the distant point where no model data is reported, there appears to be a much improved possibility of matching the field data.

3.2.3 Summary

In summarizing the field and model data, there are several conclusions which may be drawn. Specular imaging theory was found to produce results which agree quite well with smooth wall model data. It was further found, however, that the smooth wall data, and thus specular imaging theory does not correspond well to field data for street propagation. Diffraction effects were observed in the model data which increased sound levels thus not alleviating the discrepancy between specular imaging and actual street propagation.

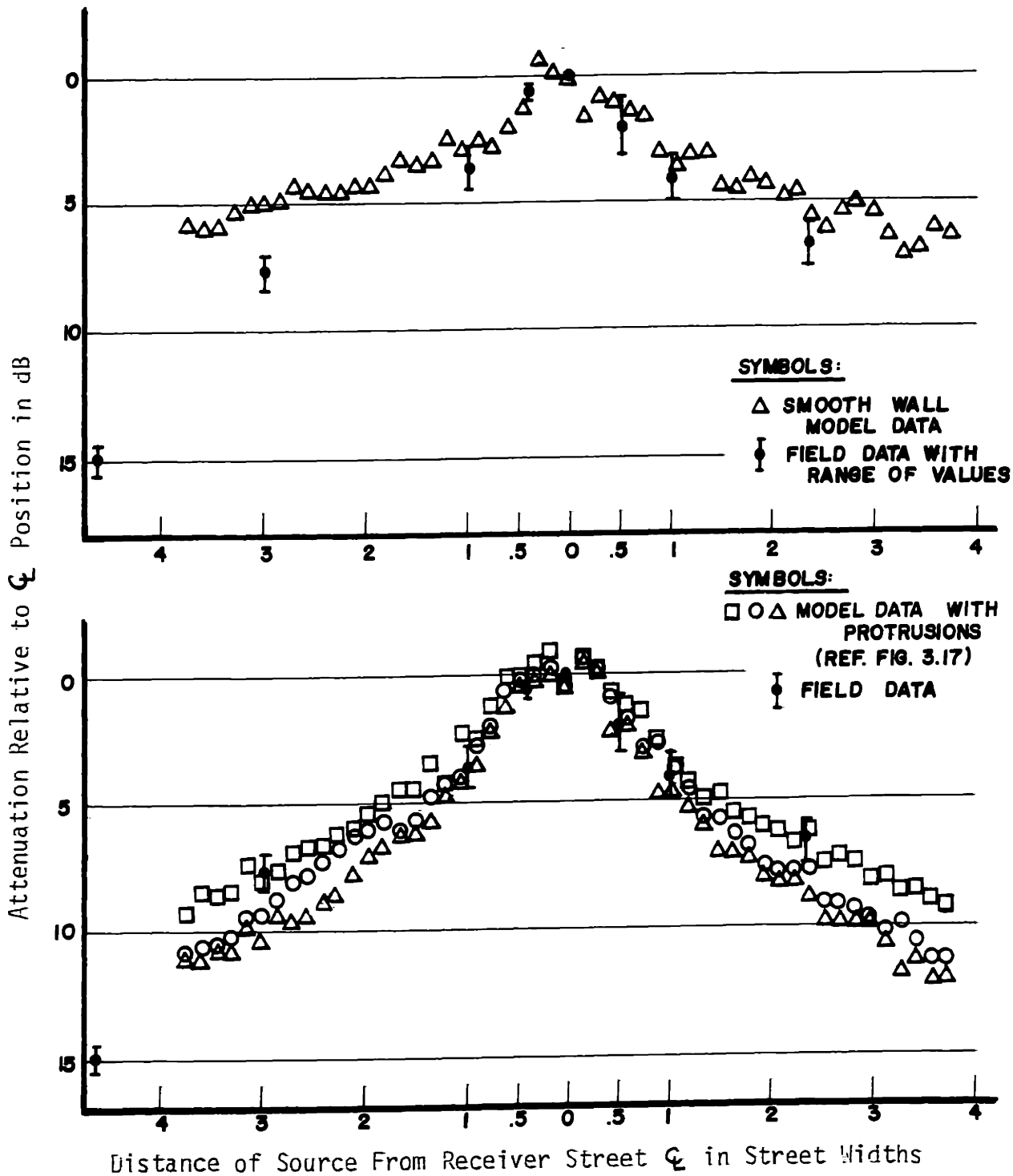

FIGURE 3.23: Comparison of Field and Acoustical Model Data with Protrusions

It was also found from the model study that the addition of periodic, rectangular protrusions to the channel surfaces, simulating building facade structure, substantially decreased the measured sound levels. Further it was shown that the model results with protrusions compared quite well to those measured in the field study. It is, therefore, concluded that in order to analytically model sound propagation in urban areas, scattering produced by rectangular irregularities in building surfaces must be considered.

3.3 First Order Approximation to Surface Scattering

3.3.1 The First Order Model

In order to develop an analytical model of the reflection of sound from a surface of periodic, rectangular protrusions, it is convenient to conceptually separate the specular or "mirror-image" component of reflection from the scattered component. Since energy goes into the scattered component, the specular portion is reduced relative to what would be expected for smooth wall reflection. If the scattered field produced by reflection is small compared to the specular, then to first order the total field can be approximated by the specular component alone if the energy of this component is reduced owing to the scattered loss. The concept of added energy loss for the specular component is quite compatible with the increased attenuations observed in the model experiments due to periodic protrusions. Incorporation of this first order model into specular imaging theory can be made simpley by decreasing the

wall reflection ratio to an empirically determined value.

To utilize this first order scattering approximation for channel propagation, the appropriate value of reflection ratio was empirically determined. This was accomplished by varying the reflection ratio until a good match was produced between the imaging theory results and model data with the periodic protrusions. The reflection ratio value was determined to be .65. This reflection ratio corresponds to an effective wall absorption coefficient of .35. Simulation of the model data using R equal to .65 is presented in Figure 3.24. For the two source locations indicated, good correspondence was achieved with the imaging simulation. It should be noted that for these two positions, the source is in or near the intersection.

3.3.2 Comparison of First Order Model and Experimental Results

Using this first order approximation, line source levels can be calculated corresponding to those obtained for the simulated facade model. A comparison of these two sets of results is made in Figure 3.25 for the tee, four-way and multiple four-way intersections. Of the three street configurations, the best correspondence between experimental and theoretical values was obtained for tee intersection shown in Figure 3.25(a). In this case, the imaging values fall within the model data for the 16 and 31.5 kHz octave bands. For 8 kHz band, the imaging values are 1 to 2.5 dB lower than the experimental. This consistent variation could be due to either diffraction effects or to

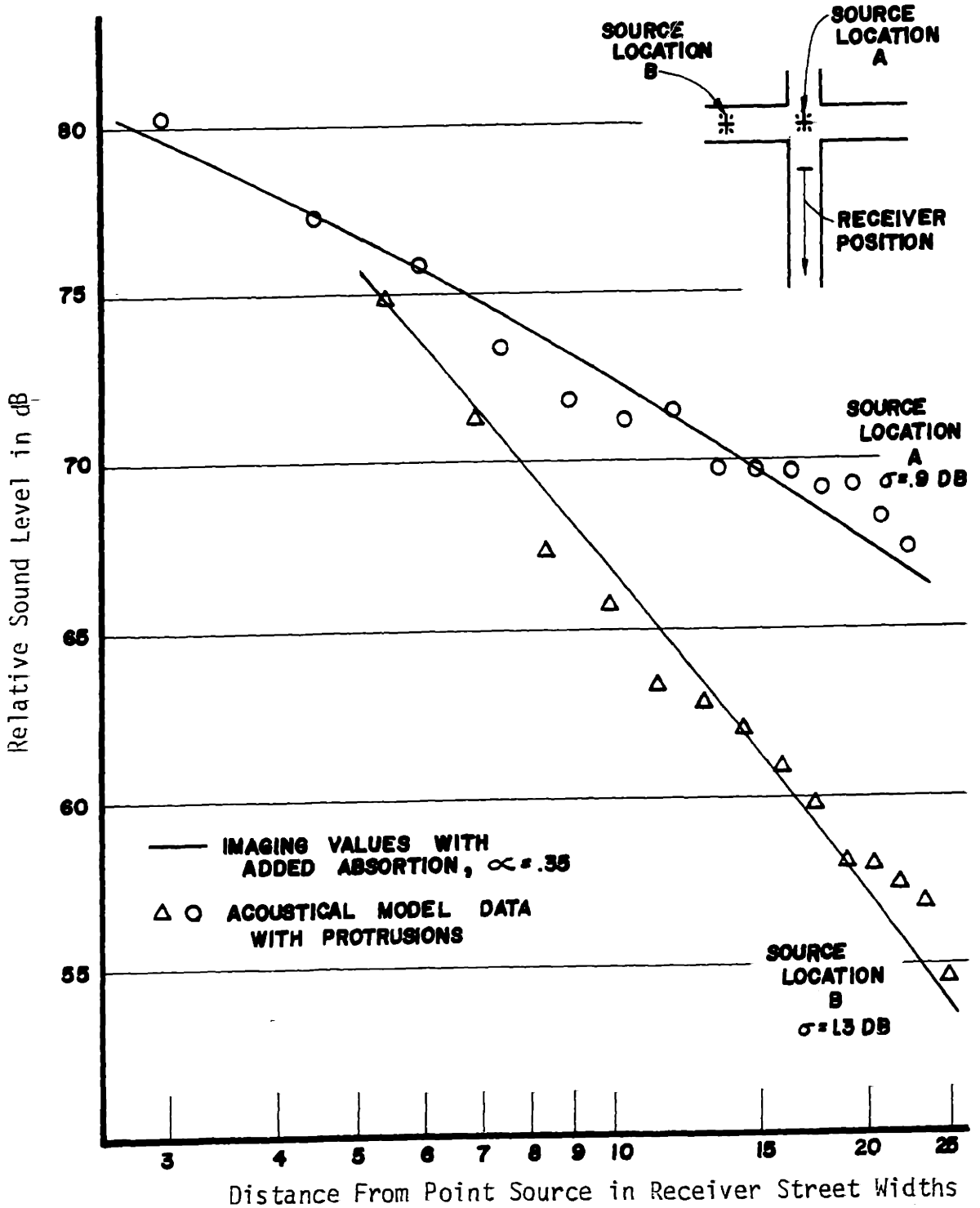

FIGURE 3.24: Simulation of Scattering with Increased Wall Absorption

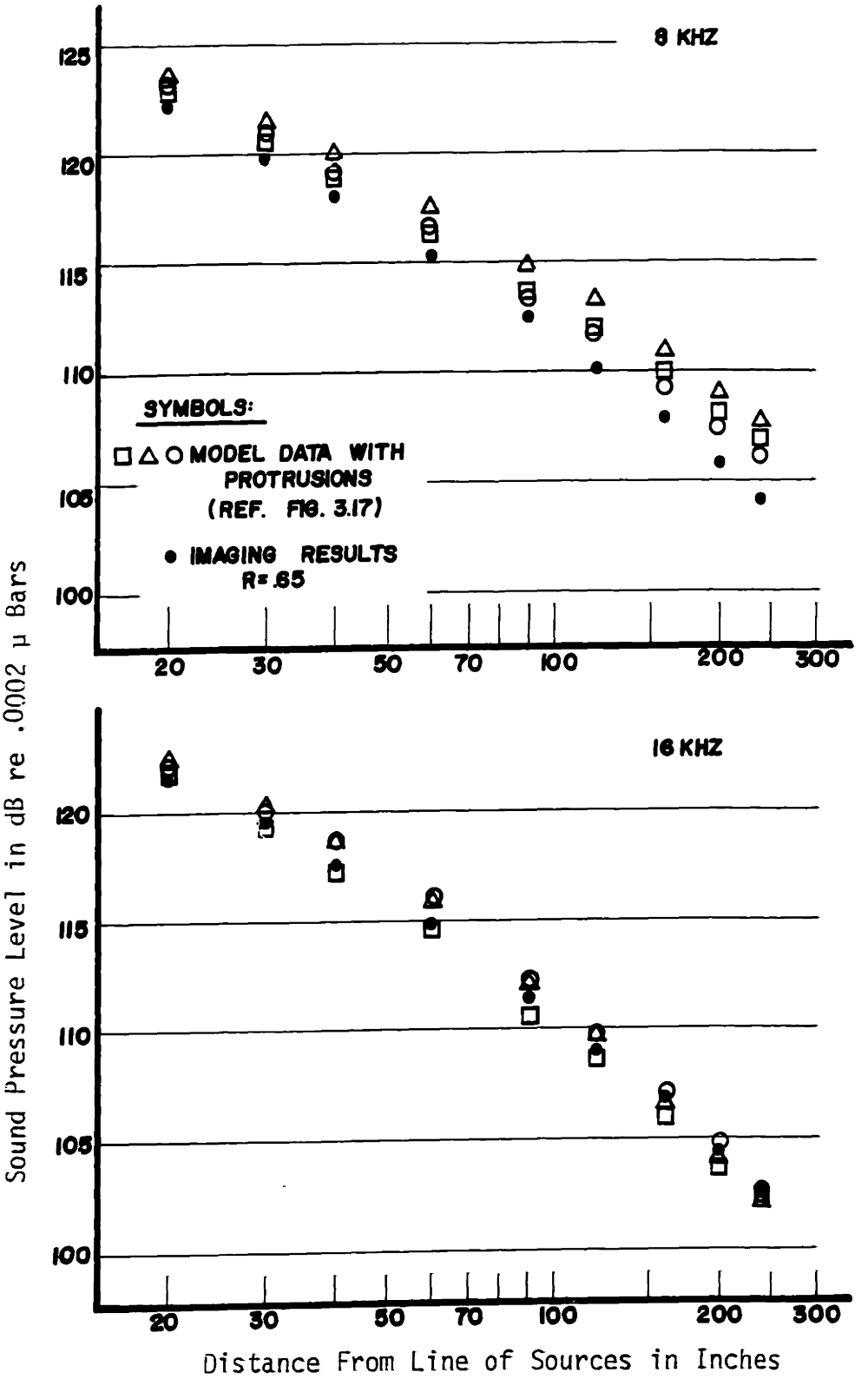

FIGURE 3.25a: Acoustical Model and Added Absorption, Specular Imaging Line Source Levels-Tee Intersection

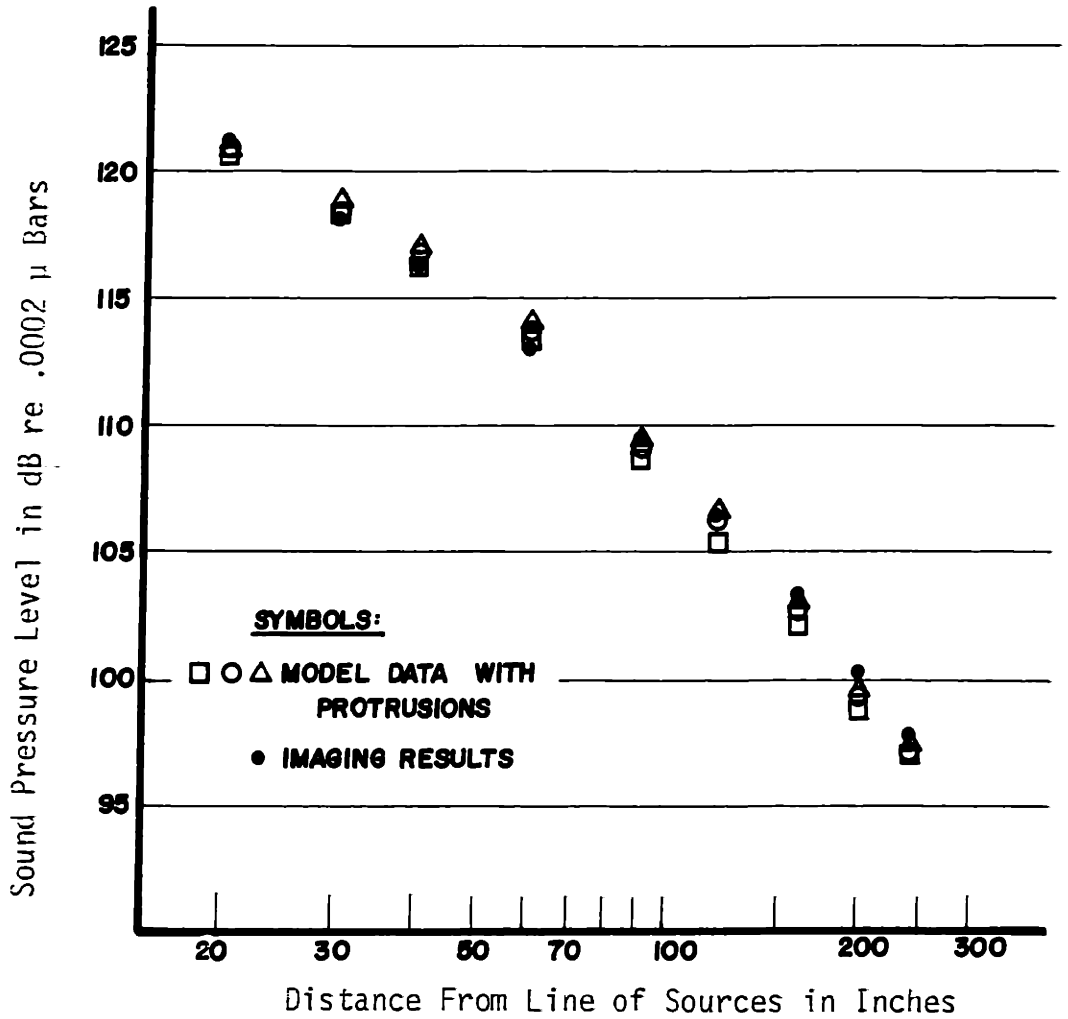

FIGURE 3.25a: Acoustical Model and Added Absorption Specular Imaging Line Source Levels - Tee Intersection

frequency dependence in the scattering processes. The line source results for the two four-way configurations is presented in Figure 3.25(b). For the intersection without a cross street, the imaging values are seen to be consistently lower than the experimental. These differences extend from near 0 to a maximum of 2.5 dB for the 16 kHz and 31.5 kHz bands, and 3.5 dB for the 8 kHz band. Similar behavior is apparent for the intersection with a cross street. In this case, however, the maximum differences in the 16 kHz and 31.5 kHz band is only about 1.5 dB.

With the first order scattering approximation, imaging results corresponding to the pass-by data taken with the facaded model can also be compared. In Figure 3.26, imaging values and model data in the 16 kHz band at three receiver positions for a tee intersection are presented. It will be observed that when the source is in the intersection, there is good agreement between the two results for all distances. However, as the source moves out of the intersection, the imaging values become increasingly lower than the experimental values. This difference reaches as much as 1 to 5 dB for 1.5 street widths, 3 to 8 dB for 4.5, and 8 to 13 dB for 10.

Comparing imaging values using the first order approximation to the field data indicates the same shortcomings as the above comparison to model data. The data from the field experiment is presented again in Figure 3.27 along with the imaging results. As with the model data, when the source is out of the intersection, imaging predicts levels which are considerably lower than the experimental values. Difference

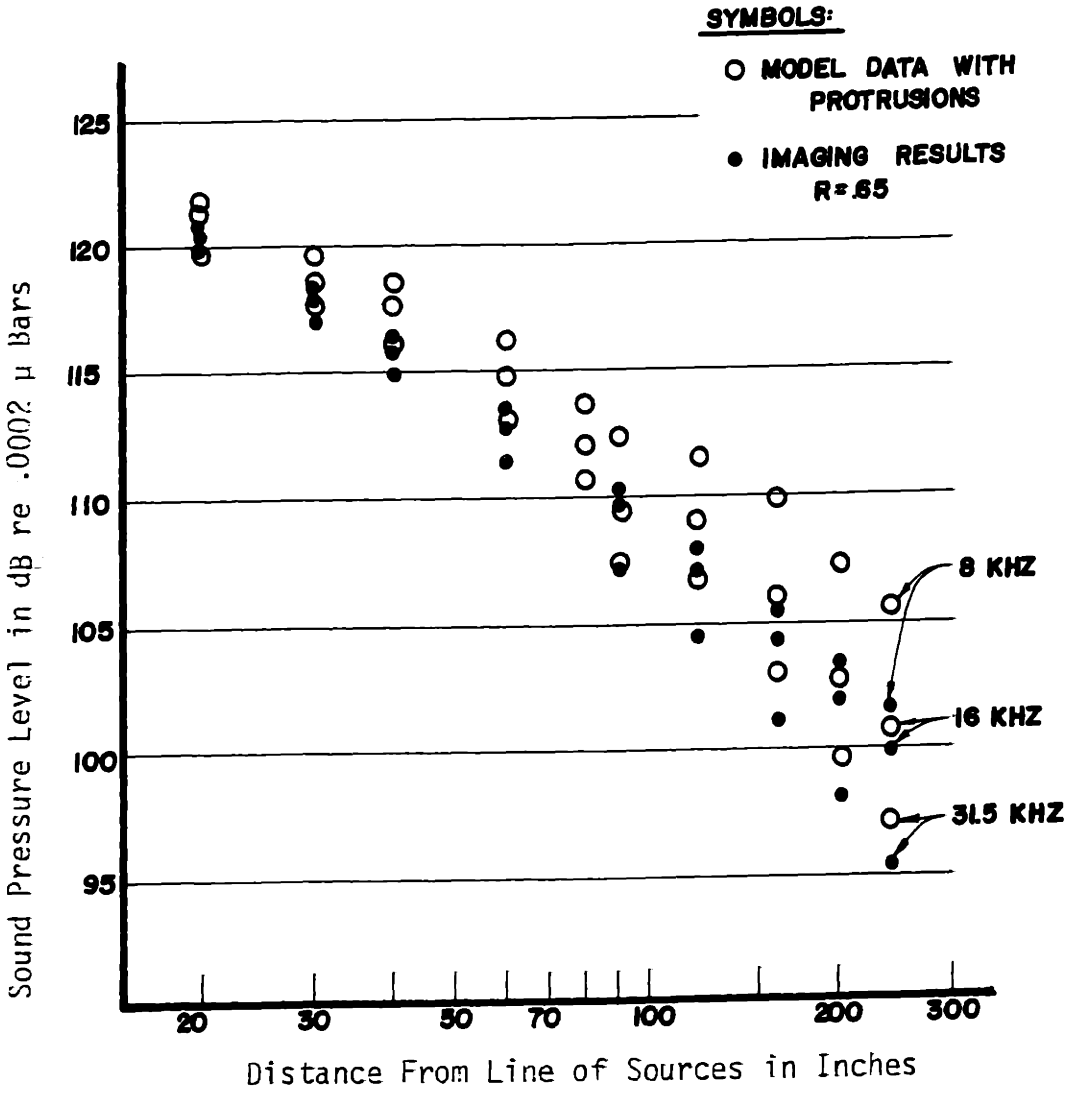

FIGURE 3.25: Acoustical Model and Added Absorption Specular Imaging Line Source Levels - Four-way Intersection

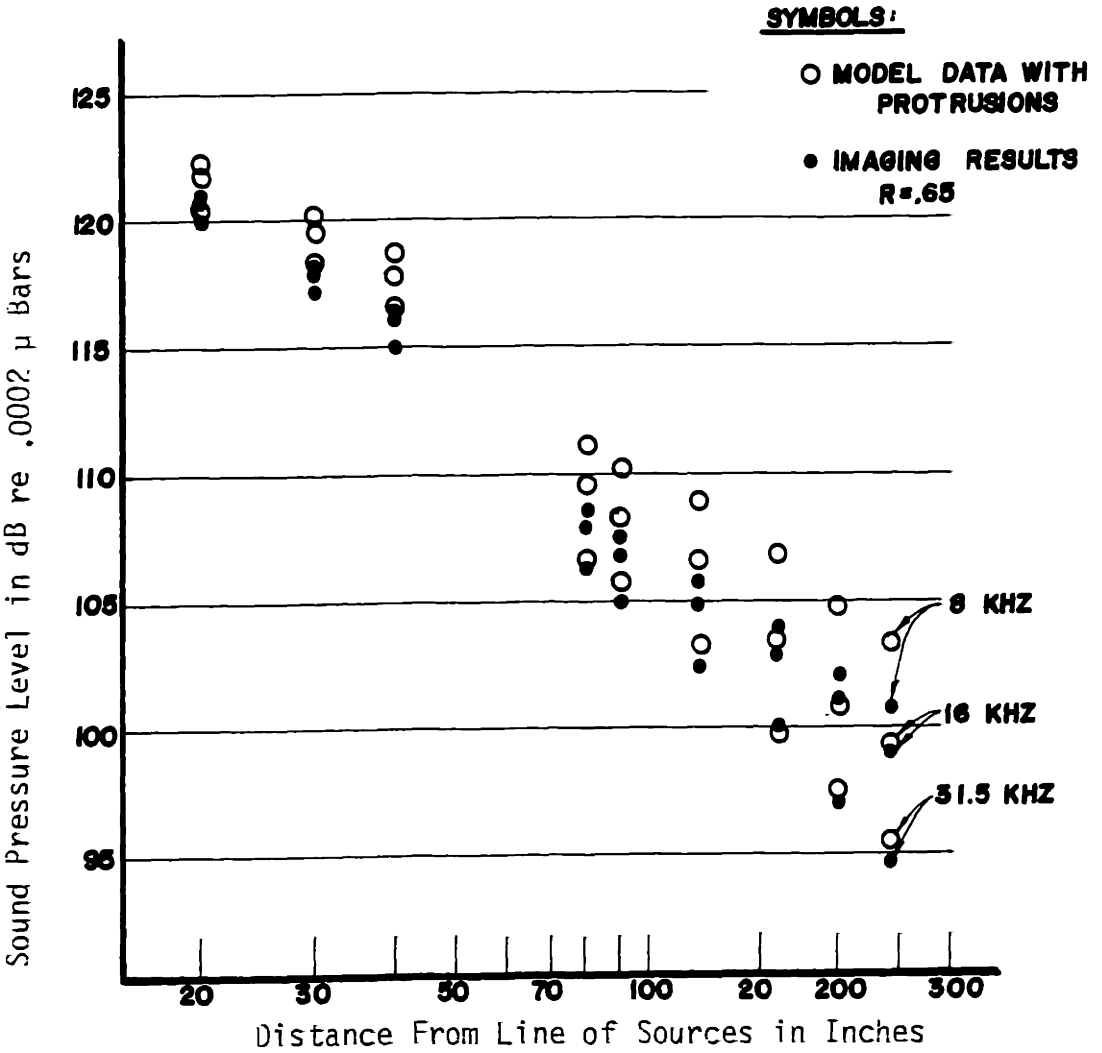

FIGURE 3.25c: Acoustical Model and Added Absorption Specular Imaging Line Source Levels - Four-way Intersection With Cross Street

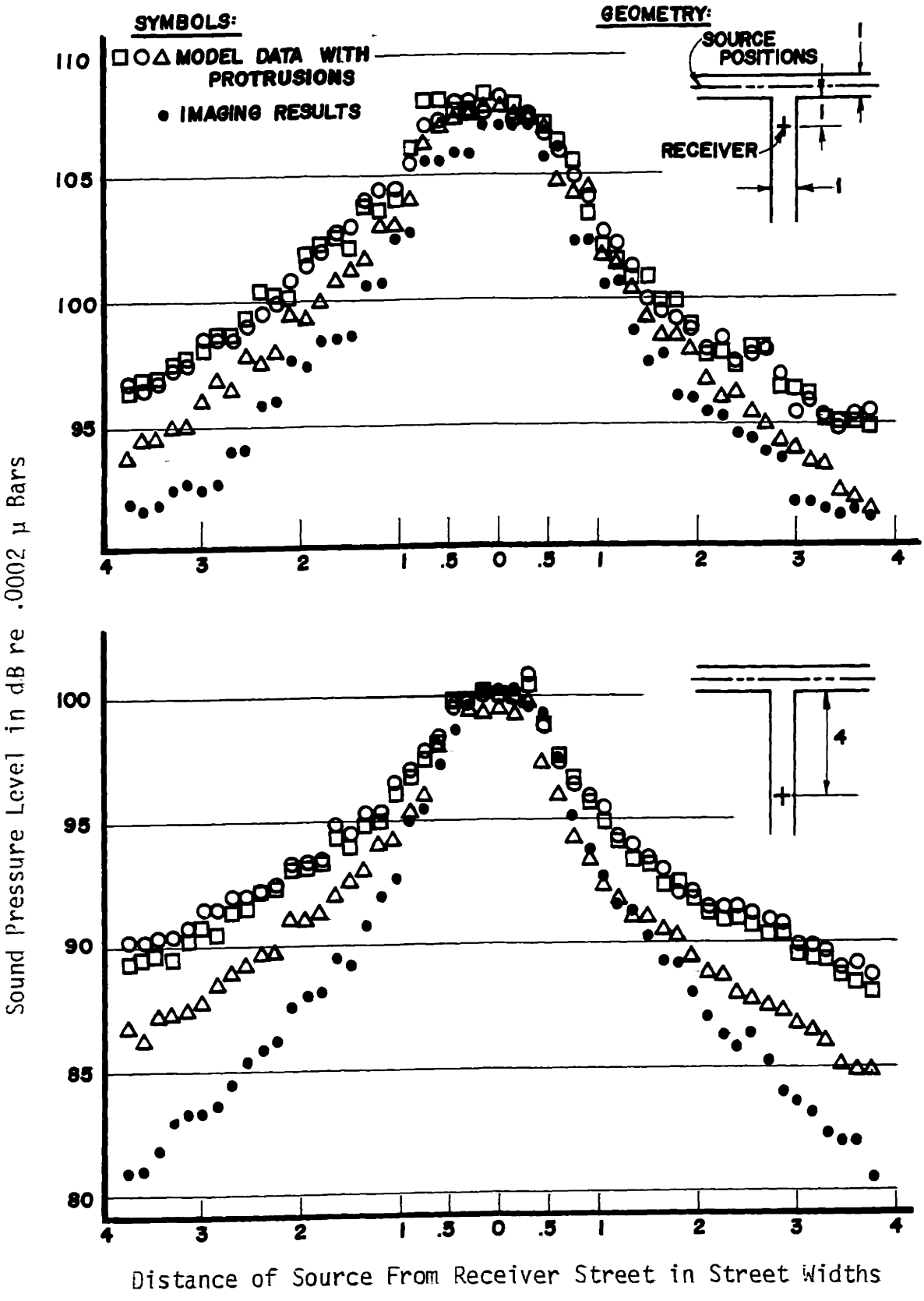

FIGURE 3.26: Acoustical Model Pass-by Data and Added Absorption Specular Imaging Simulation

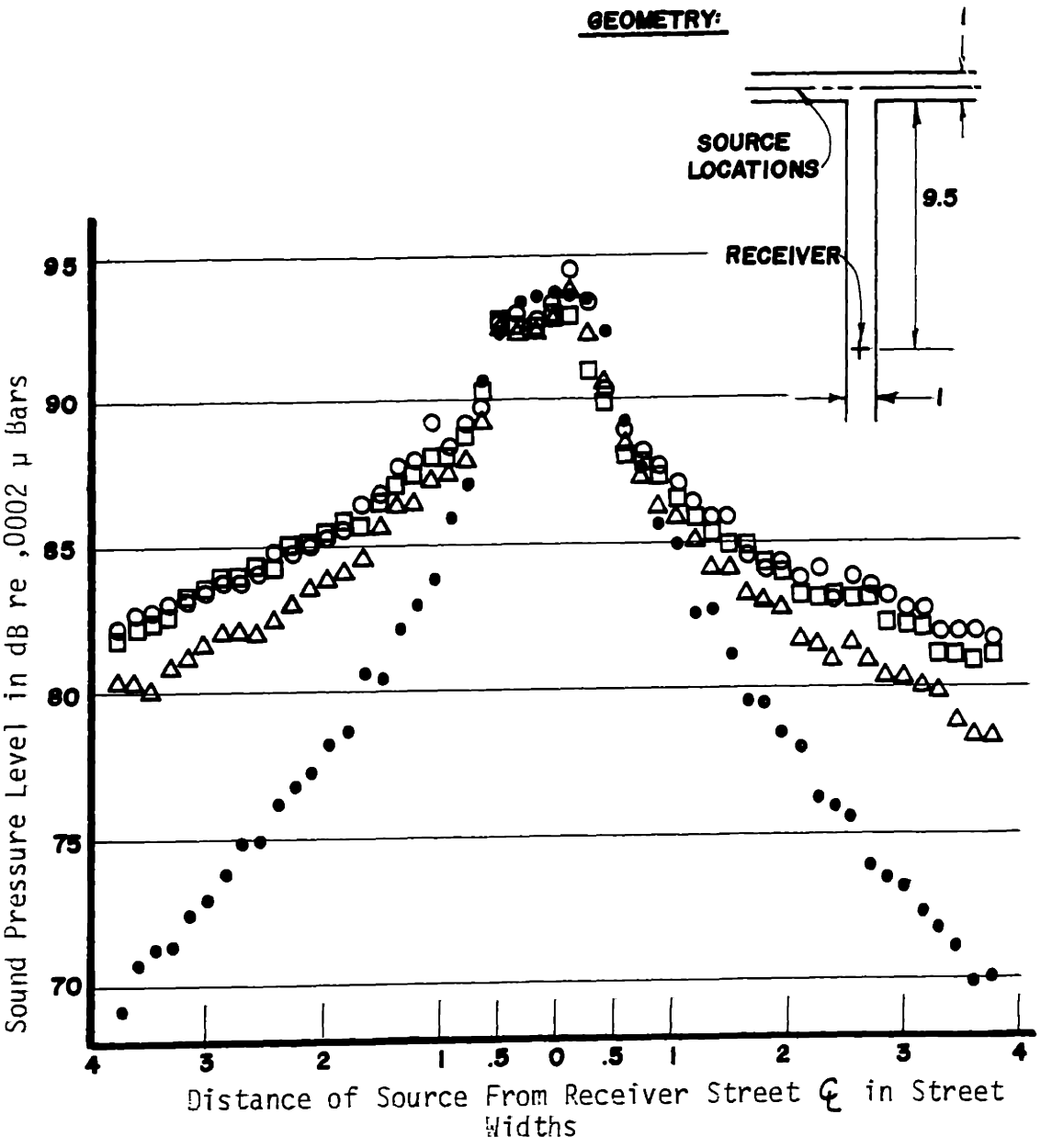

FIGURE 3.26: Acoustical Model Pass-by Data and Added Absorption Specular Imaging Simulation

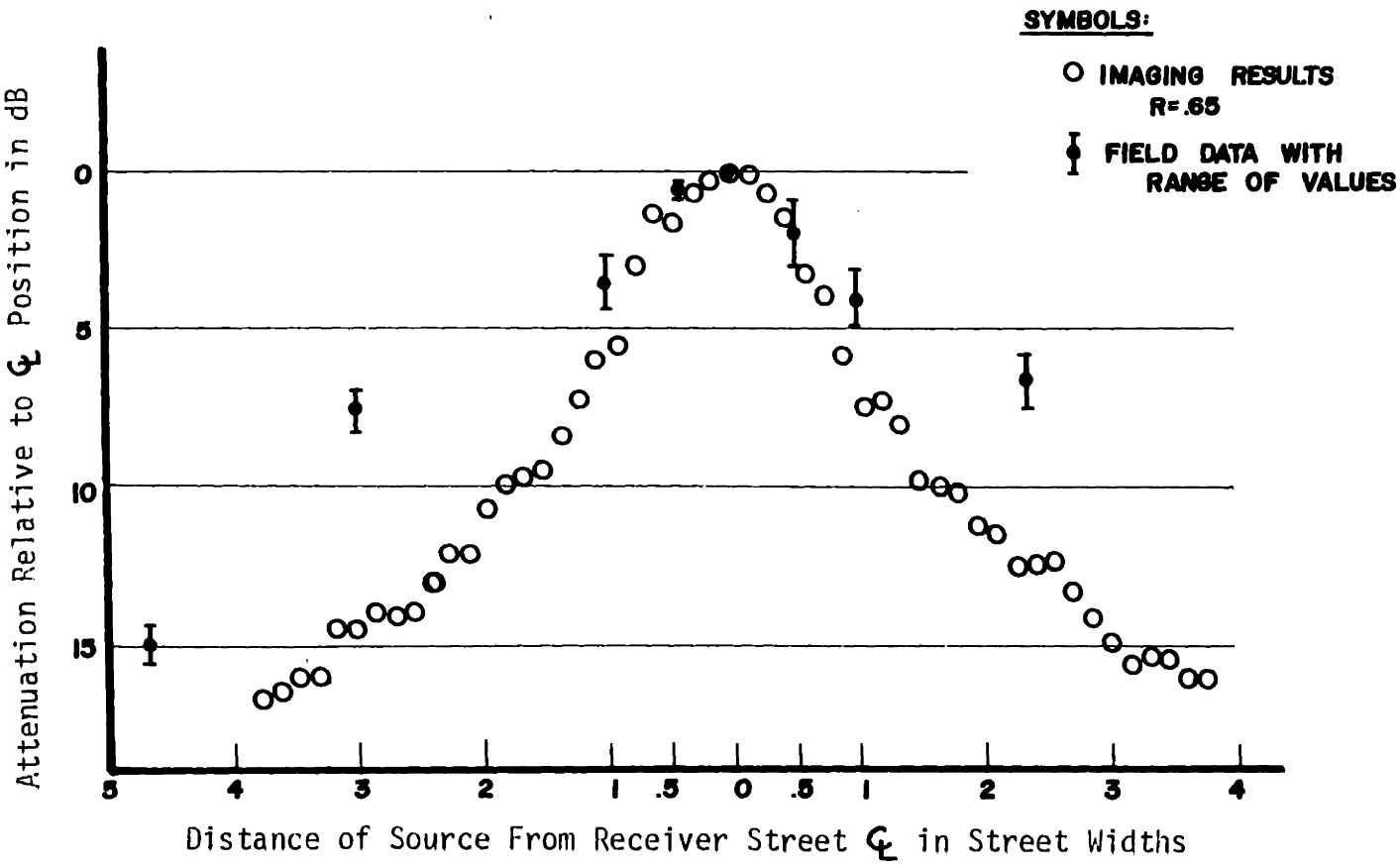

FIGURE 3.27: Comparison of Field Data and Added Absorption Specular Imaging

between the values is as much as 6 to 7 dB.

The above comparison of field and model experimental results with first order scattering imaging theory leads to several conclusions. First, it was shown that although always slightly lower, the first order approximation gives reasonable agreement with the experimental line source levels of the model. As might be expected from the nature of the approximation, it was also shown that this first order model is inadequate in predicting levels when the source is around a corner from the receiver. There is, however, good correspondence when the source is in the intersection, which is an improvement over the original specular imaging theory. Further, it is apparent that underestimation of line source levels is due to the inadequacy of the approximation when the source is around the corner. Due to the limitations of this scattering model, it is necessary to obtain a better approximation to the scattered field produced in a street channel.

3.4 Second Order Approximation to Surface Scattering

In order to develop a more detailed analytical model of reflection from a surface with periodic, rectangular protrusions, it remains convenient to conceptualize the reflection in terms of a specular and a scattered component. As an improvement over the previous first order approximation, the energy in the scattered component will now be included in a "second order" approximation to scattered reflection. Also, the requirement that the specular component be independent of incidence angle will be dropped. For reverberant channel propagation,

it must be remembered that scattered energy will be reflected thus creating specular-scattered energy and scattered producing scattered-scattered energy. As an approximation to this very complicated field, it will be assumed that energy which is multiply scattered is small compared to that which is specularly multiply reflected and once scattered. This assumption forms the basis of the second order approximation to scattered reflection.

To apply the second order approximation to channel propagation, separation of specular and scattered components is utilized. The specular component is determined using specular imaging theory with the addition of an angularly dependent reflection coefficient. The scattered component is determined with a modified form of imaging theory designed to evaluate surface scattering. Application of this modified imaging technique to propagation around a corner is illustrated in Figure 3.28. Using the constraints described in regard to specular imaging, the image sources of Figure 3.28 are allowed to produce scattering in the receiver street by reflecting from the far receiver street wall and image walls seen through this wall. The scattering produced is then observed by the receiver and its images. To account for scattering in the source street, the image receivers "look" back into the source street to observe scattering in the actual street as well as its images. The constraints on the influence of the image receivers are identical to those on image sources influencing the receiver street.

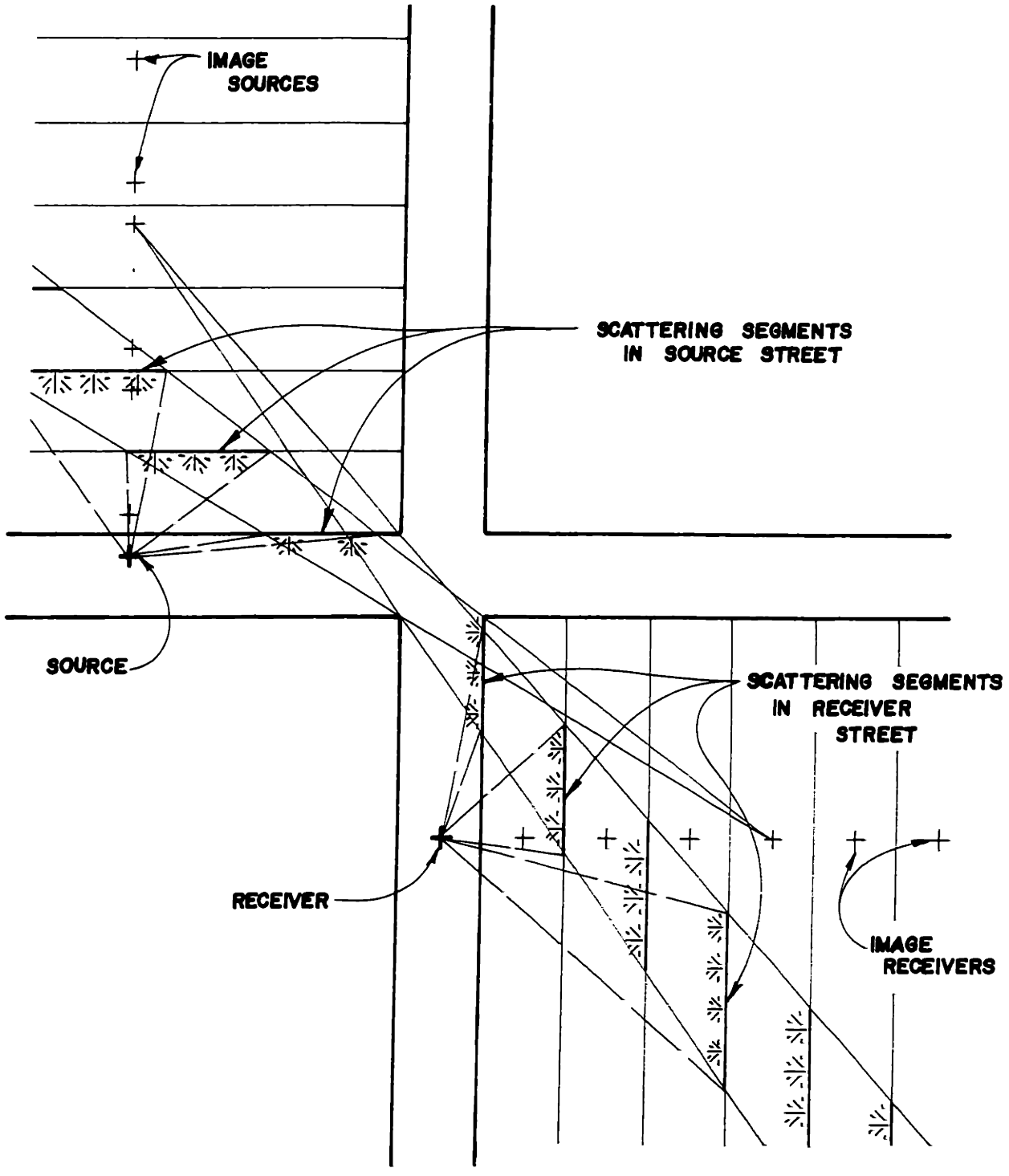

FIGURE 3.28: Application of Scattering to Imaging - Propagation Around a Corner

Before the second order approximation can actually be used, several parameters of scattered reflection must be determined. One dependence which must be determined is that of specular component reflection ratio on incident angle. Also, the angular dependence of the scattered component must be determined. In addition to angular dependence relationships between the reflection components and the geometry of the surface protrusions must be obtained. Finally, the dependence of all the above aspects on frequency expressed in octave bands must be established.

IV. SCATTERED REFLECTION FROM PERIODIC, RECTANGULAR SURFACE IRREGULARITIES

4.1 Statement of the Urban Scattering Problem

The specific details of the scattering problem to be considered are dictated by the noise sources found in urban areas and by the physical characteristics of urban architecture. As discussed in Section 3.1, rectangular irregularities in building surfaces are created by such features as recessed windows and doorways and by decorative facade structures. Facade structures typically consist of ledges and protrusions which usually accent or create the window recesses. Recesses appear on buildings in a variety of depths ranging from a few inches to one or two feet. Protrusions in building surfaces also fall within this range of depth. The width of the recesses or spacing between protrusions also has considerable variation ranging to a few feet to over ten feet. Typically protrusions (and recesses) are periodic in the building surface.

For the purposes of this study, protrusions and recesses will only be considered as occurring perpendicular to the plane of sound propagation. This simplifying assumption is made for several reasons. Protrusions in building surfaces extend either horizontally or vertically. Noise sources and listeners are often located such that propagation between them is in a nearly horizontal plane. Thus, it is more likely that vertical protrusions will have the greatest influence on propagation. Further, a common characteristic of building surfaces is that vertical protrusions

are the dominant feature of the surface as indicated in the photographs of Figure 3.1. Aside from the physical aspects, the vertical protrusion assumption is attractive for the practical reason of making the scattering problem two dimensional. This is desirable in order to keep the variables of the problem at a workable number.

The noise sources in urban areas determine the frequency range of interest in the scattering problem. One noise source of particular interest in cities is automobile, bus, and truck traffic. For these sources, the sound level spectra produced are such that when A-weighted the octave bands of importance are 250, 500, 1000 and 2000 Hz. Other sources such as industrial plants, rail systems and V/STOL aircraft also display spectra which when A-weighted have major contribution in these four octave bands [7,19]. It should be noted that these four frequency bands correspond to wavelengths which are on the order of the dimensions of the irregularities in the building surfaces. It is for this particular case that the assessment of surface scattering is most difficult.

4.2 Previous Studies Applicable to the Urban Scattering Problem

Although the problem of scattering from rough surfaces has received considerable attention in current literature, most of the work has dealt with randomly rough or sinusoidually varying surfaces. One exception to this trend is the theoretical study reported by Deringin [14] dealing with plane tranverse-polarized wave reflection from a rectangular comb. Examination of the geometry of this problem as presented in

Figure 4.1 indicates its similarity to the urban sound scattering problem. The boundary condition applied in this problem is that the comb be ideally conducting. A conducting surface produces a boundary condition on the magnetic field of:

$$\frac{\partial H}{\partial n} = 0$$

where H is the wave amplitude in the magnetic field and n is the normal direction at the surface. The amplitude H satisfies the two-dimensional wave equation. Recalling the boundary condition on the pressure field at a rigid surface,

$$\frac{\partial P}{\partial n} = 0$$

it is seen that there is a direct analogy between the magnetic field and the pressure field. With this analogy and the similarity of geometry, Deringin's results can be applied directly to the urban scattering problem.

In solving the magnetic wave equation by matching boundary conditions, Deringin's work provides some insight into the behavior of the scattered field. Referring to the geometry of Figure 4.1, it was determined that purely "mirror" (specular) reflection occurs if

$$1 + \sin \phi < \lambda/2\ell.$$

This requires that λ be greater than at least 2ℓ for totally specular reflection. Physically, this statement corresponds to having less than one step in the surface height per acoustic wavelength. This condition is very seldom met in urban propagation where 2ℓ

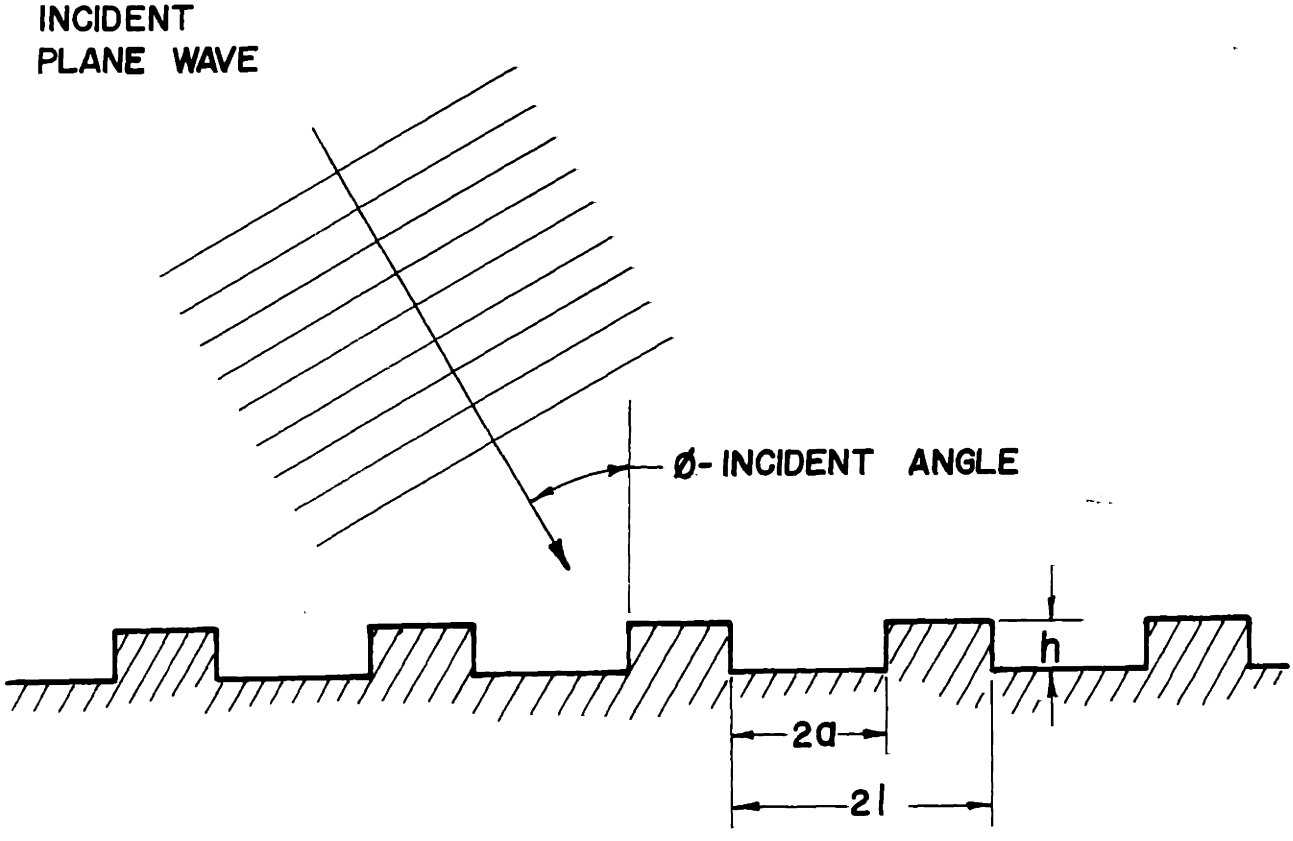

FIGURE 4.1: Geometry of Scattered Reflection from Periodic Rectangular Surface Irregularities

is typically four to ten feet and the acoustic wavelengths of importance are from four to five feet. Deringin also found that spectral content of the scattered wave was determined solely by the parameters $\lambda/2\ell$ and $\sin\phi$. It was further found that scattered waves occur at discrete angles, a result typical of Rayleigh method solutions. These discrete angles, ϕ_n, are given by

$$\sin\phi_n = \sin\phi + n \cdot (\frac{\lambda}{2\ell})$$

where n can be any positive or negative integer. For the urban case, $\lambda/2\ell$ is typically small, considerably less than 1, thus many scattering angles are present. Another result discussed in the paper is the 1/4 wavelength resonance phenomenon. Resonance in this case refers to a minimum in the energy reflected by the surface . This resonance occurs for normal incidence when

$$h = \lambda/4$$

For non-normal incidence, it occurs when

$$h = \cos\phi \cdot (\lambda/4).$$

Although Deringin outlines the method of solution of the scattering problem in general, he solves it only for a specialized, simplified case. The case considered is that of normal incidence and $2\ell/\lambda < 2$. For urban propagation, this solution is not applicable as normal incidence is too restrictive and typically $2\ell/\lambda \geq 2$. Further, although the method of solution outlined is applicable, obtaining an exact solution for the urban

case is impractical. This is due to the fact that for $2\ell/\lambda > 2$ and non-normal incidence, the number of terms corresponding to the discrete scattering angles becomes quite large. As the exact solution requires solving an infinite set of equations for each term, this method quickly becomes impractical for solving the urban scattering.

In a recent study, Wagner [15] also considers reflection from a surface with periodic rectangular protrusions. The solutions detailed in the study are for the low and high frequency limits. The low limit corresponds to the case where acoustic wavelengths are much greater than protrusion height. The high frequency limit corresponds to wavelengths much smaller than any of the dimensions of the problem thus allowing an optical or ray theory approximation. Owing to the reasons discussed above in regard to Deringin's paper, no solution is obtained for the urban case of wavelengths on the order of irregularity dimension.

4.3 Experimental Investigation of Scattered Reflection

In order to gain some understanding of the reflection process for a surface of periodic, rectangular protrusions, a model study was conducted. In addition to providing qualitative insight concerning scattering, the experiments were designed to determine the region of the surface active in scattering and to yield some information on the angular dependence of the scattered field. In order to minimize air absorption effects and yet to readily allow variation of surface parameters, a model scale of 1:8 was chosen.

The noise source used in studying scattered reflection was an electrical spark discharge. Verification of the suitability of sparks as sound sources has been made in detailed study conducted by Klinkowstein [26]. This type of source has also been used in a number of previous model studies [5, 7, 15, 21, 22]. There are several features of this type of source that make it quite desirable for use in model studies. One such feature is the high acoustic energy level produced by a spark. This is necessary to overcome air absorption and instrumentation limitations at typical modeling frequencies. Another feature of the spark source is its broad-band energy spectrum. The relative 1/3 octave band spectrum of the source used in this experiment is given in Figure 4.2. From this figure, it is seen that there is sufficient energy from 1.6 kHz to well above 31.5 kHz. A third desirable feature of the spark source is its lack of directivity. This property was verified for the particular source used in this study for the three planes indicated in Figure 4.3. The standard deviation of the level measured in 15° increments from the angular average is also presented for each plane in Figure 4.3. The technique used for the directivity measurements is discussed in Section 4.5.

The experimental instrumentation chain is presented in Figure 4.4. The settings of the various instruments are also indicated in this figure. The output from the instrumentation was plots of band-passed pressure versus time. The transient recorder was triggered by the signal itself with the recorder in a pretrigger record mode. This yielded both the

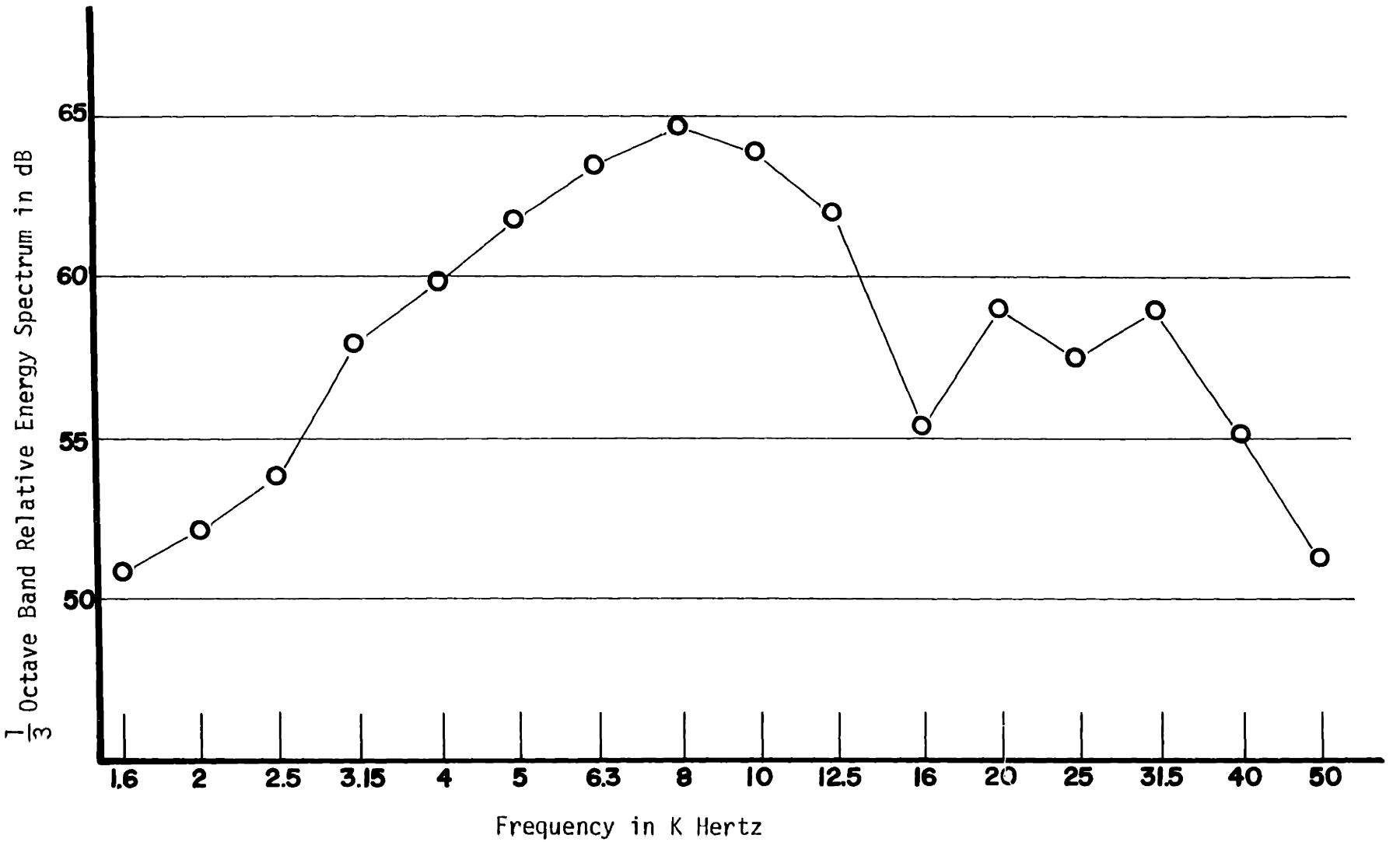

FIGURE 4.2: Energy Spectrum of Electrical Spark Source at 4 Feet

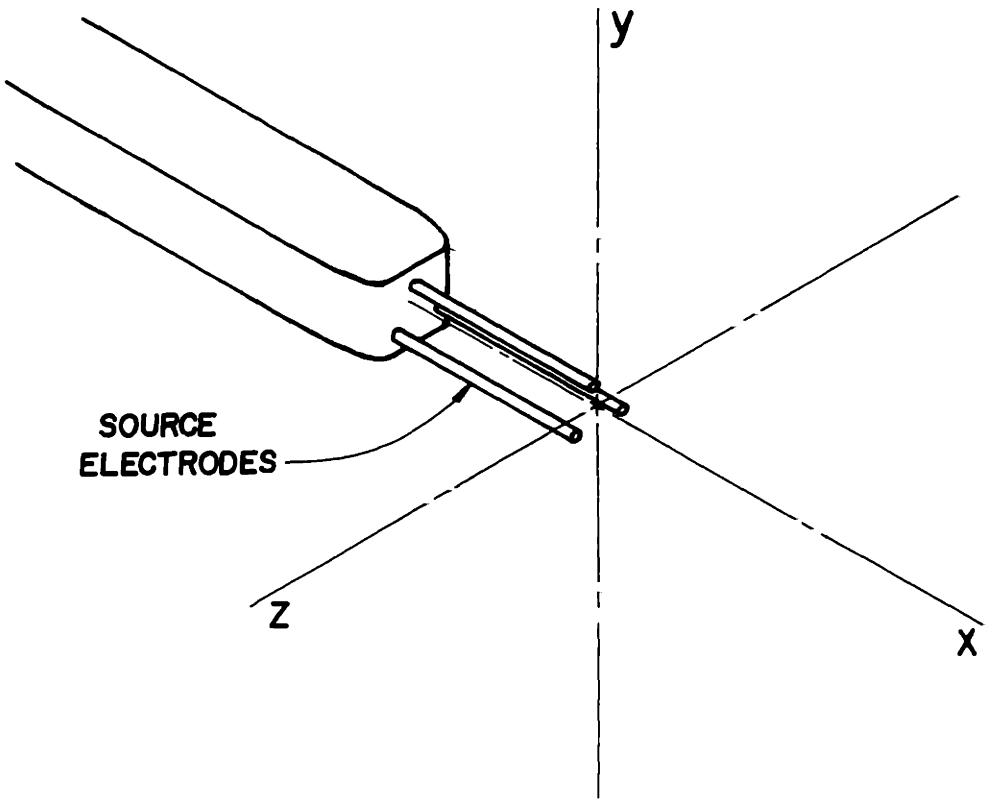

Angular Averages Relative Energy Levels in dB (O.B.'s)

Plane	Frequency	E[θ]	σ
Z-X	2k	52.4	.55
	4k	60.7	.44
	8k	65.3	.28
	16k	60.2	.33
Y-X	2k	52.7	.54
	4k	60.7	.41
	8k	65.4	.27
	16k	60.4	.38
Z-Y	2k	52.0	.36
	4k	60.3	.34
	8k	65.1	.21
	16k	60.1	.50

FIGURE 4.3: Electrical Spark Source Directivity

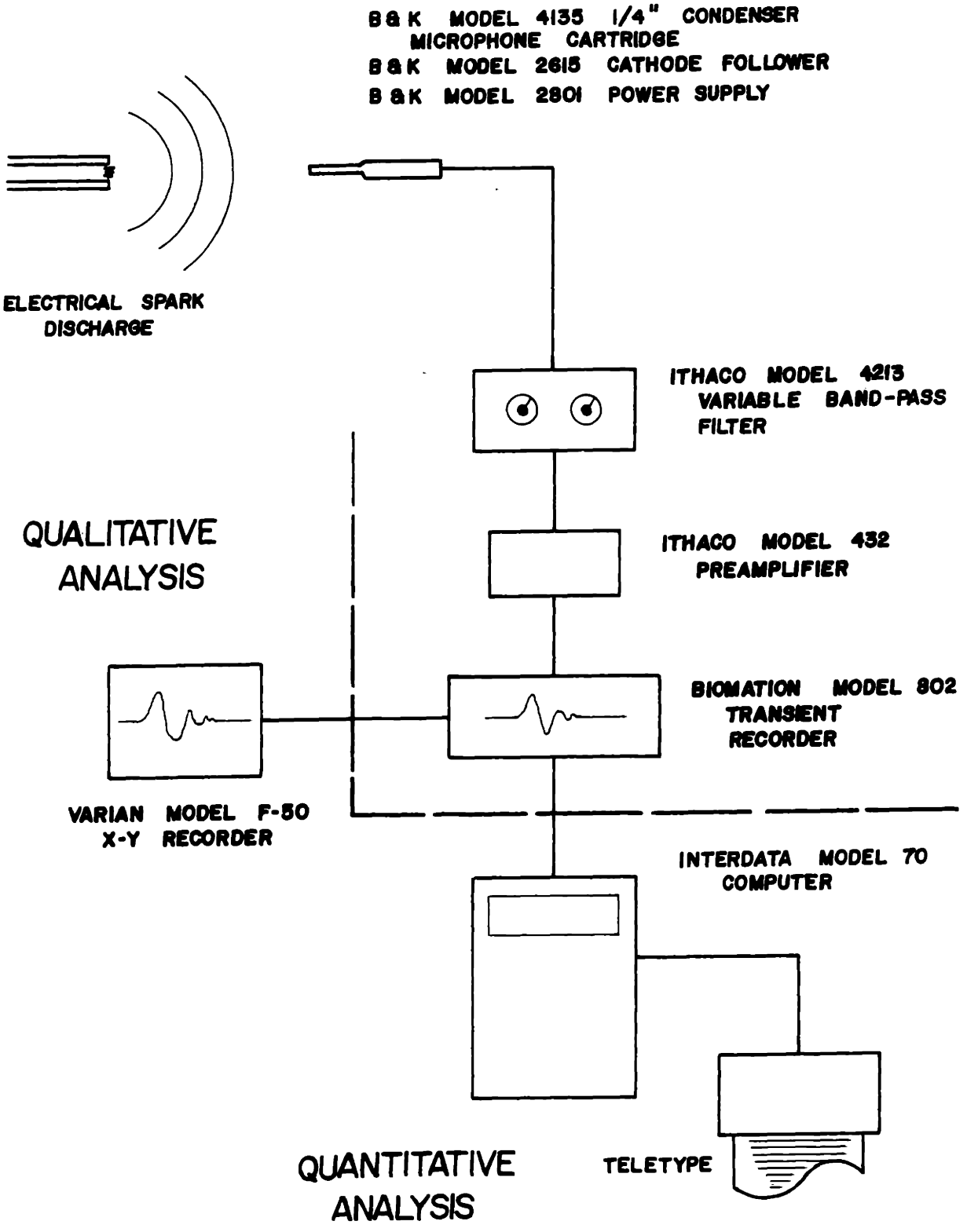

FIGURE 4.4: Transient Acoustical Model Experimental Instrumentation System

arrival of the direct pulse and the subsequent and scattered energy.

The periodic, rectangularly irregular surfaces tested were constructed by placing four foot long slats transversely on two adjacent plywood sheets. The sheets were oriented to a total surface of 4 x 16 ft. The plywood was placed directly on the concrete laboratory floor. The three sizes of slat used were 1" x 1 1/2", 1 1/2" x 1 1/2" and 1 3/8" x 2 1/2". The slats had been planed to assure square corners. A total of four surfaces were tested, one for each of the three types of slats spaced to a period of 7 1/2" and one with 1 3/8" x 2 1/2" slats at a period of 16". The rectangular slats were placed with the longer dimension on the surface. For each of the four surfaces, the reflection was separated into forward and backscattering geometries. The configurations used to achieve this are indicated in Figure 4.5.

4.3.1 Forward Scattering Experiments

For the forward scattering configuration, a detailed investigation of the surface with 1 3/8" x 2 1/2" protrusions in a 16" period was made. Slats were systematically added to the plywood surface in order that the contribution of each could be determined. One interesting phenomenon observed in experiment was the degradation of the specularly reflected pulse. A sequence indicating this is shown in Figure 4.6 along with the corresponding geometry. Breifly, it is seen that the presence of one protrusion on either side of the specular reflection point produces an almost identical phase cancellation effect which slightly reduces the specular magnitude. If, however, both protrustions are present, the phase cancelling effects of the two pro-

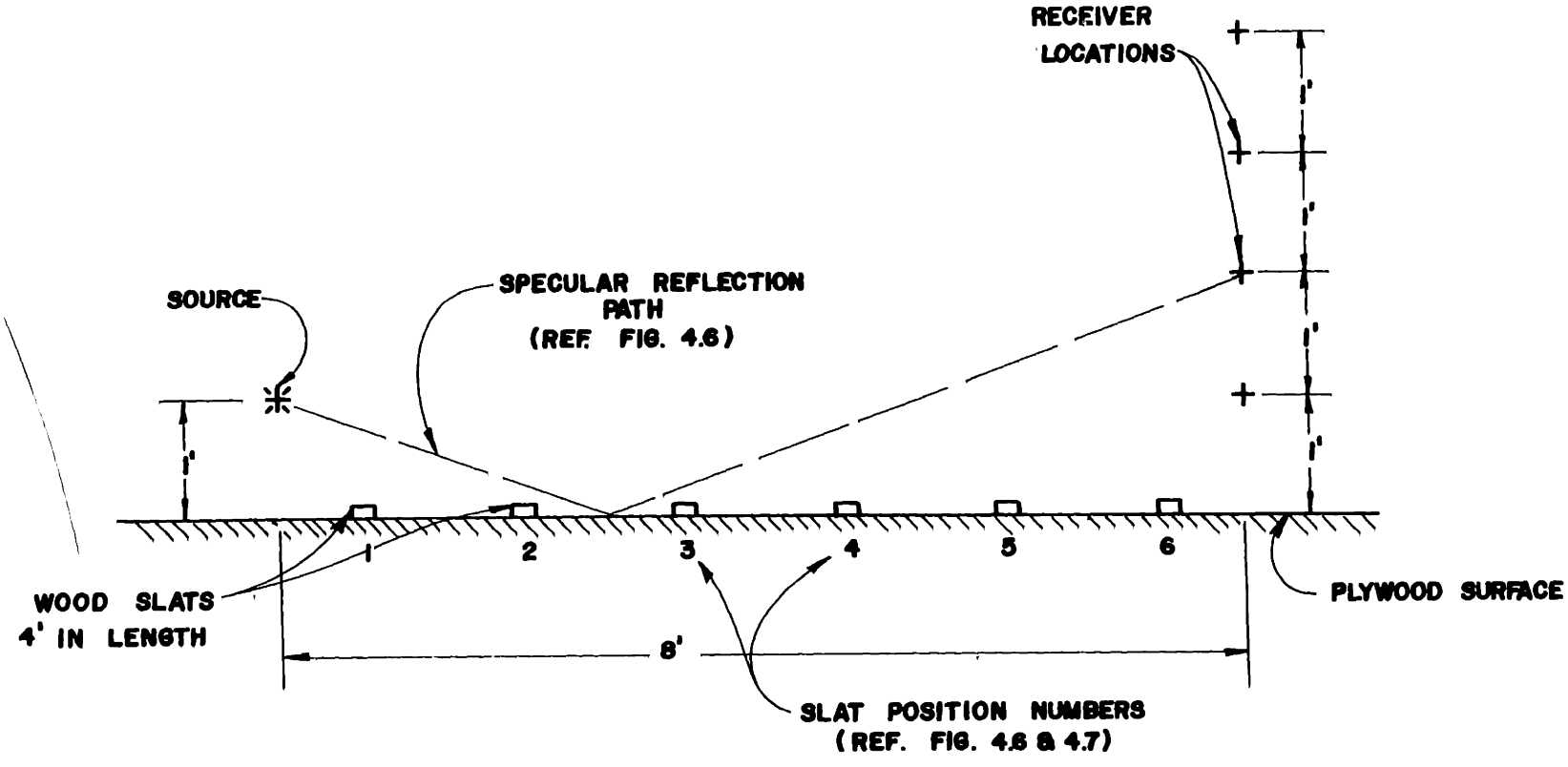

FIGURE 4.5a: Geometry for Forward Scattering Experiments

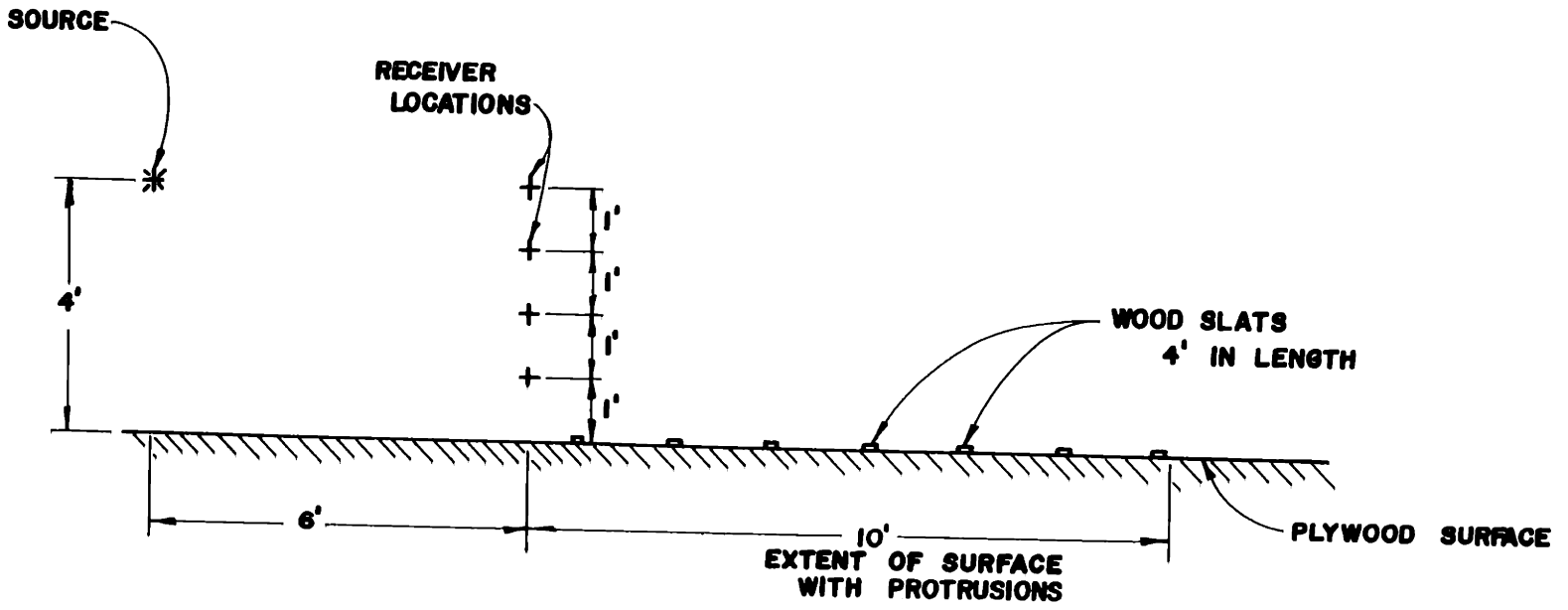

FIGURE 4.5b: Geometry for Backscattering Experiments

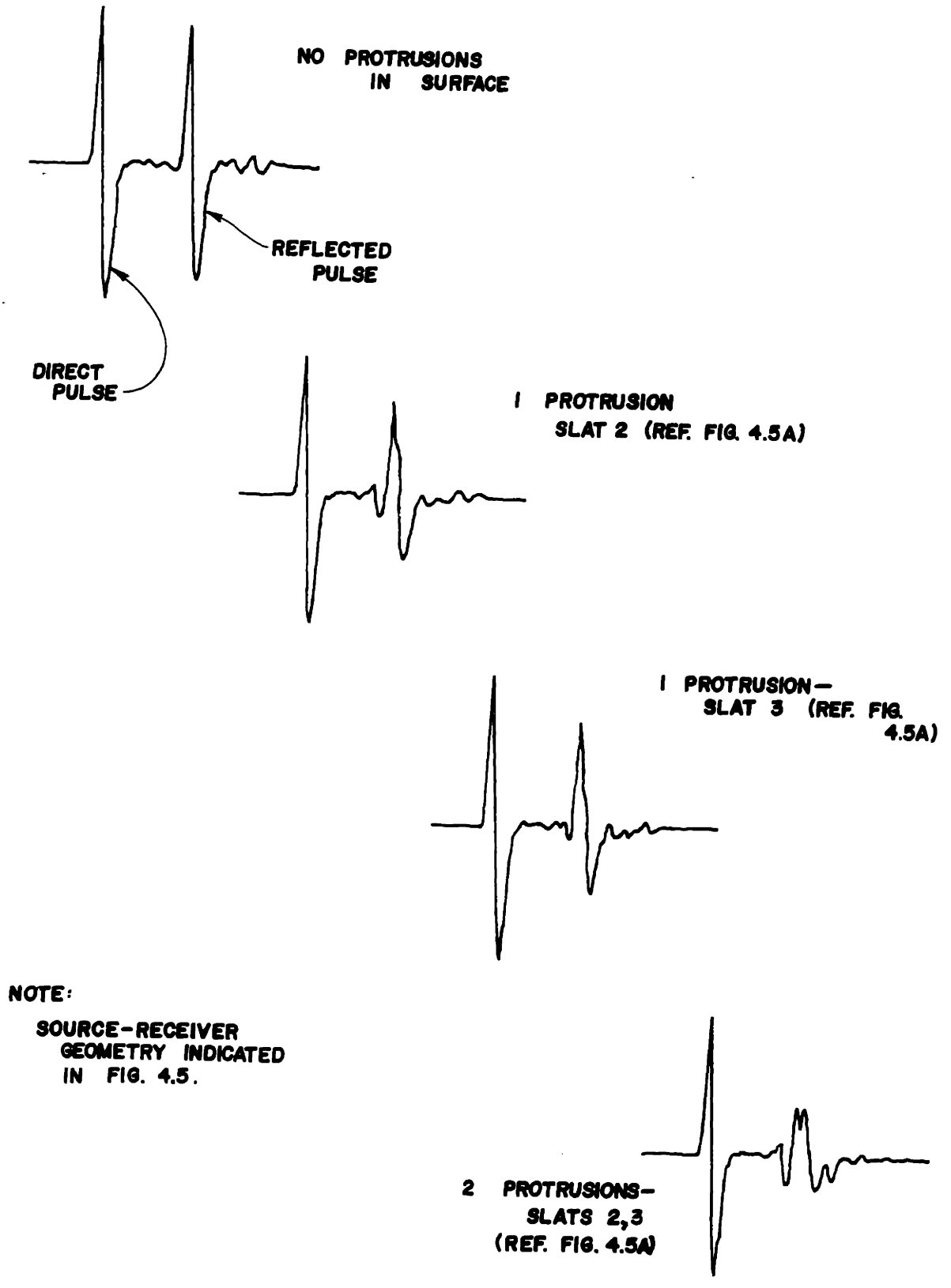

FIGURE 4.6: Degradation of the Specular Component

trusions produce a reduction in the specular magnitude which is substantially greater than for either acting alone. It should be noted that this reduction in specular magnitude is precisely that effect modeled in the first approximation to scattered reflection. By removal and addition of the slats, the contribution of each was determined for the rest of the surface. Within about 2 milliseconds after the direct pulse, all the energy which is directly attributable to individual slats has arrived at the receiver. However, examination of the time history of this reflection in Figure 4.7 reveals that energy is still being radiated from the surface after 2 milliseconds. By measurement of path length this was determined to be due to multiple reflection within the cavity formed by two slats. A schematic diagram of this phenomenon is also given in Figure4.7. The influence of pairs of slats is indicated in the time history of reflection.

Forwarding scattering experiments for other source-receiver geometries and other surfaces, yielded time histories similar to that of Figure 4.7. All the cases displayed a reduction of the specular component, the presence of scattered energy, and multiple cavity reflections. The exact details of each of the time histories were, however, found to be sensitive to individual surface geometries, incidence angle, and the placement of the source and receiver relative to the protrusions. Although this variation was present, it was not possible to formulate specific conclusions regarding pressure signal and parameter variation. Three additional examples of pressure time histories obtained for

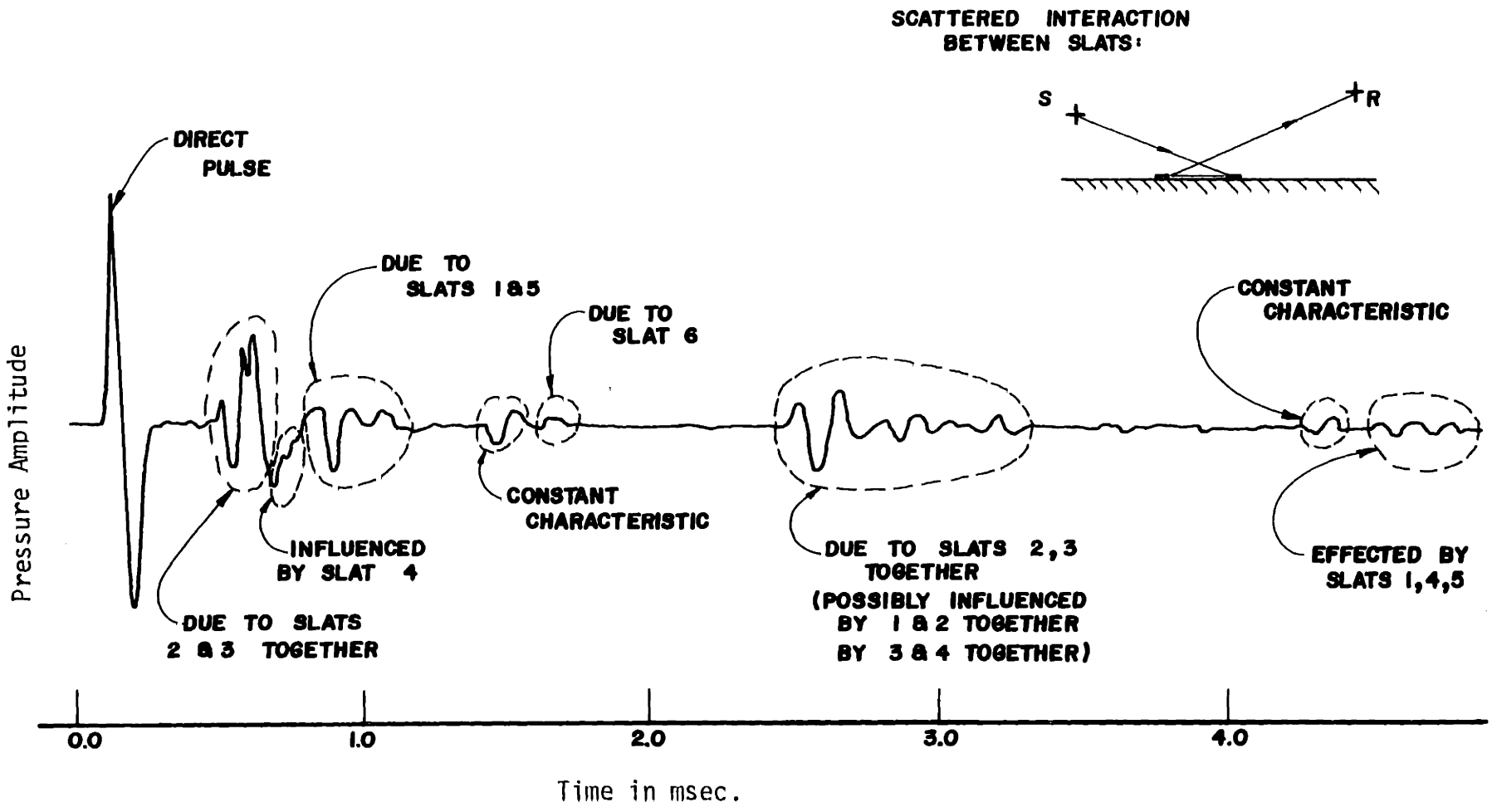

FIGURE 4.7: Time History of Scattered Refelction - Contribution of Specific Protrusions

1 1/2" x 1 1/2" protrusions are presented in Figure 4.8 for different specular reflection angles. In this figure, the pressure signal without protrusions is also presented in order that their effect can be studied.

4.3.2 Backscattering Experiments

The resultant pressure time histories for two of the surfaces studied in the backscattering experiments are presented in Figure 4.9. As for the forward scattering results, the pressure signal with no protrusions is also presented so that scattered contributions can be readily identified. The direct and specular components are indicated, but due to the averaging introduced by the plotter in its time sweep mode, their magnitude is severely reduced. It will be noted from the figure that the time in which scattered energy can be observed is limited by reflections from the test room walls.

As in the forward scatter case, the results from the backscatter experiments indicate variation for different configurations, but maintain a basic similarity. All the surfaces indicated that scattered energy was produced by a large segment of the surface. Further, angular dependence was indicated as the magnitude of the scattered energy from different protrusions varied more than can be attributed by path length divergence differences. As would be expected, the separation in time of the arrival of scattered energy was directly related to the physical separation of the protrusions.

4.3.3 Summary

To summarize the results of these experiments, several

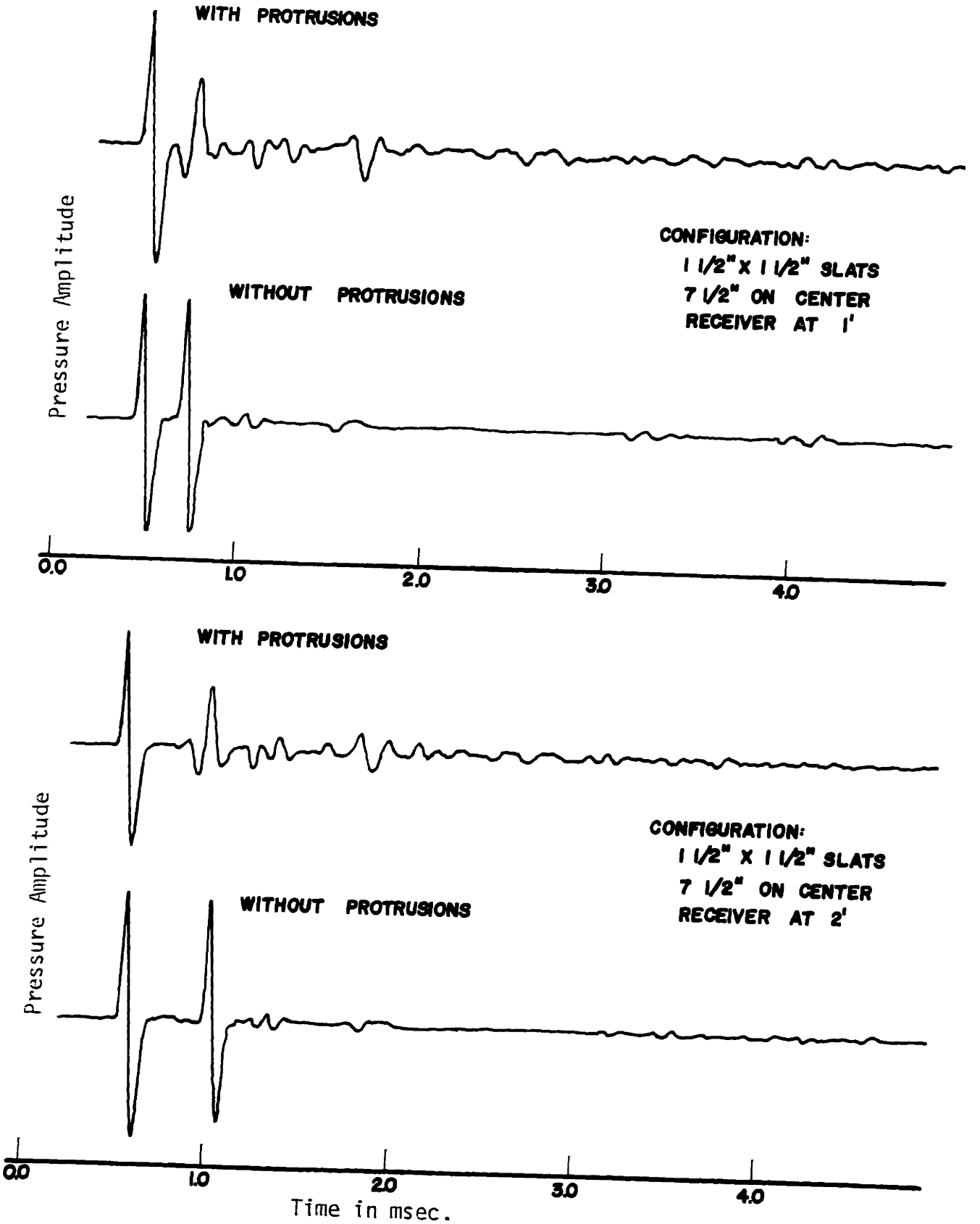

FIGURE 4.8: Time History of Scattered Reflection - Forward Scattering

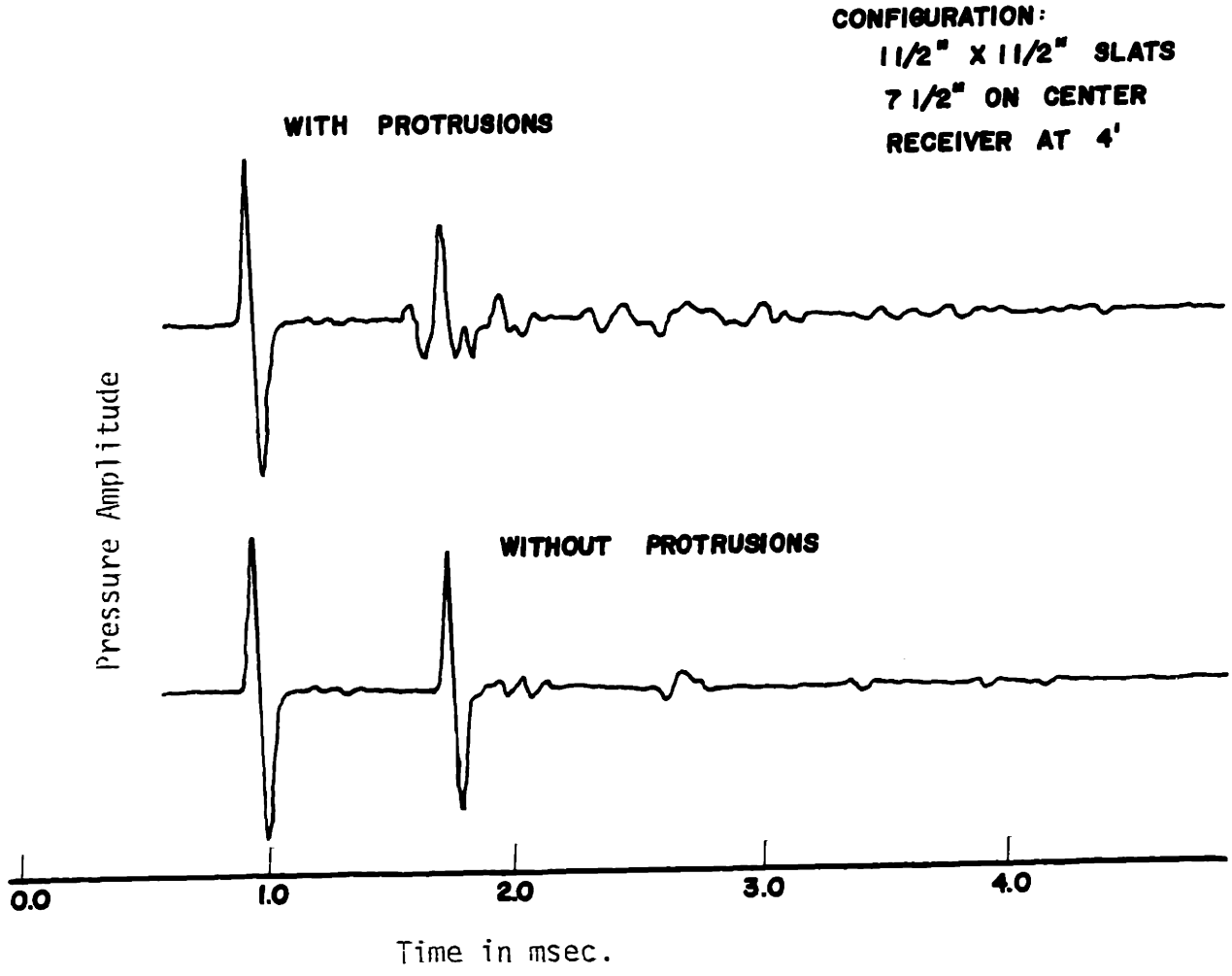

FIGURE 4.8: Time History of Scattered Reflection - Forward Scattering

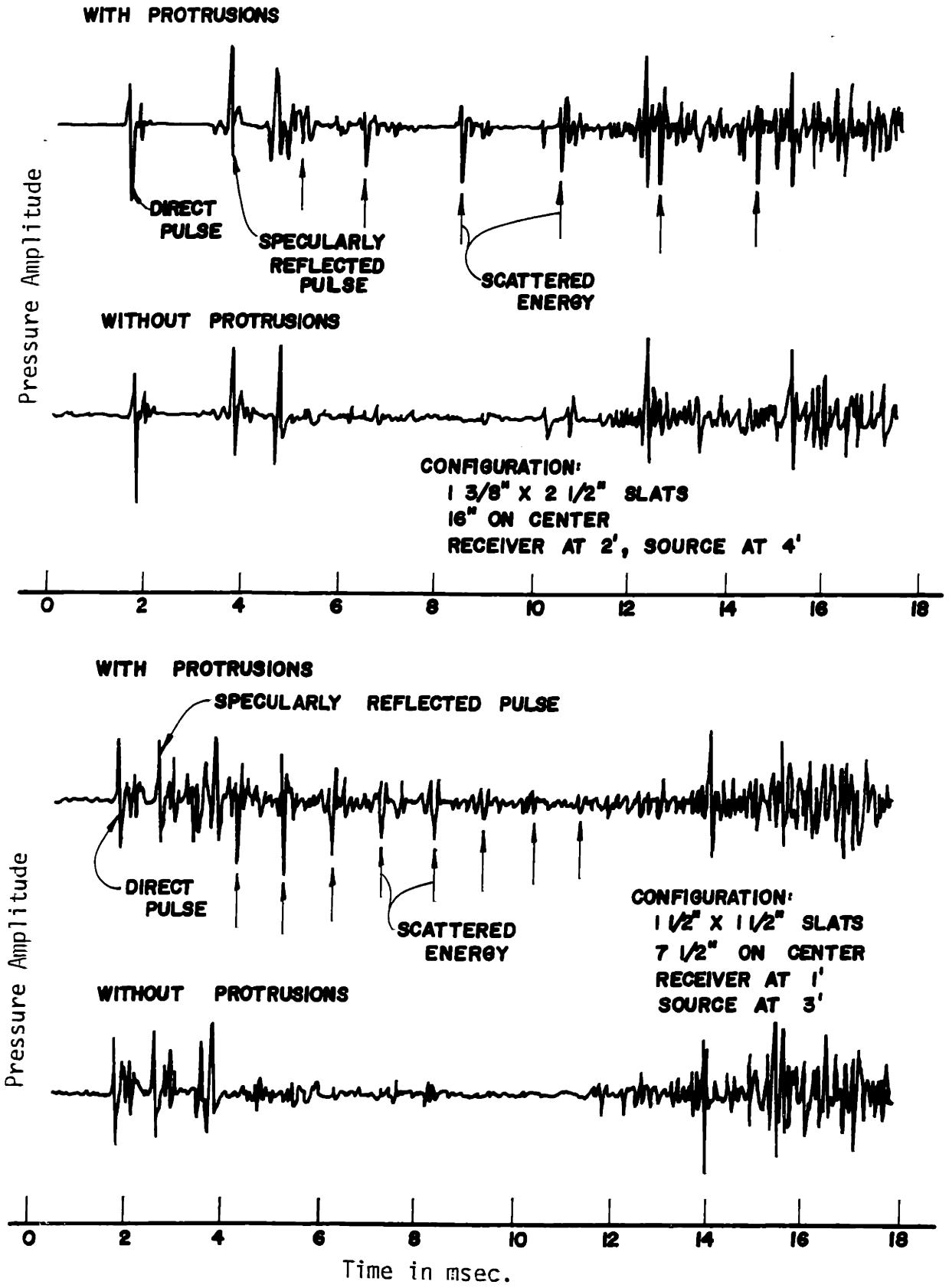

FIGURE 4.9: Backscattering From Surface Protrusions

qualitative conclusions can be drawn. Degradation of the specular component of reflection was found to occur which corresponds to an added absorption effect created by periodic protrusions. It was determined that a large portion of the surface played an active role in the reflection process and that scattered energy appeared from even the most distant protrusions. Angular dependence was also observed, but could not be quantitatively assessed in this experiment. Although some variation was observed for the surfaces studied, it was slight.

In terms of the two scattered reflection approximation theories described in Sections 3.3 and 3.4, the above conclusions are significant. The observation of the degradation of the specular component implies that there is physical basis for the first order approximation. The observation of appreciable scattered energy, however, indicates the limitations of a theory which only accounts for added absorption. By considering the pulse magnitudes it may be further concluded that when both the direct and specularly reflected pulses are present, the total scattered energy is relatively unimportant. When the direct pulse is not present and when the specular component has been reflected several times, these same relative magnitudes indicate that the second order approximation to scattering is necessary to adequately estimate the total sound level at a point.

A further conclusion which can be drawn from the backscatter experiments is that detailed quantitative measurements of the scattered field cannot be accurately made. This is due to the relatively small

amount of scattered energy produced by one protrusion for any one receiver point. Because of this limitation, the properties of the scattered field must be inferred from measurements which can be made. The measurement needed for determination of these properties is that of the energy from the surface specularly returned. If it is assumed that all energy which is not specularly returned goes into the scattered field or is absorbed at the surface, the properties can be readily determined. With the low absorption coefficients typical of building material, as an approximation, the absorbed energy can be ignored.

4.4 Reflected Energy Analysis

In order to estimate the effects of the geometric parameters on reflection from periodically irregular surfaces, a simplified reflection model was developed. The feature of irregular surfaces which was desired to be model was that of shadowing by protrusions. Because of this effect, portions of the surface are not directly illuminated by incident energy. If a high frequency or optical limit is assumed, the amount of energy which could be ideally, specularly returned by a cycle of the surface can be geometrically determined. Since the surface is periodic and if only incident plane waves are considered, the fraction of energy returned by one cycle is identical to that for the entire surface. The assumption of an optical limit ignores phase cancellation and addition effects and diffraction around the protrusions. The former assumption can be approximately met by considering a large band of frequency sufficient wide to average these effects. The reflection is then

assumed to be an energy addition process. For frequency bands in which the wavelength is considerably less than the protrusion height, diffraction effects will be minimal. Since these conditions are nearly met by the urban noise scattering problem, for those octave bands above the band with the $\lambda/4$ resonance, some correspondence may be expected for those cases.

The expression found for the fraction of reflected energy is presented in Figure 4.10(a) along with the geometry used to obtain it. There are several interesting aspects of this expression. First, it should be noted that there is no dependence on the distance between protrusions, the parameter "a". Further, there is an angle of incidence, θ, such that further reduction produces no change in R, the reflected energy. The geometry of this limitation is given in Figure 4.10(b) along with the expressions for the angle of occurrence and the minimum value of R. Examination of these expressions indicates that R_{min} is not a function of h, the step height, and that θ_{min} is not a function of ℓ, the protrusion period parameter.

The calculated values for R can be used to study the surface variables parametrically in plots of R as a function of grazing angle. The effect of protrusion width is presented in Figure 4.11. From this figure it is seen that for angles greater than θ_{min} any particular value of width yields the same value of R. The values of R_{min} are seen to increase with increasing step width and thus are all different. In Figure 4.12 the dependence of R on protrusion height is displayed. This

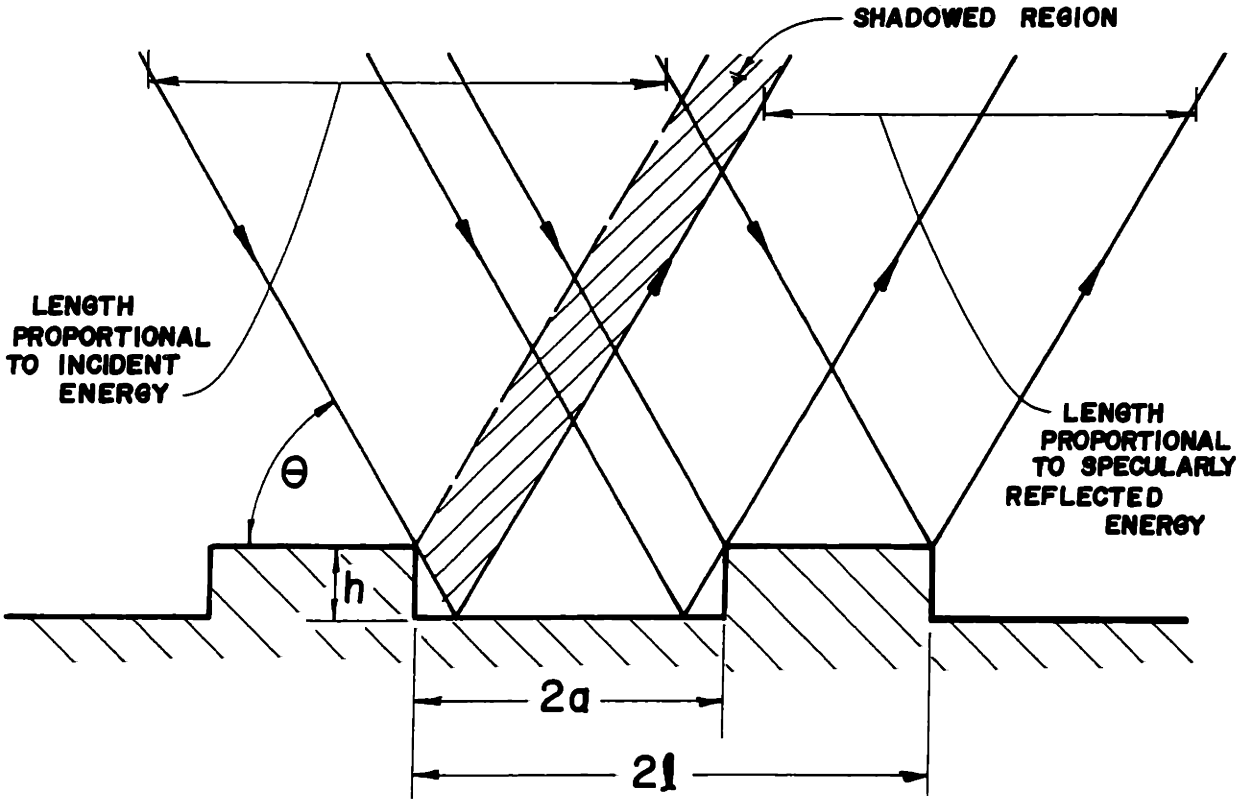

$$\text{REFLECTION RATIO} - \quad R = \frac{2\ell - 2h \cdot \cot\theta}{2\ell}$$

MINIMUM RATIO CASE:

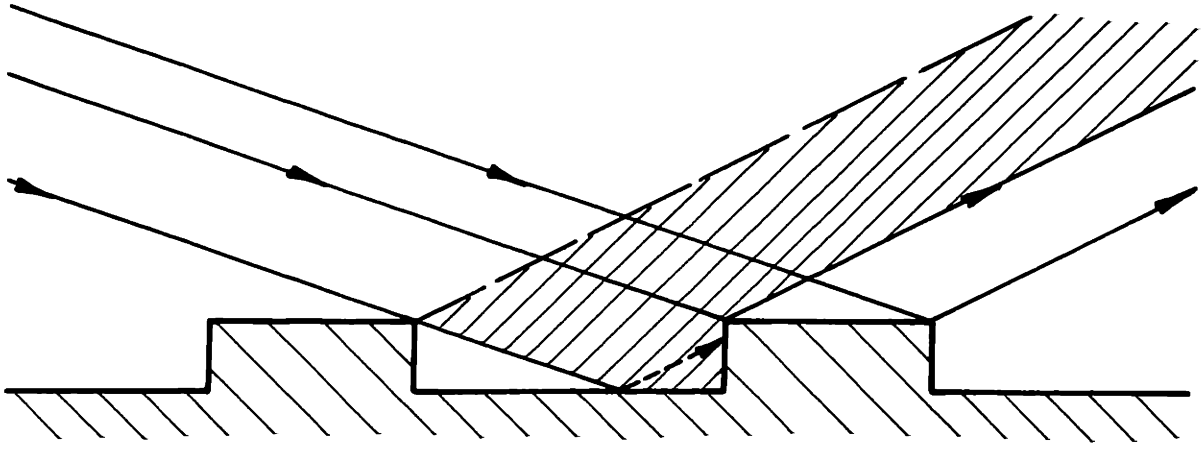

$$R_{MIN} = \frac{2\ell - 2a}{2\ell} \qquad \theta_{MIN} = \tan^{-1}\frac{h}{a}$$

FIGURE 4.10: Formulation of Reflected Energy Approximation

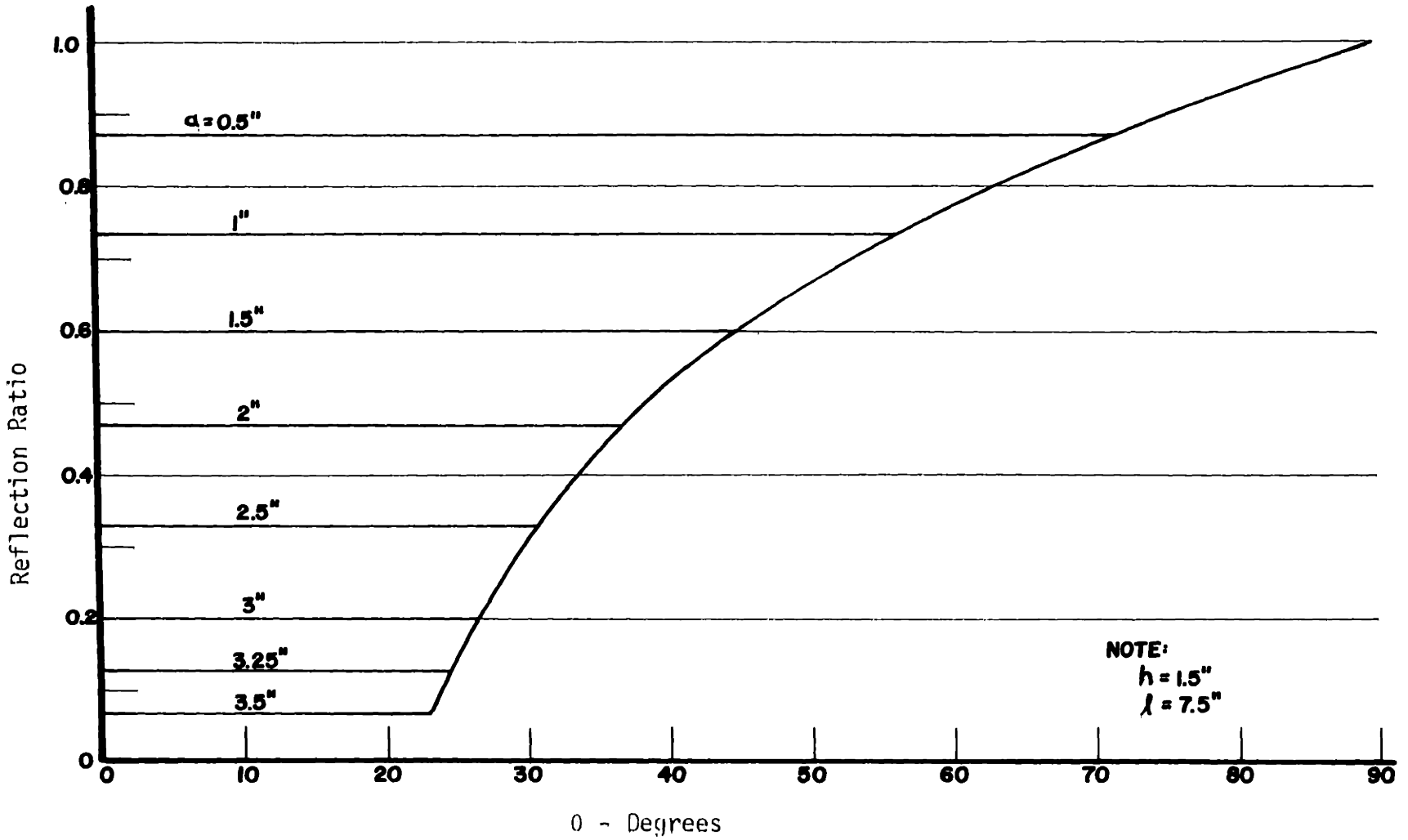

FIGURE 4.11: Variation of Reflected Energy with Protrusion Width

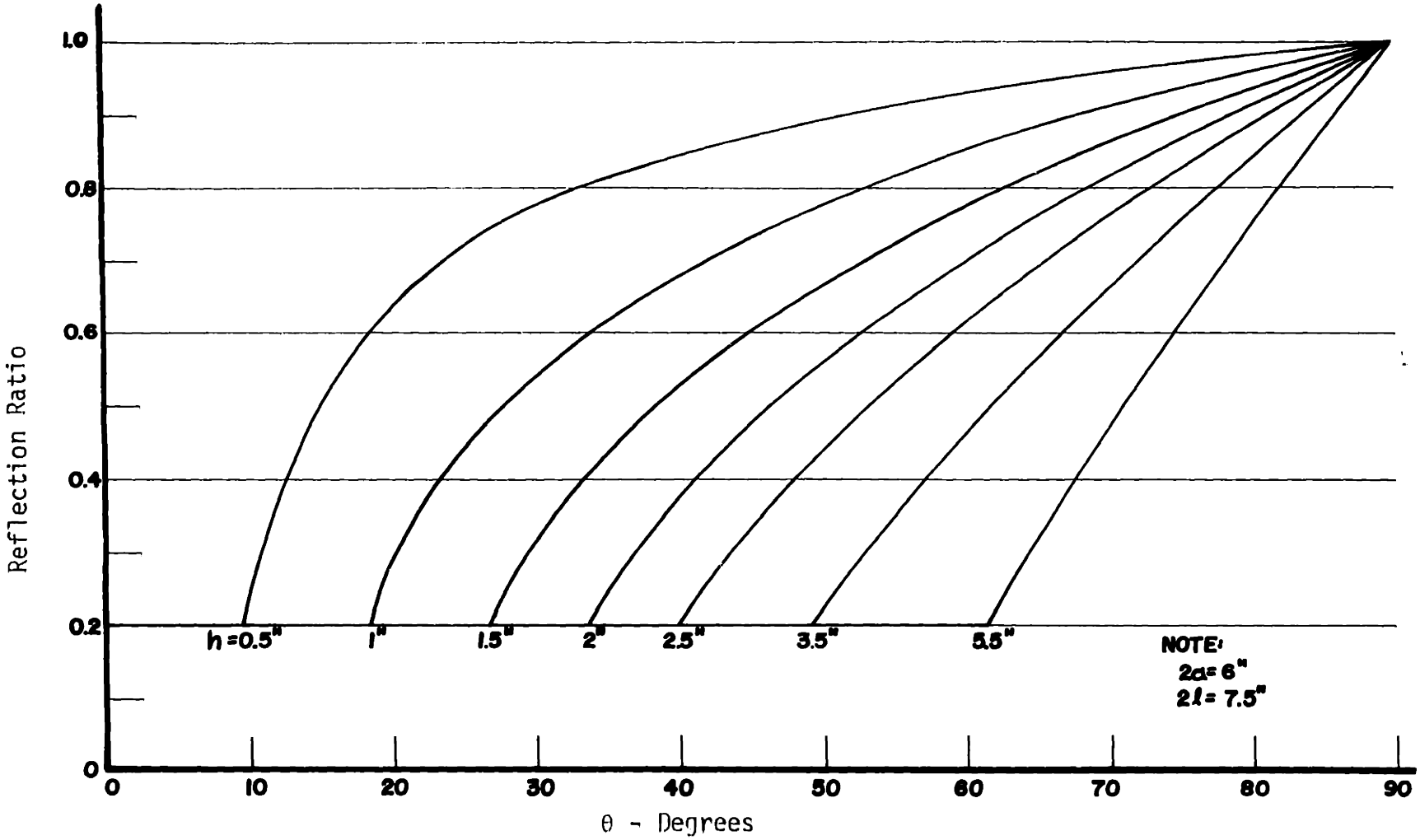

FIGURE 4.12: Variation of Reflected Energy with Protrusion Height

figure indicates that the functional relation between R and Θ is different for each value of height until Θ is less than Θ_{min}. For any one value of Θ, the value of R increases with decreasing step height. The value of Θ_{min}, however, decreases with decreasing step height. The final dependence examined was that on protrusion spacing shown in Figure 4.13. The behavior of this parameter displays characteristics of both of the previous two dependencies. For values of Θ larger than the largest Θ_{min}, R increases with increasing spacing. For values of Θ smaller than the smallest Θ_{min}, R_{min} decreases with increasing spacing. For values of Θ in between these two, there is a combination of these two behaviors.

4.5 Experimental Determination of Specular Reflection Ratio

4.5.1 Reflection Ratio Measurement

In order to adequately formulate a surface scattering model to be used for urban noise propagation assessment, quantitative 1:8 model experiments were conducted similar to the qualitative experiments discussed in Section 4.3. The experiments were designed to determine the amount of energy from the surface specularly returned. The dependence of the reflected energy on grazing anble and protrusion geometry were also to be determined. The measured reflected energy when properly averaged could also be compared to the results predicted by reflected energy analysis.

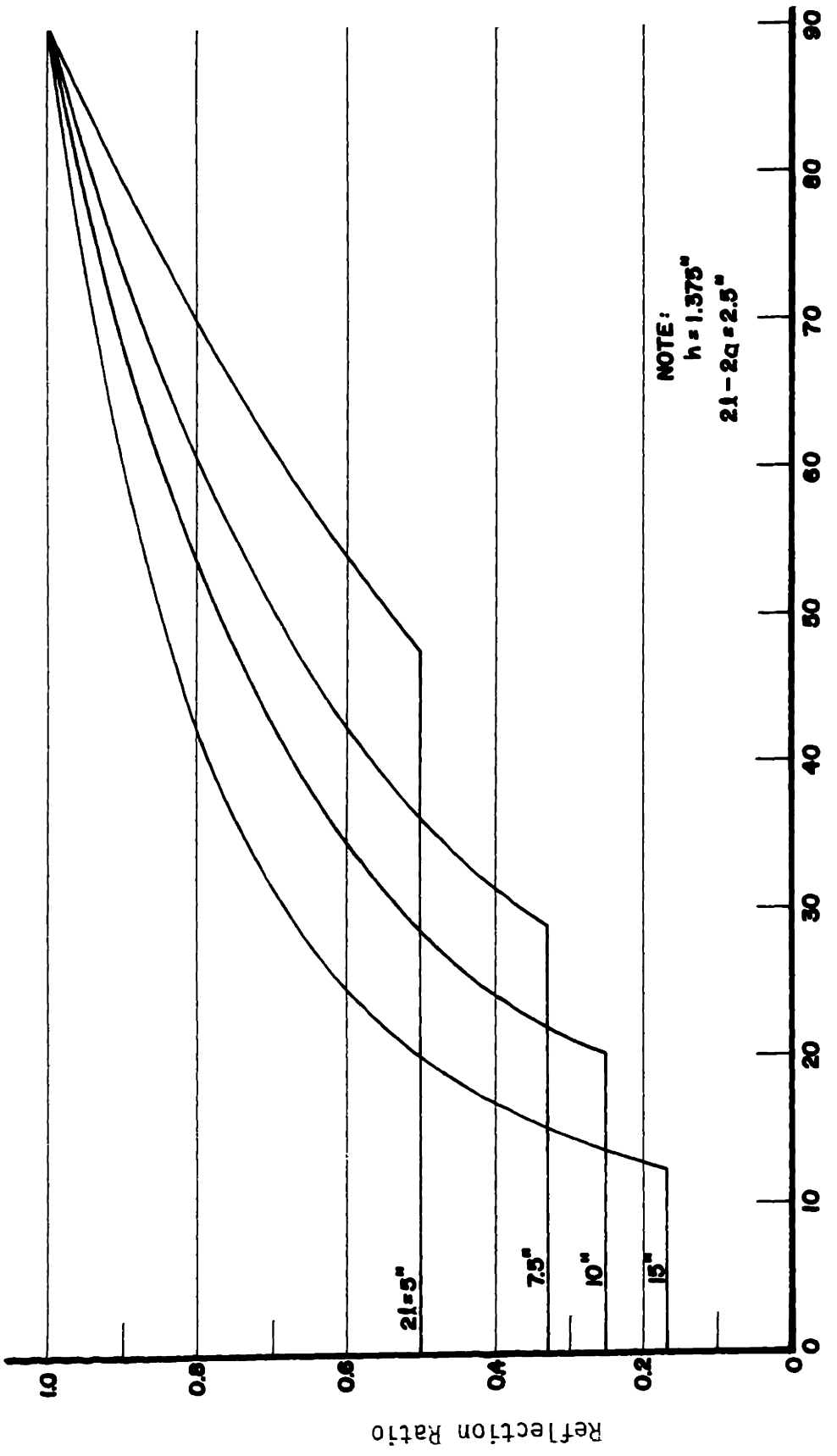

FIGURE 4.13: Variation of Reflected Energy with Protrusion Spacing

The instrumentation used to measure specularly reflected energy is given in Figure 4.4. The instrumentation is identical to that used for qualitative experiments except for the addition of a minicomputer and teletype. The computer was used to take fast Fourier transforms of the pressure signal. The energy spectra for the FFT were expressed logarithmically in octave bands. Octave bands centered at 2, 4, 8 and 16 kHz were used.

The procedure used in these experiments was developed to yield data which could be processed into a surface average reflection ratio. Data was taken by holding the source-receiver separation constant and together moving them incrementally through one cycle of the surface. The cycle or period of the surface was divided into from 5 to 10 increments depending on the size of the period. At each increment, the direct pulse along and the specularly reflected pulse without the direct were measured. A sampling time of 2 milliseconds was used on the transient recorder in order to minimize the scattered contamination of the specular energy, yet still provide adequate performance of the FFT in the lowest frequency band. Breaking up of the direct and reflected energy does produce some error particularly for near grazing incidence. However, due to the reduced energy in the reflected pulse relative to the direct, this technique was preferable to subtracting direct pulse energy from the total energy. In order to minimize the standard deviation of the measurement at each increment point, ten sparks were averaged in the computer for both the direct and specularly reflected pulses.

This technique produced standard deviations from the experimental average at each point of from .2 to .75 dB depending on the frequency. This implies a standard deviation for the reflected energy ratios of about .1 to .15.

The test configuration used was similar to that of the qualitative, forward scattering experiments as illustrated in Figure 4.5(a). The spark noise source was kept at 1 1/2 ft from the surface while the receiver height was varied to achieve different incidence angles for the specular component. In this manner, data was obtained for angles of 11.8, 20.6, 36.9, 51.3, 71.6 degrees where grazing incidence is taken to be 0 degrees. The surface geometries examined were chosen to include the range of parameters which are typically displayed in urban architecture. The three parameters of protrusion height, width and spacing were varied in order than any functional dependences could be observed. The nine surfaces tested are detailed in Figure 4.14.

The results from the experiment are expressed in the ratio of energy specularly reflected from the surface to the incident energy. Incident energy was determined from the direct pulse which was corrected for divergence to correspond to the reflected path length. The ratios were determined using the energy of the direct and reflected components. The ratios obtained for each increment of a surface cycle were averaged to produce the average reflected energy ratio. It should be noted that over a given cycle considerable variation in the reflection ratio

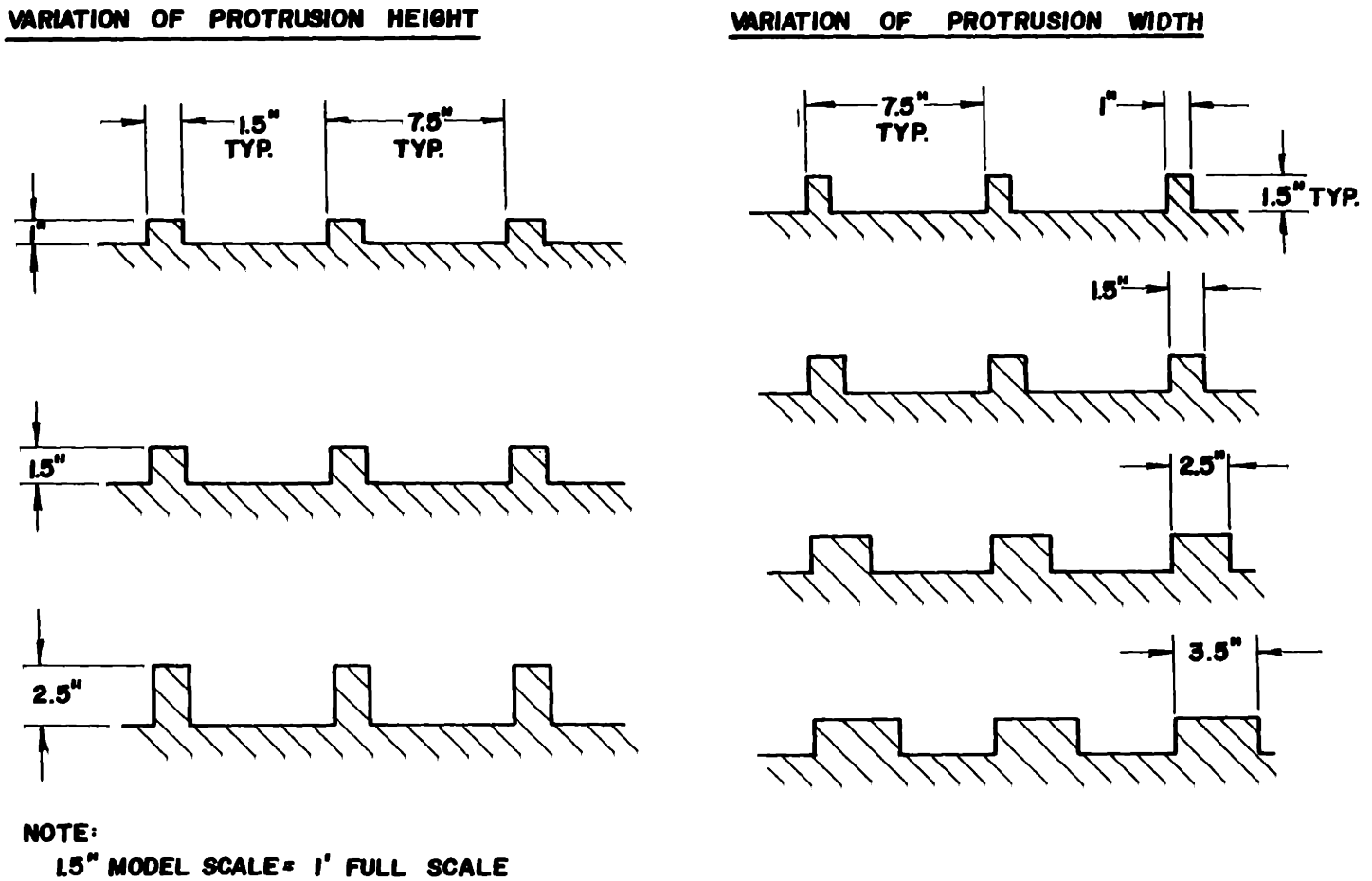

FIGURE 4.14: Surface Geometry for Reflection Ratio Measurements

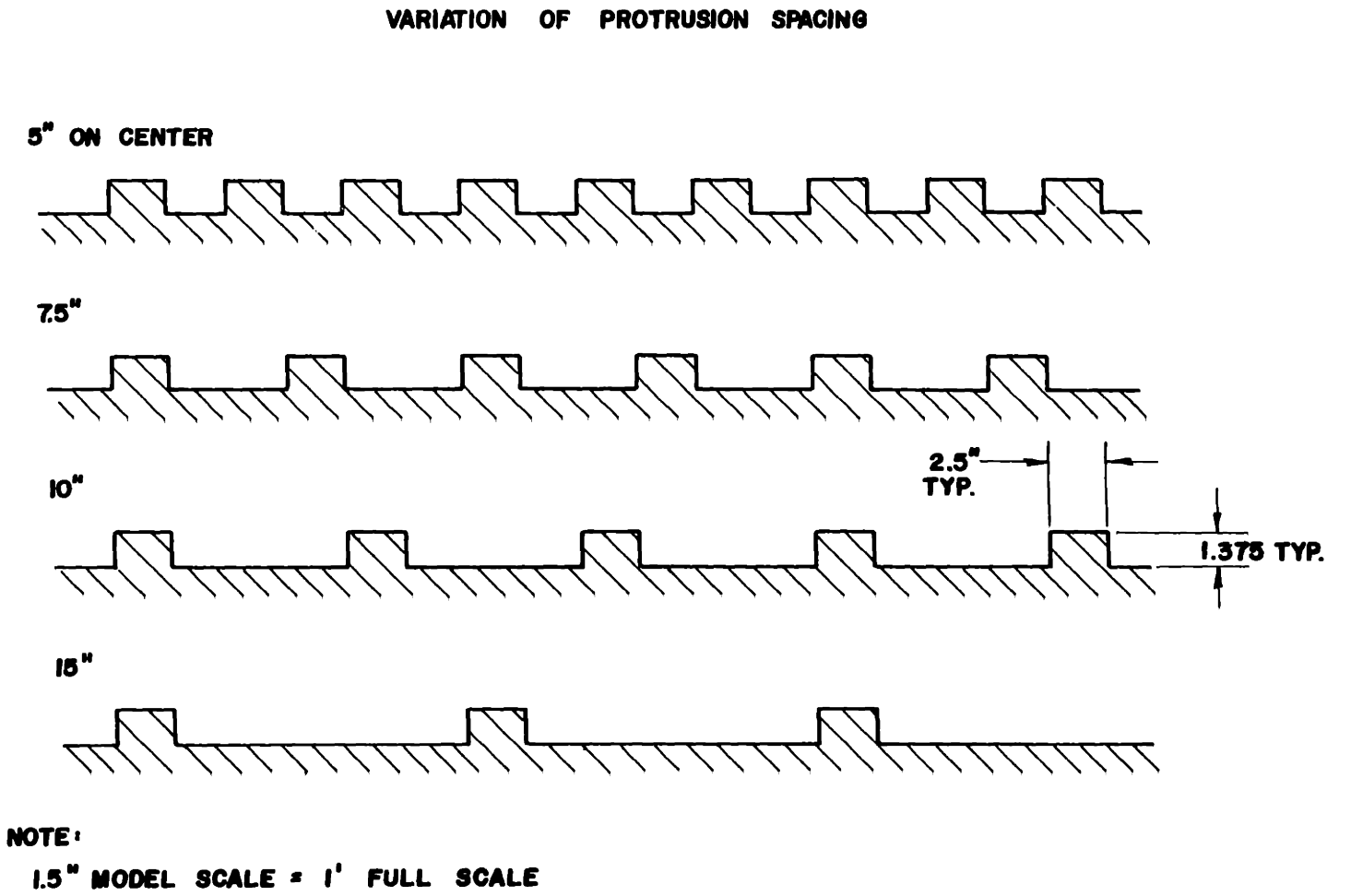

FIGURE 4.14: Surface Geometry for Reflection Ratio Measurements

was observed.

4.5.2 Parameter Dependence of Reflection Ratio

Experimental results indicating the variation of average reflection ratio with surface parameters are presented in Figures 4.15 to 4.17. For all plots, the grazing angle, θ, is a parameter. Reflection ratio as a function of protrusion height is plotted in Figure 4.15 for the four experimental frequencies. It will be observed that generally there is a reduction in reflection ratio with increasing height. This is consistent with the observation made with the reflected energy analysis of Section 4.4. The exception to this occurs in the 2 kHz octave band where reflection ratio increases with step height. This is apparently due to the $\lambda/4$ resonance phenomenon as $\lambda/4$ is about 1 1/2" in this band which corresponds to the intermediate protrusion height. As would be expected, as the height increases, the resonance effect decreases producing a higher value of reflection ratio. The relationship between reflection ratio and protrusion width is presented in Figure 4.16. This figure indicates that there is generally little dependence of reflection ratio on protrusion width. Intuitively, this result is anticipated. Because steps in the surface are responsible for relative phase shifting, it is expected that scattering is more strongly dependent on the number of steps per wavelength rather than on the position of their occurrence. This result was also predicted by the reflected energy

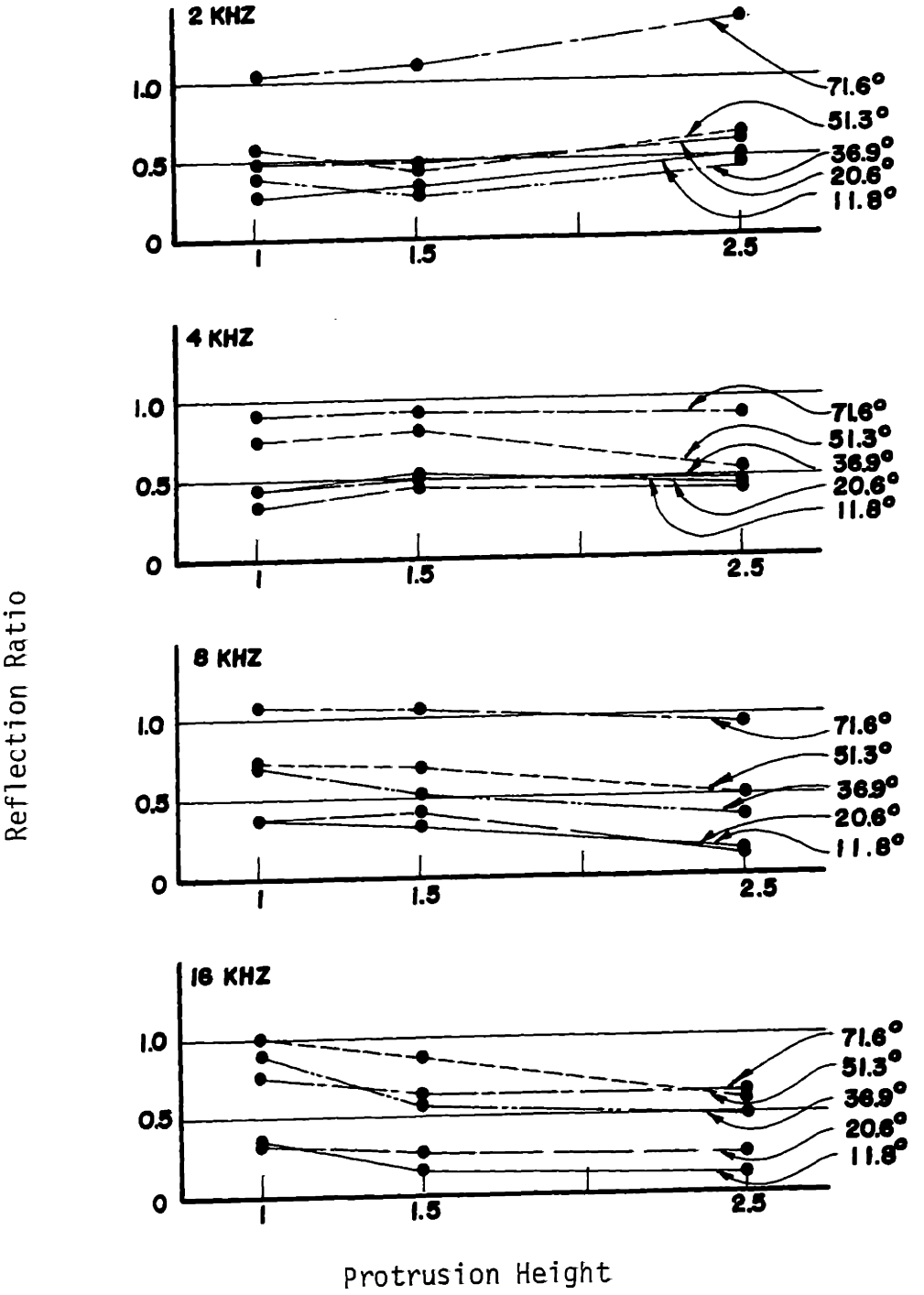

FIGURE 4.15: Variation of Measured Reflection Ratio with Protrusion Height

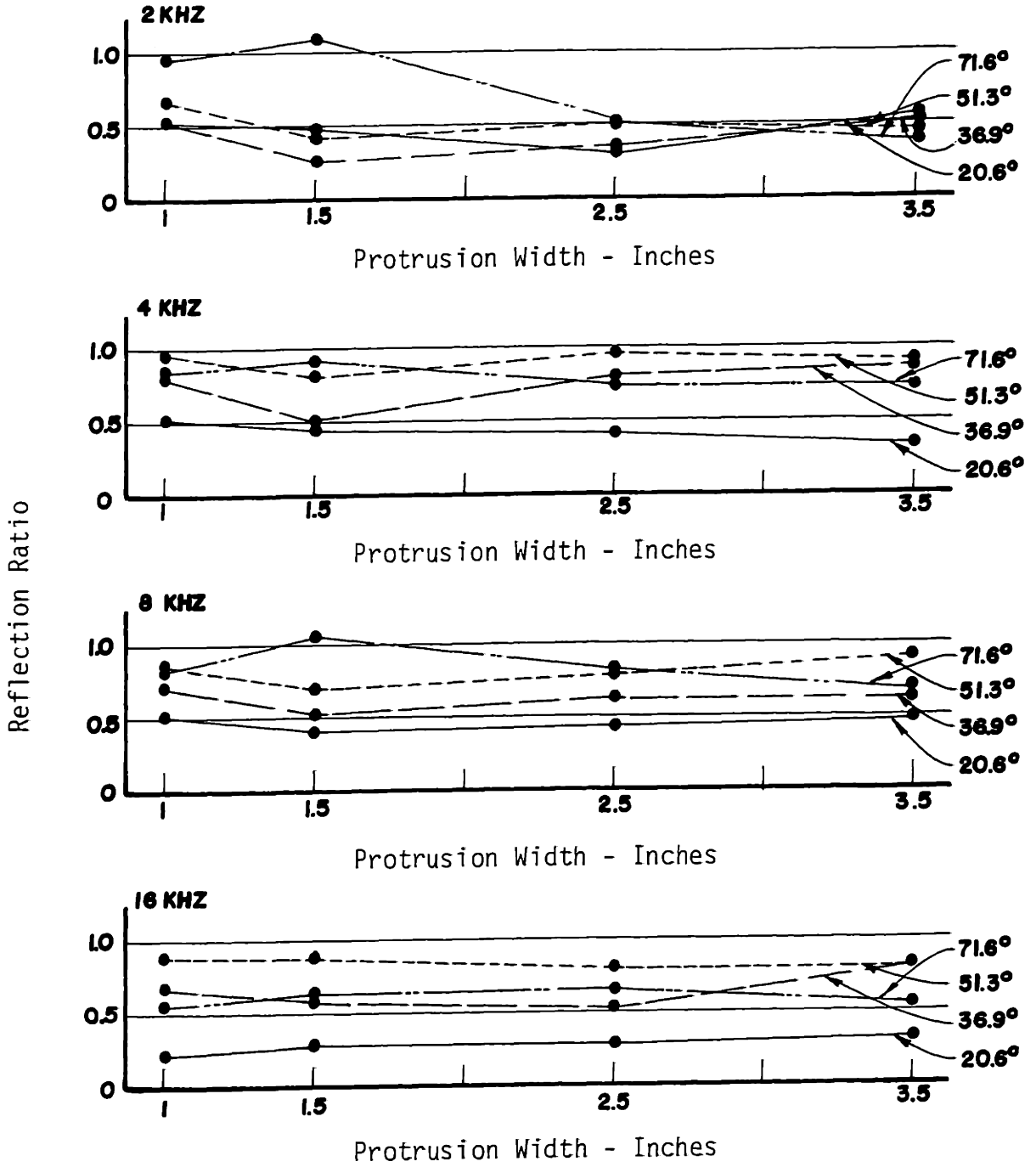

FIGURE 4.16: Variation of Measured Reflection Ratio with Protrusion Width

analysis of Section 4.4. The final parameter dependence of protrusion spacing is examined in Figure 4.17. The results for this parameter indicate some, but not appreciable, variation in reflection ratio with spacing. Also included in this figure are results calculated with reflected energy analysis. It will be observed that there is reasonable agreement between these predicted results and the experimental for the 4 and 8 kHz octave bands.

Another method of considering the experimental results is to plot reflection ratio as a function of grazing angle with the surface variables as parameters. Such plots are presented in Figure 4.18 for each of the three sets of surface variables and each frequency band, 2 through 16 kHz. From this figure it is seen the variation of reflection ratio with grazing angle is the most pronounced and consistent of the four possible parameters. Also included with these plots are corresponding results calculated using reflected energy analysis. It will be observed that there is generally good correspondence between the analysis results and the measurements both in angular and parametric dependence. For the 2 kHz band where $\lambda/4$ resonance effects are present, there is, however, only limited correspondence between the two sets of results. Considering the extreme simplifications made in developing reflected energy analysis, and remembering the experimental 10 to 15% standard deviation for the measured ratios, there is remarkable agreement between the analysis and the measured values if the 2 kHz is excluded.

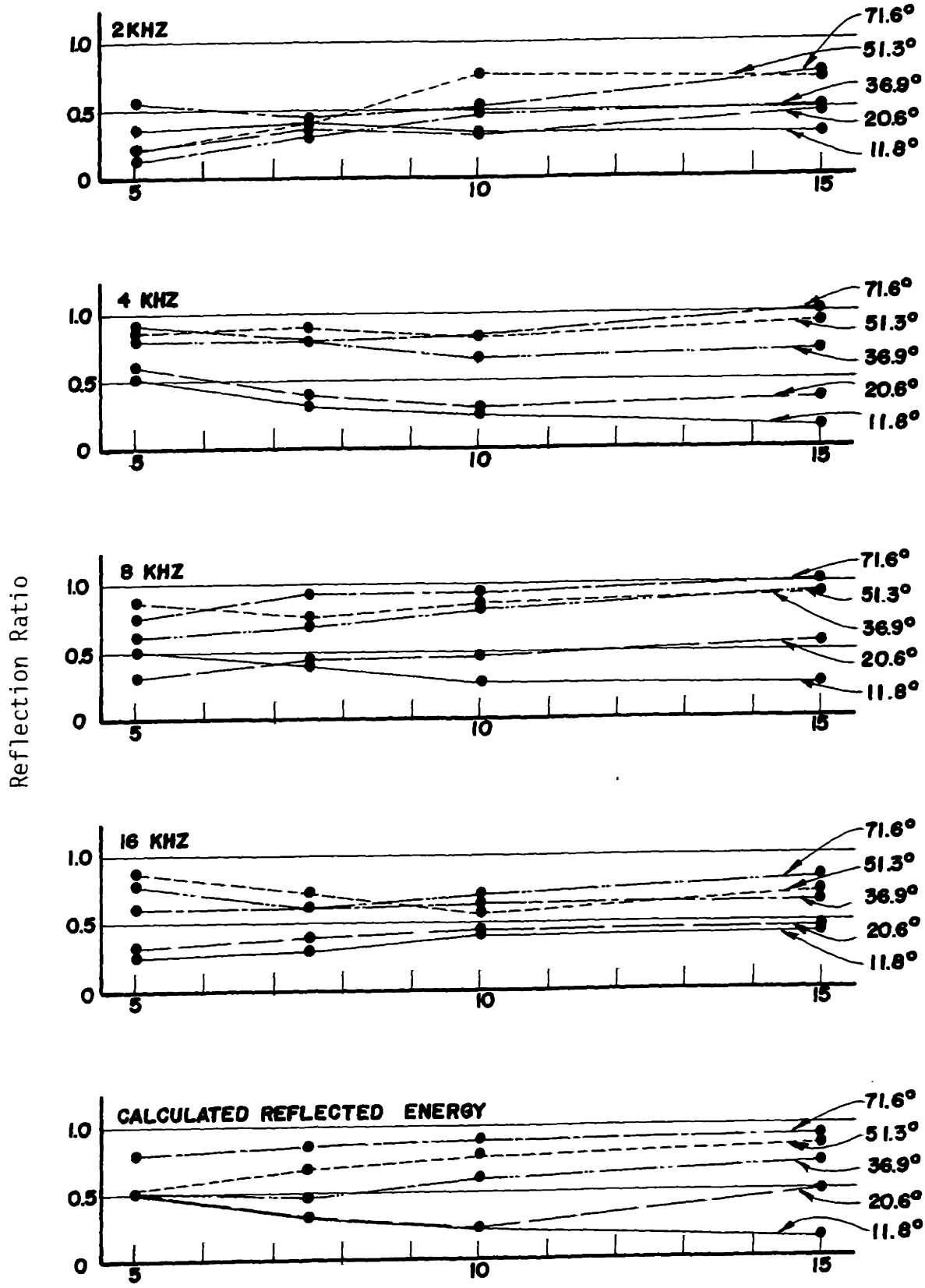

FIGURE 4.17: Variation of Measured Reflection with Protrusion Spacing

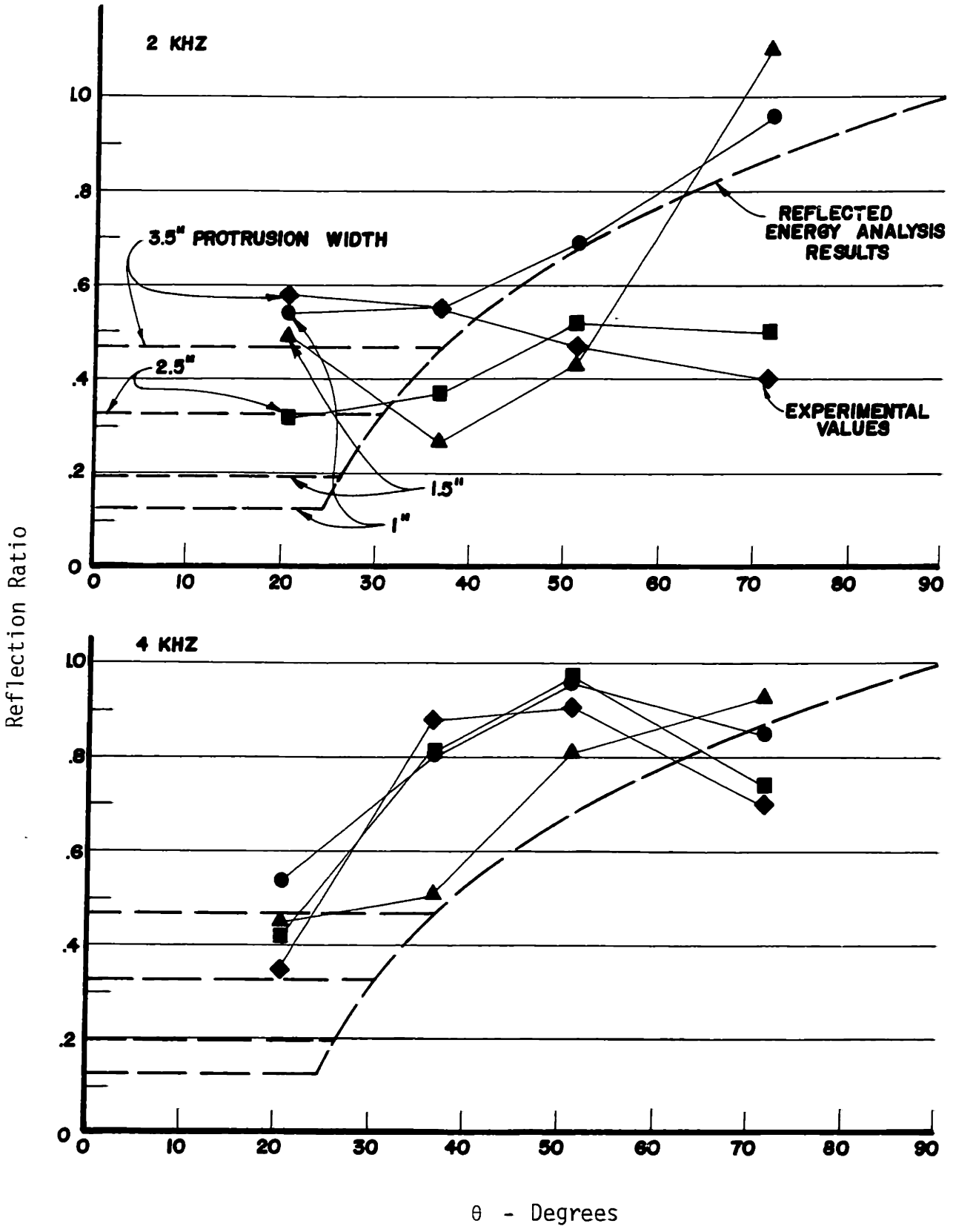

FIGURE 4.18: Variation of Measured Reflection Ratios with Grazing Angle

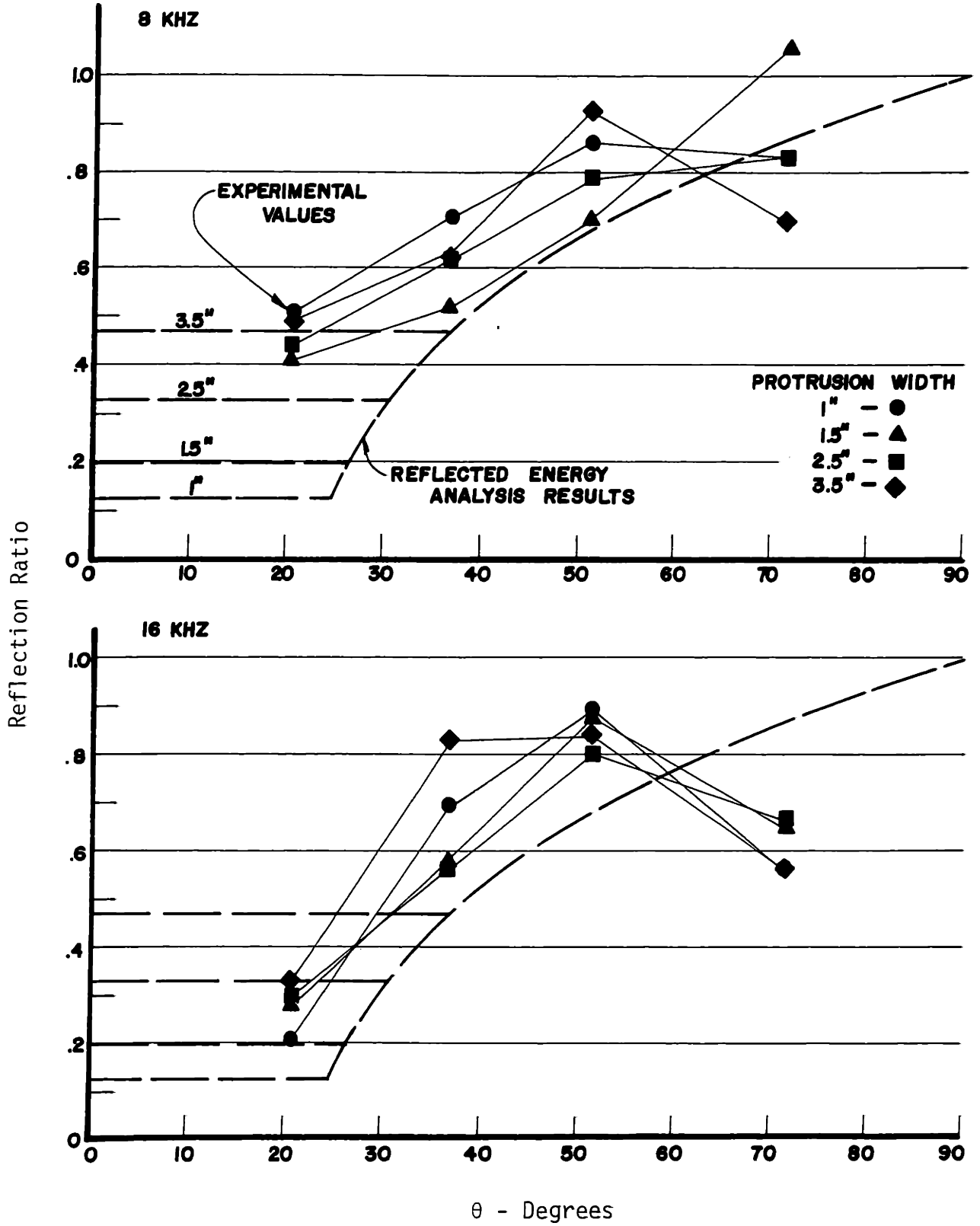

FIGURE 4.18: Variation of Measured Reflection with Grazing Angle

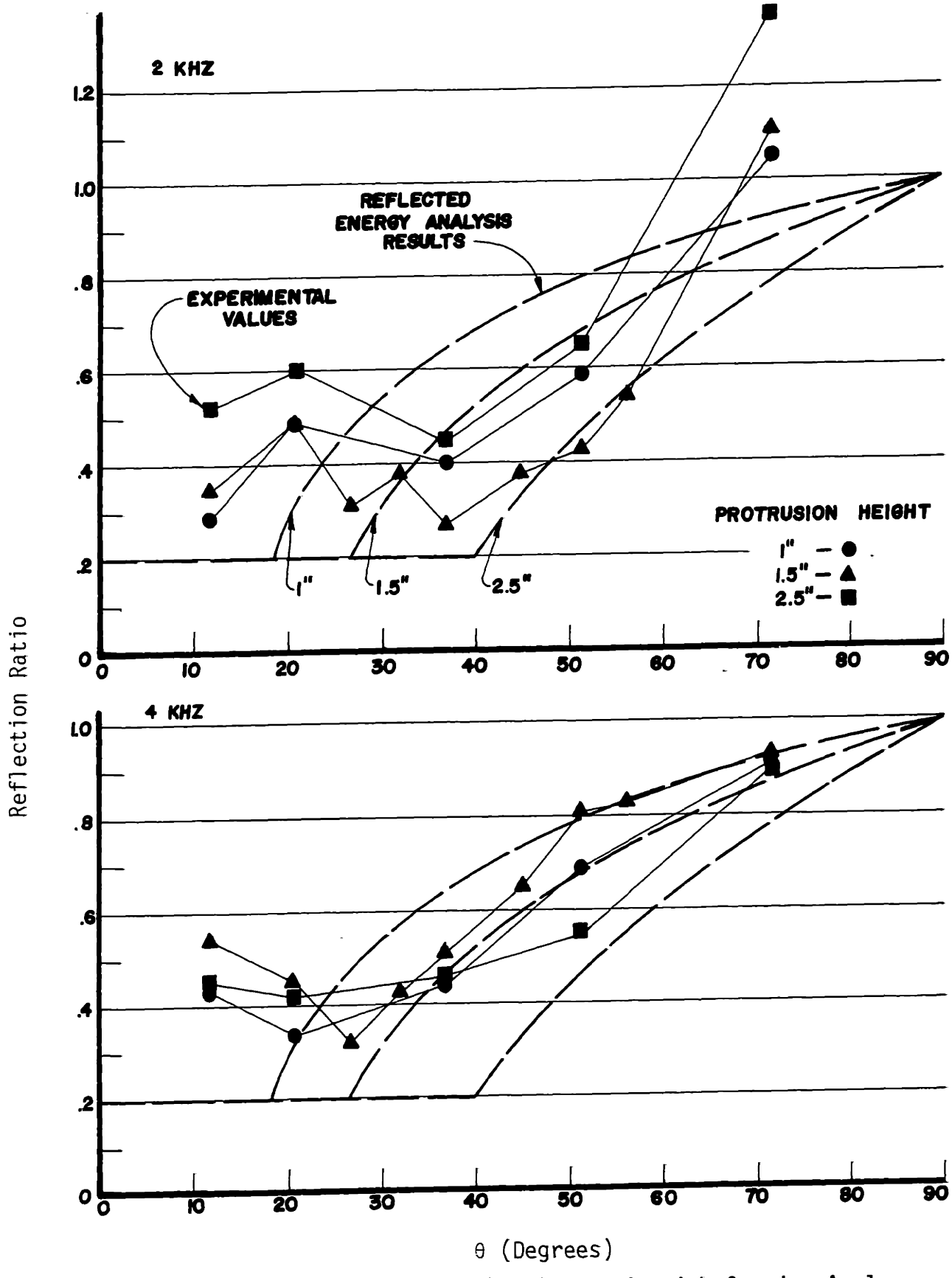

FIGURE 4.18: Variation of Measured Reflection Ratio with Grazing Angle

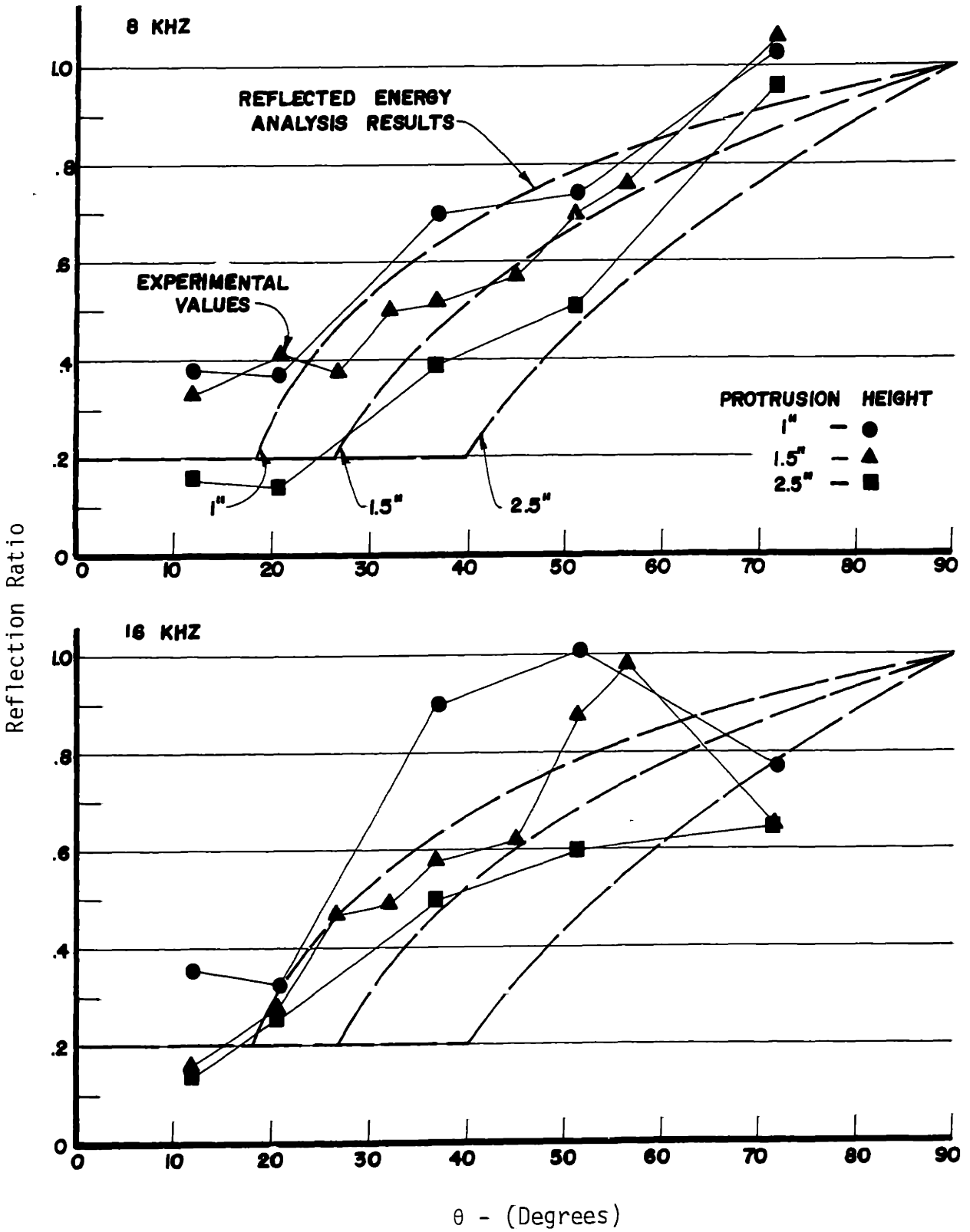

FIGURE 4.18: Variation of Measured Reflection Ratio with Grazing Angle.

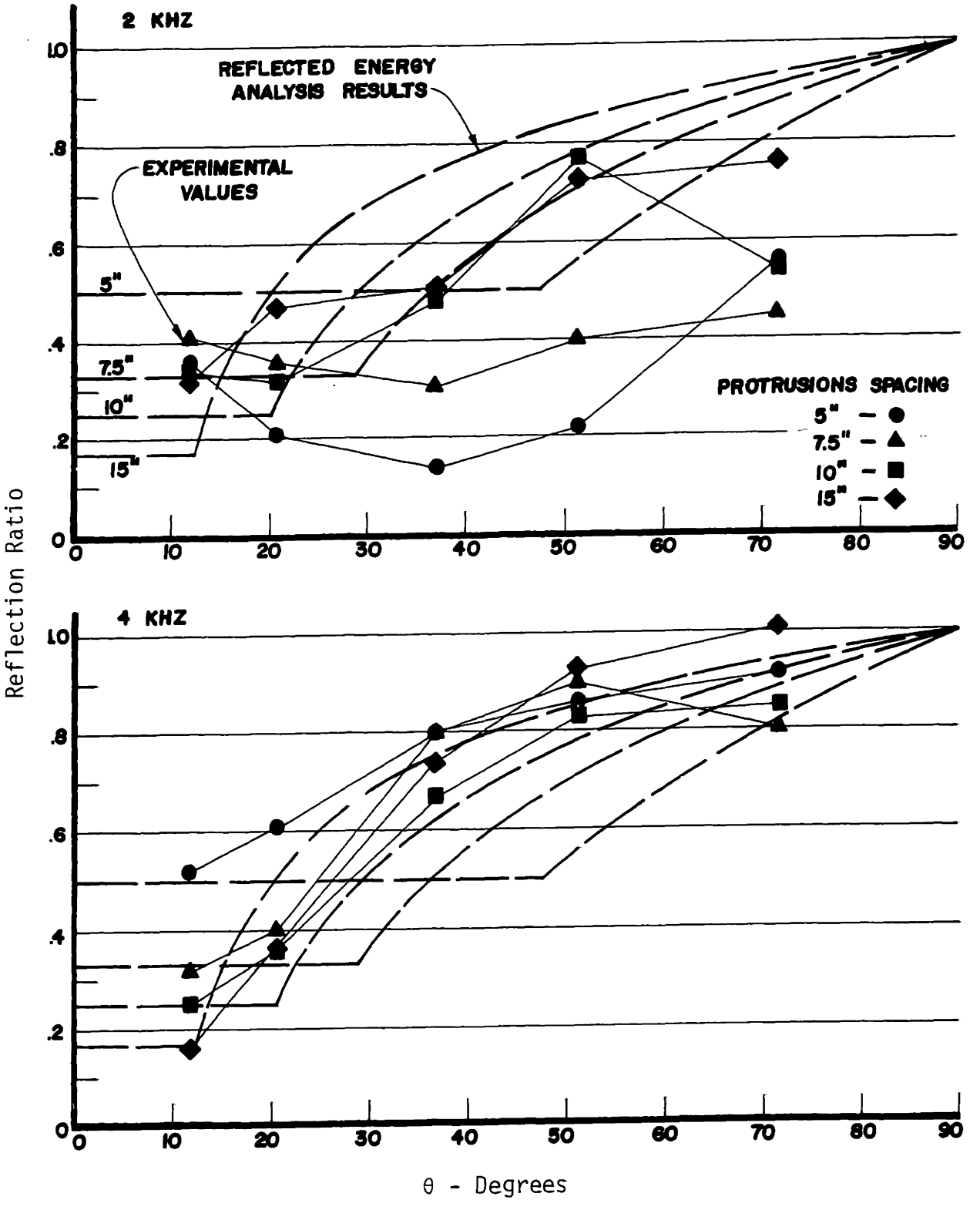

FIGURE 4.18: VARIATION OF MEASURED REFLECTION RATIO WITH GRAZING ANGLE

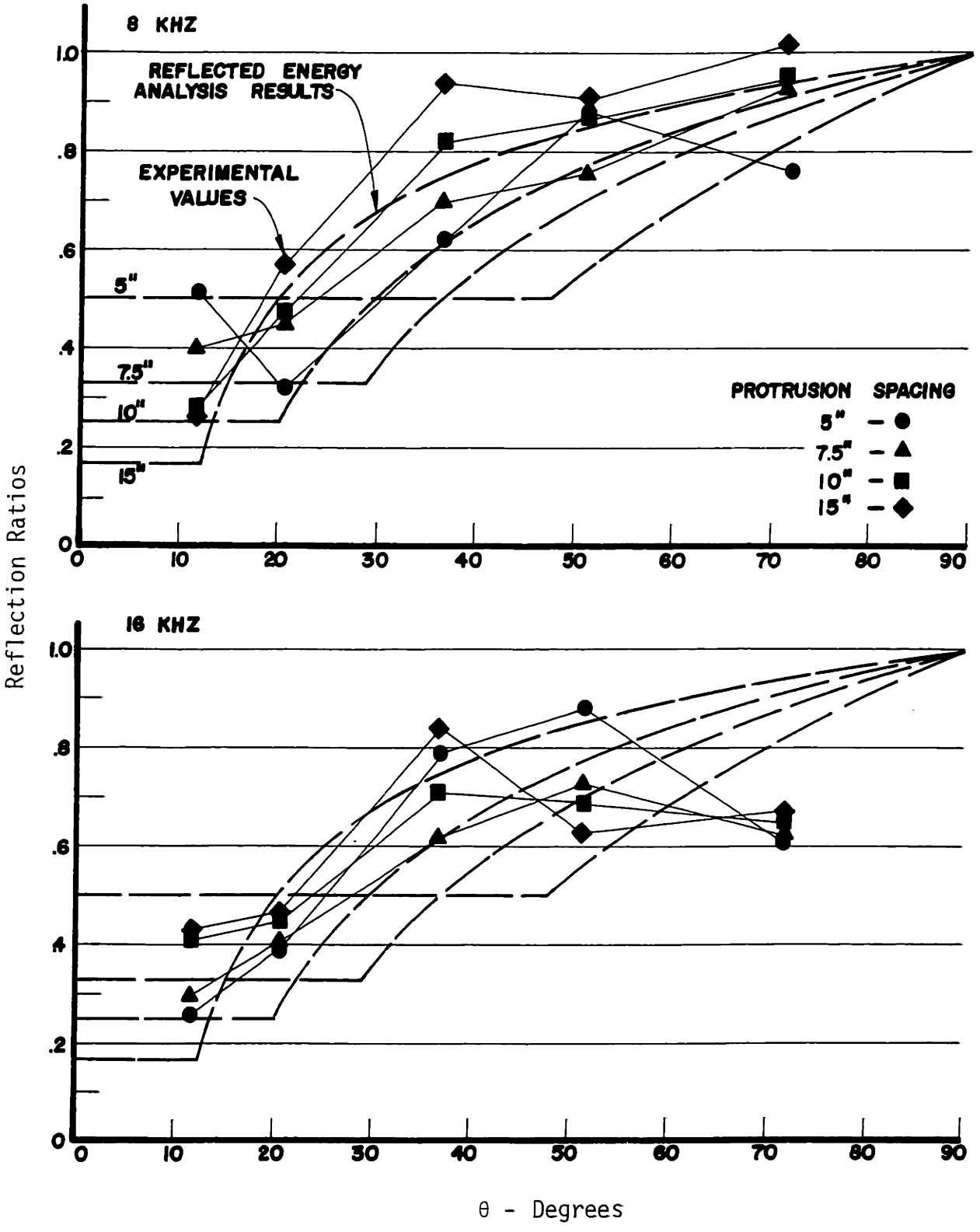

FIGURE 4.18: Variation of Measured Reflection Ratios with Grazing Angle

As noted in regard to Figure 4.18, the most pronounced dependence for surfaces typical of the urban problem is that of reflection ratio with angle. This suggests the retention of angular dependence and the exclusion of surface variable dependence for the development of a scattering model widely applicable to urban propagation. By averaging the reflection ratios over the nine surfaces investigated at each angle and frequency, such exclusion of surface parameters was made. In performing this average, it is important to consider the uncertainty introduced by the simplification. In Table 1, the results of the surface average are presented along with the corresponding standard deviations for each angle and frequency. The expected value of the reflection ratio is also plotted versus incident angle in Figure 4.19. It should be noted that the standard deviations of Table 1 typically ran from .1 to .15. This deviation is the same as that due to measurement themselves implying an uncertainty no greater than the experimental. From Figure 4.19, it will be noted that reflection ratio surface averages are very nearly equal for the 4, 8 and 16 kHz bands. These values fall within .1 of each other everywhere except 71.6° at 16 kHz. Further, the 2 kHz band is also seen to fall within this limit except at 36.9° and 51.3°. The large deviation at these angles in the 2 kHz band is probably due to the $\lambda/4$ resonance phenomenon. For this band, the protrusion depths vary from 1 to 2 1/2 inches and the quarter wavelength at this frequency is 1.69 inches.

With the noticeable lack of frequency dependence in the 4, 8 and 16 kHz bands for the surface average reflection ratios of Figure 4.19, an

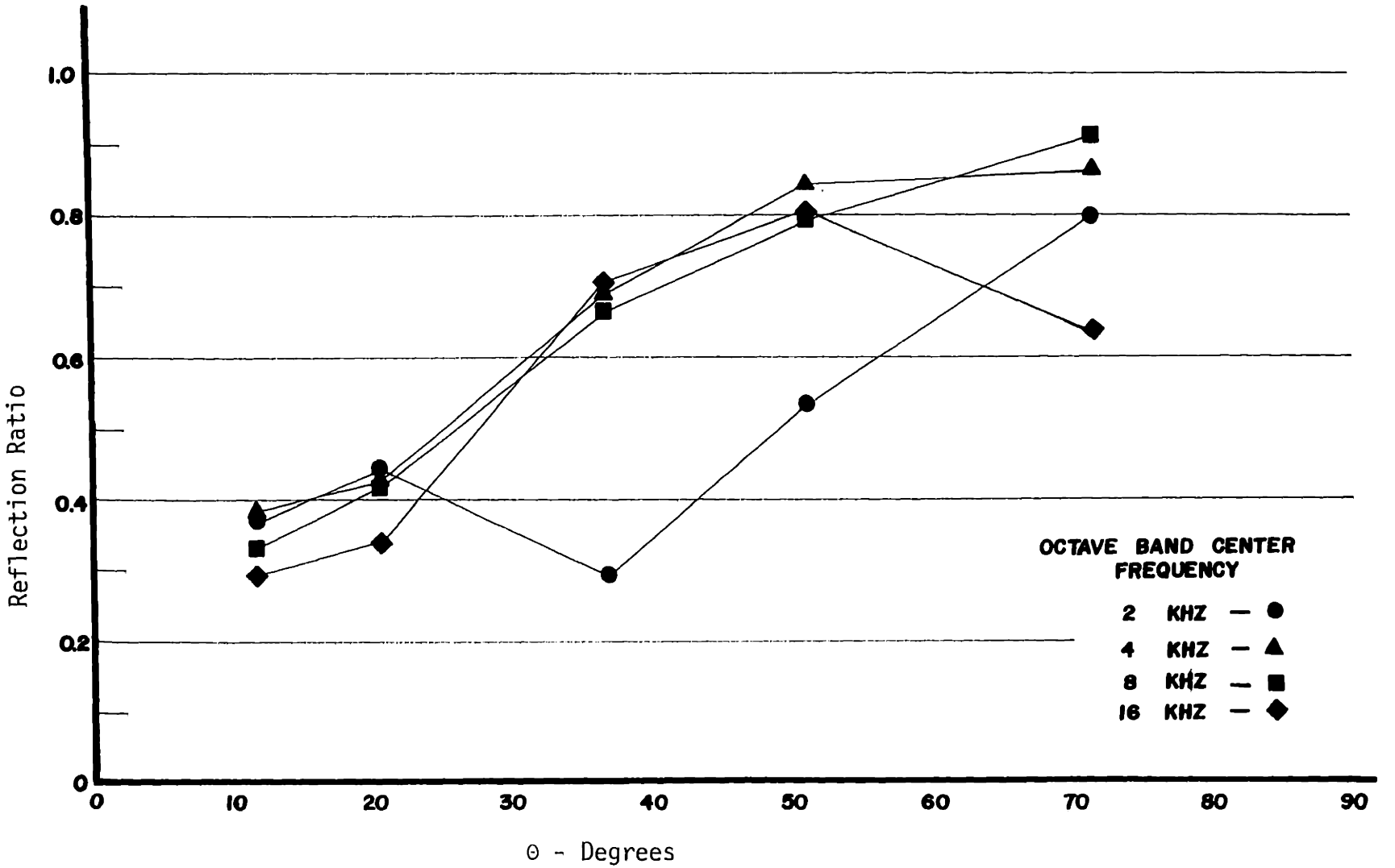

FIGURE 4.19: Measured Reflection Ratios: Averaged for all Surfaces

TABLE I

REFLECTION RATIO AVERAGED FOR ALL SURFACES

Octave Band Center Frequency	Incidence Angle	Reflection Ratio Expected Value	Standard Deviation
2 kHz	11.8°	.37	.07
	20.6°	.44	.12
	36.9°	.39	.13
	51.3°	.54	.16
	71.6°	.80	.32
4 kHz	11.8°	.38	.13
	20.6°	.43	.08
	36.9°	.69	.15
	51.3°	.85	.12
	71.6°	.87	.08
8 kHz	11.8°	.33	.10
	20.6°	.42	.11
	36.9°	.67	.14
	51.3°	.80	.12
	71.6°	.91	.12
16 kHz	11.8°	.29	.11
	20.6°	.34	.08
	36.9°	.70	.13
	51.3°	.81	.11
	71.6°	.64	.06

averaging over frequency for these bands was implied. To get an accurate indication of the uncertainty involved, this averaging was performed using the original ratios, averaged over a surface cycle. The result of this average along with the corresponding standard deviations are plotted in Figure 4.20. The uncertainty produced by this averaging is seen to be approximately equal to that obtained for averaging over the surfaces and for the actual measurements. Although averaging of the 4, 8 and 16 kHz bands produces a desirably small amount of uncertainty, the 2 kHz with its $\lambda/4$ resonance must also be incorporated into an urban scattering model. Inclusion of this band is necessary because for A-weighted urban noise predictions, a band with a $\lambda/4$ resonance will always be included unless protrusions are two feet or greater in height. To include this resonant band, another frequency average was performed. The result of this average is given in Figure 4.21. As indicated in the figure, the uncertainty introduced by this average is slightly greater than the previous three band frequency average. The standard deviations for this case range from about .1 to .2. Although this increased uncertainty is not desirable, this frequency average is preferable because of its incorporation of the resonant frequency band.

4.6 A Model of Scattered Reflection

4.6.1 The Specular Component of Reflection

With the averaged experimental results of Figure 4.21, a model of scattered reflection can now be formulated. As discussed in the last section, the actual details of building surfaces are not an important factor in assessing scattering. The dependence which must be included

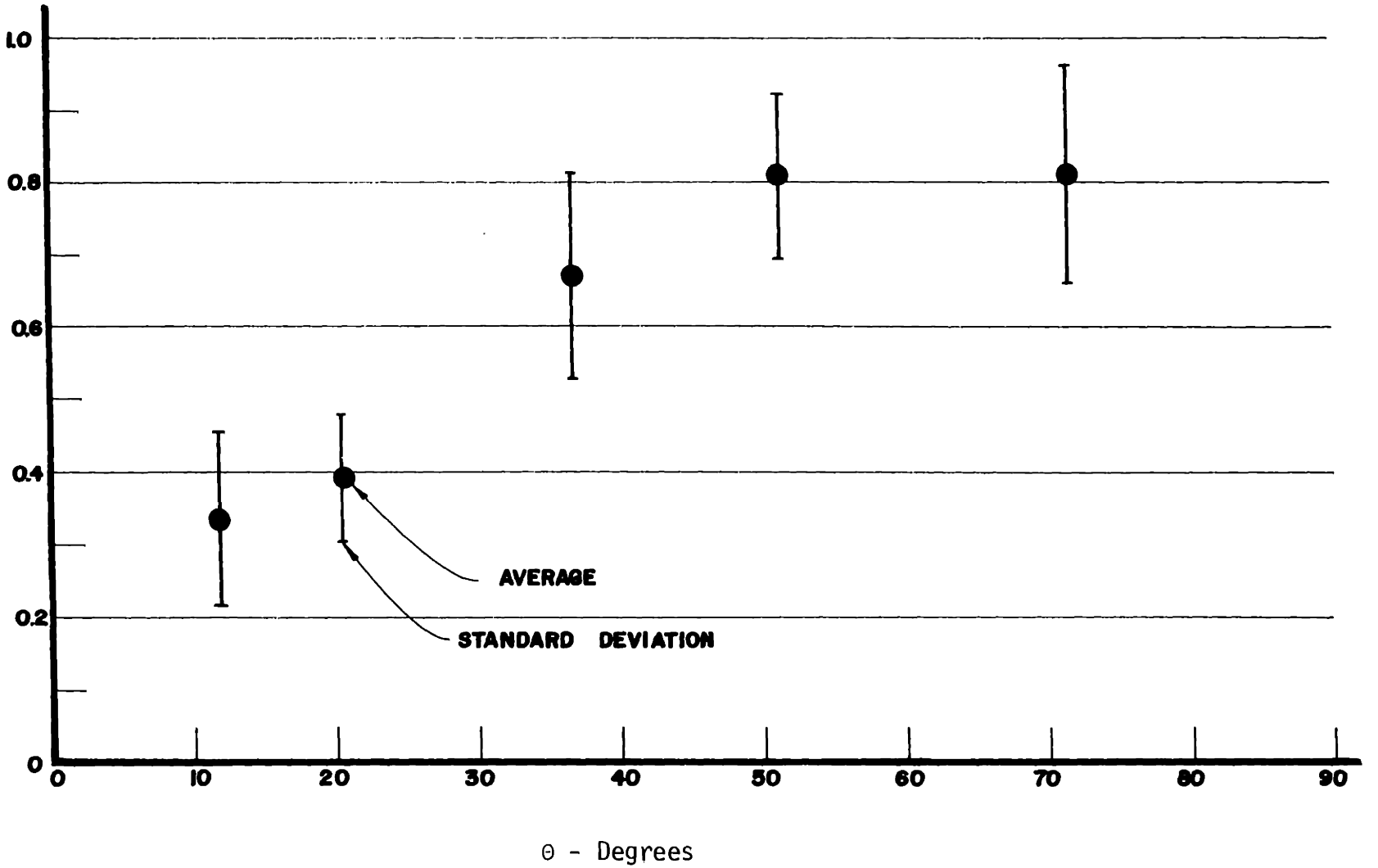

FIGURE 4.20: Measured Reflection Ratios: Averaged for 4, 8, 16 kHz

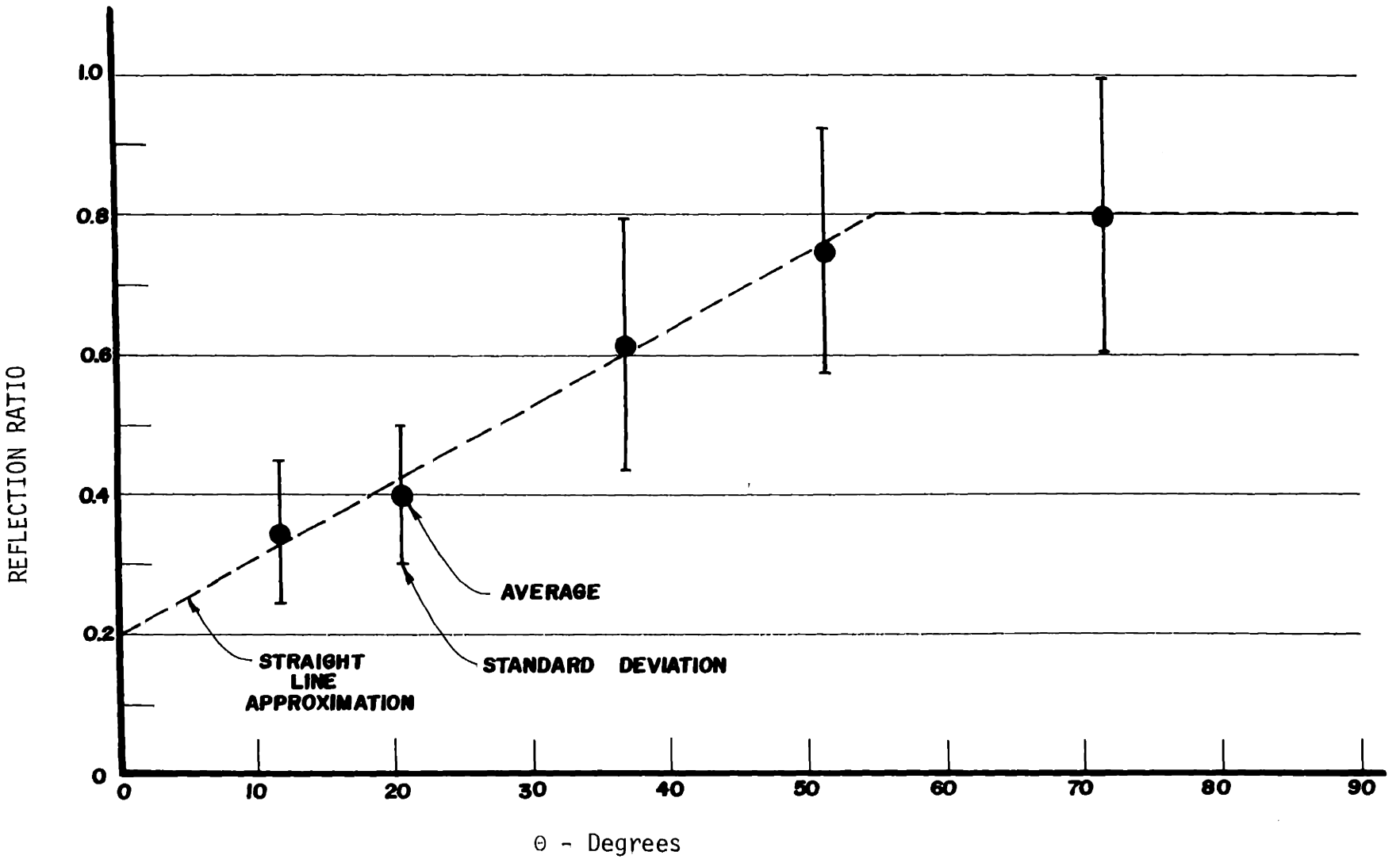

FIGURE 4.21: Measured Reflection Ratio: Averaged for 2, 4, 8, 16, kHz

in a scattering model is that of reflected energy on incident angle. Inclusion of this dependence requires that an approximate relationship between reflection ratio and incident angle be assumed. With the amount of uncertainty present in the averaged ratio, a number of approximations could be chosen. In an attempt to best match the average values and yet have a simple relationship, a two segment, linear approximation was assumed. This approximation is indicated in Figure 4.21. The value of reflection ratio as a function of incident angle is given by:

$$r(\theta) = .6245\ \theta + .2 \qquad 0 \leq \theta < .9599$$

$$r(\theta) = .8 \qquad \theta \geq .9599$$

where θ is in radians. In making this approximation, behavior at the extreme values of 0 and 90 degrees had to be assumed because of the experimental difficulties in obtaining data. For the grazing incidence case, the direct and specularly reflected pulse merge and can not be experimentally separated. At normal incidence, either the source or receiver is necessarily an obstacle in the propagation path. For the behavior at 0 degrees, it was decided to extend the straight line implied by the values at 11.8°, 20.6°, 36.9°, and 51.3°. Because of expected net phase cancellation effects at normal incidence, the behavior of r near 90° was assumed to be constant and less than 1.0.

4.6.2 The Scattered Component of Reflection

With an approximate expression formed between reflection ratio and incident angle, the scattered reflection model can now be formulated.

The geometry of scattered reflection is given in Figure 4.22. To develop the model, first consider one ray incident on the surface. A portion of the energy in this ray is reflected specularly while some is available for scattering. For the purposes of the model, the specular component will be ignored and considered separately. The scattered component is assumed to lie totally in the plane normal to the surface and containing the source and receiver. The component does, however, diverge in three dimensions on its path to the receiver. It should be noted that this divergence is not as if a source were located two-dimensionally on the surface, but rather is the total divergence along the path from the point source to the receiver. The amplitude of the energy available for scattering is given by the fraction of initial energy which is not specularly reflected, but is $1-r(\theta)$. Because the available energy can be scattered into π directions, the energy at the receiver point is further reduced by a factor of $1/\pi^2$. Finally, since the angular dependence of the scattered energy may not be constant, a weighting factor dependent on the scattering angle is necessary. Using the notation of Figure 4.22, the expression for the scattered energy due to one ray incident on the surface is

$$P^2_{R/X} = \frac{A^2[1-r(\theta)]S(\beta)}{\pi^2(d_D+d_S)^2}$$

where $S(\beta)$ is the scattered energy angular dependence factor. To determine the scattered energy due to a region of the surface, the above expression is integrated between the limits of the region. As the above

FIGURE 4.22: Formulation of Scattering Model

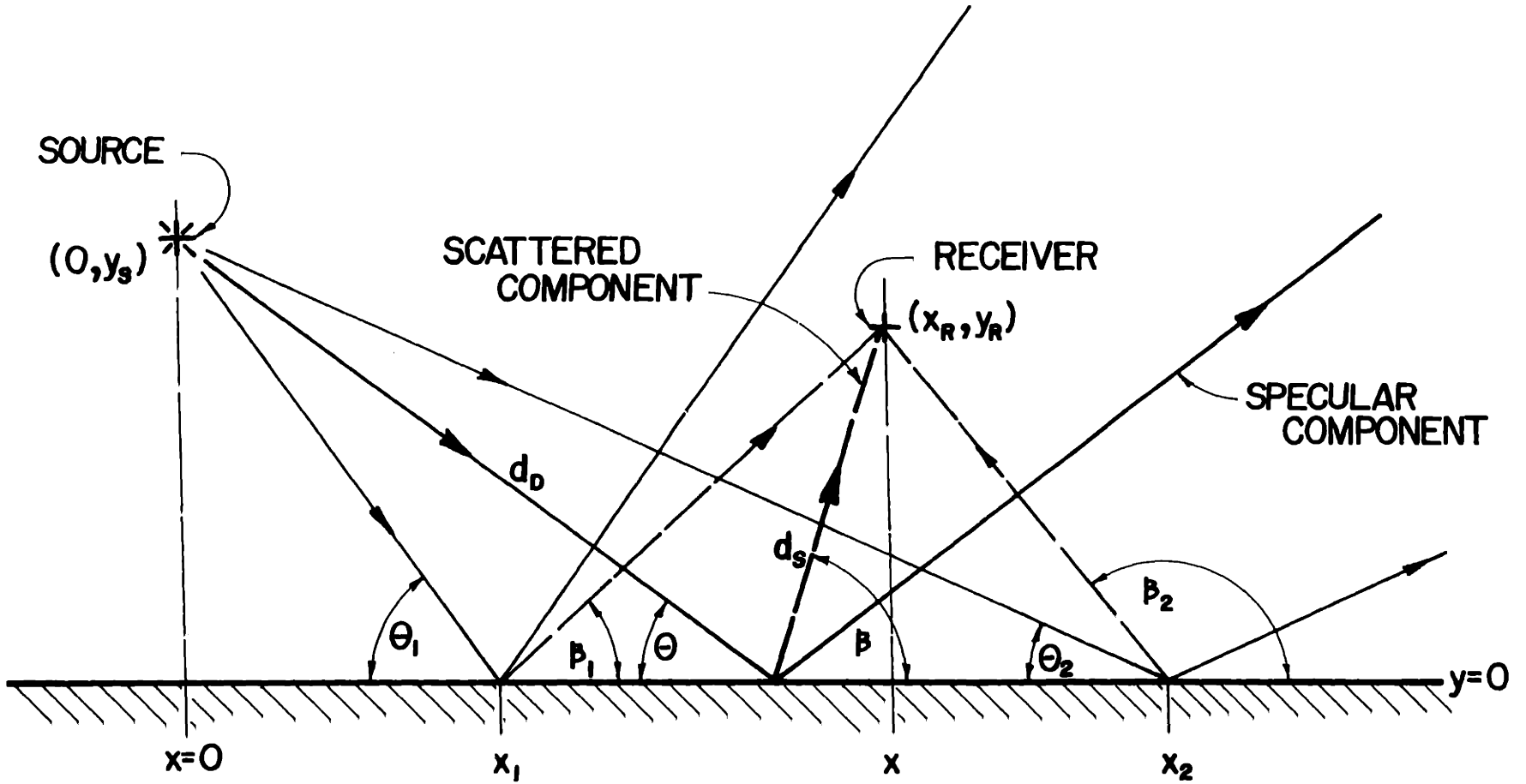

Energy at Receiver Point from Path Through X:

$$P^2_{R/X} = \frac{A^2[1-r(\theta)]\ S(\beta)}{\pi^2(d_o+d_s)^2}$$

where A^2 is pressure amplitude of source
$r(\theta)$ is energy fraction returned by specular component

expression is considerably complicated by the divergence term, $1/(d_D+d_S)^2$, integration must be done numerically.

A remaining question for the scattering model is the angular dependence of the scattered energy. Owing to the small amount of energy in the scattered component at any given angle, this dependence can not be determined experimentally. An expression for the angular dependence can be obtained, however, by application of the principle of reciprocity [17]. Briefly, this principle states that the measured pressure will remain constant upon exchange of the source and receiver positions. Applying this to the scattering model, the requirement becomes

$$[1-r(\theta)]\ S(\beta) = [1-r(\beta)]\ S(\theta)$$

using the notation of 4.22. This condition implies that the functional form of $S(\beta)$ is same as $[1-r(\theta)]$. Further, because $S(\beta)$ is a weighting factor over π radians, another condition on $S(\beta)$ is

$$\int_0^{\pi} \frac{S(\beta)}{\pi} = 1.$$

With these conditions, the expression for the scattered energy angular dependence was determined to be

$$S(\beta) = .2114 - .1652\beta \qquad 0 \leq \beta < .9599$$

$$S(\beta) = .0528 \qquad \beta \geq .9599$$

where β is in radians.

4.6.3 Application to Propagation in City Streets

The scattering model which has been developed can readily be applied to street sound propagation. Application of the model is quite similar to the techniques of specular imaging theory. Image sources and receivers are used although the criterion for scattering becomes the amount of building surface "seen" rather than the number of images. Determination of the amount of surface contributing to the scattered field is subject to the same geometric limitations imposed on determining the influence of an image array. Once the portion of surface contributing scattered energy is established, the geometry of Figure 58 is then applicable.

As an application of the scattering model, propagation around a corner at a four-way intersection is considered in Figure 4.23. In Figure 4.23(a) scattering in the receiver street is examined. The extent that each image source can influence the receiver street is the same as for specular theory and is indicated in the figure. Energy from the image source produces scattering on the receiver street walls and their images. This scattered energy is observed by the actual receiver as well as by its images. Thus, generally, sound can be multiply reflected in source street, multiply reflected in the receiver street, scattered, and then multiply reflected to the receiver. For each of these reflections, the associated energy loss of reflection must be applied. Scattering in the source street is indicated in Figure 4.23(b). This case

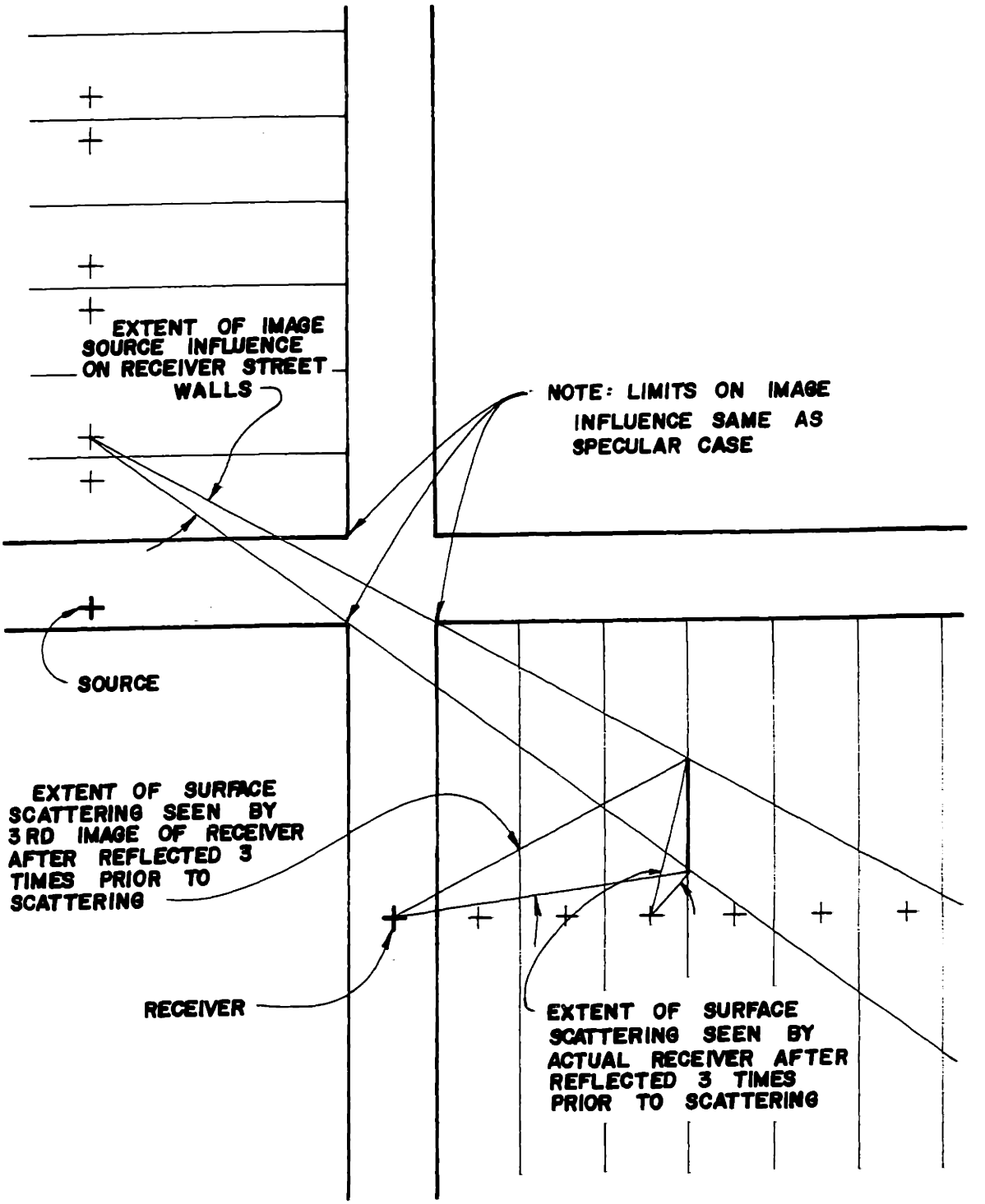

Figure 4.23(a): Application of Scattering Model to Propagation Around A Corner -- Scattering in Receiver Street

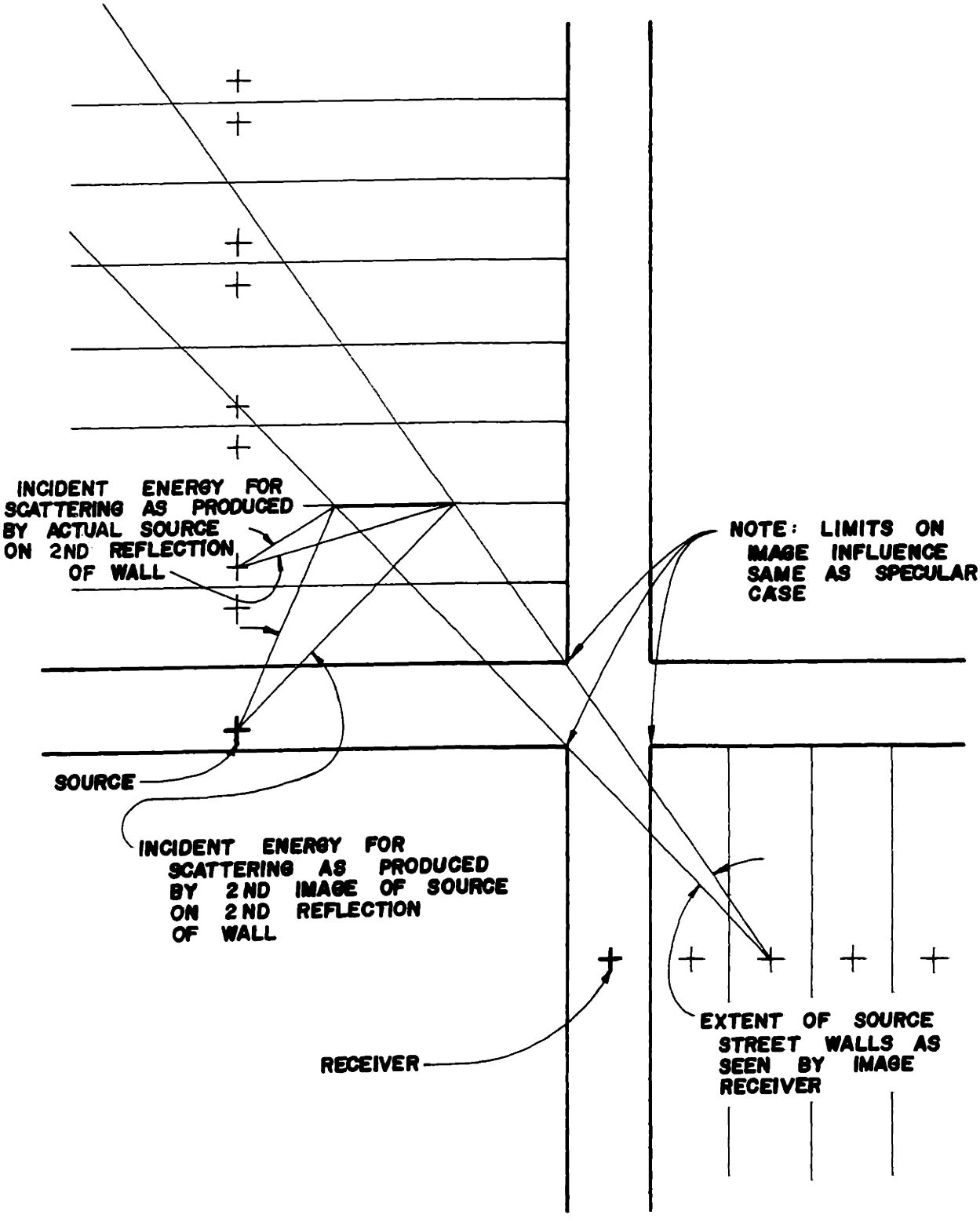

FIGURE 4.23(b): Application of Scattering Model to Propagation Around A Corner - Scattering in Source Street

is almost identical to the previous case except for a slight geometrical and sequential reorientation. For this case, sound is multiply reflected in the source street, scattered, multiply reflected further in the source street, and then multiply reflected in the receiver street to the receiver. As can be easily seen from both of these cases, the total scattered field becomes quite complicated and therefore computer solution is almost mandatory. The results of the scattered field computation can be added on an energy basis to corresponding values of the specular field to produce the total sound field. The specular field is determined as discussed in section 2.2 with exception of using the angularly dependent reflection ratio.

4.7 Data Simulation Using the Scattering Model and Imaging Theory

4.7.1 Scattered Reflection from a Single Surface

In conjunction with the forward scattering measurements described in section 4.5, backscatter measurements were taken for comparison to results from the scattering model. The instrumentation used in these measurements was the same as that for the reflection ratio measurements as given in Figure 4.4. The energy scattered by a portion of a surface containing periodic, rectangular protrusions was measured by first measuring the direct pulse strength and then the amount of energy received after arrival of the specularly reflected pulse. The geometry used for this experiment is given in Figure 4.24. Three receiver positions were used to give several different ranges of scattering angle. The nine protrusion configurations described in section 4.5 were also used

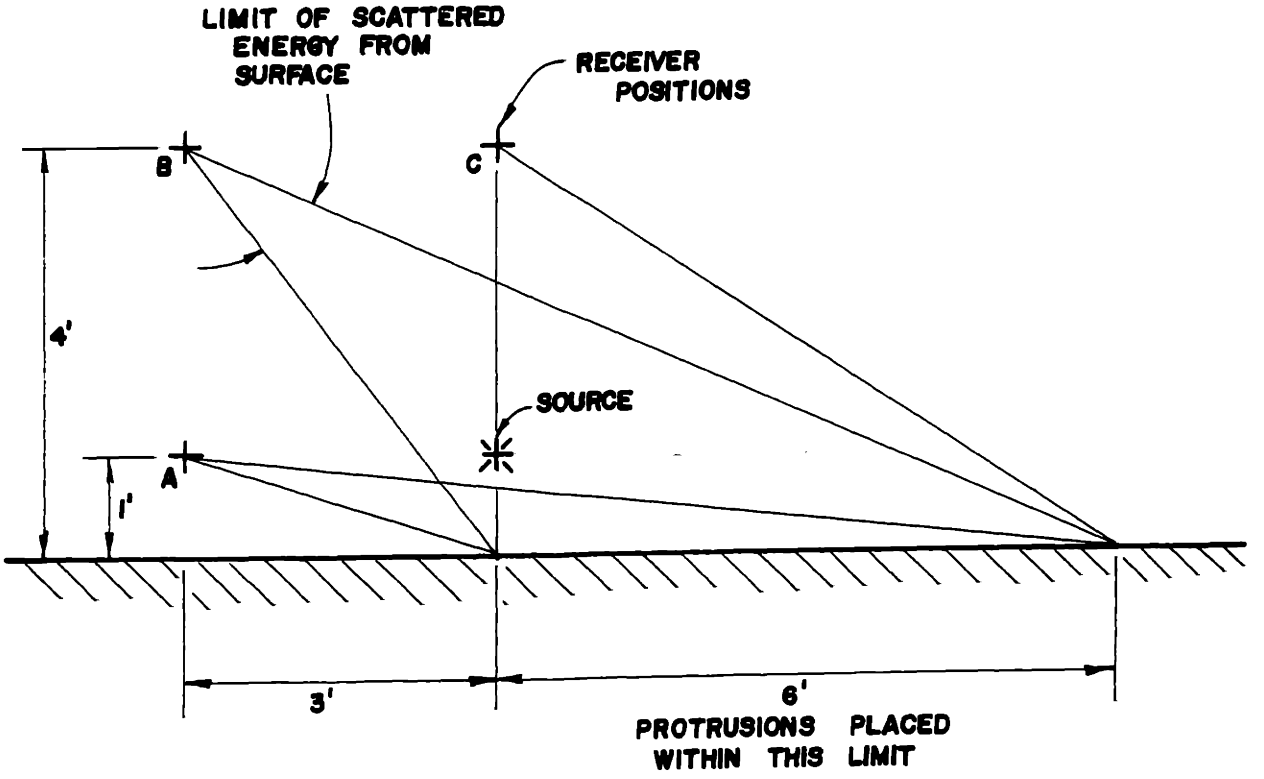

FIGURE 4.24 Geometry for Quantitative Backscatter Experiments

in this experiment. The levels obtained from the measurements were averaged over the 2, 4, 8 and 16 kHz octave bands and over the nine surface configurations. The levels were corrected for background noise which was typically on the order of 10 dB below the signal, and normalized to correspond to a free field source level of 80 dB at 3 ft. For the comparison, the experiment was simulated by computer using the scattering model. The results of the experiment and the simulation are presented below:

Receiver Position	Experimental Level in dB	Scattering Model Level in dB
A	68.5	68.1
B	71.7	67.6
C	64.6	64.4

Agreement of the two sets of result is quite good except for receiver position B. For this position, the experiment is about 4 dB higher than predicted, while for the other two positions, levels are within .5 dB. The experimental standard deviation is on the order of 1 dB. A partial explanation of the poor correspondence for receiver position B may lie in an observation about backscattering made by Wagner [15] for the high frequency limit. It was observed that for this optical limit, there is a preferred backscatter angle which corresponds to intersection of the line determined by the source and receiver with the surface. If such preferred scattering was present for the experimental frequencies, it would only occur for position B. Although this question is raised, it is not pursued as the agreement of the two sets

of results is quite sufficient in terms of the total energy of the sound field.

4.7.2 Simulation of Acoustical Model Data

Using the scattering model and specular imaging theory with appropriate inclusion of air absorption attenuation, the pass-by data reported in Section 3.2.2 for walls with protrusions was simulated with computer programs. Comparison of the acoustical model and simulation results for the tee intersection configuration are presented in Figure 4.25. In this figure, values are given for the 8, 16 and 31.5 kHz octave bands at the three receiver positions. These positions are 1.5, 4.5 and 10 street widths from the line of travel of the source. For the receiver position closest to the source, the simulation values consistently lie within the range of the experimental values for all three octave bands as illustrated in Figure 4.25(a). This agreement is also maintained at the intermediate position as indicated in Figure 4.25(b), except when the source is in or near the intersection. For the source at these positions, the simulation values are slightly higher than experimental with differences being less than 2 dB for all bands. At the farthest receiver position, as for the previous positions, simulation values fall within the range of the experimental when the source is 1 to 2 street widths from the receiver street centerline. When the source is in or near the intersection, the simulated values tend to overpredict the experimental with a maximum difference of about 3 dB at some points. These results are given in Figure 4.25(c).

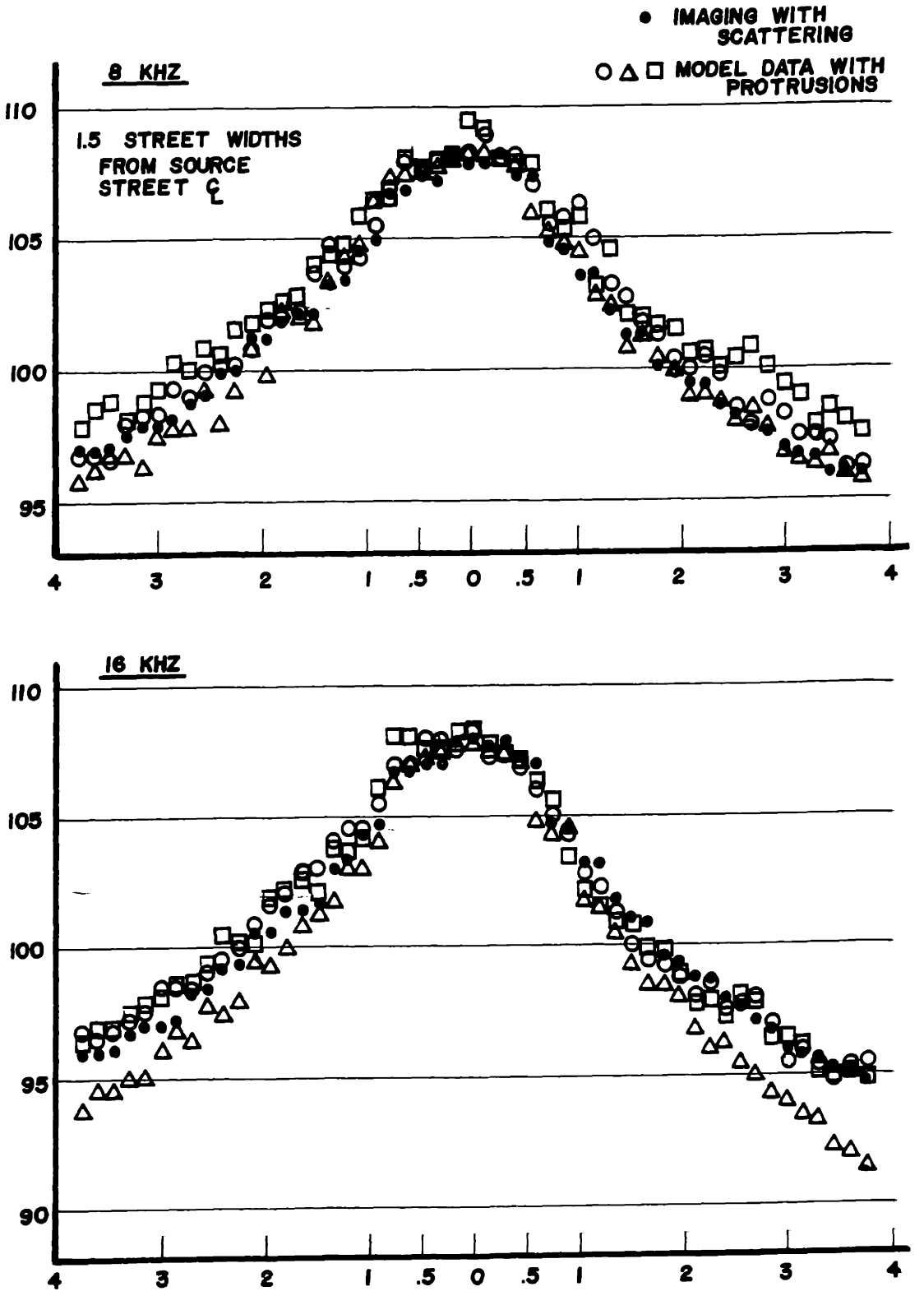

Distance of Source from Receiver Street ℄ in Receiver Street Widths

FIGURE 4.25: Acoustical Model Pass-By Data and Image/Scattering Results - Tee Intersection

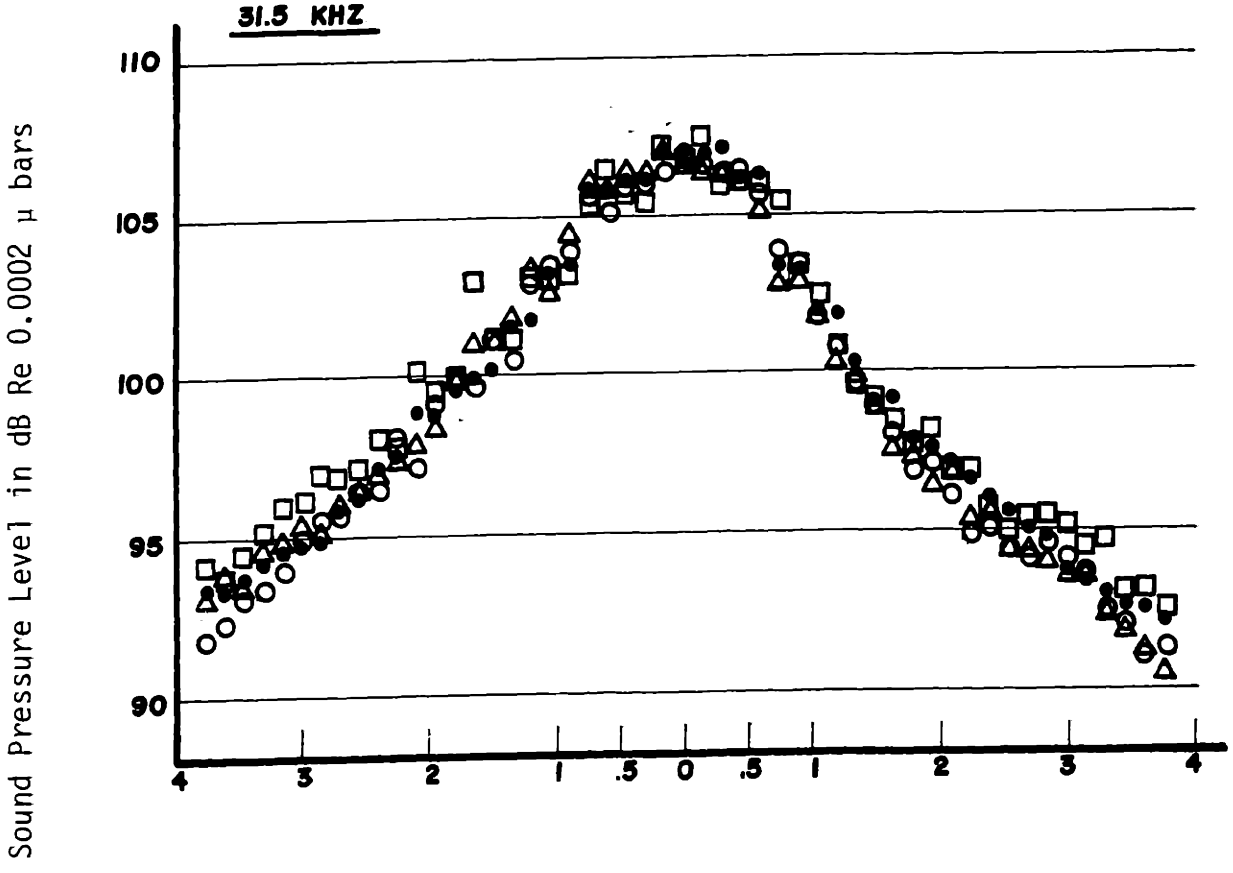

FIGURE 4.25: Acoustical Model Pass-By Data and Imaging/Scattering Results - Tee Intersection

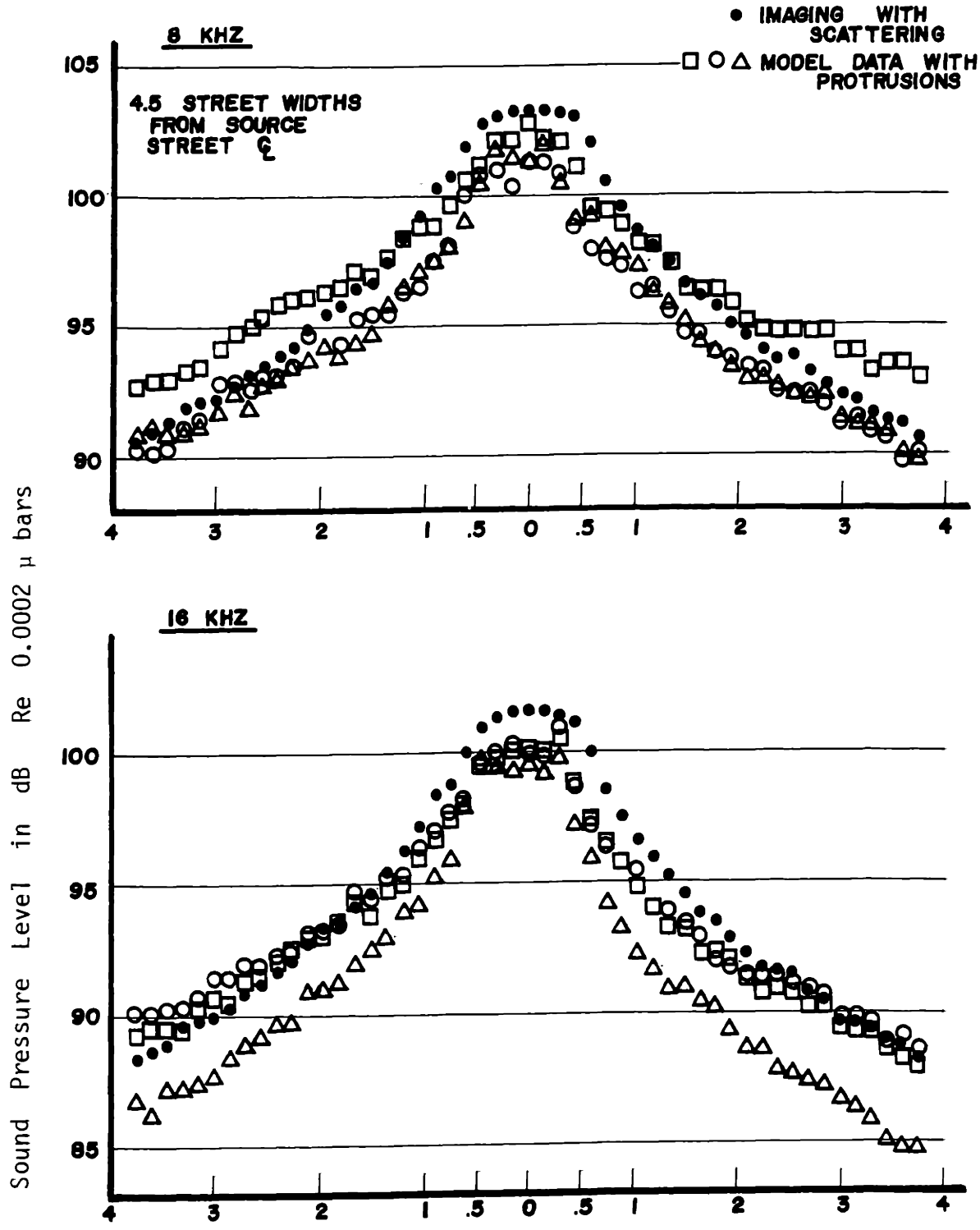

FIGURE 4.25 Acoustical Model Data and Imaging/Scattering Results Tee-Intersection

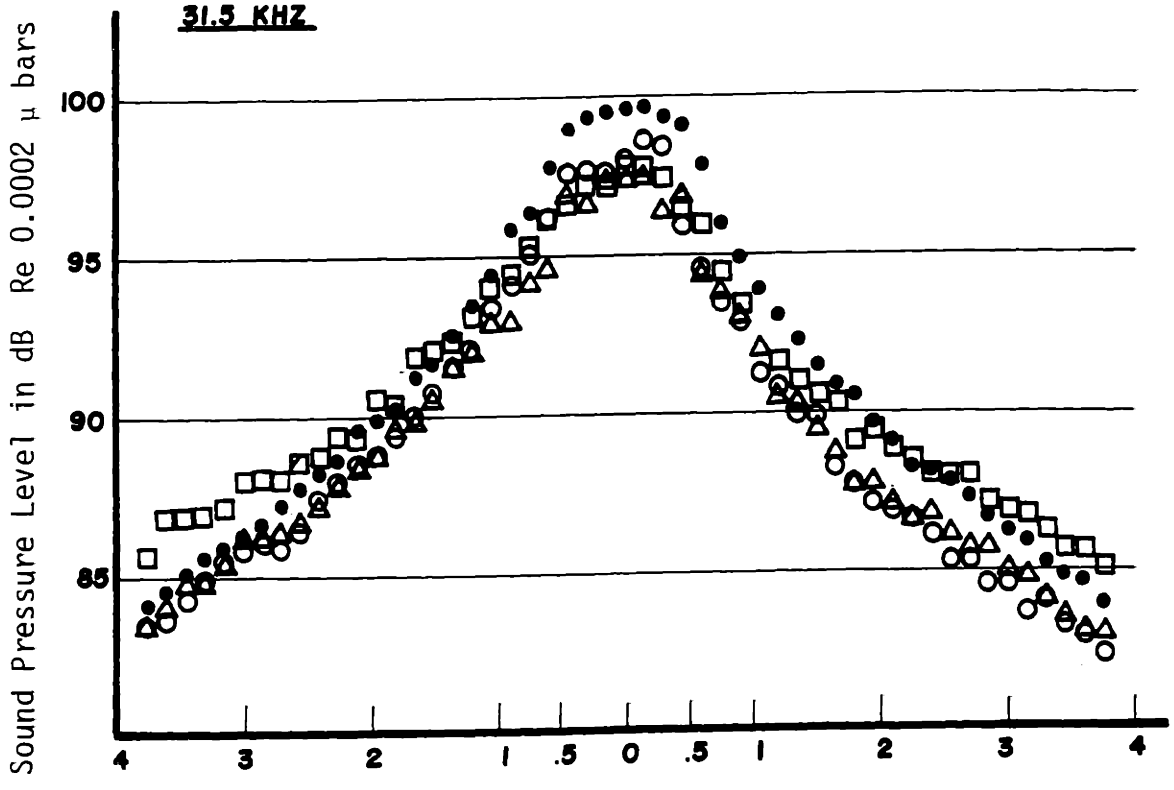

FIGURE 4.25: Acoustical Model Data and Imaging/Scattering Results -- Tee Intersection

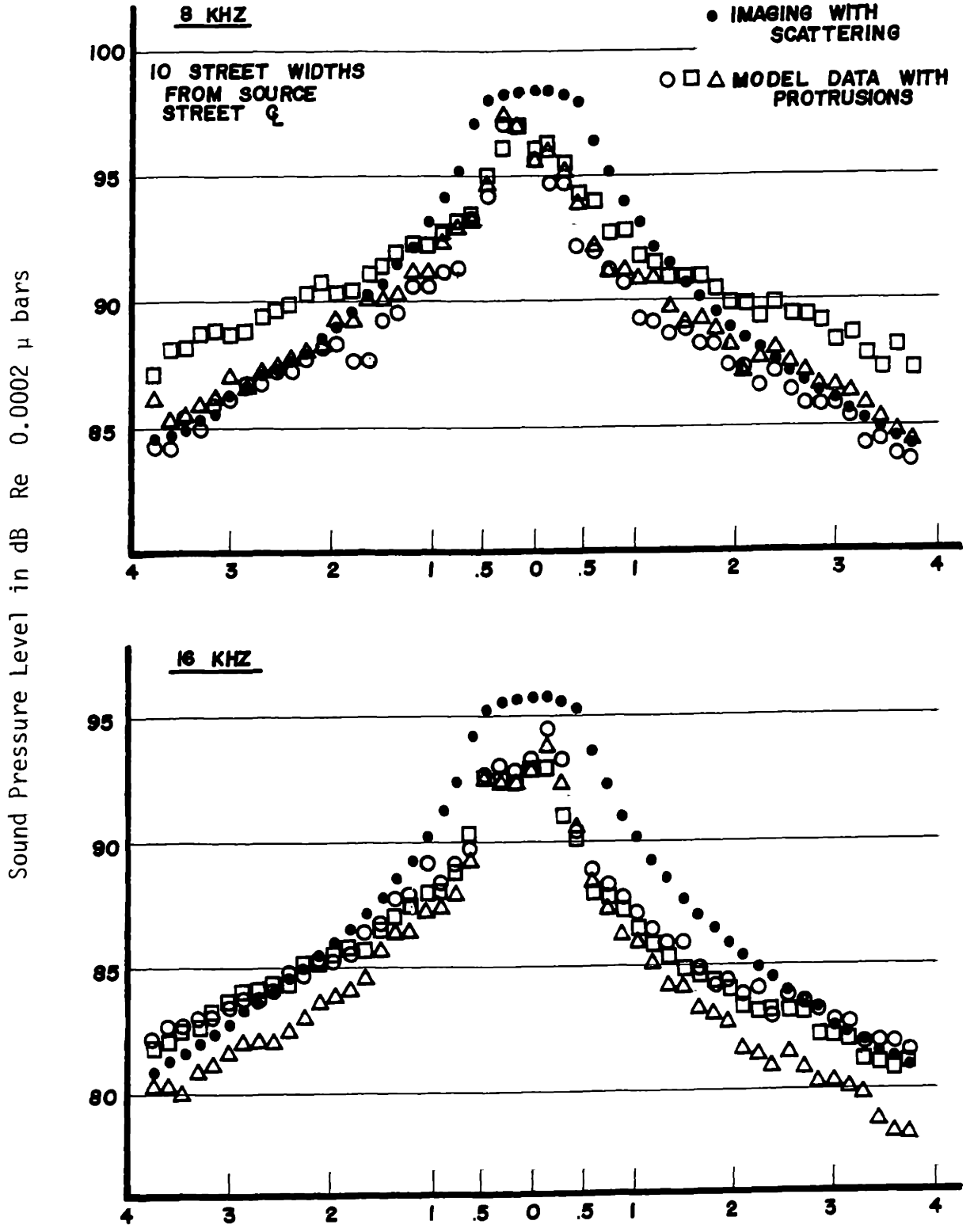

FIGURE 4.25: Acoustical Model Pass-By Data and Imaging/Scattering Results - Tee Intersection

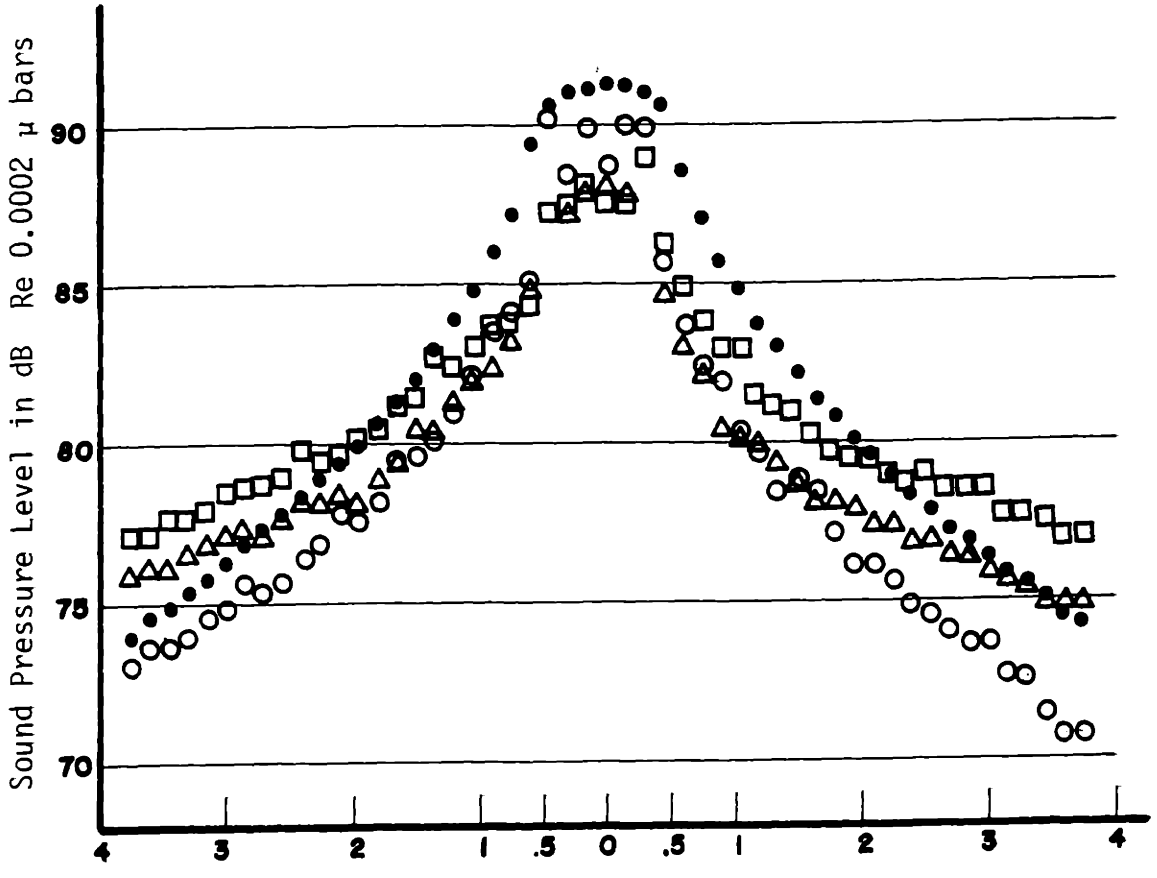

FIGURE 4.25: Acoustical Model Pass-By Data and Imaging/Scattering Results - Tee Intersection

Comparison of simulated and experimental values for the four-way intersection is afforded in Figure 4.26. For this case, only the 16 kHz band is presented for the nearest and farthest positions. All three bands are reported for intermediate position. This was done because of the similarity in the comparison for the three bands. For this street configuration, only one facade structure was tested. The tendencies noted for the tee intersection are also seen for this configuration although the differences between the values at the more distant microphone positions are slightly more accentuated. These differences are particularly apparent in Figures 4.26(b) and 4.26(c) where the simulation values range from nearly equal to at most 4 dB higher than the measured. Further, in Figure 4.26(b), it will be noted that for the 8 and 31.5 kHz bands there is some underprediction by the simulated values. This effect is small, however, ranging from 1 to 3 dB at most. Also, it may be more apparent due to the lack of a range of values as for the tee case. The overprediction by the simulated values seen in Figures 4.26(b) and 4.26(c) is in part due to the finite size of the model. Because of space limitations, extension of the receiver street was not possible. Thus, backscattering from surfaces beyond the receiver position was reduced. This effect was enhanced for the farther receiver positions as the finite termination of the street became closer. This effect was only accounted for in the tee simulation and was found to produce a lowering of the simulation values of about .5 dB. A similar lowering can be expected for the four-way intersection simulation.

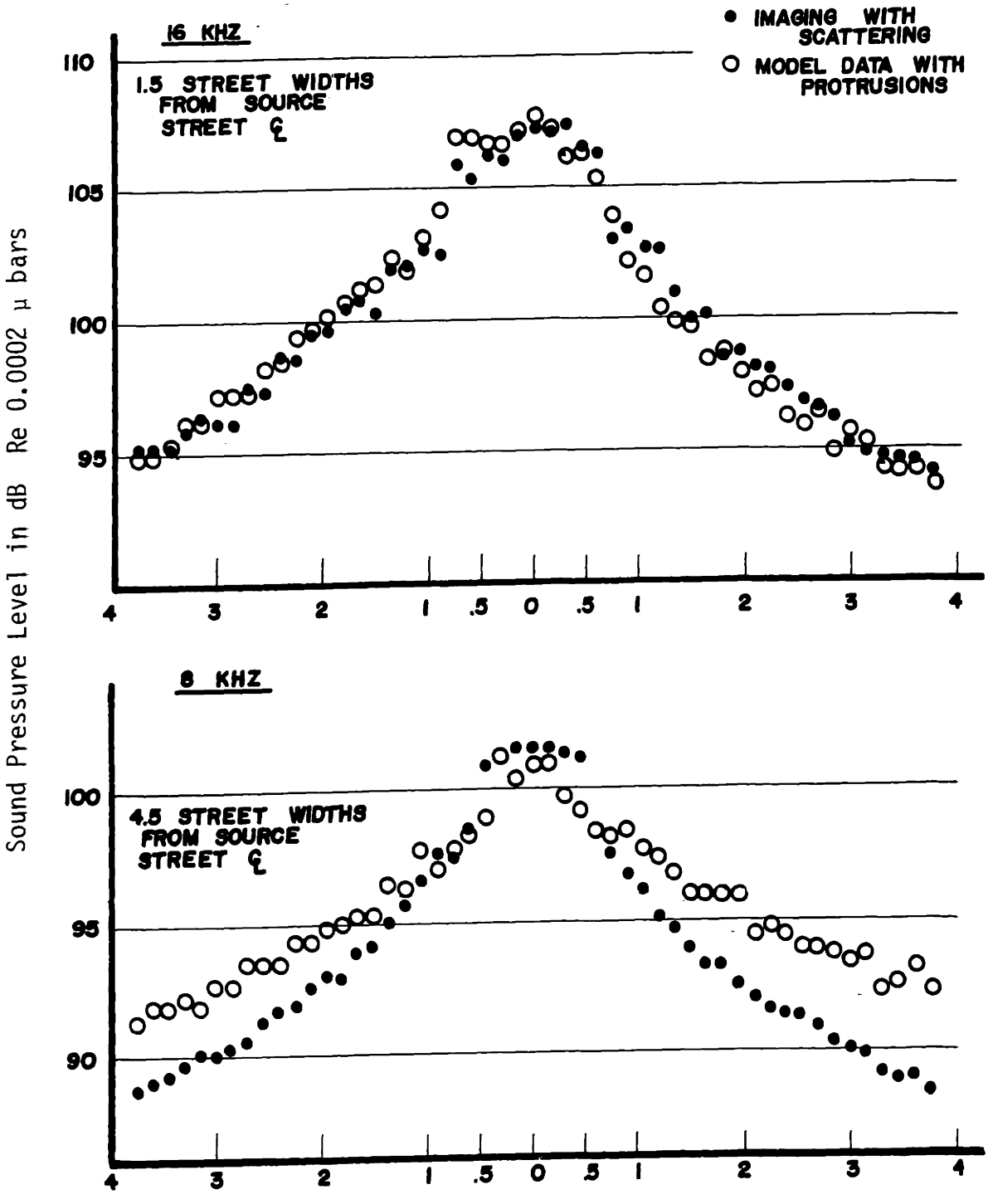

FIGURE 4.26: Acoustical Model Pass-By Data and Imaging/Scattering Results - Four Way Intersection

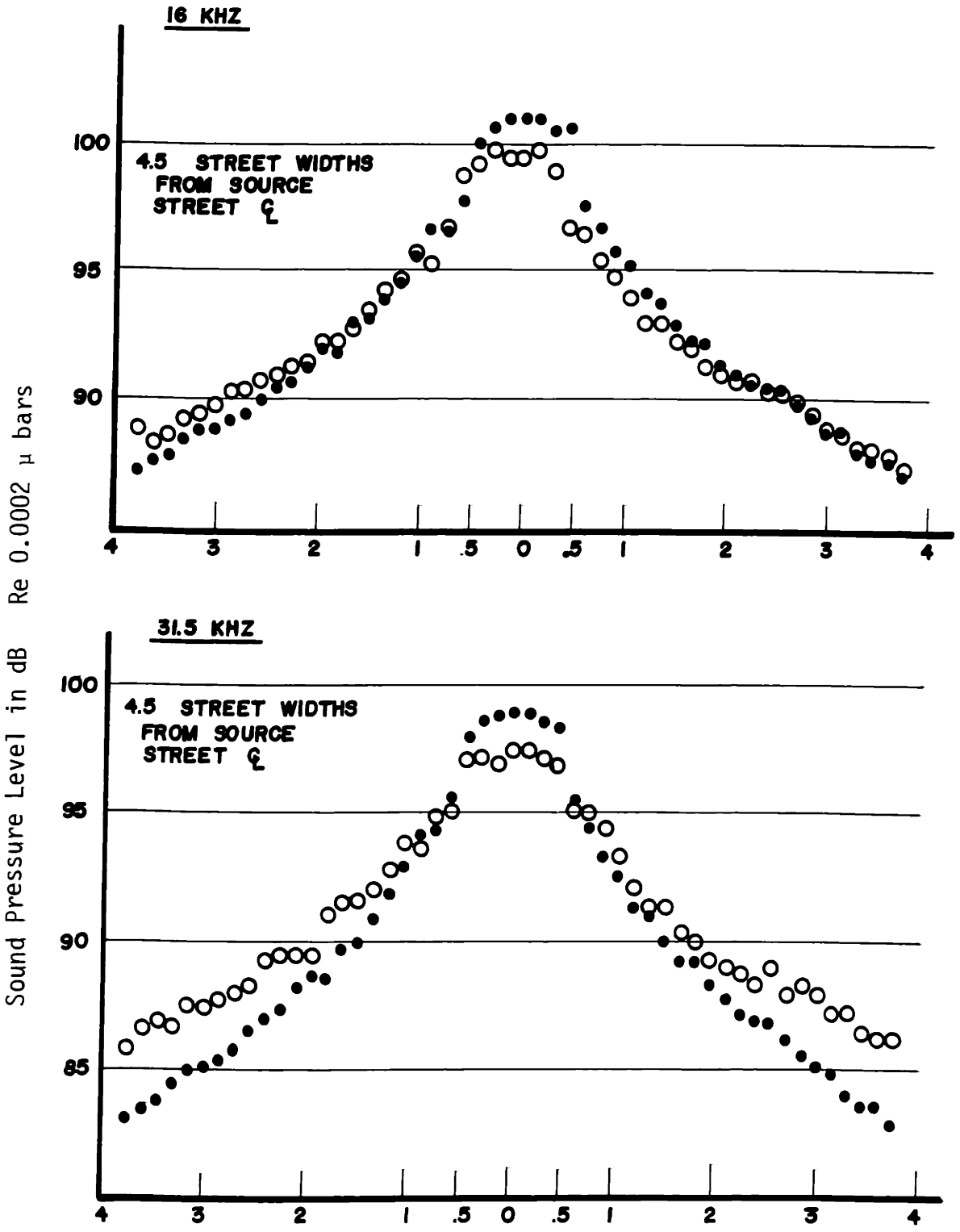

FIGURE 4.26: Acoustical Model Pass-By Data and Imaging/Scattering Results - Four Way Intersection

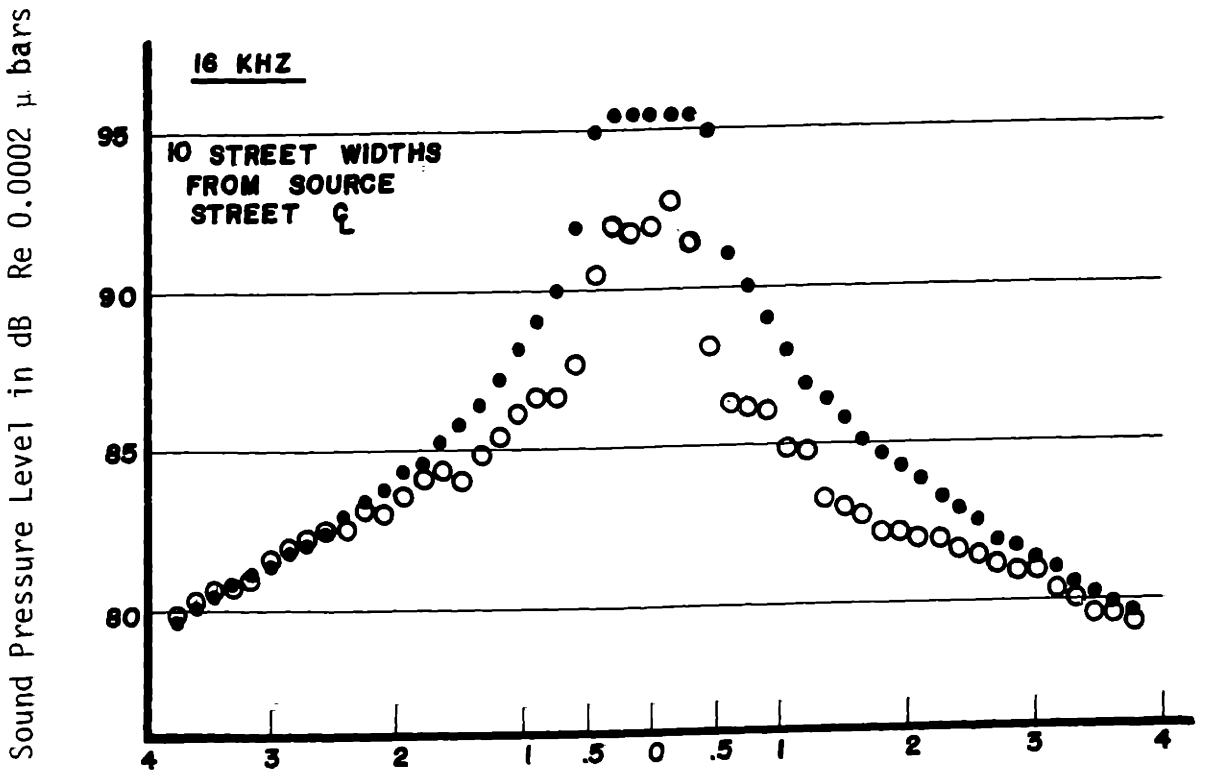

FIGURE 4.26: Acoustical Model Pass-By Data and Imaging/Scattering Results - Four Way Intersection

Experimental and simulation results are compared for a four-way intersection with a cross street in Figure 4.27. The results indicate generally good agreement and display tendencies identical to the plain four-way intersection. The maximum differences observed for this case are also about 4 dB which occur at the farthest receiver position. Discussion regarding the previous case is also applicable to this.

The final comparison of simulated and experimental pass-by values is made in Figure 4.28 for the cross street. These results indicate good agreement between the theory and experiment with simulation values being within 2 dB of the measured for all receiver positions and all frequency bands.

The levels computed with imaging theory and the scattering model for pass-by data simulation can be summed into line source levels to be compared with the corresponding experimental levels. These levels are compared in Figure 4.29 for the tee intersection, in Figure 4.30 for the four-way intersection,in Figure 4.31 for the four-way intersection with a cross street, and in Figure 4.32 for the cross street. As would be expected from the tendency of overprediction by the simulation values for the source near the intersection, the theoretical line source levels tend to be slightly higher than acoustical model levels. This difference is greatest for those positions farthest from the line of the sources. It should be noted the overprediction is greatest in the 16 kHz octave band where the difference ranges from 2 to 4 dB. The range is less for the other two bands, typically 0 to 2 dB. This difference of

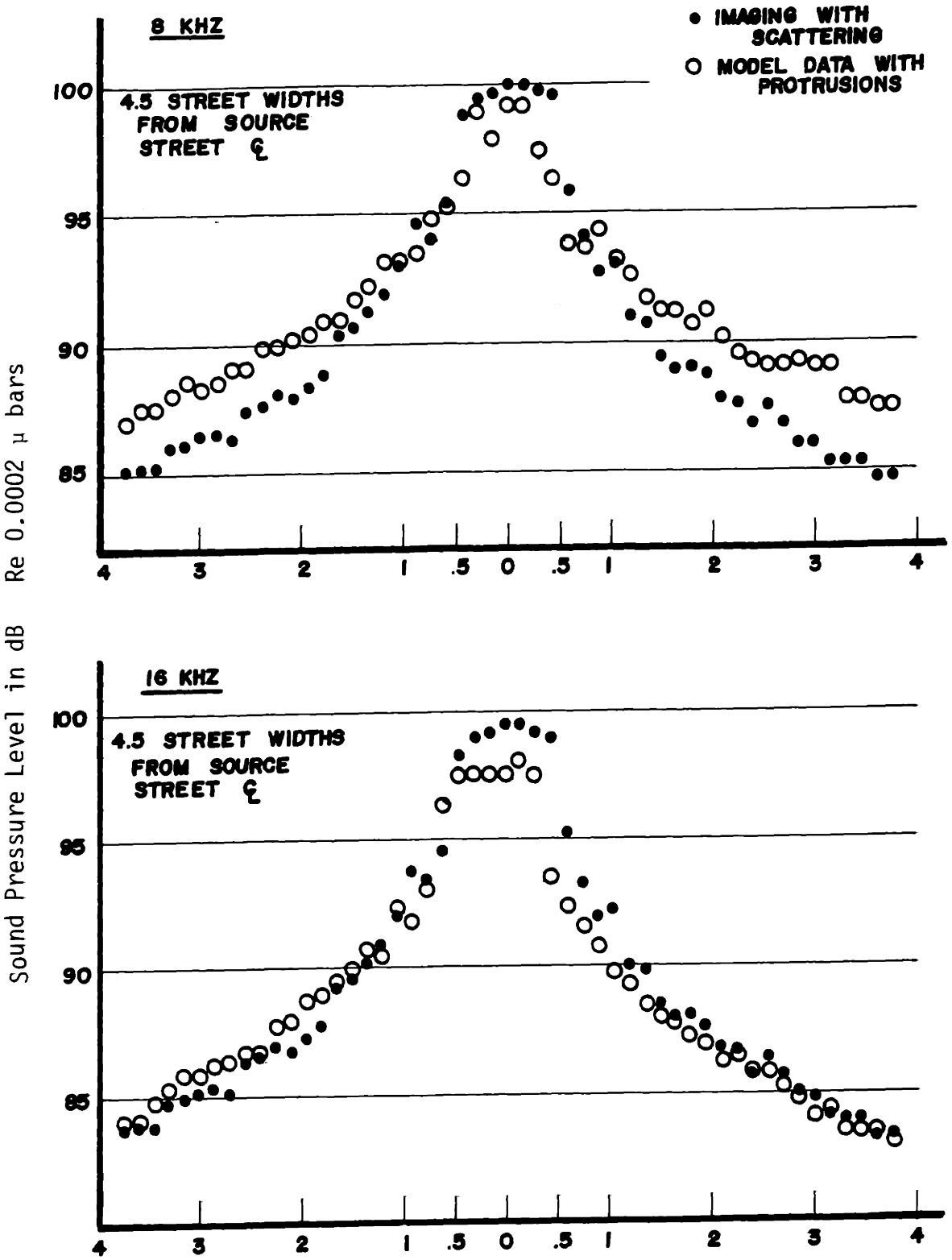

FIGURE 4.27: Acoustical Model Pass-By Data and Imaging/Scattering Results - Four Way Intersection with Cross Street

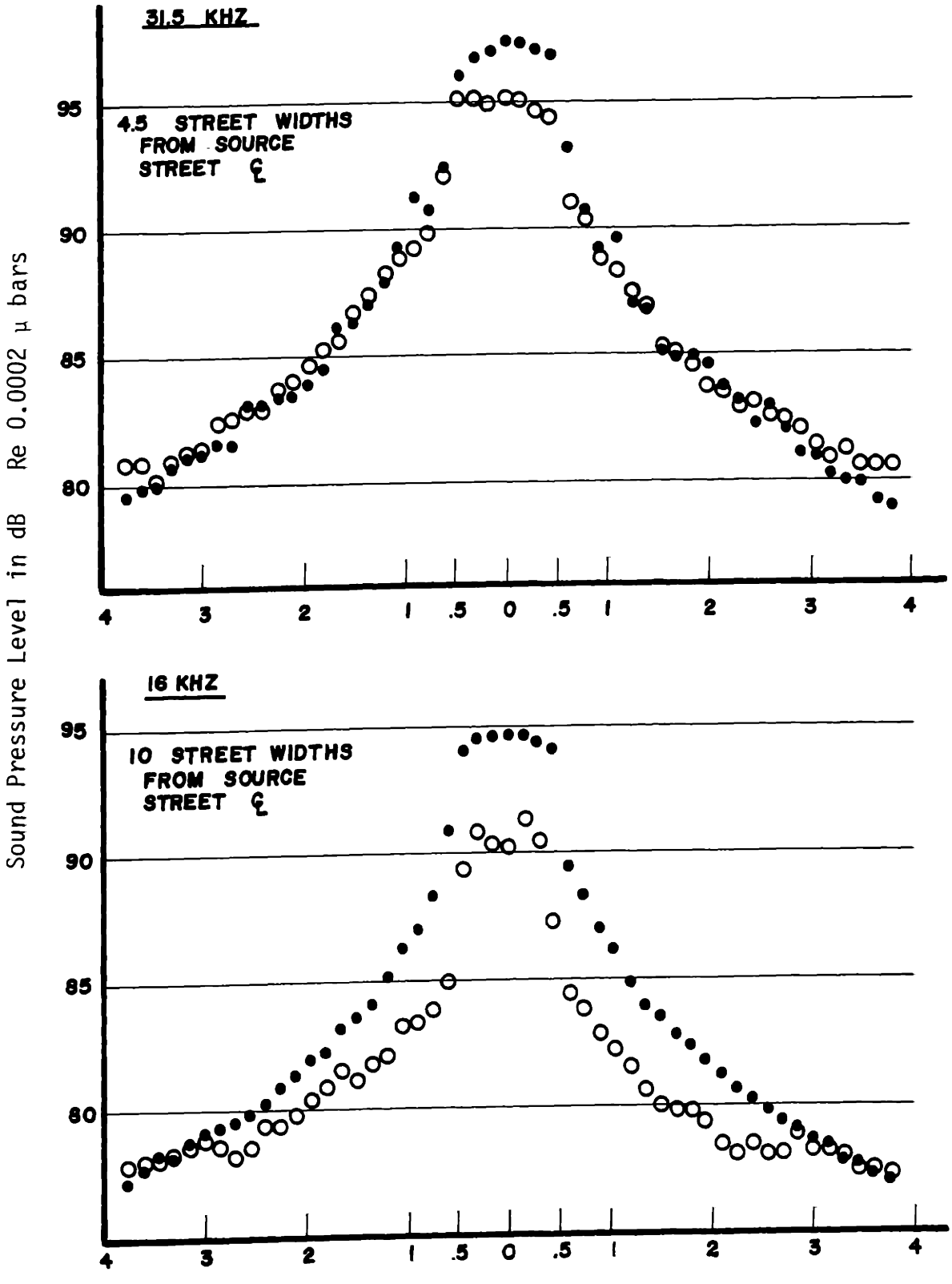

FIGURE 4.27: Acoustical Model Pass-By Data and Imaging/Scattering Results - Four Way Intersection with Cross Street

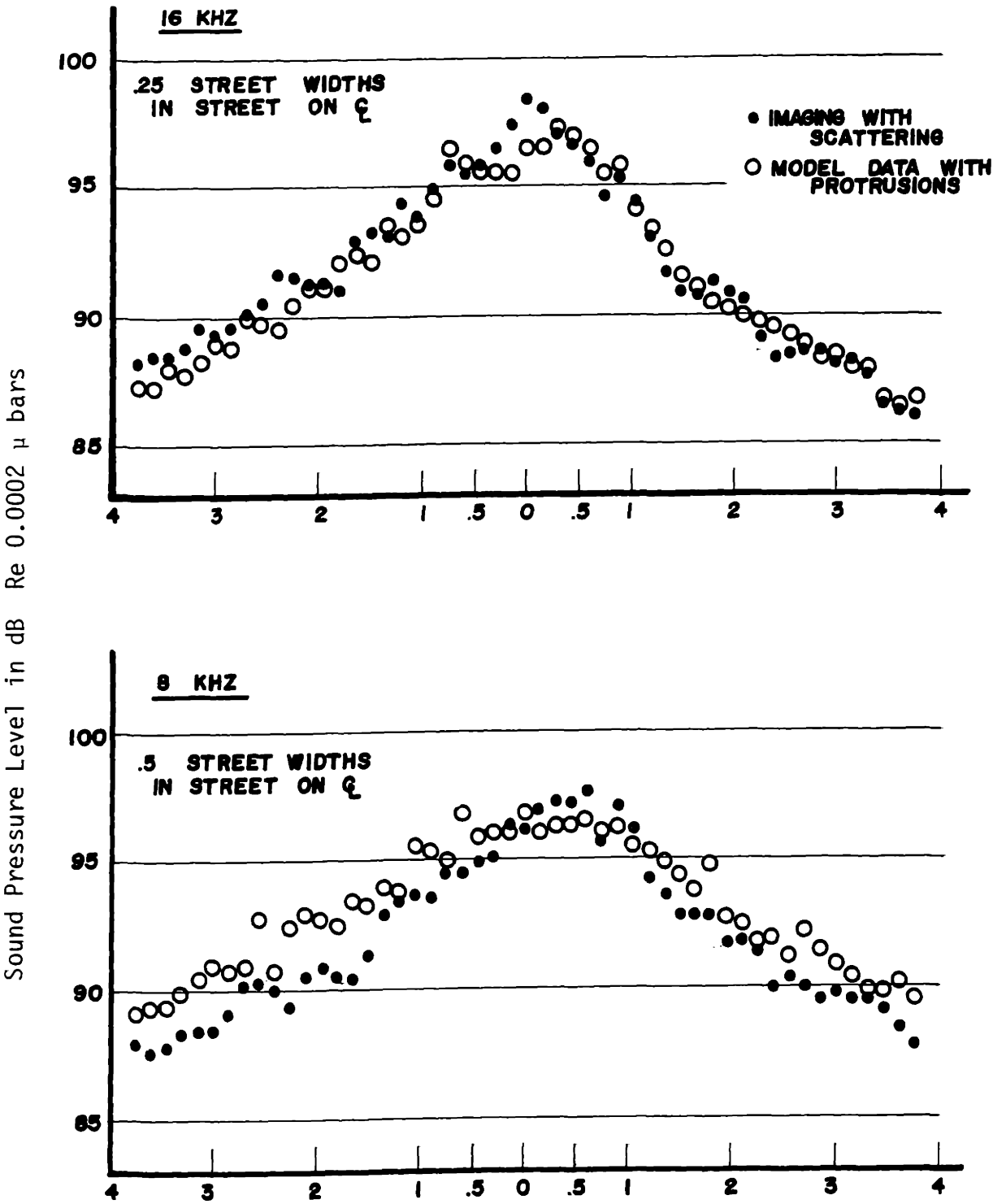

FIGURE 4.28: Acoustical Model Pass-By Data and Imaging/Scattering Results - Cross Street

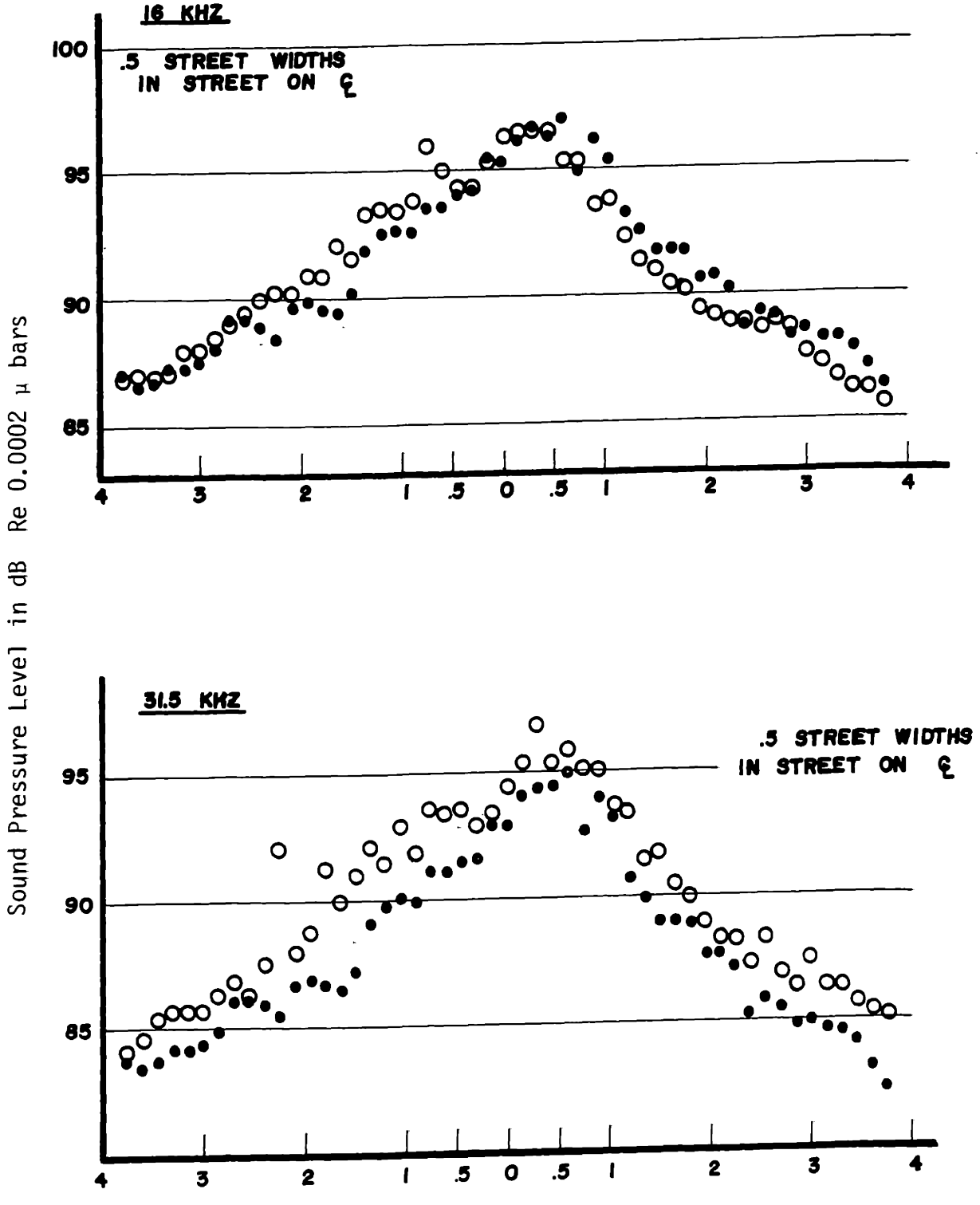

FIGURE 4.28: Acoustical Model Pass-By Data and Imaging/Scattering Results - Cross Street

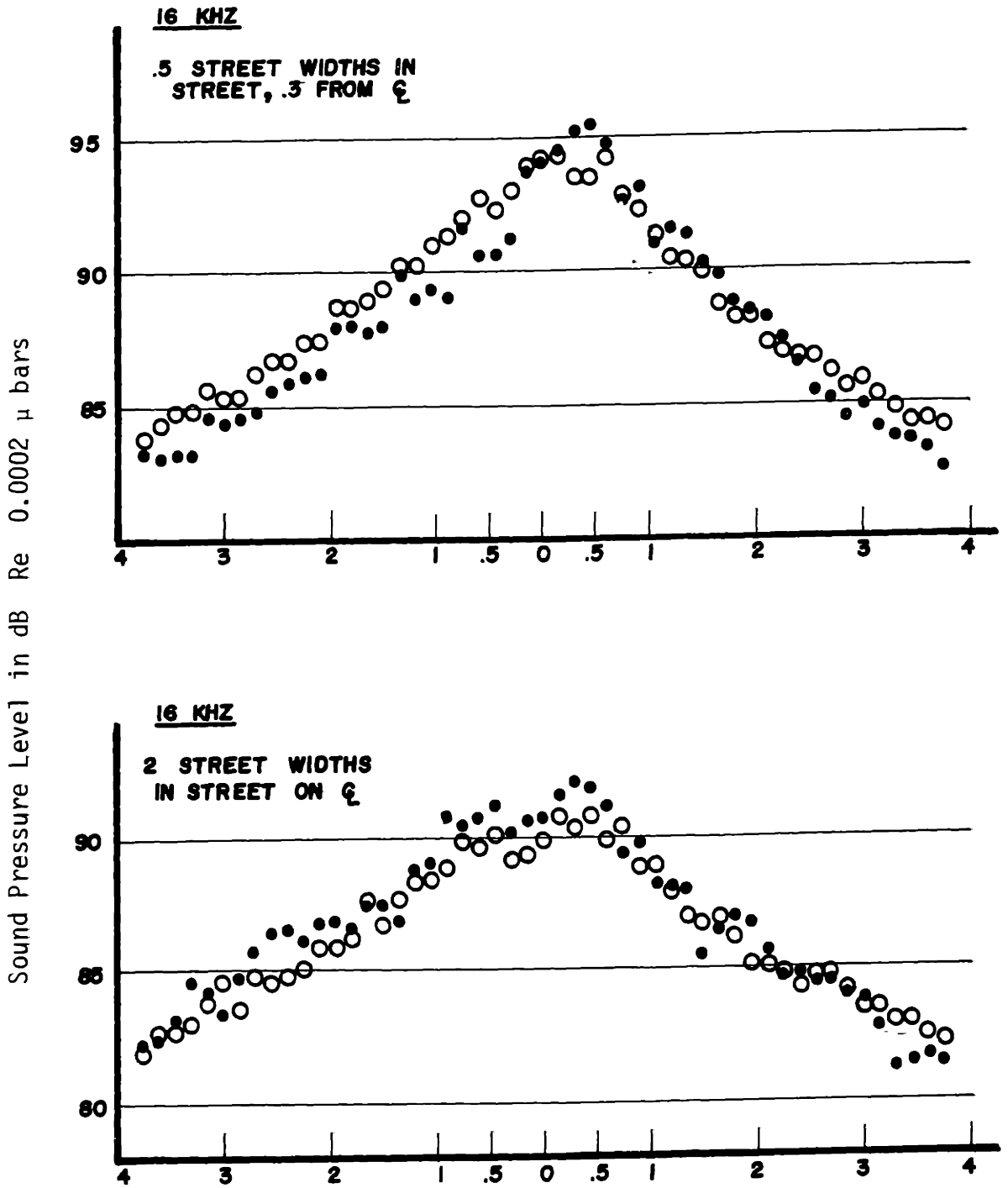

FIGURE 4.28: Acoustical Model Pass-By Data and Imaging/Scattering Results - Cross Street

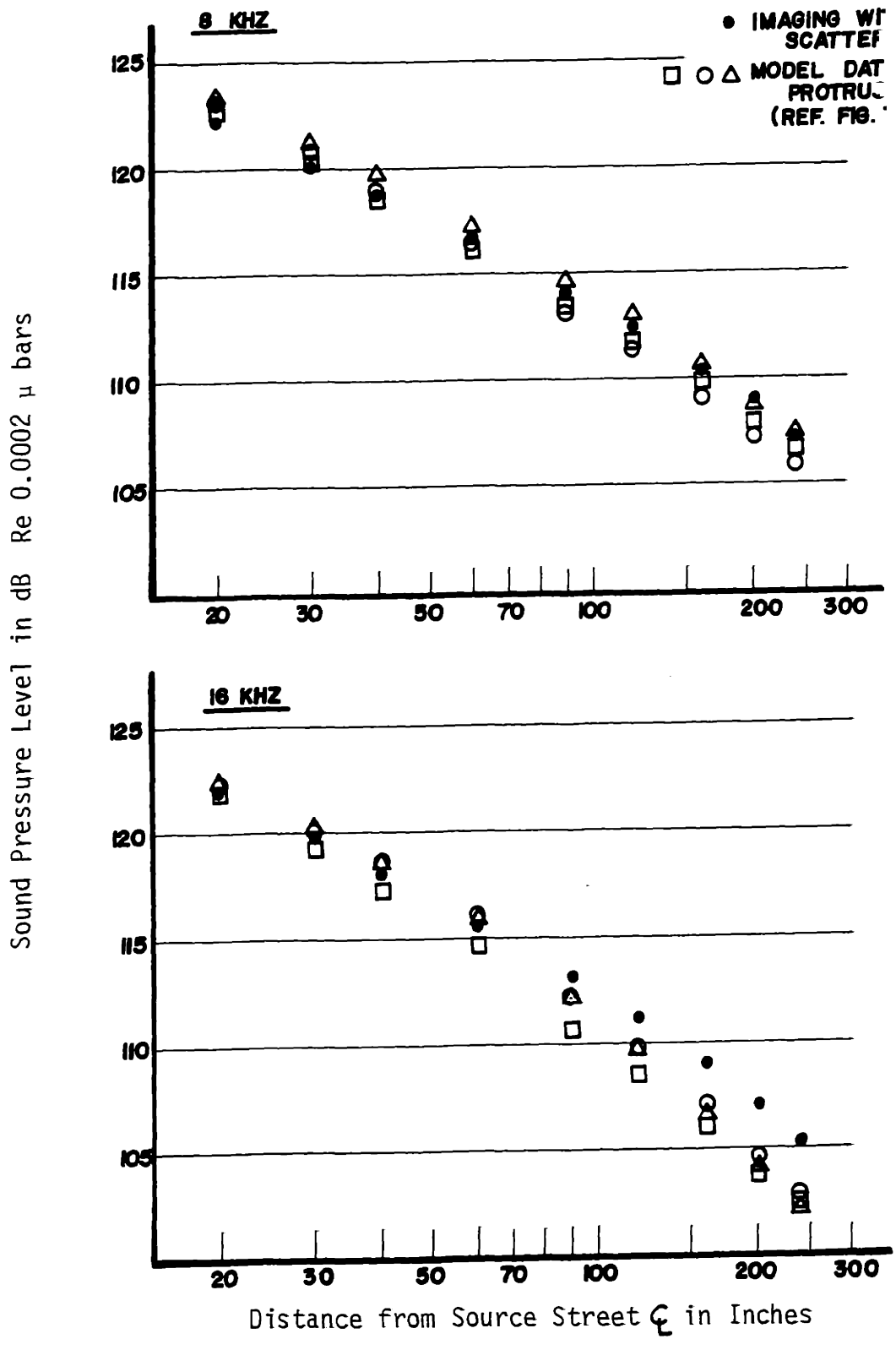

FIGURE 4.29: Comparison of Acoustical Model and Imaging/Scattering L
Source Lines - Tee Intersection

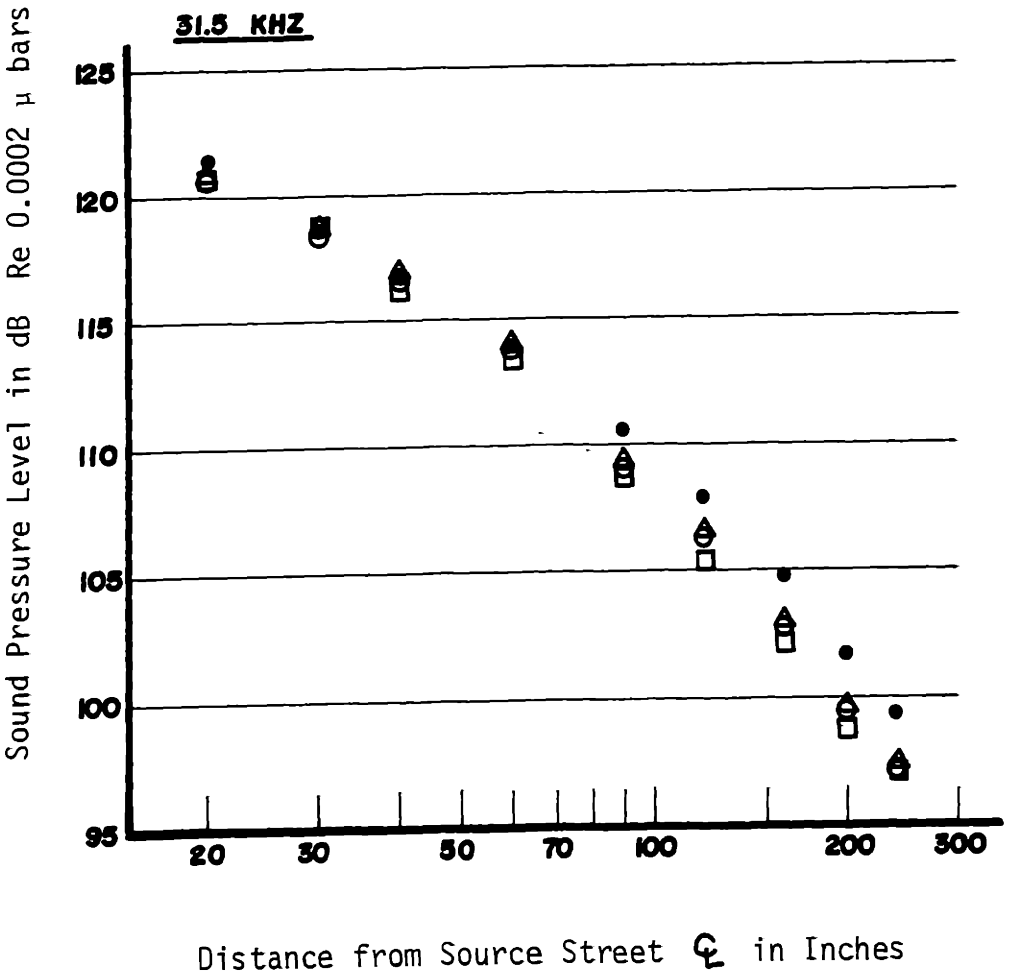

FIGURE 4.29: Comparison of Acoustical Model Data and Imaging/ Scattering Line Source Levels - Tee Intersection

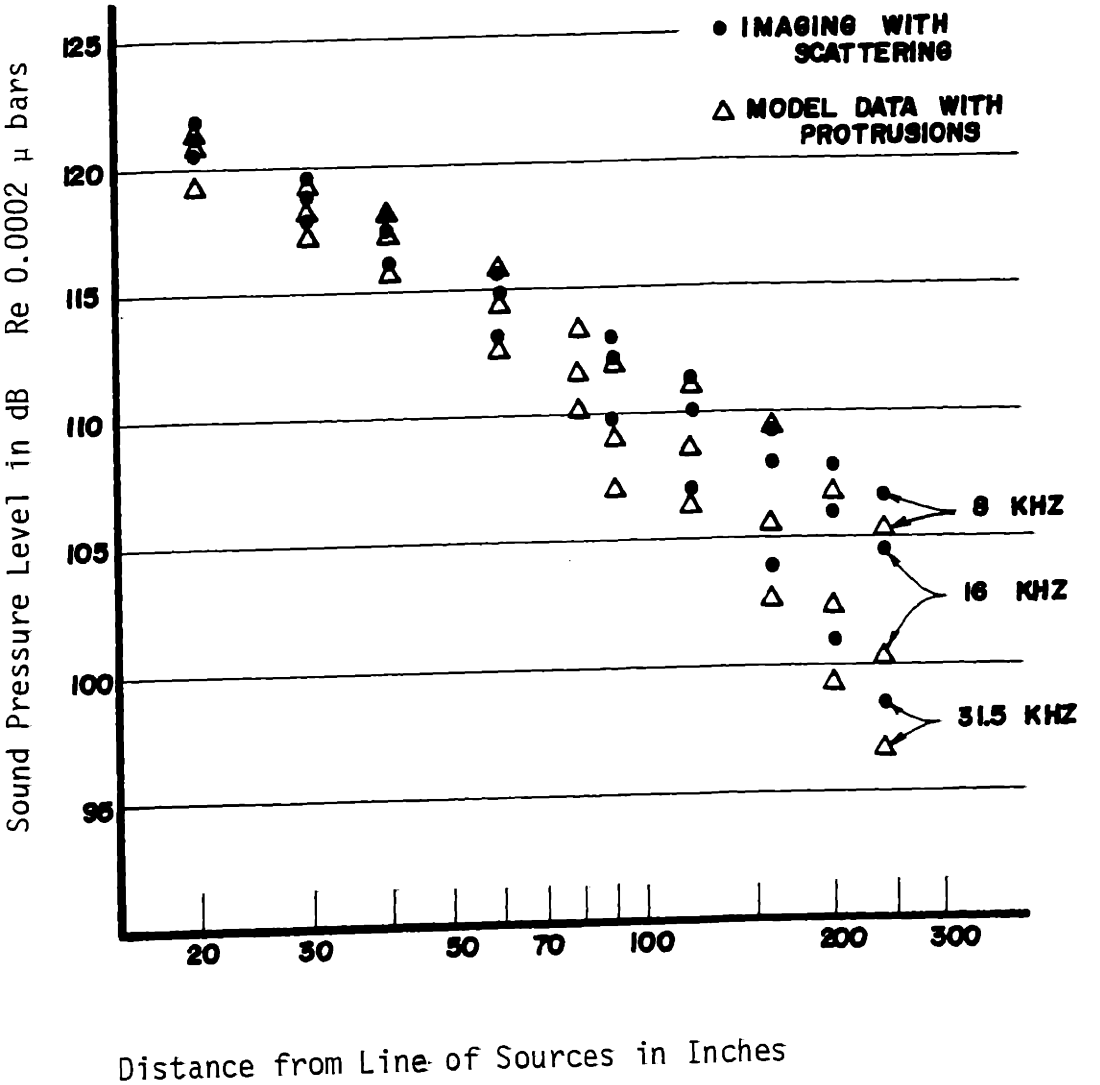

FIGURE 4.30: Comparison of Acoustical Model and Imaging/Scattering Line Source Levels - Four Way Intersection

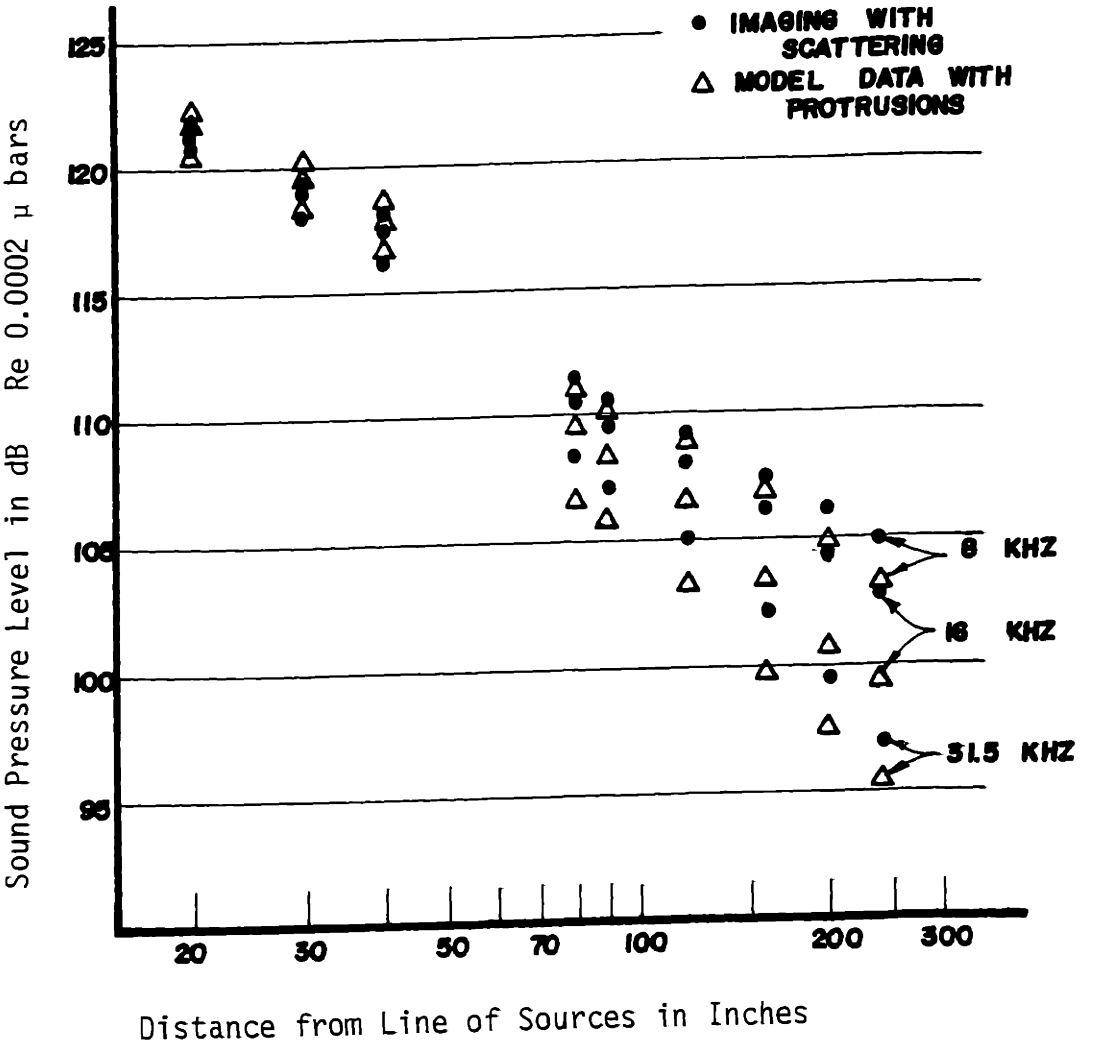

FIGURE 4.31: Comparison of Acoustical Model and Imaging/Scattering Line Source Levels - Four Way Intersection with Cross Street

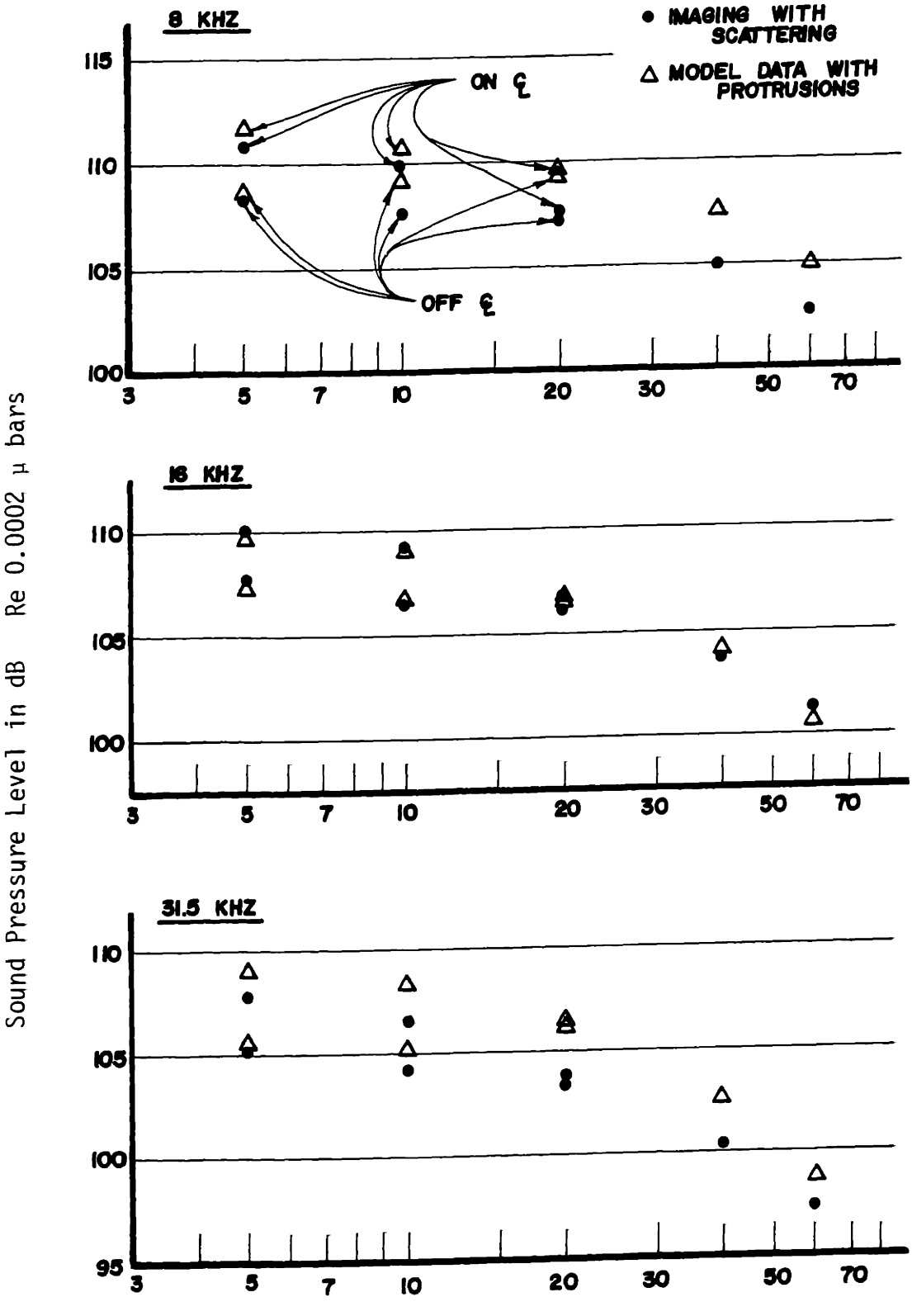

FIGURE 4.32: Comparison of Acoustical Model and Imaging/Scattering Line Source Levels - Cross Street

behavior for the 16 kHz band can be attributed to the $\lambda/4$ resonance phenomenon. The data reported in Figures 4.30 and 4.31 is for a protrusion depth of .188 inches. A quarter of a wavelength at 16 kHz is .211 inches. Thus resonance effects are expected to occur in this band producing relatively lower levels than for the 8 and 31.5 kHz bands. In comparing the simulation results to the model results for this band, it should be recalled that the scattering model is band averaged and, therefore, will not predict the details of the octave band containing the $\lambda/4$ resonance. Even with this phenomenon, however, there is good correspondence between the imaging with scattering values and the acoustical model data.

4.7.3 Simulation of Field Data

The scattering model and imaging theory can also be applied to the field data reported in Section 3.2.1. In Figure 4.33 the field data is shown along with the corresponding results using the prediction technique. From this figure, it will be noted that there is good correspondence between the two sets of results. The theoretical values fall within about 2 to 3 dB for all the field data points. As attenuation due to air absorption is quite minimal for the frequencies and distances of the field data, it was not included in the analytical values.

With the comparisons given in Figures 4.25 through 4.33, it can be concluded that imaging theory with the second order scattering model provides a propagation model which is appropriate for urban

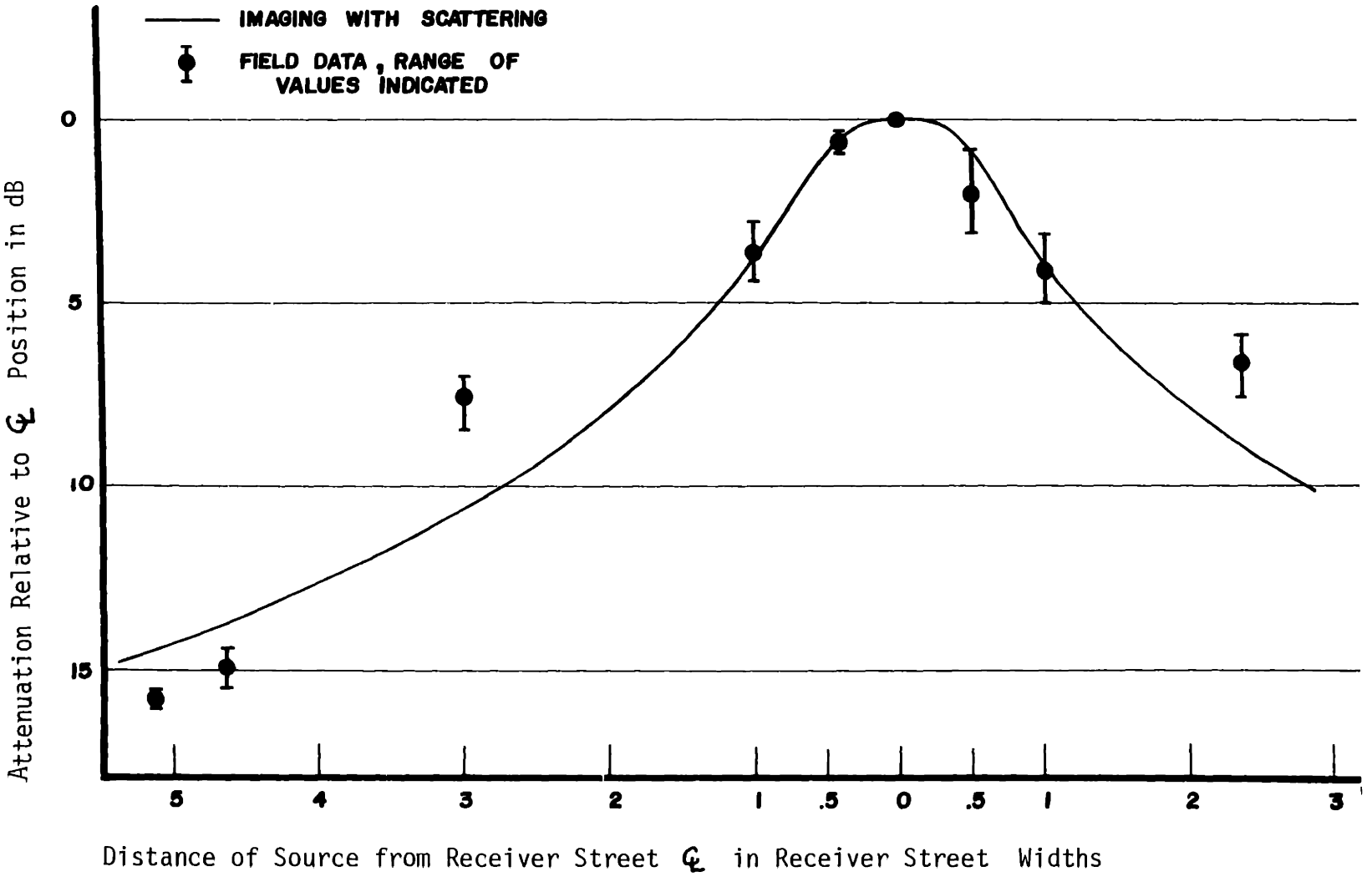

Figure 4.33: Comparison of Field Data and Imaging/Scattering Results

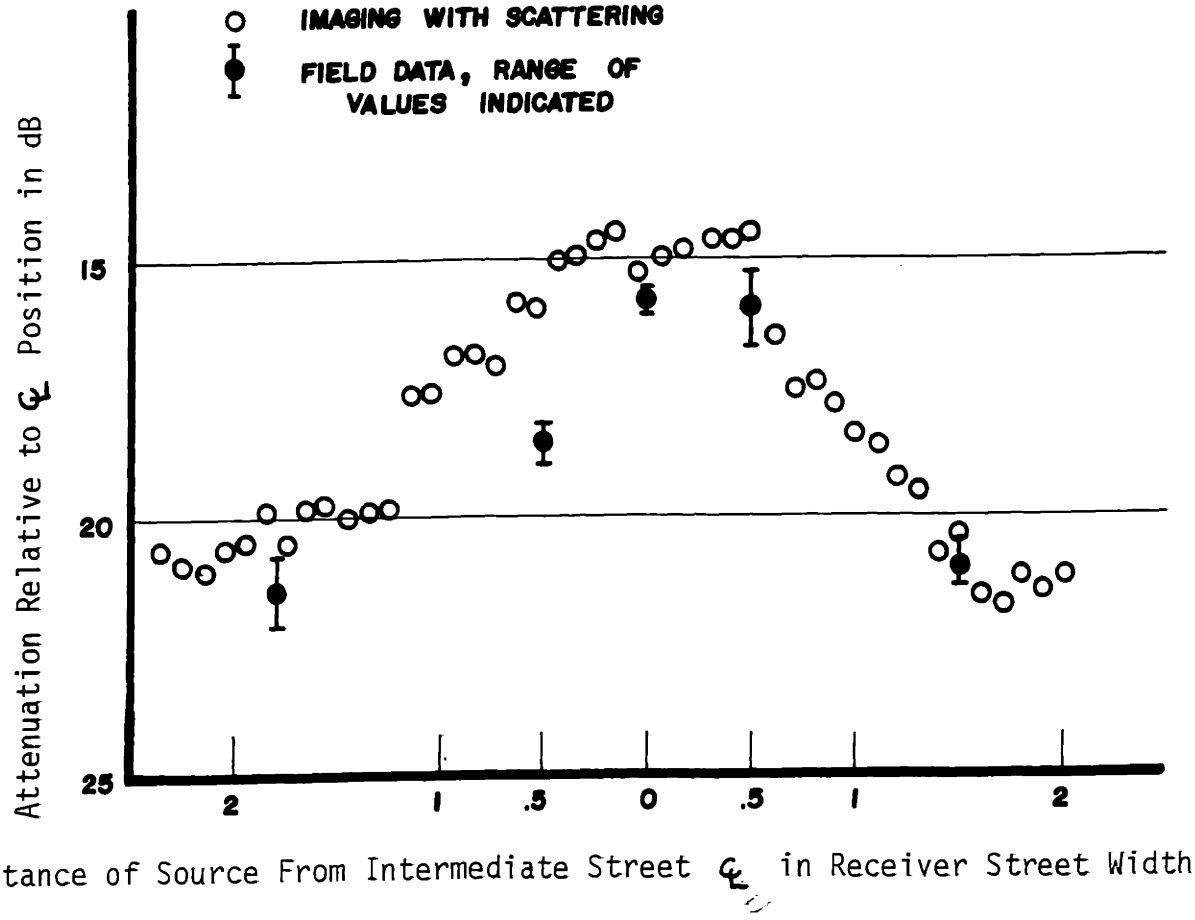

FIGURE 4.33: Comparison of Field Data and Imaging/Scattering Results

sound propagation. With the use of this model, it has been shown that sound levels can be predicted typically within at least 2 or 3 dB of measured data.

4.7.4 Comparison of Scattering Models and Experimental Data

In order to compare the first and second order scattering models in relation to field and acoustical model data, the results given in Figures 3.23, 3.27 and 4.33 are combined in Figure 4.34. This figure affords a direct comparison of field data, acoustical model data and imaging utilizing the first and second order scattering models. As the source power level was only known for the acoustical model data, the figure was constructed by first simulating the model data with the two imaging results. The model data was then matched to the zero attenuation position of the field data. For propagation around two corners, no corresponding acoustical model was taken. For this case, the field data and the two imaging results are given.

For propagation from the single intersection, Figure 4.34 indicates a close correspondence bwtween the field data, the acoustical model data and imaging with second order scattering. The imaging values utilizing the first order scattering model are consistently lower than the other three sets of values. This difference is a maximum of about 5 to 6 dB for the more distant source positions. When the source is in or near the intersection, the first order results are within 1/2 to 1 dB of the other three values. In regard to both the field and acoustical model data, this same behavior of the first order

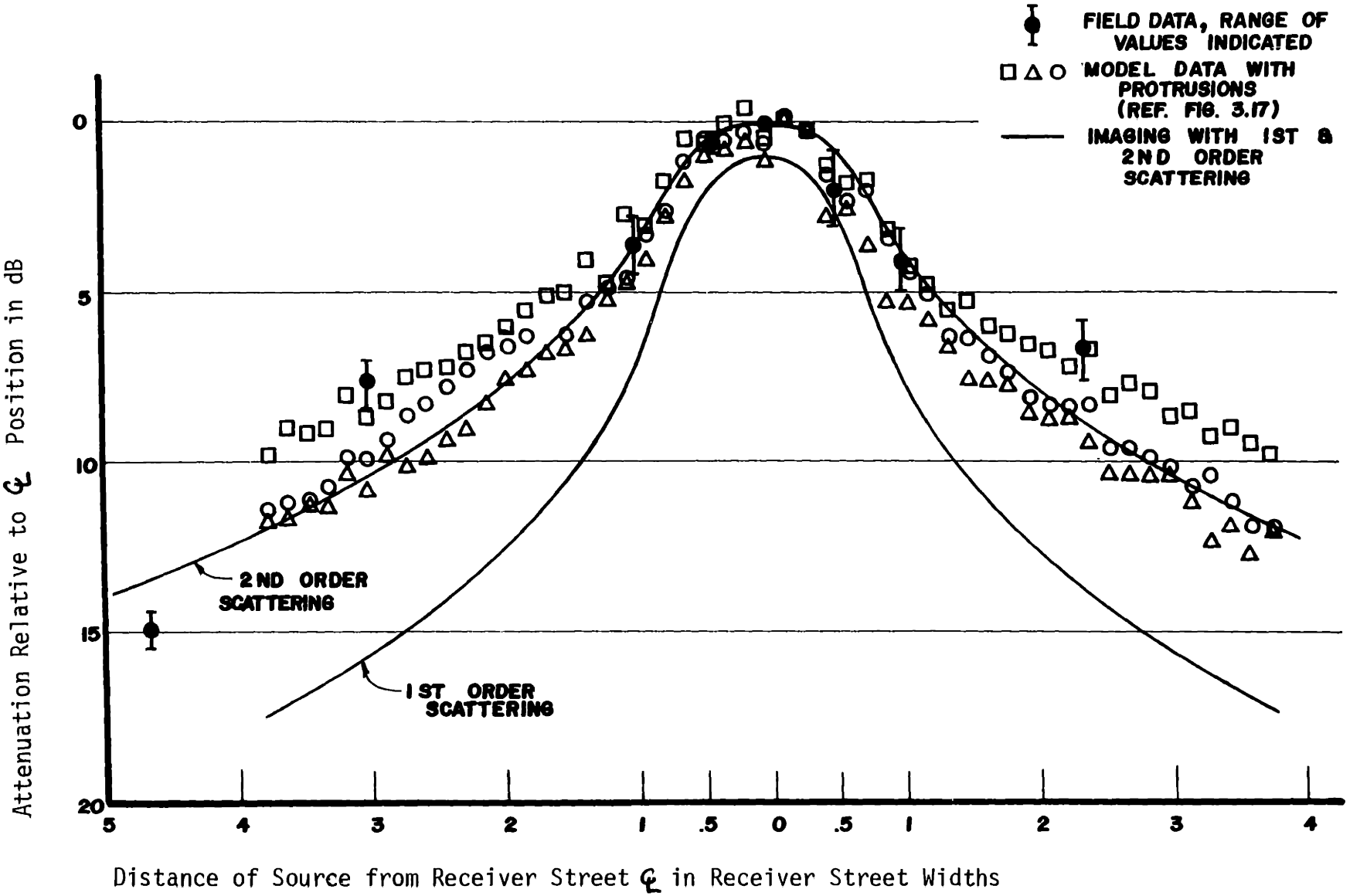

FIGURE 4.34: Comparison of Field Data, Acoustical Model Data and Imaging with First and Second Order Scattering Models

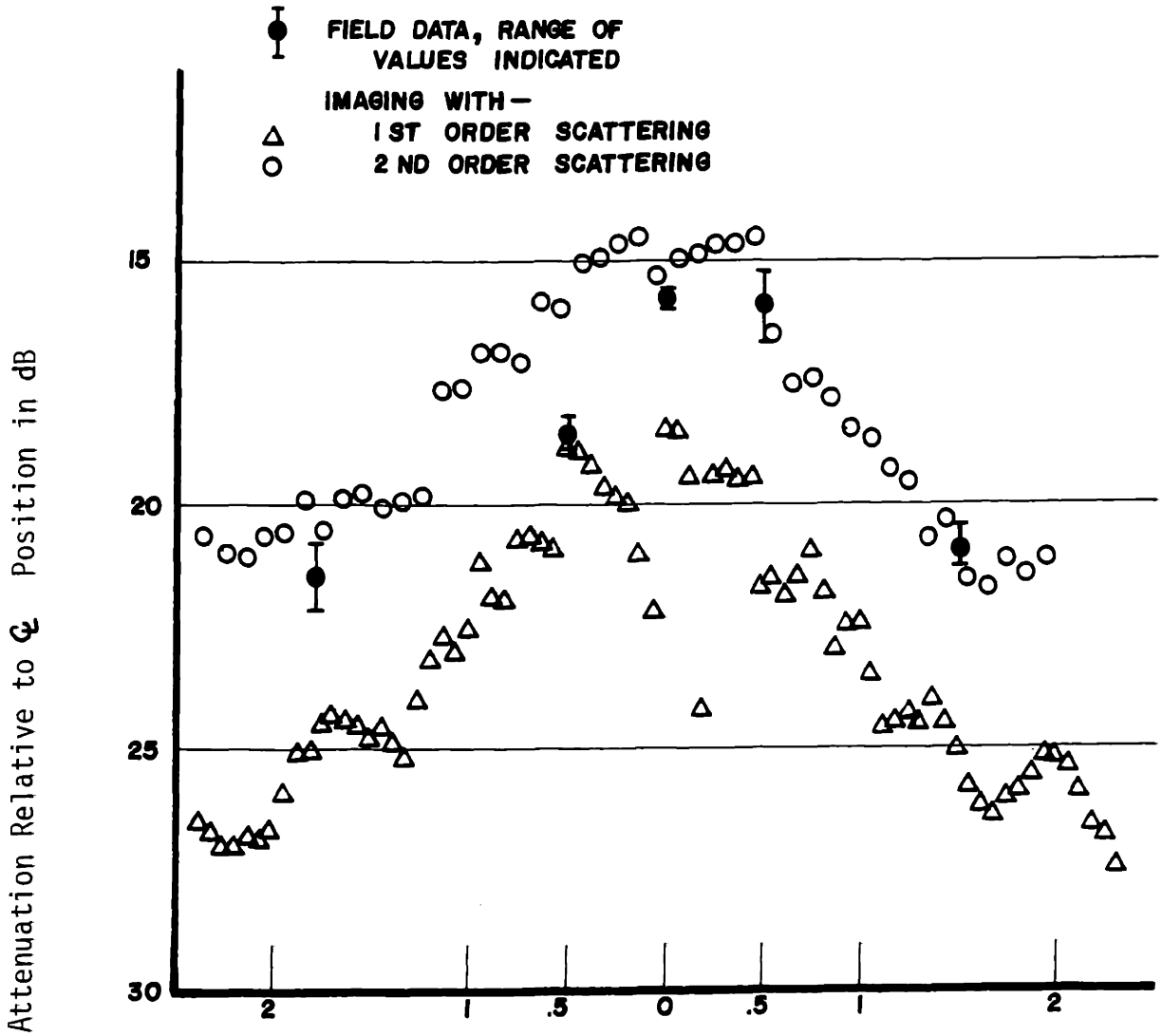

FIGURE 4.34: Comparison of Field Data and Imaging with First and Second Order Scattering Models

scattering model was noted in Section 3.3.2 and was responsible for the development of the second order approximation.

For propagation from the second intersection, it will be noted that the first order scattering results are again lower than the second order results and the field data. The first order results are quite similar in shape to those of the second order approximation although they are approximately 4 to 5 dB lower. The imaging results with second order scattering are also seen to agree well with the field data for all but one point. For this particular source position, the simulated result is about 2 dB higher than the data. All other points are well within 1 dB of the field data.

V. URBAN NOISE PROPAGATION PREDICTION

5.1 Application of the Propagation Models

With the verification of the second order scattering model in Section 4.7, imaging with angularly dependent reflection ratio and surface scattering can be used for more general propagation prediction. The computer programs used for simulation of acoustical model data in Section 4.7.2 were expanded for this purpose. The expansion included decreasing source spacing to .1 receiver street widths from the original .15. Decreased spacing provided better line source simulation from the total array of source locations. Further, source positions up to 10 receiver street widths from the intersection center were added to the original 3.75 street widths. Receiver positions up to 20 street widths were also added for the street intersecting the source street. Two receiver positions across the street width were averaged at each receiver distance. For propagation into a second intersecting street, positions up to 8 street widths were added. In addition to the original four simulation programs, two new programs were developed. Programs for straight channel propagation and propagation from an open intersection were added.

Although in principle the propagation model can be applied to any urban geometry, only the cases arising from the common "grid pattern" have been developed here. This choice was made in order to limit the cases to a reasonable number and yet to obtain results

applicable to most urban areas. The cases comprising the grid pattern include propagation from a single intersection, propagation from one intersection through another, and propagation into the street of the second intersection. For the single intersection case, the variations of four-way, tee, and open intersections were also included. A final necessary case was propagation for sources located in the receiver street. Utilizing all these cases, the sound level due to sources in any given street in a region as pictured in Figure 5.1 can be determined.

In applying the predictions based on imaging theory to actual streets and sources, one limitation must be realized. This limitation is in regard to the energy addition assumption used in imaging theory as discussed in Section 2.1. As will be discussed to a greater extent in Section 5.3.1, the energy addition assumption breaks down if the difference in length between the direct and reflected paths to the receiver is less than one wavelength. For channel propagation, this limitation is of concern when the receiver is sufficiently far from the source that the difference in length between the direct and wall reflected paths is less than a wavelength. This limiting situation can be readily formulated in terms of the street geometry. With the various relative positions that the source and receiver can assume across the street width, it is easiest to examine the average case of the source and receiver lying on the centerline of the receiver street. This situation is presented in Figure 5.2. Using the geometry of this

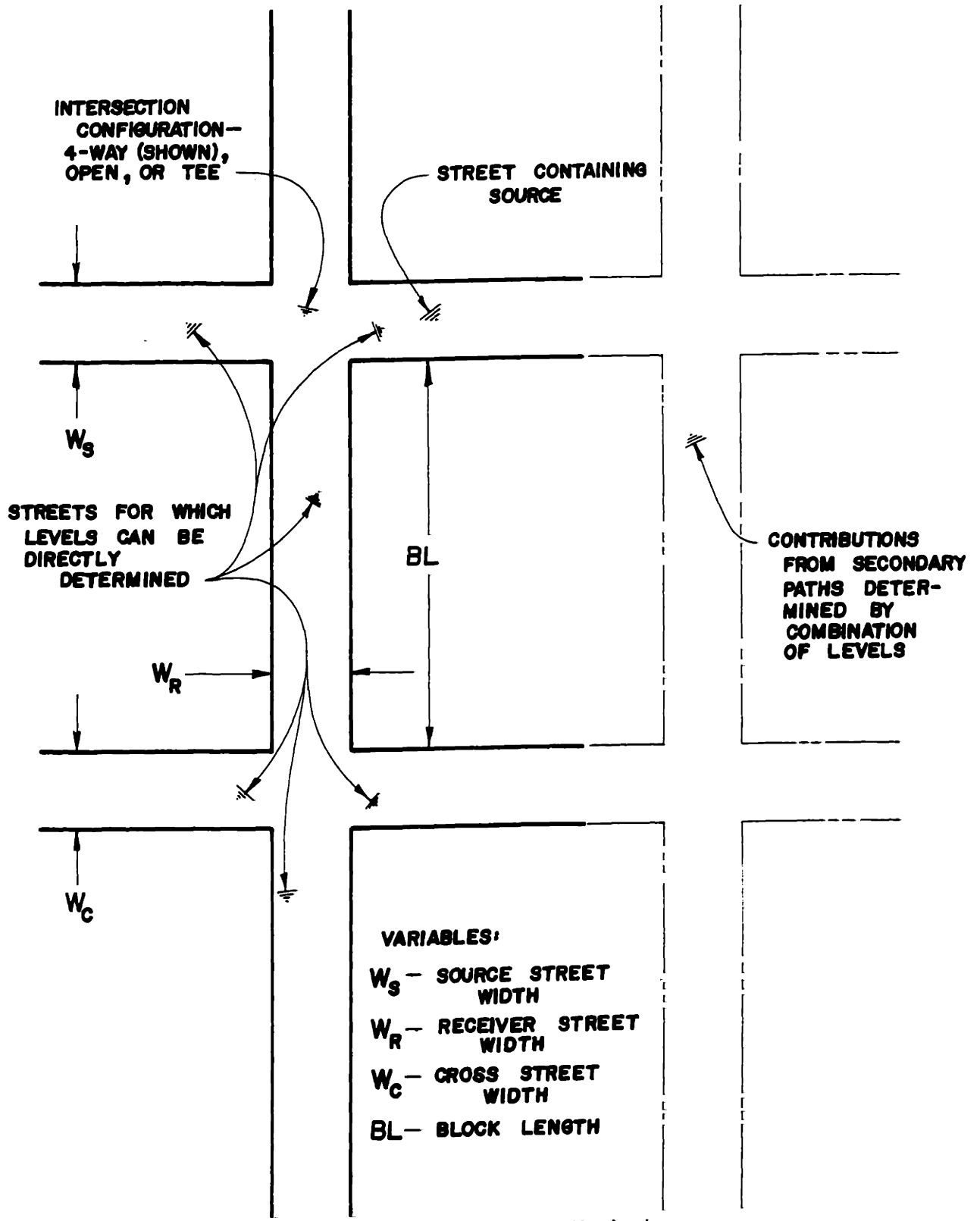

FIGURE 5.1: Applicability of Prediction Method

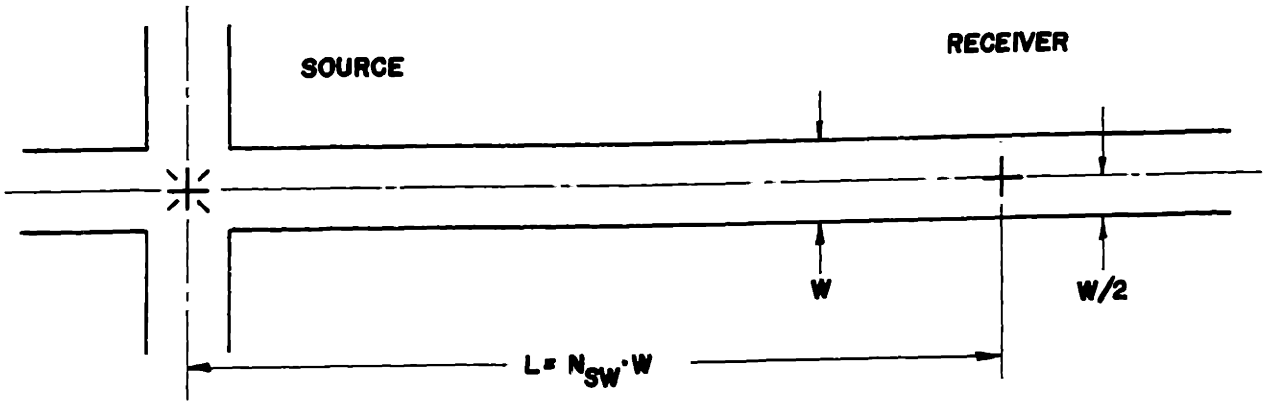

PATH LENGTH DIFFERENCE = $W \cdot (\sqrt{1 \quad N_{SW}^2} - N_{SW})$

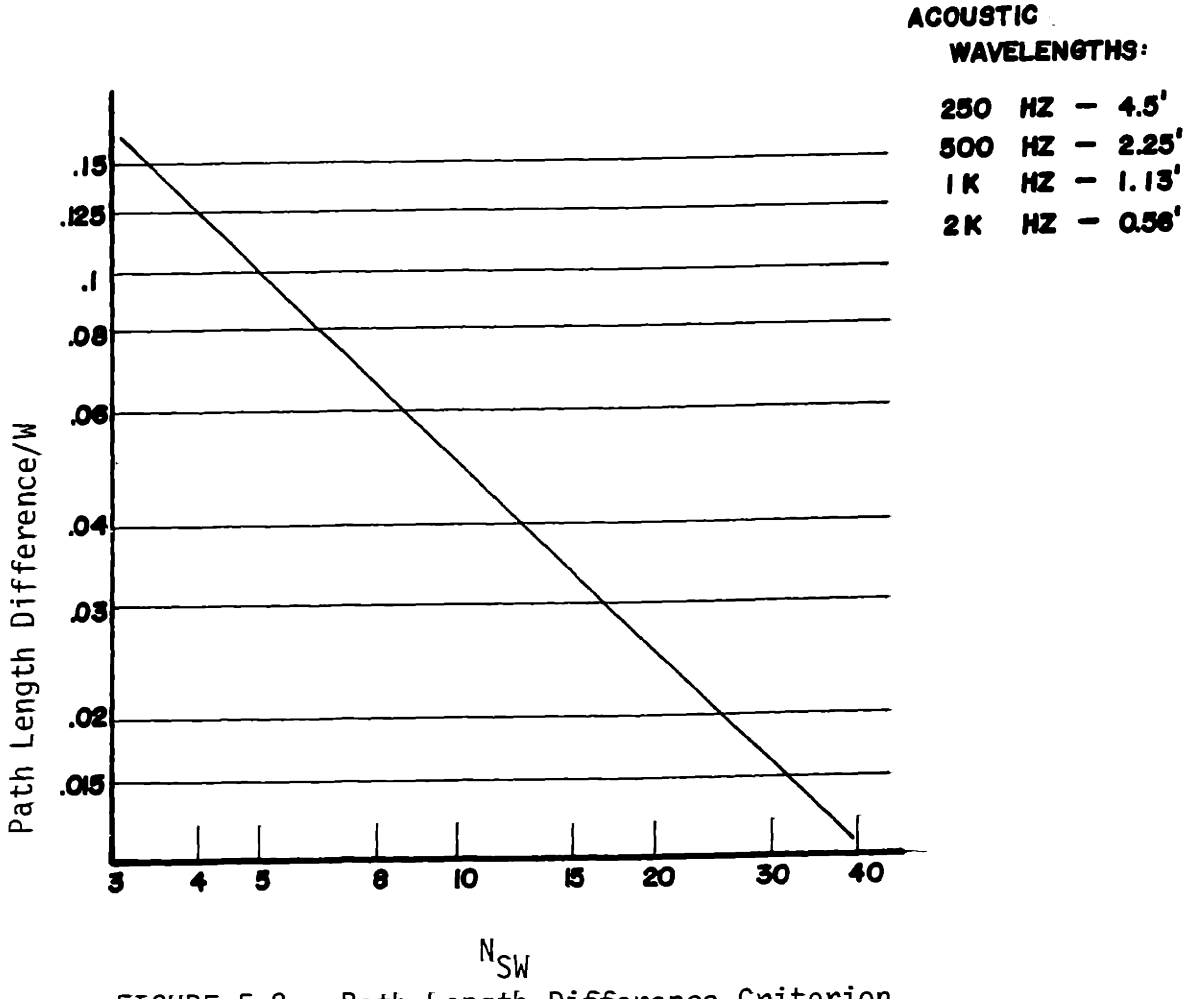

FIGURE 5.2: Path Length Difference Criterion

figure, the difference in length for the direct and wall reflected paths is

$$\delta D = (2x\sqrt{(W/2)^2 + (L/2)^2}) - L$$

where W is the street width and L is the distance between source and receiver. Letting N_{SW} equal the separation expressed in street widths, this expression can be simplified to:

$$\delta D = Wx\ (\sqrt{1 + N_{SW}^2} - N_{SW}).$$

The factor in parenthesese was determined for values of separaticn from 2 to 50 street widths and is presented in Figure 5.2. The acoustic wavelengths corresponding to the octave band center frequencies of importance for urban noise are also given in this figure. As example of application of this criterion, consider a street width of 75 feet. Calculating the corresponding values of δD, it is found that imaging theory predictions can be used up to 8 1/4 street widths for 250 Hz, 16 1/2 for 500 Hz and could be used beyond 20 street widths for both the 1 kHz and 2 kHz bands. For A-weighted urban noise owing to the significant contribution of the 500 Hz band, the imaging predictions should not be employed beyond about 16 street widths for this example. For general application, this criterion should be checked before using imaging results for prediction beyond 10 street widths. If the criterion is violated, errors on the order of 3 to 6 dB should be expected.

5.2 Prediction for Basic Source Types

5.2.1 Point Sources

Attenuation values obtained from computer programs employing angularly dependent imaging and scattering can be applied directly to predict point source sound levels. The computed values are expressed in attenuation relative to the free field sound level of the source at one receiver street width. The source level can be expressed in octave bands for the range of 250 to 2000 Hz or in A-weighted sound level. The geometry of the situation for which prediction is desired must be converted to dimensions in ratios of the receiver street widths. The corresponding attenuation can then be determined from the computed values. This attenuation is then subtracted from the source level at one receiver street width to obtain the predicted sound level. Corrections for ground reflection and environmental conditions may also be applied to this predicted sound level if necessary. These corrections are described in Section 5.4.

An example of computer generated attenuation values for a particular propagation case is presented in Figure 5.3. This figure plots results for propagation from a four-way interesction with equal source and receiver street widths. For this figure, relative attenuation is plotted as a function of source distance from the receiver street centerline. The distance of the receiver from the source street centerline is the parameter.

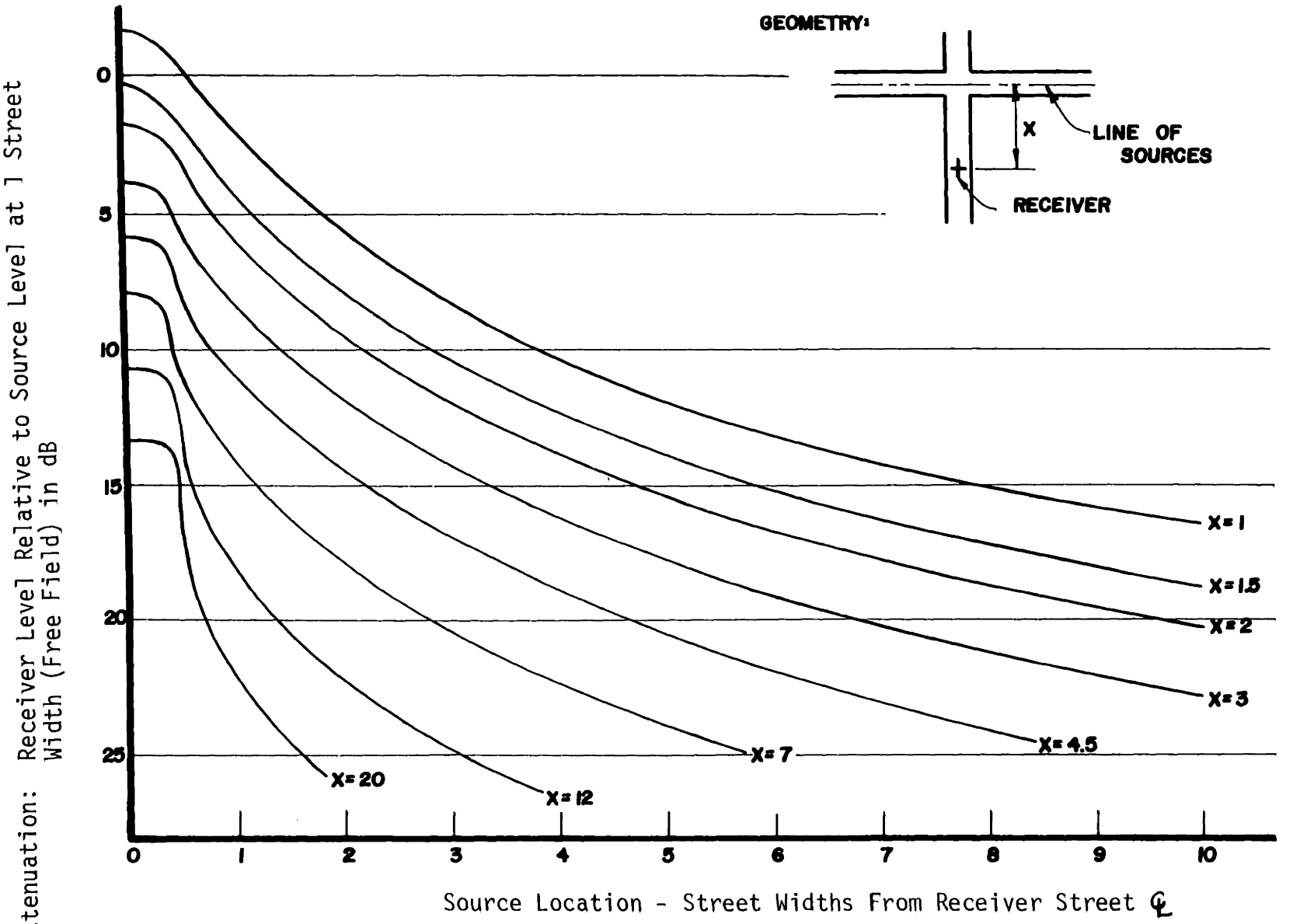

FIGURE 5.3: Point Source Attenuation - Four Way Intersection

In applying the computed values to propagation from a point source, the assumptions made in determining these results must be considered. One such assumption is that the source is an ideal point source, that is, omnidirectional and of no dimension. For traffic noise sources, the omnidirectional assumption is quite commonly employed [19]. Other sources must be examined individually. The assumption of no dimensional extent is not met by actual sources. However, as most sources are typically considerably less than a street width in extent, this condition is approximately satisfied. Another assumption employed is that the geometry be "urban". As applied to the propagation model, urban is taken to mean that buildings extend in height at least one street width above the source position and that buildings are spaced closely together. These conditions are necessary to insure that the sound level measured at the receiver position is due to propagation along the street channels. As will be indicated in the Section 5.3.2, building spacing should be less than 1/4 of a street width to produce no appreciable effect on the propagation. The final assumption used in developing the propagation model is that building walls display surface irregularities. As long as some irregularity is present, the details of the surfaces may be ignored.

5.2.2 Line Sources and Traffic Flows

The point source attenuation values for any one receiver position can be summed for all the source positions. This summation

gives an effective line source attenuation level at the receiver position. This attenuation corresponds to that which would be obtained if a line source were located in the source street. For such a source, the computed attenuation is used directly as was done for a single point source. To apply the predicted attenuation for some particular geometry, the level of the source measured at one street width in a free field must be known. The attenuation value is subtracted from this source level to determine the sound level at the receiver point. The procedure gives only an approximation to the attenuation produced by an infinite line source. The approximation is quite good, however, as largest contribution to the line source level occurs from those segments of the source in or near the intersection. The relative magnitude of the contribution is apparent from Figure 5.3. It should be noted that for a line source in a free field measured at one street width, that portion of the source beyond 10 street widths contributes only an additional .3 dB to the level of the finite source.

The line level source attenuation values can also be applied to traffic flows. This is done by visualizing the curves of attenuation versus source position given in Figure 5.3 as time histories of single vehicle pass-bys. More accurately, the curves correspond to position histories of pass-bys which are related to time histories through the vehicle speed. If a particular vehicle speed is assigned, the line source level corresponds directly to the Equivalent Energy Level (L_{EQ}) produced in the time of the single

vehicle pass-by. By examination of the definition of L_{EQ}, it can be further shown that the L_{EQ} of the pass-by corresponds to the line source level regardless of vehicle speed if the L_{EQ} integration time is the duration of the pass-by. Equivalent Energy Level is defined as [26]:

$$L_{EQ} = 10 \log_{10} \{\int_{t_1}^{t_2} P_A^2 \, dt/[P_o^2(t_2-t_1)]\}$$

where t_1 and t_2 define the time interval of the L_{EQ}, P_A^2 is the mean square A-weighted sound pressure, and P_o is the reference pressure,

$$P_o = 2x10^{-5} \text{ N/M}^2 .$$

For direct correspondence to the line source level, the integration interval must be taken to be the time interval of the pass-by. This time interval is equal to the distance of 20 street widths divided by the vehicle speed. If the same time is kept, but now N vehicles are allowed to pass-by in the time period, the L_{EQ} can still be determined from the line source level. As a specific example, consider N = 4. The L_{EQ} is then given as

$$L_{EQ}^{(4)} = 10 \log_{10} \{\int_{t_1}^{t_2} P_{A_t}^2 dt/[P_o^2(t_2-t_1)]\}$$

where

$$P_{A_t}^2 = P_{A_1}^2 + P_{A_2}^2 + P_{A_3}^2 + P_{A_4}^2$$

is the sum of the individual A-weighted mean square pressures. Each of these pressure terms can be integrated separately and then summed. The four terms separately correspond to the energy of the individual pass-bys. If the average of the P_A^2's is used, the L_{EQ} becomes

$$L_{EQ}^{(4)} = 10 \log_{10} \{4 \int_{t_1}^{t_2} P_{A_{AV}}^2 \, dt/[P_o^2 (t_2-t_1)]\}$$

or

$$L_{EQ}^{(4)} = 6 + 10 \log_{10} \{\int_{t_1}^{t_2} P_{A_{AV}}^2 \, dt/[P_o^2 (t_2-t_1)]\}.$$

The effect of four pass-bys compared to one pass-by is thus to add 6 dB to the single event L_{EQ}.

The observations in regard to L_{EQ} can be formalized into a normalization scheme which accounts for traffic density. To develop this scheme, the traffic flow is considered as a line source made from many discrete point sources of acoustic power W_i. To obtain an expression for the incremental intensity produced by a segment of the source, consider an increment dx along the source. The power per unit length of source is determined by the density of point sources and is given by:

$$W(x) = \frac{W_i N}{R}$$

where N is the number of sources in the length of one receiver street width, R. The incremental intensity is then

$$dI = \frac{W(x)\,dx}{4\pi r^2}$$

where r is the straight line distance from the receiver to the increment dx. Substituting (R+x) for r, expressing W(x) with its x independent value, and integrating in x from $-\infty$ to $+\infty$ yields the following expression for the intensity

$$I = \frac{W_i N}{4R^2}$$

In this expression, the power W_i of an individual point source can be written in terms of pressure amplitude at one receiver street width, R

$$W_i = \frac{4\pi P^2 R^2}{\rho c}$$

where P^2 is the corresponding pressure amplitude, and ρc is the characteristic impedance of air. This value of W_i is then substituted in the expression for I, and the intensity level taken to give

$$L_I = 10 \log_{10} (\pi N P^2/\rho c\ I_{REF}).$$

This expression can be simplified to:

$$L_I = 10 \log_{10} \pi + 10 \log_{10} N + 10 \log_{10} (P^2/P^2_{REF}$$

$$+ 10 \log (P^2_{REF}/\rho_c\ I_{REF})$$

For a free progressive wave, the sound level is related to the intensity

level by [27]

$$L_p = L_I - 10 \log (P^2_{REF}/\rho c\ I_{REF}).$$

The total sound level for the source is, therefore, given as

$$L_p = 5 + 10 \log_{10} N + L_p^{(1)}$$

where $L_p^{(1)}$ is the average free field sound level of the individual sources at one receiver street width. The level L_p corresponds to the sound level produced by the line source made up of individual point sources in a free field as measured at one receiver street width.

With the use of the appropriate line source attenuation from the computed values, the L_{EQ} of a traffic flow for a specified urban geometry can now be determined. The L_{EQ} is found by simply calculating the total level, L_p, using the above equation and subtracting the appropriate line source attenuation from it. If a traffic flow is comprised of two vehicle types such as automobiles and trucks, the L_{EQ} of the flow is found by calculating the total L_p for each flow separately, combining the two levels, and applying the appropriate attenuation. Similarly, if flows from two different streets contribute to the sound level at a receiver point, the L_{EQ} for each can be determined separately using the corresponding attenuation values. The total L_{EQ} at the receiver is then the combination of the two individual L_{EQ}'s. In this manner, the total L_{EQ} from any number of traffic flows each with a mix of vehicle types can be calculated. As for point sources, corrections to traffic flow L_{EQ}'s and to line source sound levels may

also be necessary for ground reflection and environmental conditions.

The assumptions made in developing line source attenuation values are similar to those used in the point source case. A true line is assumed to produce uniform power per unit length and to be cylindrically homogeneous. For traffic flows, the individual sources possess the same attributes of the point sources of Section 5.2.1. The geometry of particular propagation cases is again assumed to be urban. For the L_{EQ}'s of traffic flows, there is no requirement on vehicular spacing. Further, the individual source need not have equal acoustic power output as long as the average level of the sources is used.

An example of line source attenuation is presented in Figure 5.4. The intersection geometry applicable is that of a four-way intersection with equal sources and receiver street widths. The figure plots attenuation versus distance of the receiver from the line source center.

5.3 Aspects of Urban Noise Propagation

5.3.1. Point Sources

There are numerous features of point source propagation in urban areas which could be contrasted. To keep the number of comparisons to a reasonable limit, some of the more important features for the six propagation cases are discussed in this section.

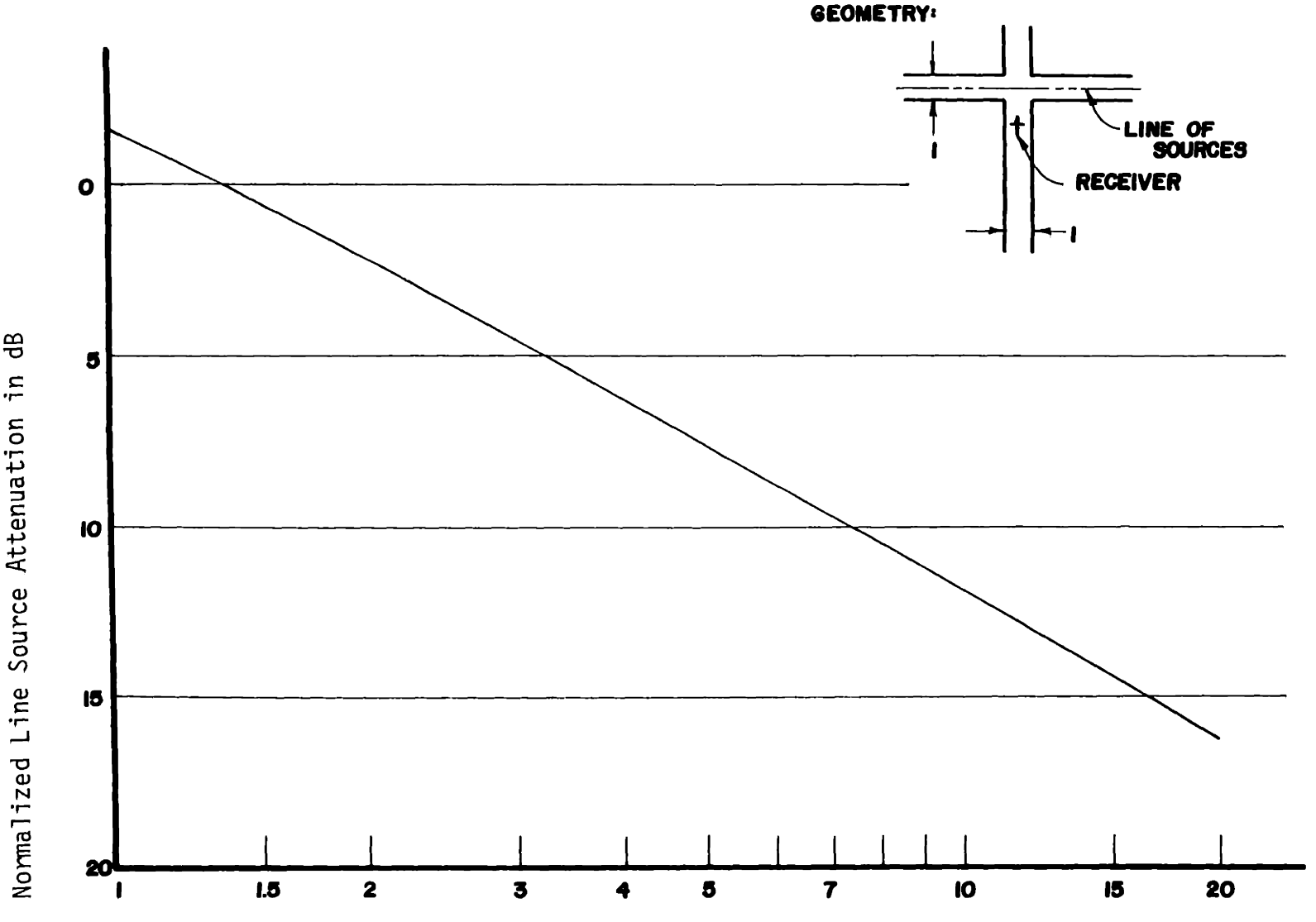

FIGURE 5.4: Line Source Attenuation - Four Way Intersection

The simplest case for which values were obtained is propagation in a straight street with no intersection. For this case and only this case, the values were obtained using the first order scattering model. This scattering model was chosen because of the accurate simulation it produces of the corresponding acoustical model data. The point source attenuation values for this case are presented in Figure 5.5. In this figure, attenuation relative to the free field source level at one street width is plotted as a function of source distance from the receiver. It will be noted that for those source positions very near the receiver, within 1/4 street width, the level is shown to be constant. This is done in order that the attenuation remain finite as well as correspond more accurately to the approach of an actual, finite source. Also displayed in this figure are the values for free field attenuation for a point source. At distances from the receiver of 3/4 street widths or less, the free field and channel attenuation values are approximately equal. This is due to dominant influence of the actual source relative to its images at these positions. As the source recedes from the receiver, the two sets of values diverge. The difference between the values corresponds to the reverberant build-up produced by the channel. At four street widths separation, this build-up is seen to be about 4 dB. When the separation is 10 street widths, the difference reaches 5 dB.

Several aspects of point source propagation from an intersection into the receiver street are presented in Figure 5.6 and 5.7.

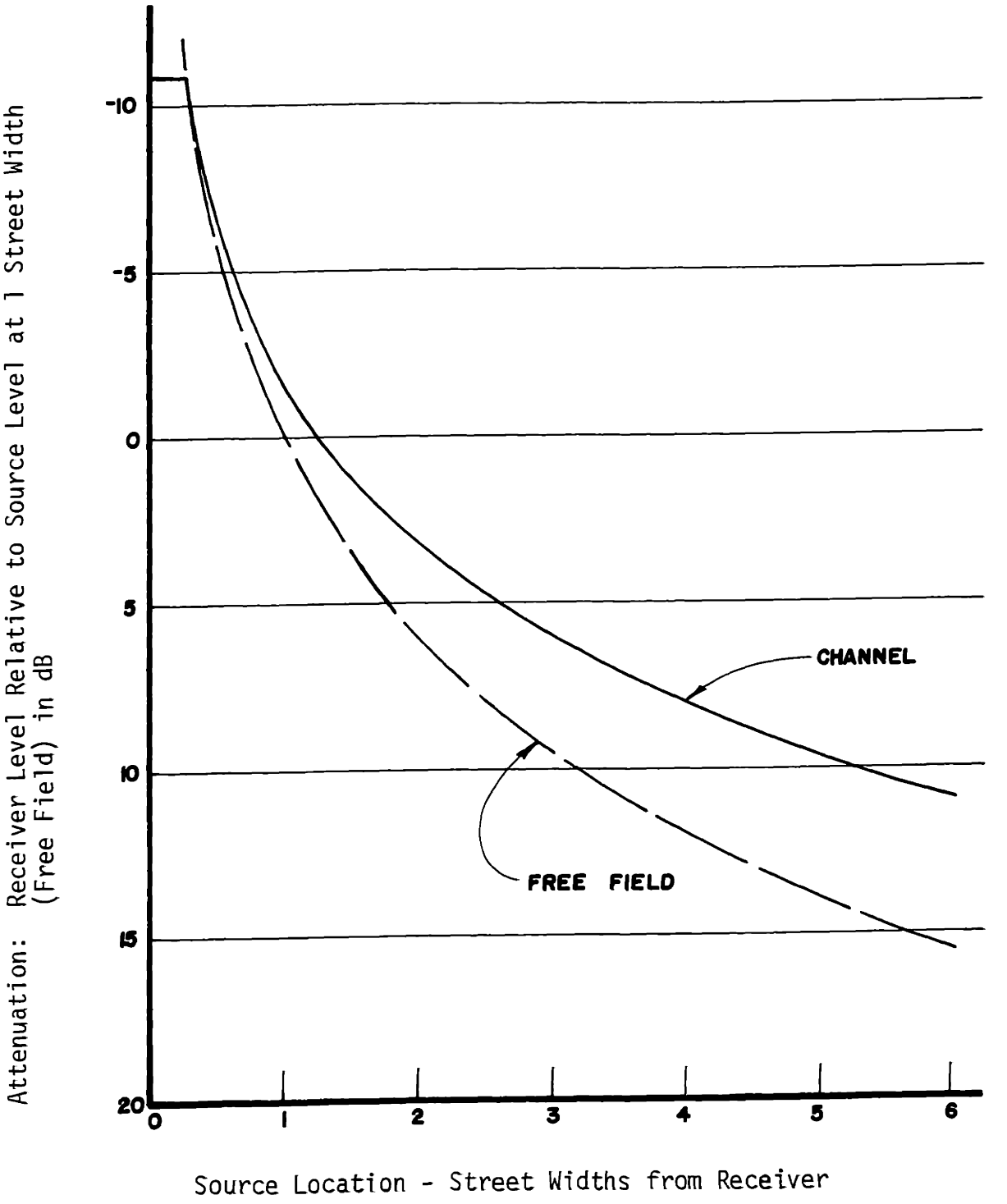

FIGURE 5.5: Point Source Attenuation - Source and Receiver in Same Street

In Figure 5.6 attenuation for various receiver positions for a four-way intersection is examined. From this figure, it is seen that the attenuation increases more rapidly with receiver distance for those source positions around the corner from the receiver than for those in which the source is in the intersection. This difference in attenuation rate creates a narrowing of the pass-by shape with receiver distance. Also, it will be noted that for all receiver locations, the attenuation is not strongly dependent on the location of source when it is in the intersection.

The point source attenuation values produced at receiver location of 4 1/2 street widths from the line of sources are contrasted in Figure 5.7 for an open, tee and four-way intersection. Comparison of the values for the tee and four-way intersection indicate very little difference between the two configurations. The values for the tee intersection are slightly higher than for the four-way, approximately 1/2 dB for the source in the intersection, and as much as 1 dB for source positions around the corner. Comparison of the open intersection with the four-way and the tee is more dramatic. Because of the absence of the second reflecting surface in the source street and hence the lack of reverberant build-up, the attenuation increases more rapidly with source position around the corner for the open intersection. At a distance of 4 street widths from the receiver street centerline, the open intersection attenuation values are seen to be 14 to 15 dB higher than those of the four-way and tee. When the source

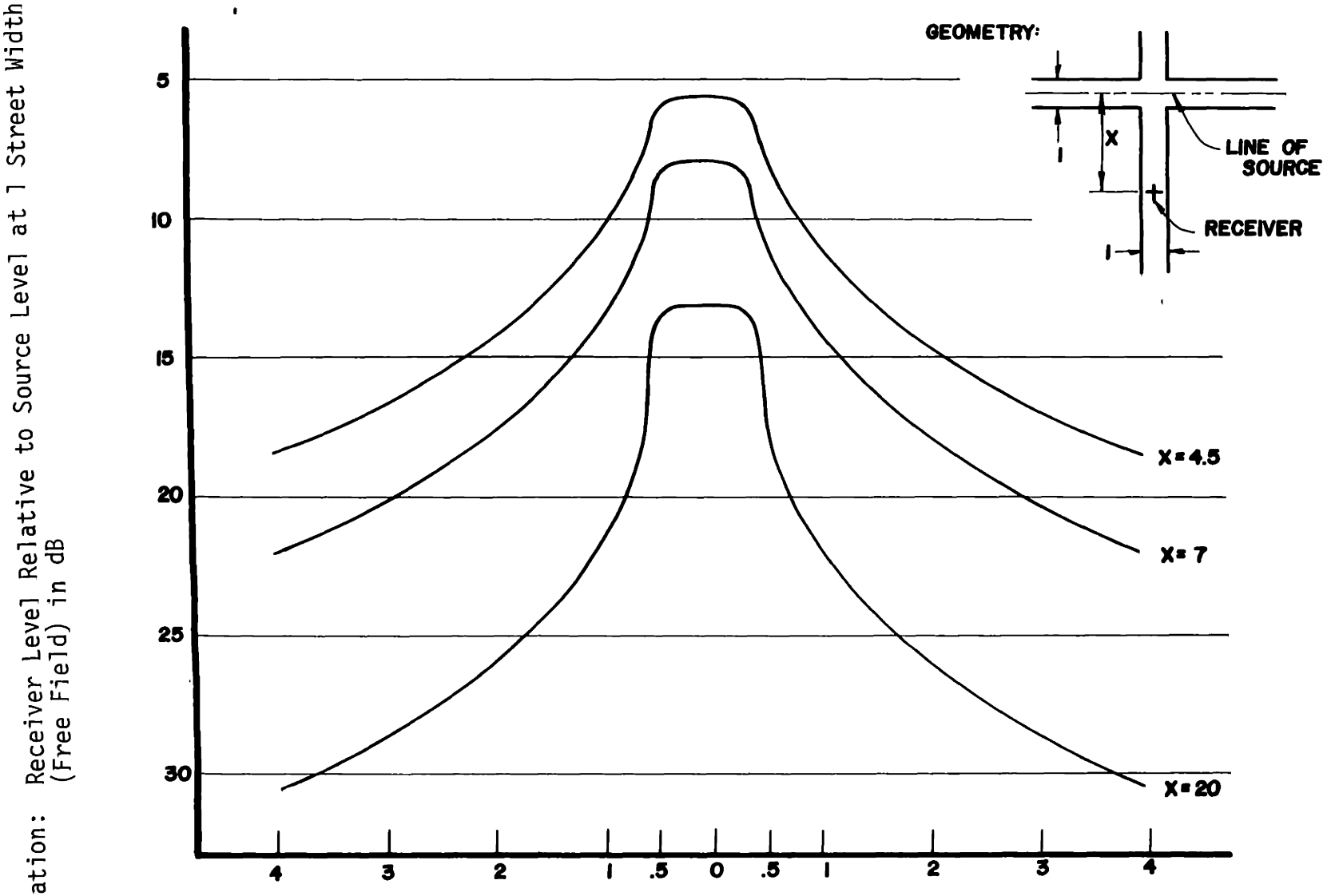

FIGURE 5.6: Point Source Attenuation - Variation with Distance, Four-Way Intersection

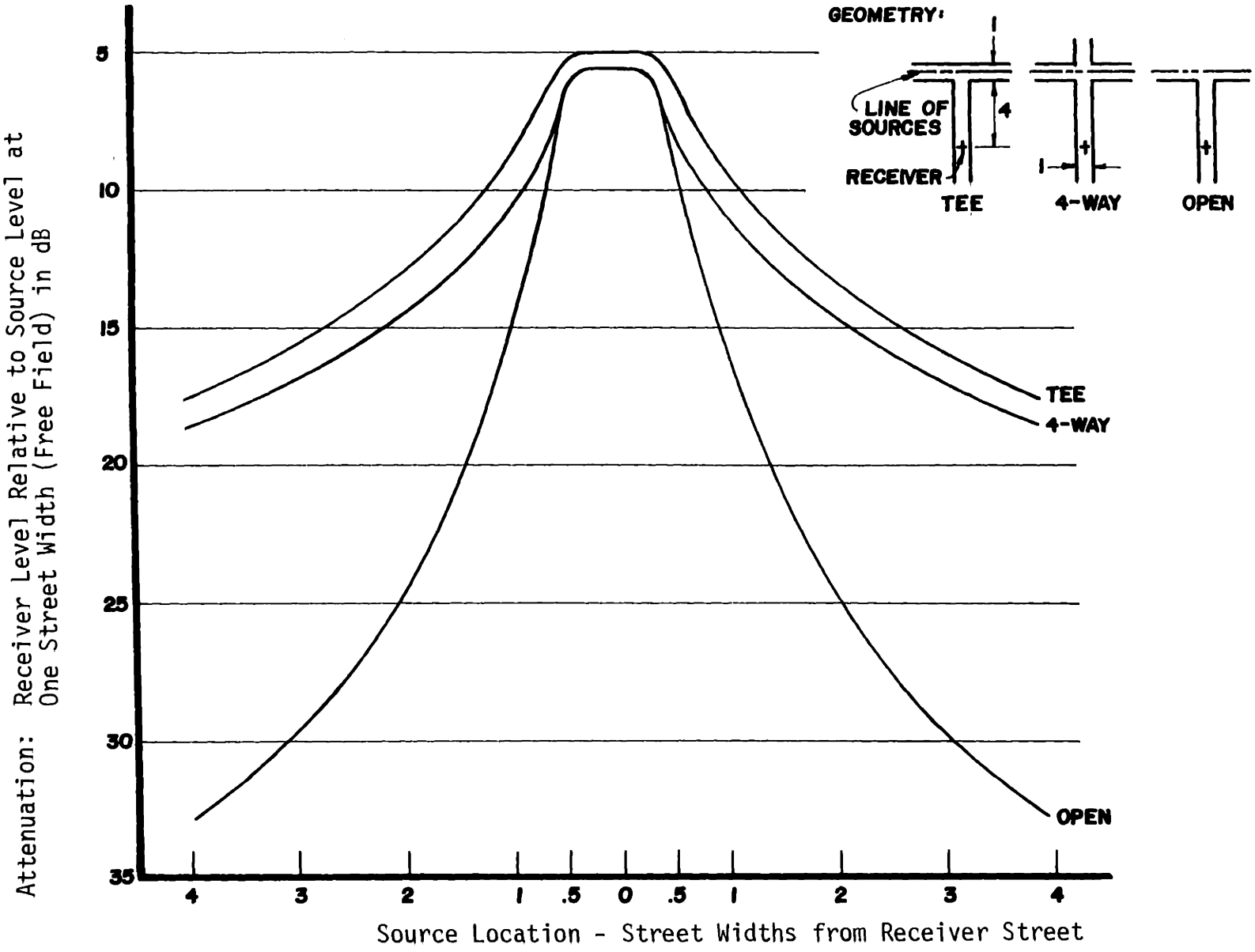

FIGURE 5.7: Point Source Attenuation - Tee, Four-Way and Open Intersections

is in the intersection, however, the values for the four-way and open intersections are the same.

In Figure 5.8, the attenuation values with and without an intervening intersection between the source street and the receiver is examined. The geometry of the comparison is given in the figure. From the figure, it is apparent that the change in attenuation produced by the intervening intersection is slight. It produces greater attenuation values for all source positions with differences of about 1/2 dB when the source is in the intersection and up to 1 1/2 dB when the source is around the corner. The increase of attenuation indicates that the effect of the second intersection is to subtract some of the energy that would otherwise reach the receiver. This subtraction of energy is particularly effective for those specular paths which are reflected many times in the receiver street. These paths have a higher probability of propagating into the opening of the second intersection.

The propagation of sound into a second intersection for a point source can also be examined for a variety of geometries. In Figure 5.9, the attenuation values at two different distances into the second street are presented for the receiver located at the street centerline as indicated in the figure. Contrary to the other five propagation cases, the values for propagation around a second corner can not be matched exactly by a smooth curve. To illustrate this more erratic behavior, the discrete attenuation values obtained for source spacings of 1/10 of a street width are given in this figure along

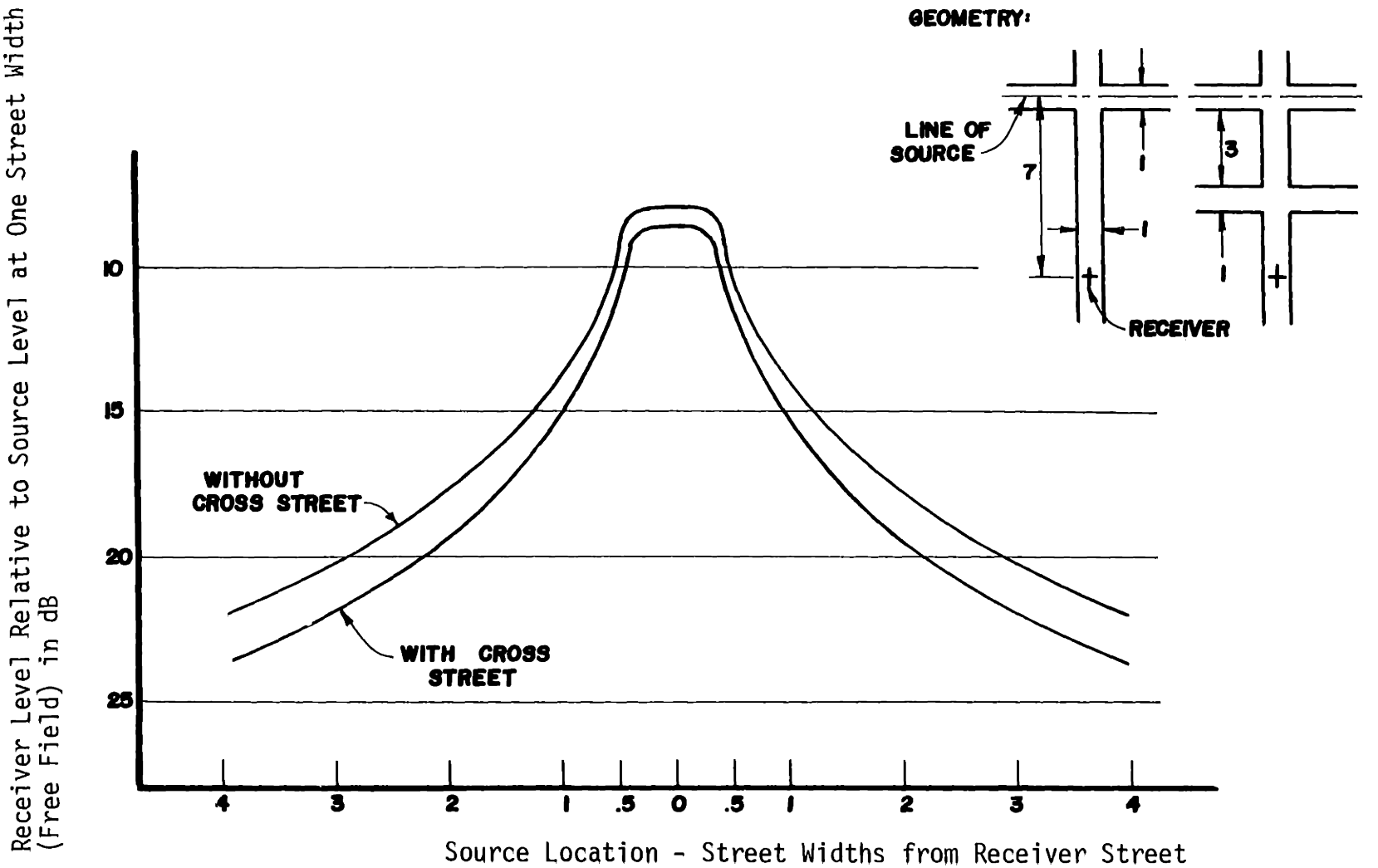

FIGURE 5.8: Point Source Attenuation - Four Way Intersection, With and Without Opening

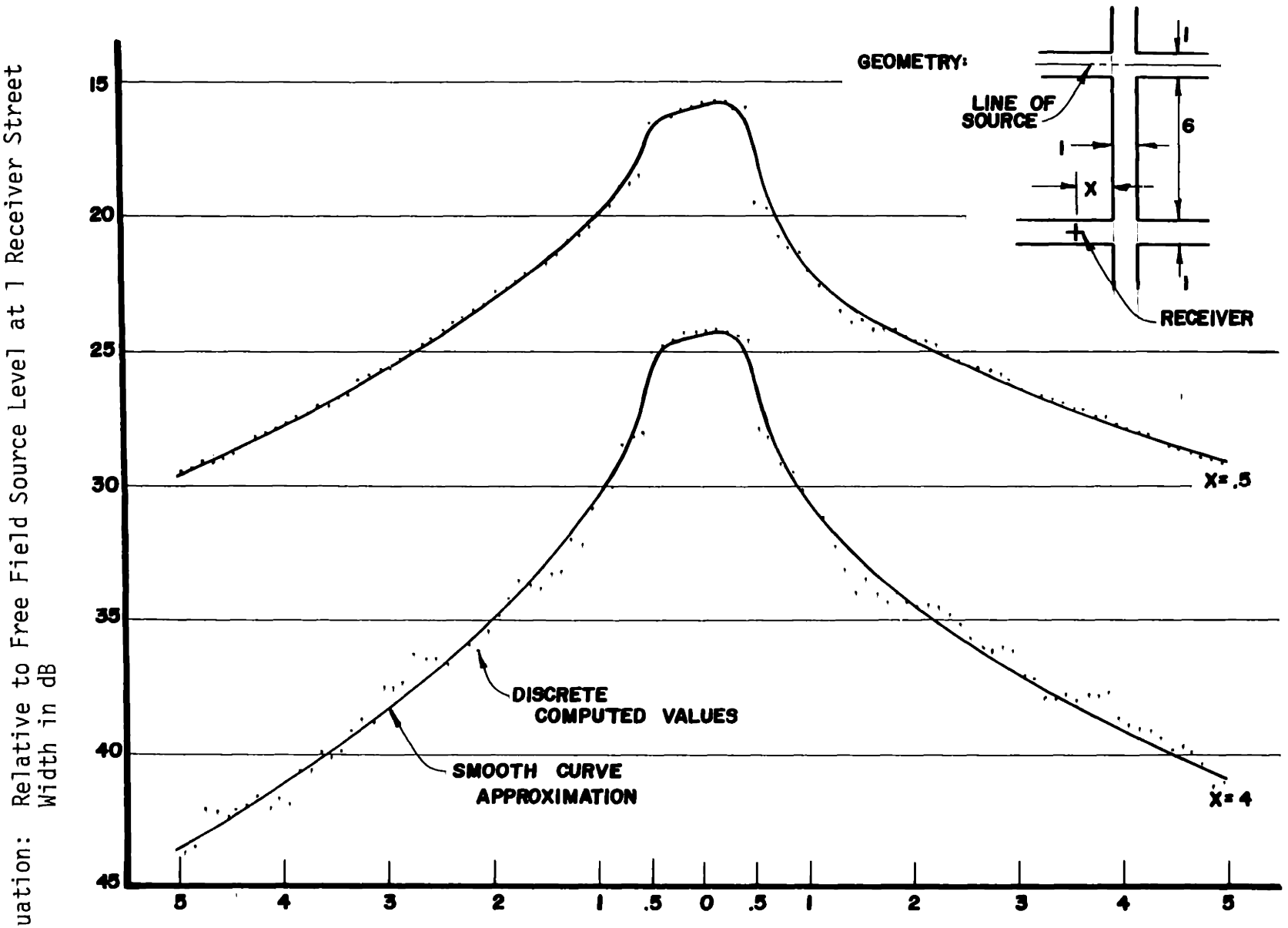

FIGURE 5.9: Point Source Attenuation - Variation with Distance into Second Intersection

with a corresponding smooth curve approximation. The deviations from a uniform increase of attenuation are attributable to the complicated geometry of this propagation case and the point nature of both source and receiver. These two factors produce rapidly changing "windows" through which portions of the image arrays are viewed. Because of the geometry, only a few images contribute to the sound level relative to other propagation cases. Thus, the loss or gain of one image as the source moves incrementally is noticed in the position history of the pass-by. Since real sources are finite in extent, the erratic behavior of the attenuation increase is not expected to be seen in actual situations. For this reason, as well as for ease in implementation of the predicted values, the smooth curve approximations are preferred. Use of these approximations can introduce an error of at most about 1 dB for the ideal point source as illustrated in Figure 5.9.

The shape of the pass-by attenuation position histories for the two distances down the second street in Figure 5.9 are somewhat similar to those for propagation from a single intersection. The behavior with distance from the source street is also similar to single intersection case. It will be observed that while the source is in the first intersection, the attenuation in the second street for a given receiver distance remains relatively constant. As the source moves out of the intersection, the sound level decays at a faster rate for the farther receiver position. This produces a narrowing of the pass-by shape with distance from the source street. As illustrated by

comparison to Figure 5.6, such narrowing was also observed for propagation into a receiver street from a single intersection.

Another feature of propagation into a second intersection is presented in Figure 5.10. The attenuation values presented in this figure are for two receiver positions located at the same distance into the street. The positions are 1/8 of a street width from each of the street walls. From the figure, it will be observed that there is some difference between the two pass-by histories. The attenuation values for that position closer to the source street are consistently lower than those obtained at the other position. This difference is about 1 1/2 to 2 dB when the source is in the intersection, and at most about 4 to 5 dB when the source is around the second corner. Although there is the possibility of extensive shadowing for the receiver position closer to the source street, the difference observed indicates only limited shadowing occurs.

Attenuation values for corresponding receiver positions in second streets located at different distances from the source street are presented in Figure 5.11. The pass-by position histories illustrated in this figure indicate that there is a narrowing in the shape of history with increased separation of the source and secondary street as well as a general lowering of the sound level. This behavior was also noted for increasing distance into second street for the constant street separation of Figure 5.9. In regard to Figure 5.11, it should also be noted that there is considerable difference between the attenuation

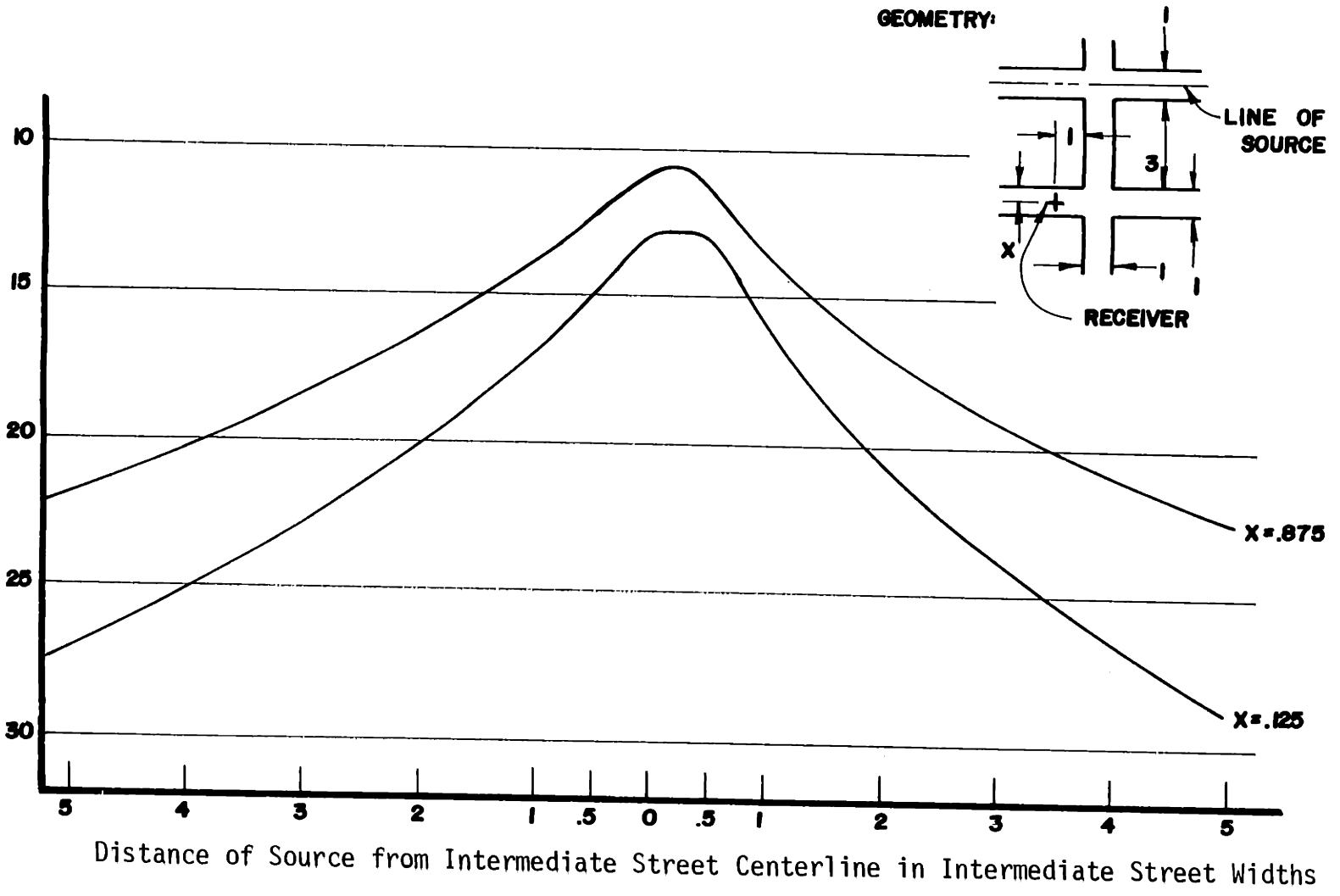

FIGURE 5.10: Point Source Attenuation - Variation of Position Across Street of Second Intersection

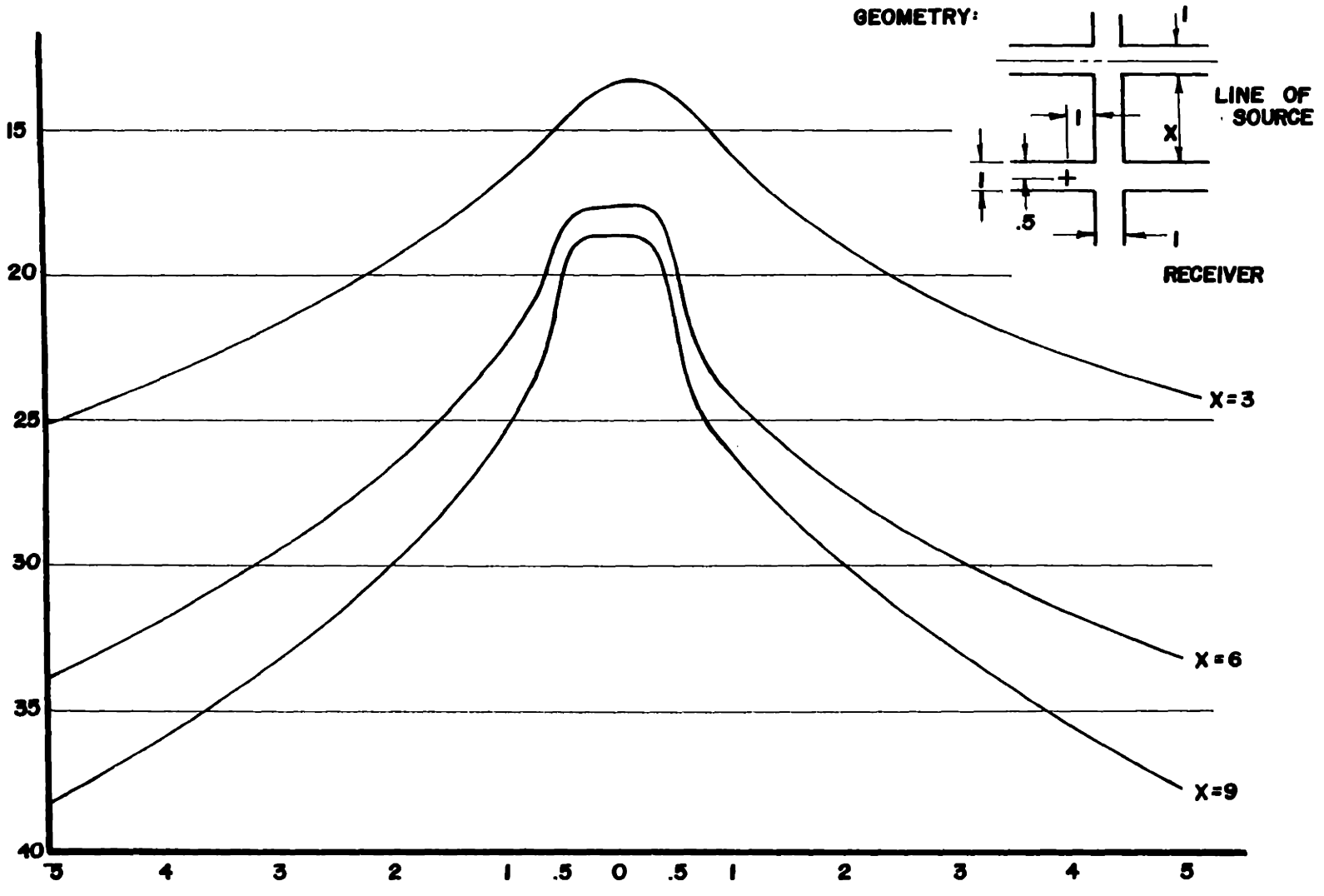

FIGURE 5.11: Point Source Attenuation - Variation of Intersection Location, Into Second Intersection

values for a 3 and 6 street width separation while there is only slight difference between the 6 and 9 street width separation values. The former two separations give differences of at most 8 1/2 dB while the later give at most 4 1/2 dB.

5.3.2 Traffic Flows and Line Sources

As discussed in Section 5.2.2, normalized line source attenuation values are applicable to both physical line sources and to traffic flows of any density. In this section, some of the features of line source or traffic flow noise propagation are discussed.

The first propagation case of interest for a line source is that situation in which the source is located in the same street as the receiver. The point source equivalent of this case was given in Figure 5.5. Since there is only one receiver position relative to the line source, there is only one normalized attenuation value. This value was found to be 7.0 dB. Examination of Figure 5.5 yields the observation that virtually all of this line source level is determined by those portions of the source within 1 or 2 street widths from the receiver. For this reason, if an intersection is located 2 or more street widths from the receiver, it will have negligible effect on the line source attenuation value.

A second case of interest concerns propagation from a line source in one street into an intersecting receiver street. In Figure 5.12 the attenuation values produced for three different intersection

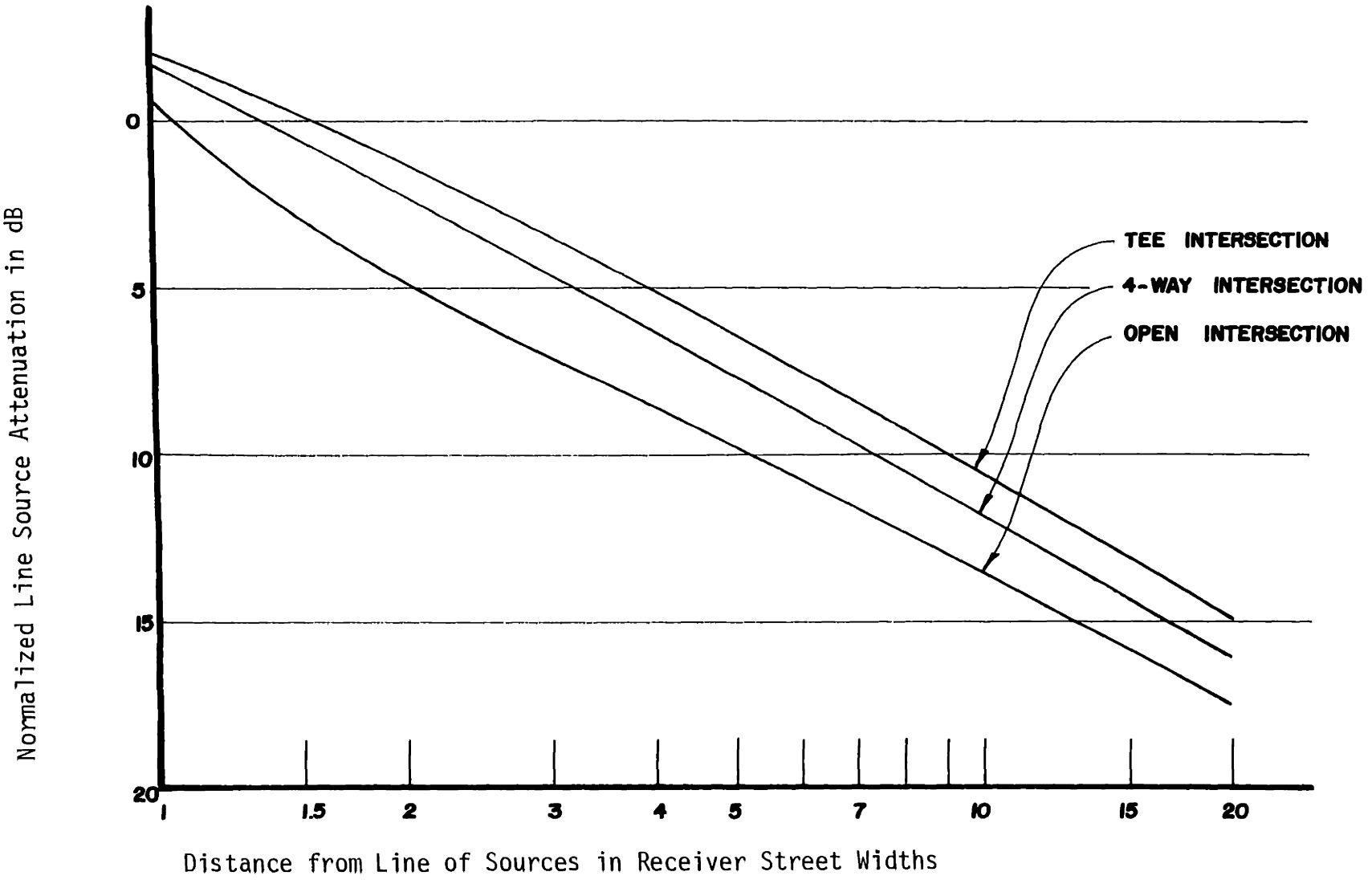

FIGURE 5.12: Line Source Attenuation - Tee, Four-Way, Open Intersections

geometries are given. The geometries include a tee, four-way and open intersection. Due to the additional reflecting surface, the tee intersection attenuation values are lower than the other two. This difference is about 1 1/2 dB compared to the four-way intersection and 3 to 4 dB for the open. With the lack of reverberant build-up in the source street, the open intersection values are lower than the other two configurations.

Concentrating on the four-way intersection, variations in attenuation with the width of the source street is presented in Figure 5.13. Detailed examination of this figure indicates that there is some variation with source street width. However, a more remarkable feature is the general similarity in both fall-off rate and absolute level for the various configurations. The figure indicates that all the values lie within a 3 dB range for all receiver positions. Another aspect of the four-way intersection is shown in Figure 5.14. This figure plots attenuation for different source offsets in the source street for a fixed street width. As the attenuation values are only computed for receiver positions in the receiver street, the attenuation values begin at different distances from the line of the source. As in the previous figure, there is detailed differences in the attenuation values for the three cases. Also as before, considering the maximum difference displayed in Figure 5.14 of 3 dB, the three cases are functionally similar.

Another line source propagation case of interest is that in which there is an intervening intersection between the intersection formed by the source and receiver streets and the receiver. One

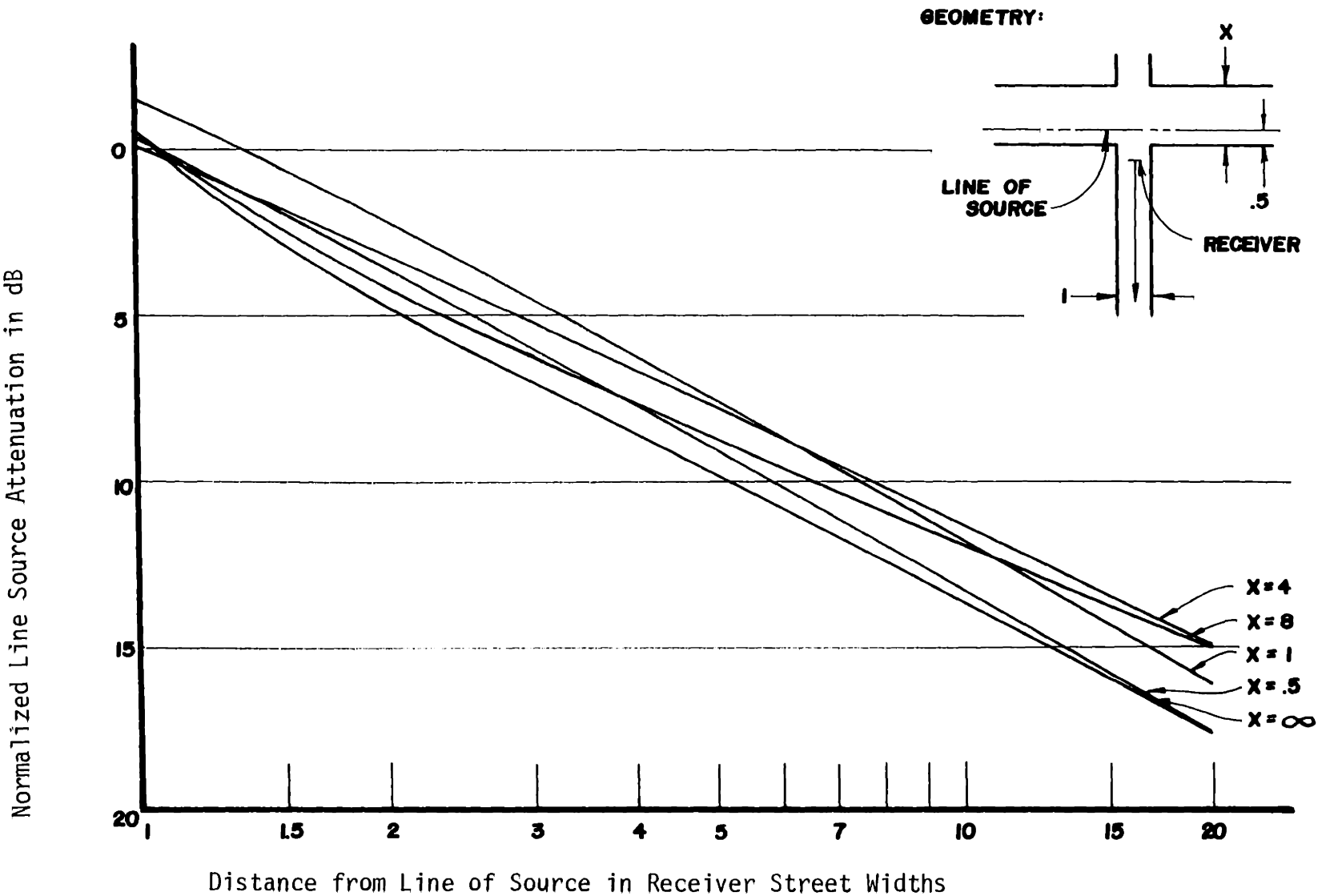

FIGURE 5.13: Line Source Attenuation - Variation of Street Width, Four-Way Intersection

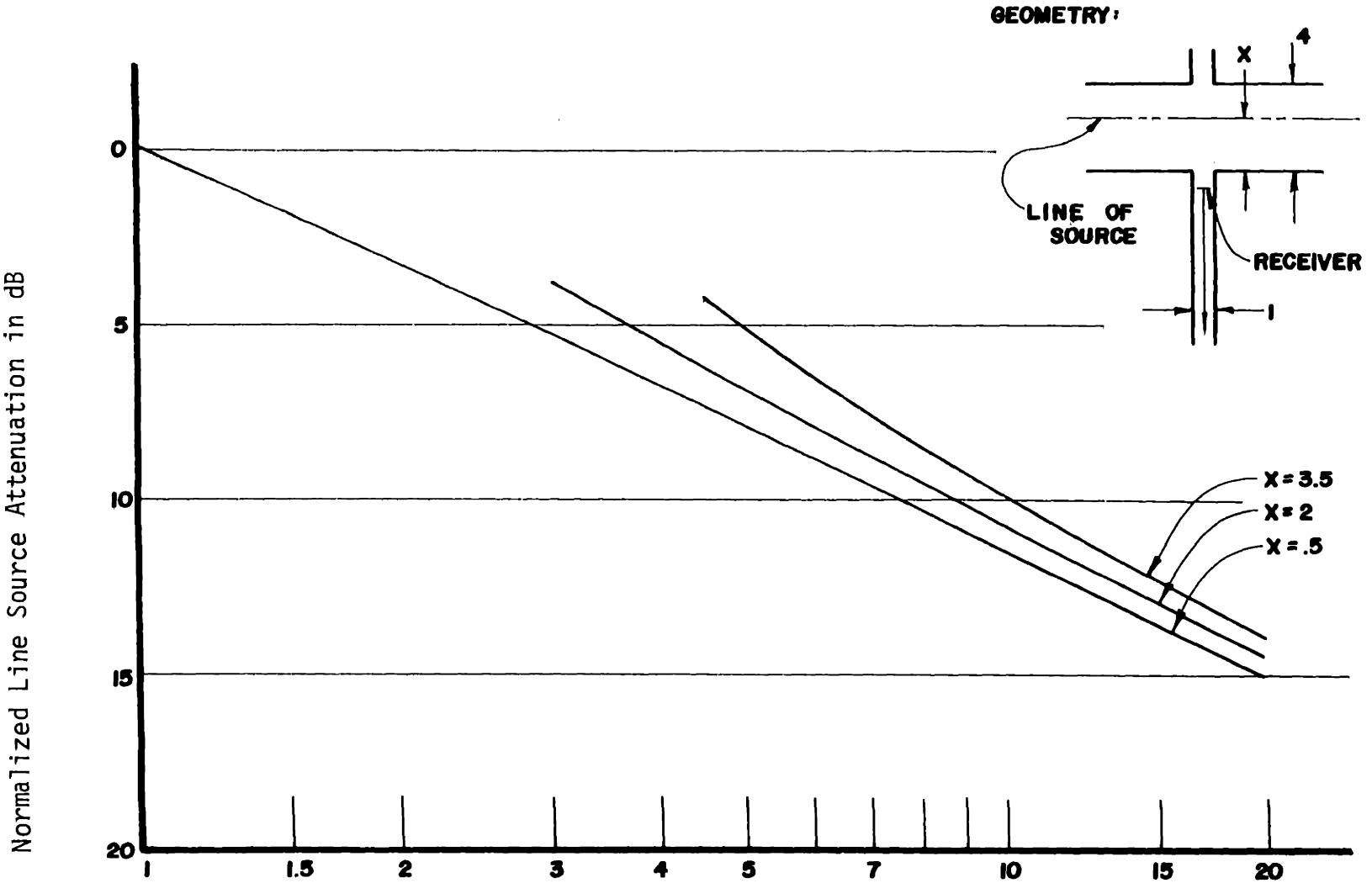

FIGURE 5.14: Line Source Attenuation - Variation of Source Offset, Four-Way Intersection

variable in this propagation case is the location of the intervening intersection for a given source-receiver separation. The dependence of attenuation on this variable is quite minimal as evidenced by Figure 5.15 in which attenuation values for three locations are presented.

Another variable which can be examined is the width of the intervening intersection. Attenuation values for intersection widths from 0 to 7 receiver street widths are presented in Figure 5.16. There are two features of particular interest illustrated in this figure. The first feature is that for intervening street widths less than 1 receiver street, the attenuation is at most 1 1/2 dB greater than for no intervening street at all. Thus, if alley ways or spacing between buildings of this magnitude occur along the receiver street, their effect is negligible if the total opening area between the source street and receiver is less than 1 street width. The second feature of interest is the reduction in sound level that can be achieved by the opening. For an opening of 7 receiver street widths, this reduction can be as much as 5 1/2 dB.

A final variable to be considered for propagation through an intervening intersection is the ratio of source and intervening street width to receiver street width. Computed attenuation for several values of this ratio are presented in Figure 5.17. This figure indicates detailed variation in attenuation for the different ratios. However, for all cases, the attenuation values lie within a range of at most 2 1/2 dB.

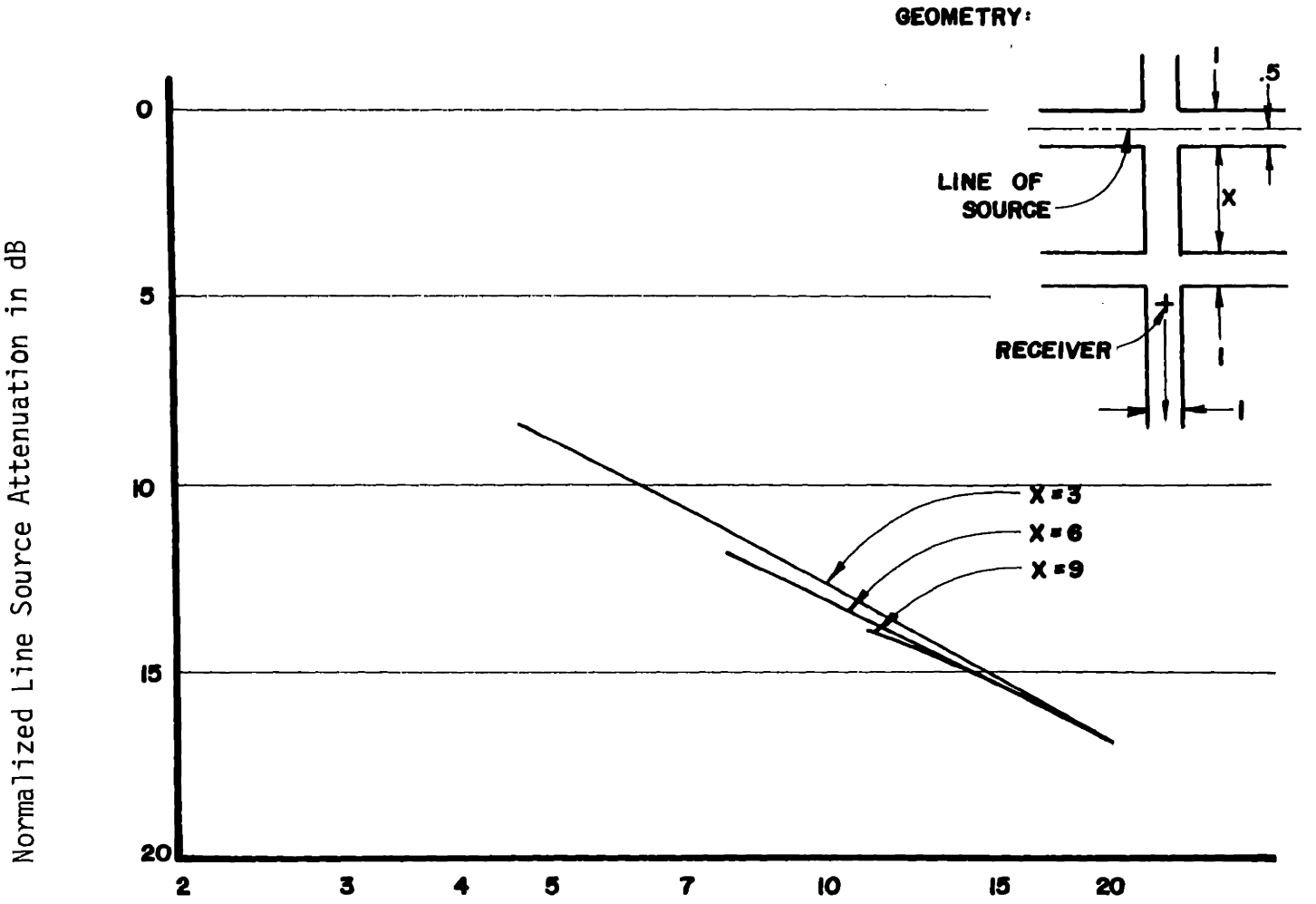

FIGURE 5.15: Line Source Attenuation - Variation of Street Separation, through Second Intersection

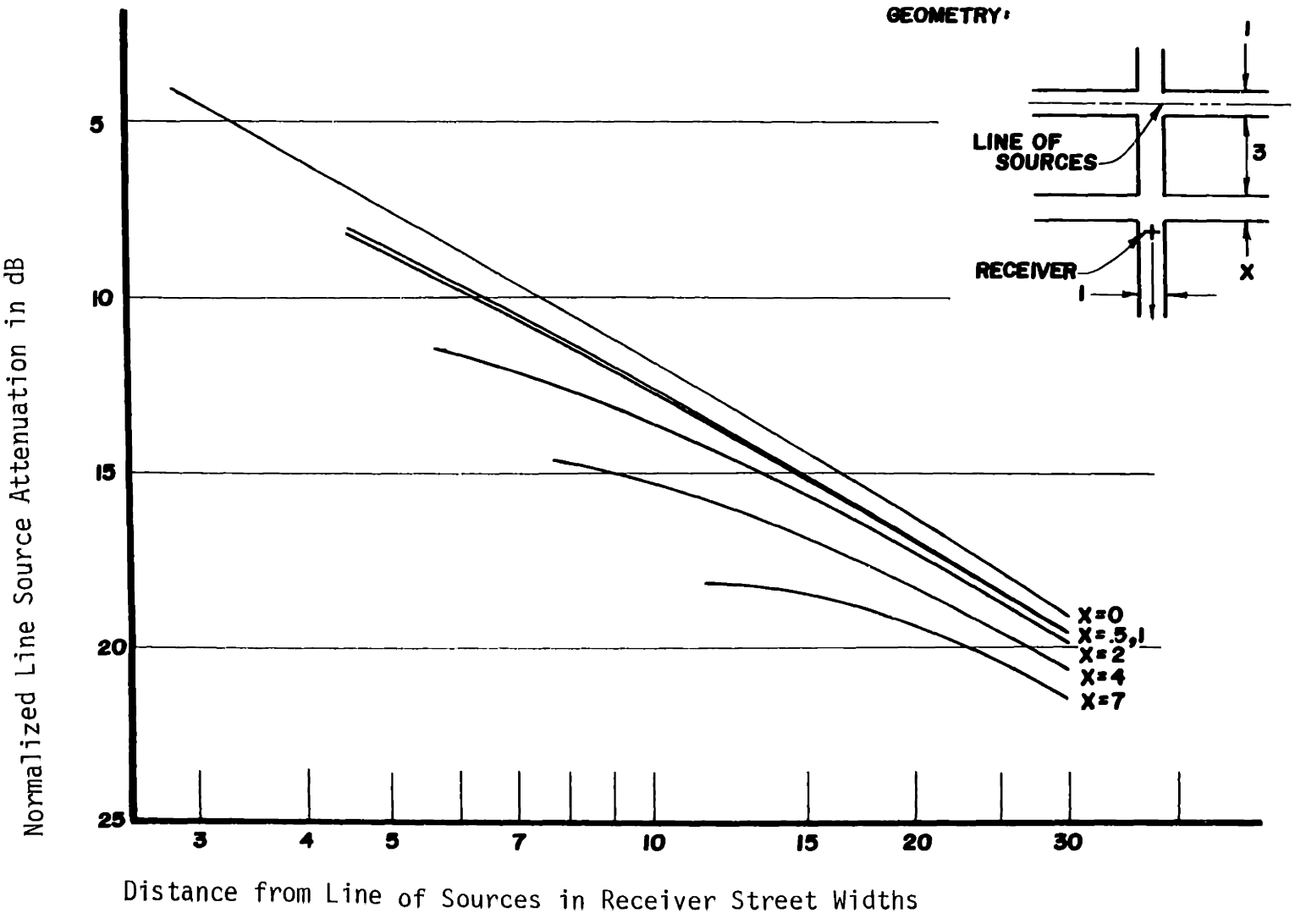

FIGURE 5.16: Line Source Attenuation - Variation of Second Street Width, through Second Intersection

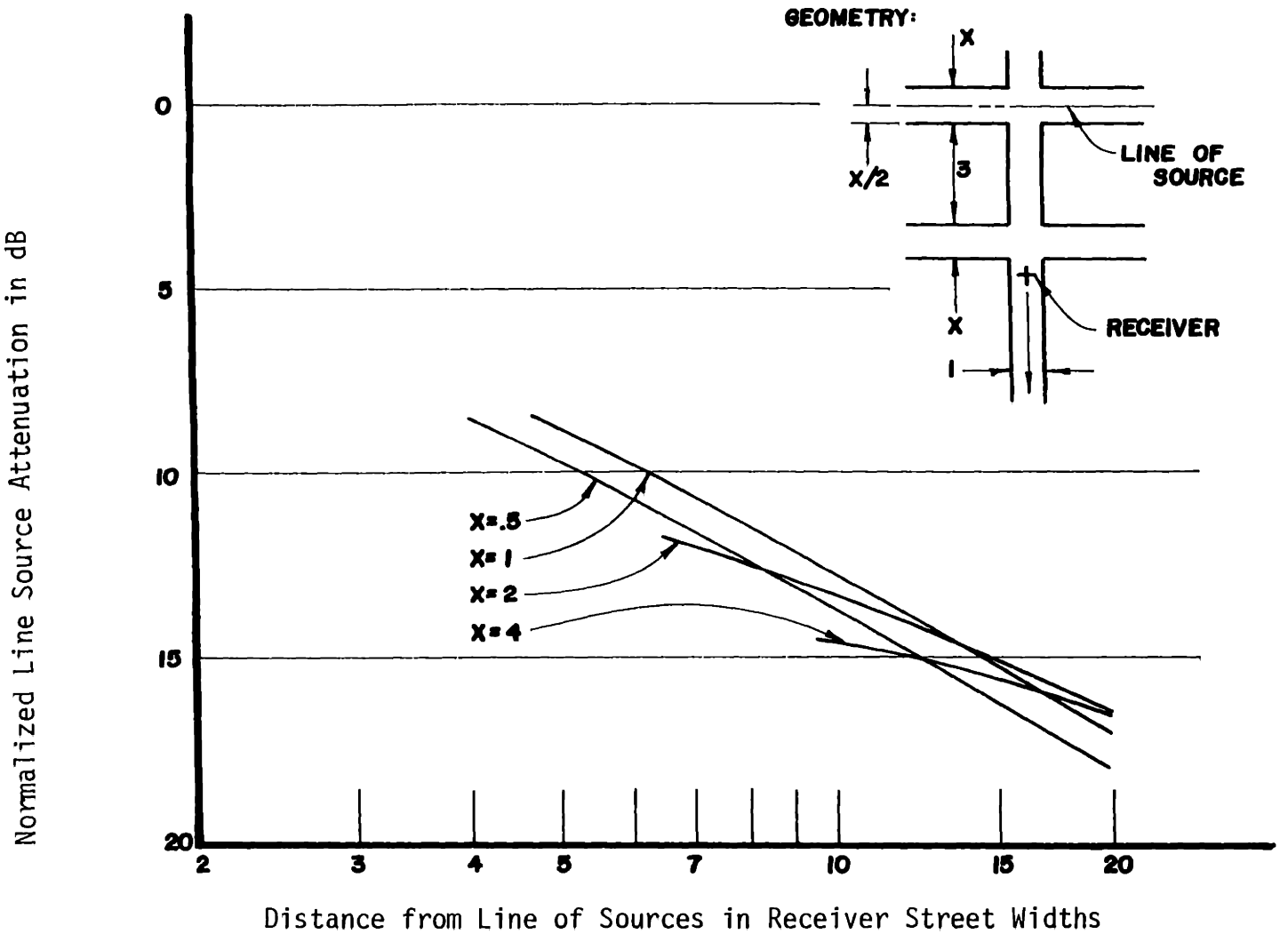

FIGURE 5.17: Line Source Attenuation - Variation of Street Widths, through Second Intersection

The final line source case of interest is propagation from the source street intersection into a parallel receiver street forming a second intersection. The normalized attenuation for this case can be plotted against two different distance scales. In Figure 5.18, attenuation is plotted as a function of the total distance between the receiver and the line of the source for three separations between the source and receiver streets. From this plot, it will be observed that the fall-off of sound level down the street is quite rapid, from 9 1/2 to 18 1/2 dB per distance doubling. Further, the fall-off rate increases with increased separation between the two streets. As illustrated by Figure 5.19, a second method of plotting the attenuation is as a function of the distance the receiver is from the centerline of the intermediate street. This plotting method produces attenuation curves which all have similar fall-off rates with distance. An attempt was made to relate the displacement of these attenuation curves to the level in the intermediate street corresponding to the location of the second intersection. Unfortunately, no quantitative relationship was found.

Another aspect of line source propagation into a second intersection is the variation of sound level across a street section. Variation for one particular geometry is given in Figure 5.20. This figure indicates that the sound level decreases as the side of the street nearest the source street is approached. At 1/8 of a street width from either side, the difference in level across the street is 3.4 dB. From this figure, it can be concluded that some shadowing occurs due to the second corner. Shadowing does, however, decrease with

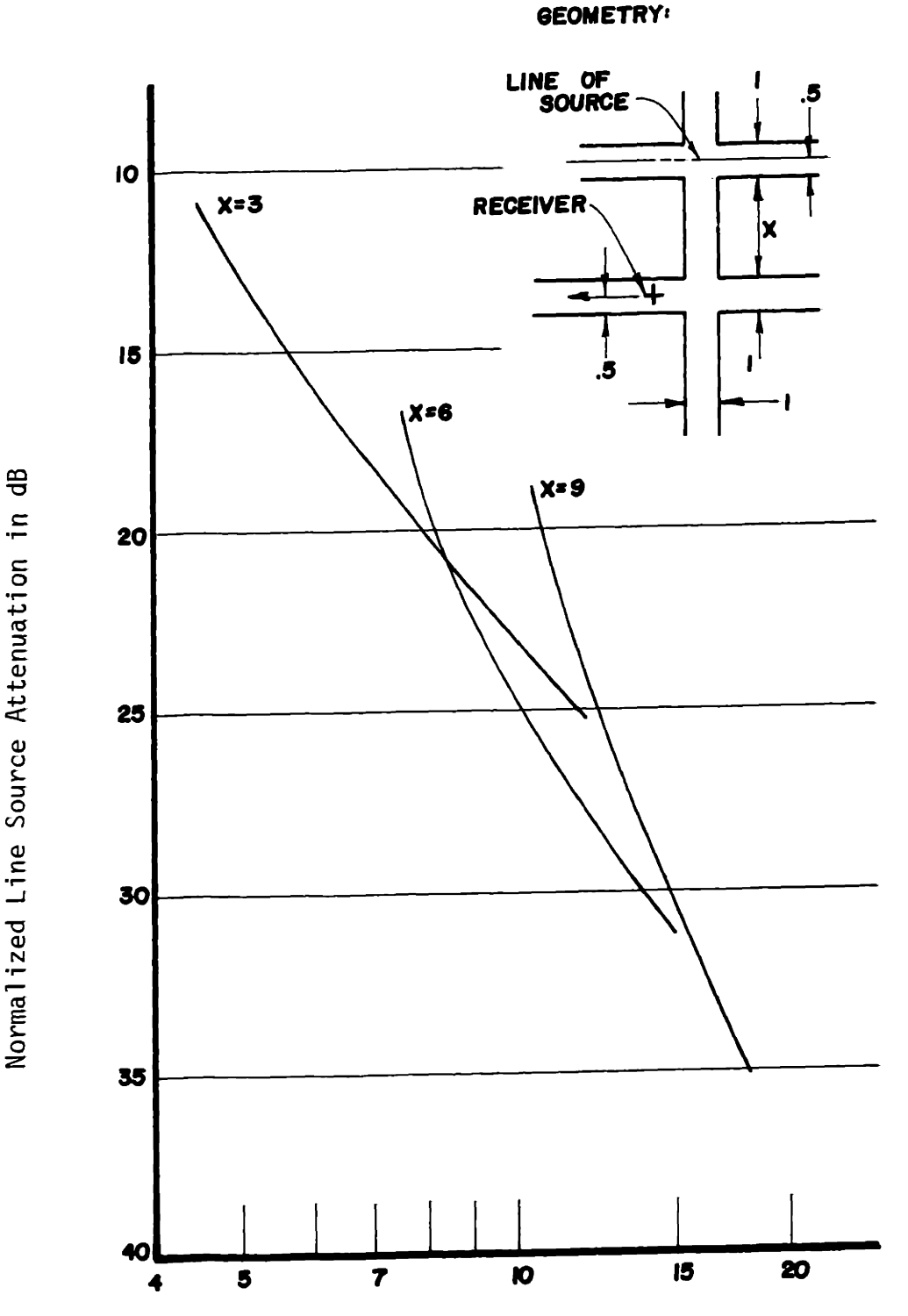

FIGURE 5.18: Line Source Attenuation - Distance from Source, into Second Intersection

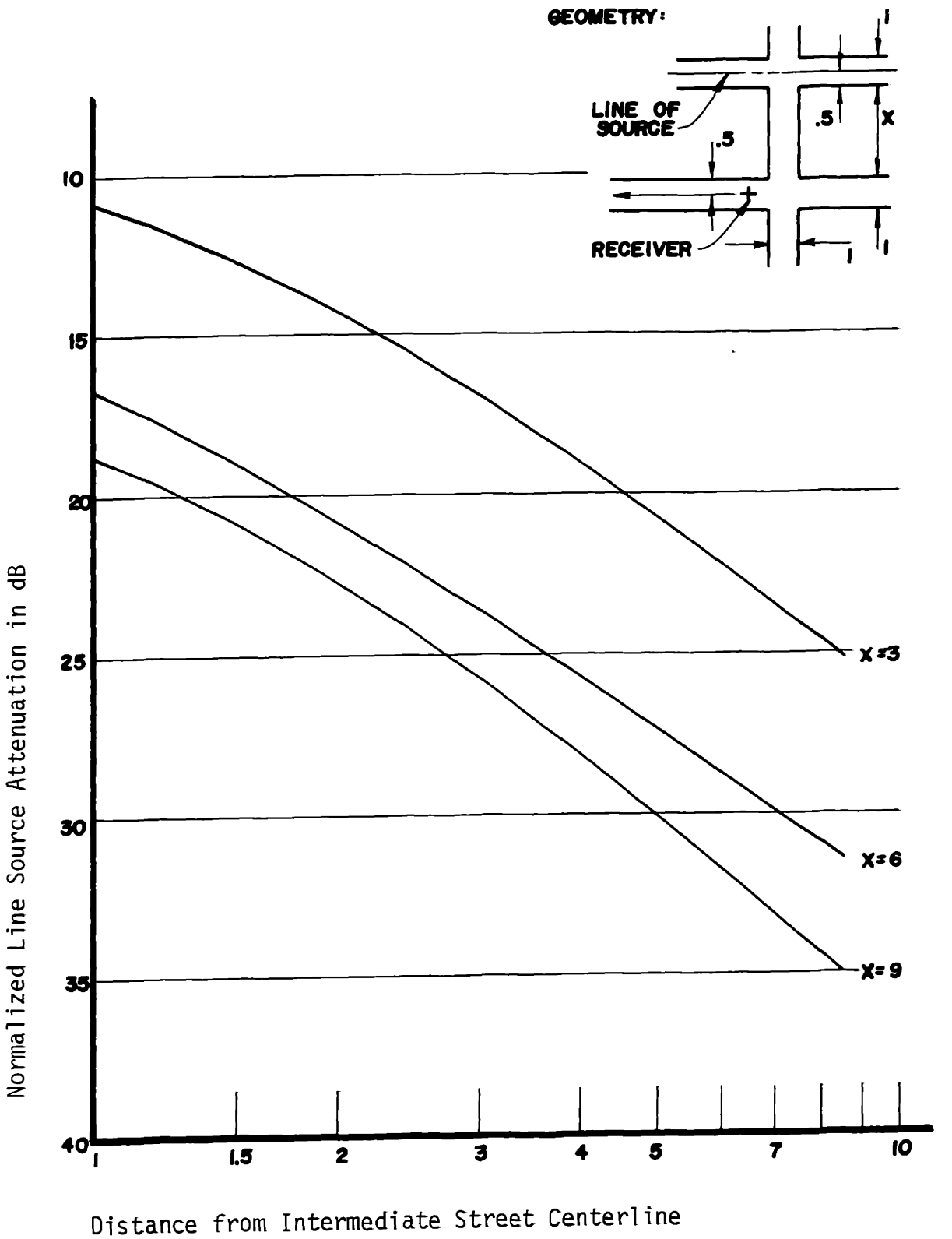

FIGURE 5.19: Line Source Attenuation - Distance from Second Intersection Center, into Second Intersection

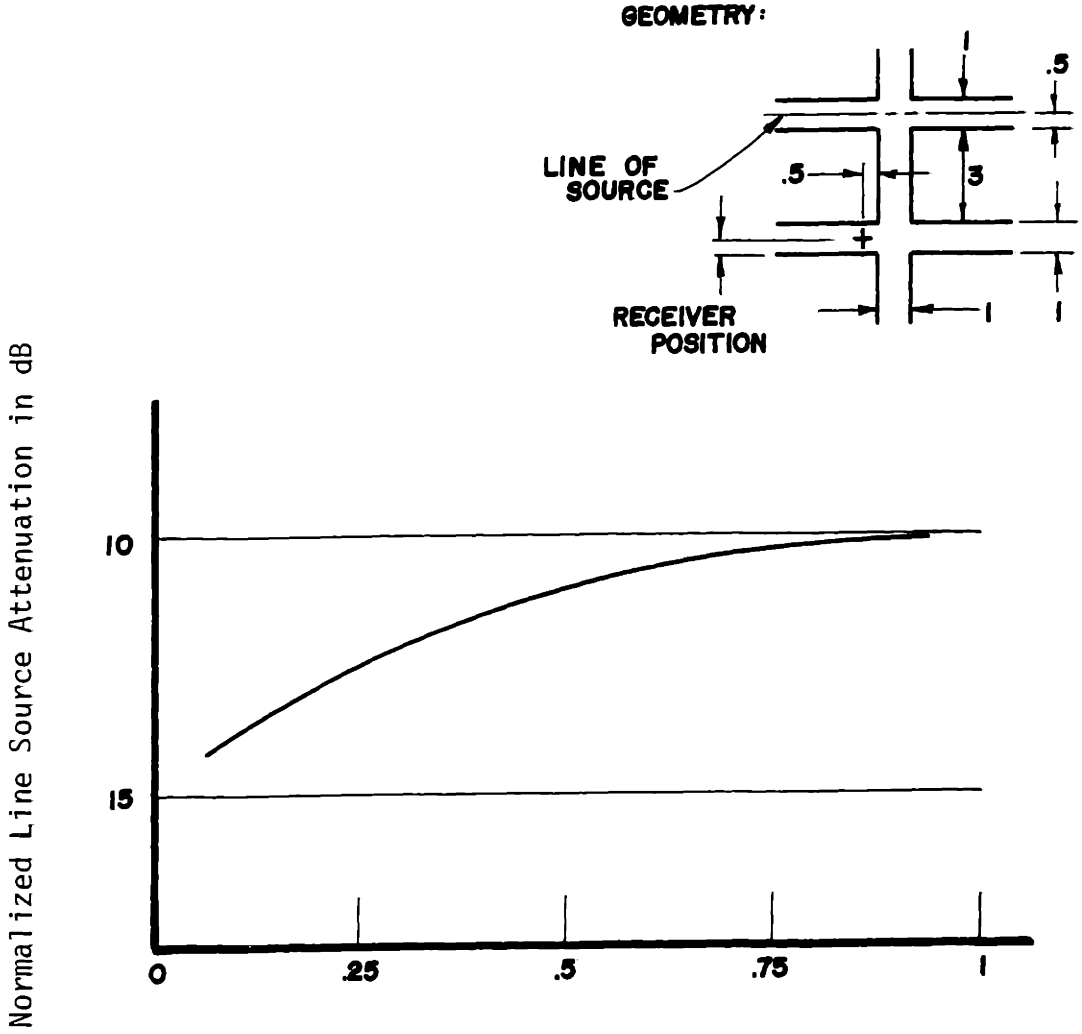

FIGURE 5.20: Line Source Attenuation - Variation Across Street, into Second Intersection

increased distance from the intersection.

5.3.3 Summary

A number of important observations regarding urban sound propagation were made in Sections 5.3.1 and 5.3.2. Some of these observations are summarized in this section.

For propagation from a single intersection, it was observed that the configuration of the intersection, four-way, tee, or open, only slightly effects the predicted sound level for similar source and receiver positions. The variation was found to be at most 3 1/2 dB for all three configurations. One exception to this result, however, was found for point source propagation for source positions around a corner from the receiver. For this case, the open intersection attenuation was substantially greater than for the other two cases. In regard to propagation from a four-way single intersection, it was also noted that variation of source position within the source street and variation of the source street width produced only small variation in sound level, no greater than 3 dB.

For most cases, the propagation of sound from an intersection was found to be insensitive within 1 to 2 dB to the presence of an intervening intersection. This conclusion was shown to be valid when the second intersection introduced an opening of about one street width. Further, for this size opening, only very slight variation in level, less than 1 dB, was observed for different locations of the

second intersection relative to the source and receiver. For openings of 2 street widths or greater, the sound level was found to be dependent on the size of the opening. It was observed that sound level decreased with increased opening such that for an opening of 7 street widths, a maximum reduction of 5 1/2 dB was achieved.

In the case of propagation around the corner of a second intersection, no simplifying behaviors were observed. It was observed, however, that there is only slight variation across the street section, this variation being about 3 to 4 dB.

5.4. Additional Factors in Urban Sound Propagation Prediction

In addition to the basic inclusion of multiple reflection and surface scattering in an urban noise propagation model, there are other phenomenon which may influence propagation. Using the experimental results of Section 3 and results available in the current literature, some of these factors are discussed in this section.

5.4.1 Environmental Conditions

A number of environmental conditions are known to influence outdoor sound propagation [27]. Among these, the most appropriate to urban propagation are wind and temperature gradients and the absorption of sound by air. In conducting a series of urban propagation experiments, Wiener, Malme and Gogos [12] obtained micrometeorological data corresponding to their sound propagation data. The experiments were conducted in both summer and winter and spanned several weeks. In

their investigation of temperature gradient, no appreciable gradients were measured at any time. Data was taken for several wind conditions with a mean flow up to 10 miles per hour. Although this flow was present, no appreciable wind gradient was measured. Further, no appreciable effect on the sound level measurements was observed. The results of this study lead to the conclusion that wind and temperature gradients in urban areas are such as not to influence sound propagation.

Unlike wind and temperature gradients, the absorption of sound by air is always present in urban propagation. However, the magnitude of this phenomenon is sufficiently small for the distances and frequencies of concern in urban noise propagation that it can often be ignored. As an example, for propagation with air at 68°F and 60% relative humidity, the total absorption in 1000 ft is .4 dB at 250 Hz, .7 dB at 500 Hz, 1.0 dB at 1 kHz, and 2.0 dB at 2 kHz [24]. If the distances of propagation and frequency content of the source is sufficient to warrant correction for air absorption, the appropriate values for the 250, 500, 1 kHz and 2 kHz octave band center frequencies can be found in Figure 5.21. For frequencies beyond 2 kHz, the original report of Evans, Bass and Sutherland [24] should be consulted.

5.4.2 Diffraction Around Corners

In Section 3.2.2, the presence of diffraction was implied by the data obtained in the acoustical model experiments with no periodic protrusions. A significant role for diffraction around a

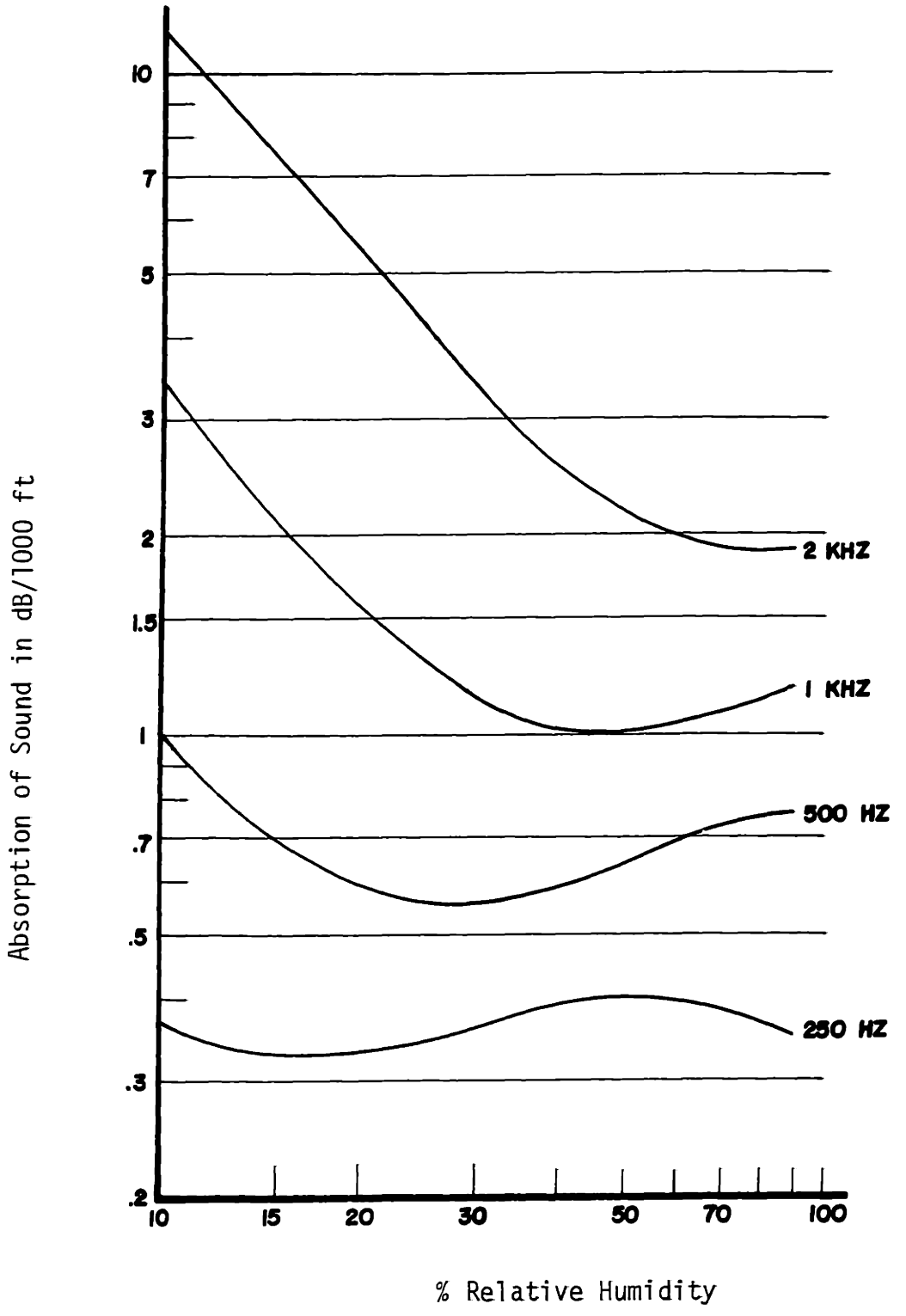

FIGURE 5.21: Absorption of Sound in Air

corner appears, however, to only occur for this special propagation case. Diffraction effects are not apparent for propagation in the presence of surfaces which scatter sound. For the acoustical model data taken with periodic protrusions reported in Section 3.2.2 and for the field data reported in Section 3.2.1, there is little or no frequency dependence displayed which could be attributed to diffract The absence of diffraction in this data is probably due to the preser of surface scattering and the added effective absorption created by s face irregularities. The presence of surface scattering creates a mc effective path by which sound may turn a corner thus masking the presence of diffraction. Further, with surface irregularities, addec effective absorption implies that those images representing many reflections are of considerably less strength than those of the ideal smooth wall case. It is these higher order images which are of majc importance in creating diffraction around a corner. For these reason no correction factor for diffraction around a corner is necessary.

5.4.3 Ground Reflection

In the development of the urban noise propagation predicti model, the reflection of sound from the street surface was not explic included. This reflection was not included because the amount of energy added by the reflection varies with frequency, the nature of t surface, the height of the source and receiver and their separation. discussed in Section 3.2.2, for simulation of the model data, path length difference was less than 1/4 of a wavelength. For hard,

non-porous surfaces, a difference of this amount implies pressure addition of the direct and reflected signal leading to a 6 dB increase of the predicted level. In many situations of urban noise propagation, the geometry of source and receiver and the source spectrum are such that the path length difference is less than 1/4 of a wavelength. Although this difference implies pressure addition, due to the nature of typical street surfaces, a 6 dB increase in the level is not expected for ground reflection. In these situations, ground reflection is best accounted for by specification of reference source level in the presence of the street surface as would normally be done. No correction is needed for this type of specification. If, however, the path length difference for the specification measurement is less than one wavelength, further consideration is necessary.

For those cases in which the direct and reflected path length difference is greater than 1/4 of a wavelength and less than 1 wavelength, the expression for reflection from a surface developed in Section 2.1 can be utilized to determine the contribution of the reflection. This expression was used to develop a computer program which produces the added energy of reflection in octave bands for given source and receiver geometries. The program was experimentally verified using the instrumentation and processing system described in Section 4.5. The geometry and results of the experiment are presented in Figure 5.22. Also included in the figure are the results given by the computer program. Comparison of the two sets of results indicates generally good agreement. The computed values

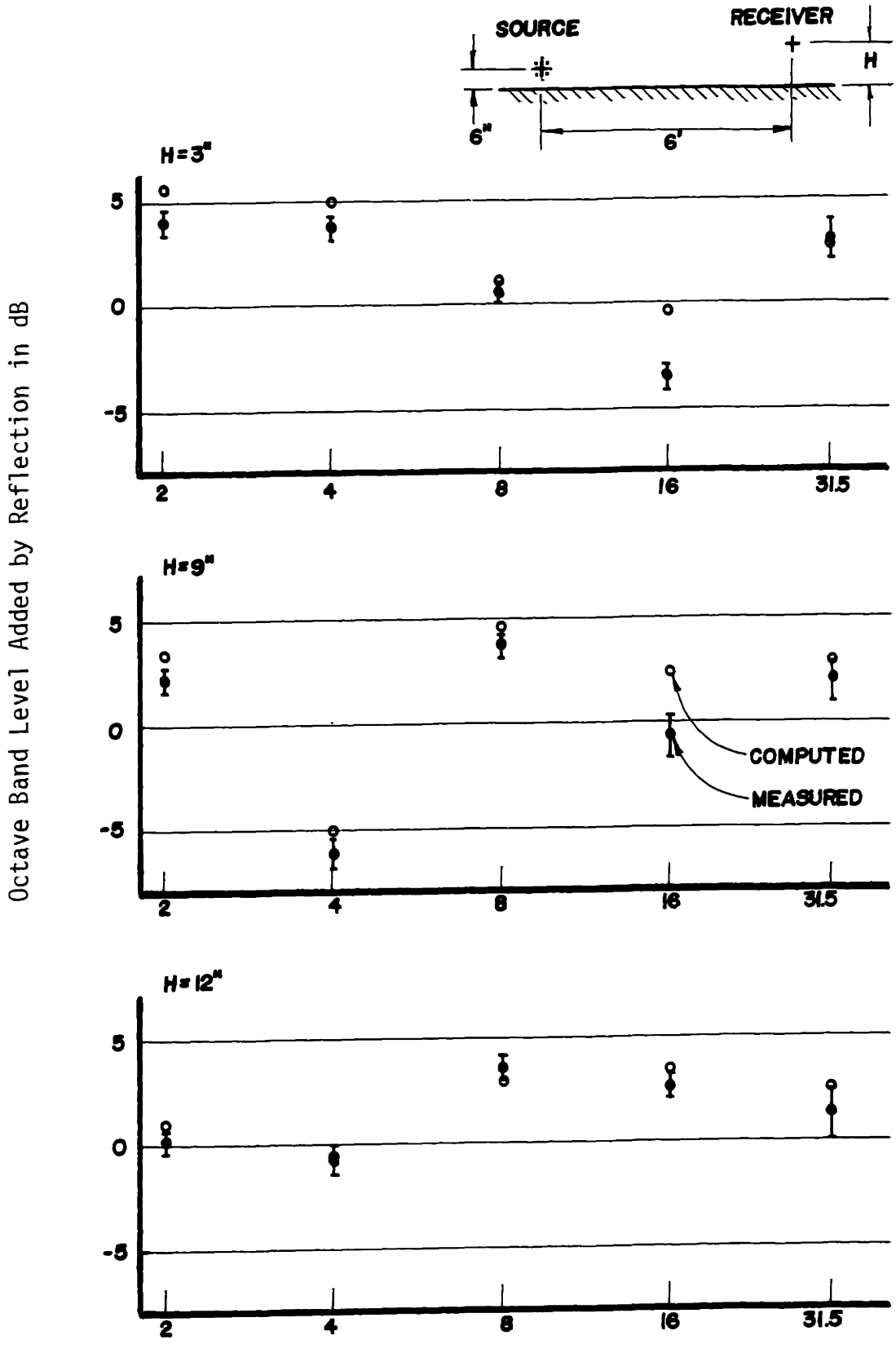

FIGURE 5.22: Ground Reflection - Experimental Results

typically lie within 1 dB or less of the standard deviation of the experimental values, with the largest differences being about 2 dB.

The expression for reflected energy can be used to generate functional relationships between path length difference in wavelengths and additional level created by the reflection. Examination of the expression for the squared pressure ratio indicates that the additional level is a function both of frequency band and direct path length between source and receiver. For the octave bands centered at 250, 500, 1kHz and 2 kHz and for separations up to 2000 ft, the dependence on frequency and separation was found to create differences of about .1 dB. With this minimal dependence, only one curve is needed to express the pressure squared ratio for these ranges. It was further found that the ratio is only slightly dependent on absorption coefficient assuming it is less than 0.2. The values of additive level due to reflection obtained for an ideally hard, non-porous surface are presented in Figure 5.23.

Unless the source and the geometry of a particular situation are such that the line of sight direct and reflected path length difference is less than 1/4 wavelength, application of the ground reflection information is in detail quite difficult. This is true because each multiply reflected and scattered path represents a different length difference between ground reflected and non-ground reflected paths. For this reason as well as the non-ideal nature of the surface, the minimum in the additive level at .4 to .5 wavelengths is not

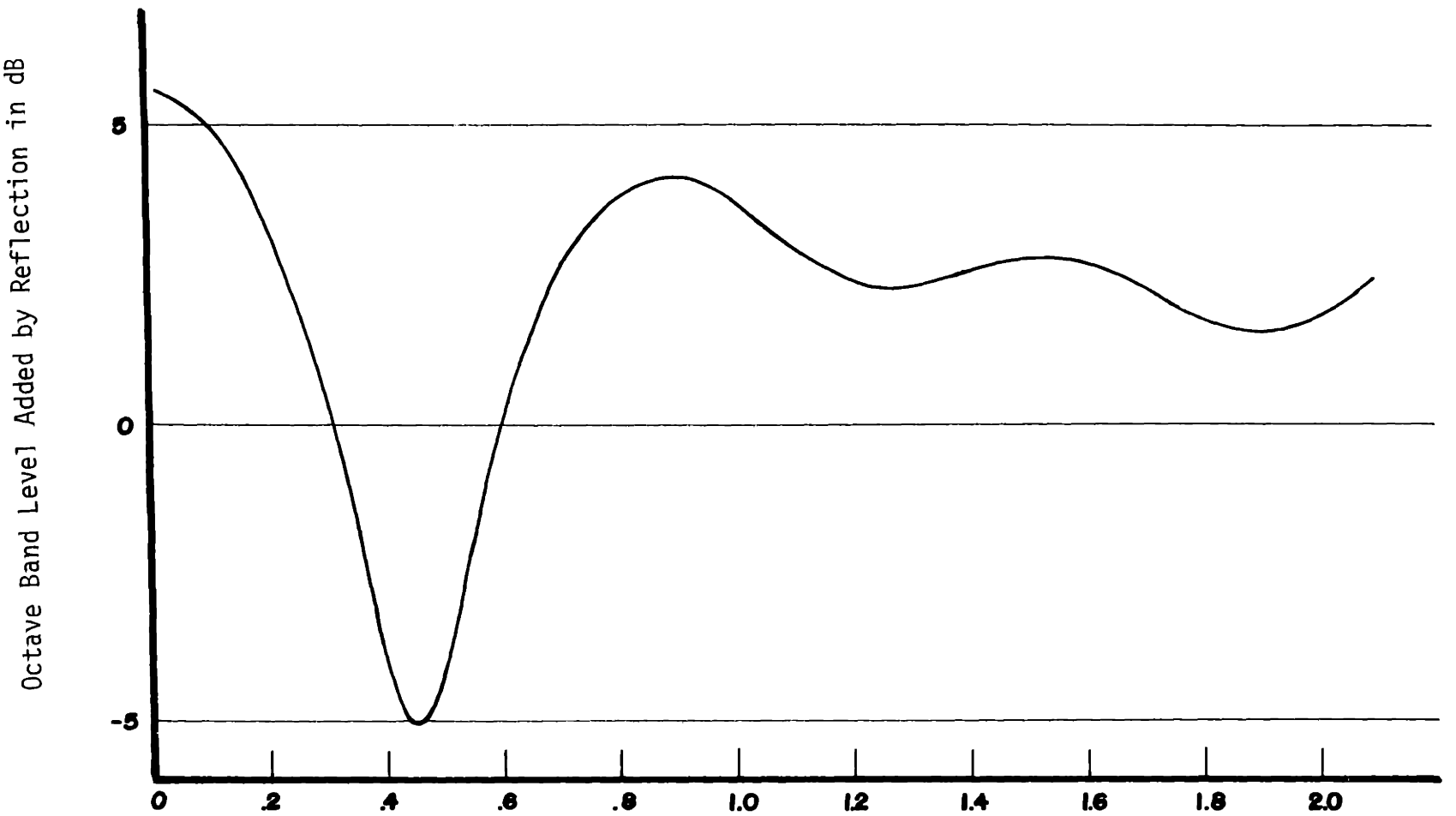

FIGURE 5.24: Normalized Ground Reflection Prediction

expected to be observed. The effect of multiple paths is further expected to create a smooth transition from energy to pressure addition. Because of the nature of the street surface, pressure addition will yield an additive term less than that of Figure 5.23. It is, therefore, suggested that if the source level is specified without the presence of a reflecting surface, the effect of ground reflection be approximated by an additional 3 dB. If the source is specified in the presence of a ground plane and the difference of the direct and reflected path lengths is greater than 1 or less than 1/4 wavelength, no correction is required for ground reflection. Specifications not meeting this requirement should not be used. For A-weighted level specifications in the presence of a ground plane, no correction is needed.

5.4.4 Temporal Level Variation for Traffic Flows

Unless traffic flow densities are such that at least several vehicles are present in an intersection at any instant, there will be temporal variation in the sound level measured in the street intersecting the flow. Variation of this sort is attributable solely to the spatial dependence of sound level with source position and not to variation in individual vehicles or in their spacing. This temporal variation can be simulated with the aid of a computer and point source pass-by position histories. Simulation is accomplished by assuming a traffic density and corresponding uniform vehicle spacing. The total contribution of these sources can be determined at a receiver point as

the array uniformly, incrementally passes through the intersection. In this manner, a pass-by position history for the array of point sources is constructed. Once this position history is obtained, the statistics of L_{10} and L_{50} can be determined. As an example, several position histories corresponding to different traffic densities are given in Figure 5.24 along with the corresponding L_{10} and L_{50} values.

Using the method outlined above, L_{10} and L_{50} values can be computed as a function of traffic density for those propagation cases for which point source pass-by position histories were obtained. The utility of such values are, however, questionable. The assumptions needed in obtaining the values are restrictive and probably not met by most real traffic flows. The assumption of uniform spacing is probably only met in those cases where the traffic is flowing freely and the density is such that vehicles are at constant minimal spacing. The assumption of uniform strength of individual sources is probably never observed in traffic flows. This later assumption is particularly important in the calculation of L_{10} as this statistic is considerably more sensitive to individual vehicle variations that is L_{50}. Although there are these limitations on the utility of the calculated statistics, they may be useful as an indicator of variation.

As an example of the use of the statistics which can be determined for a traffic flow, the L_{50} data reported by Delaney, Copeland and Payne [13] for Bulwer Road was simulated. The L_{50}

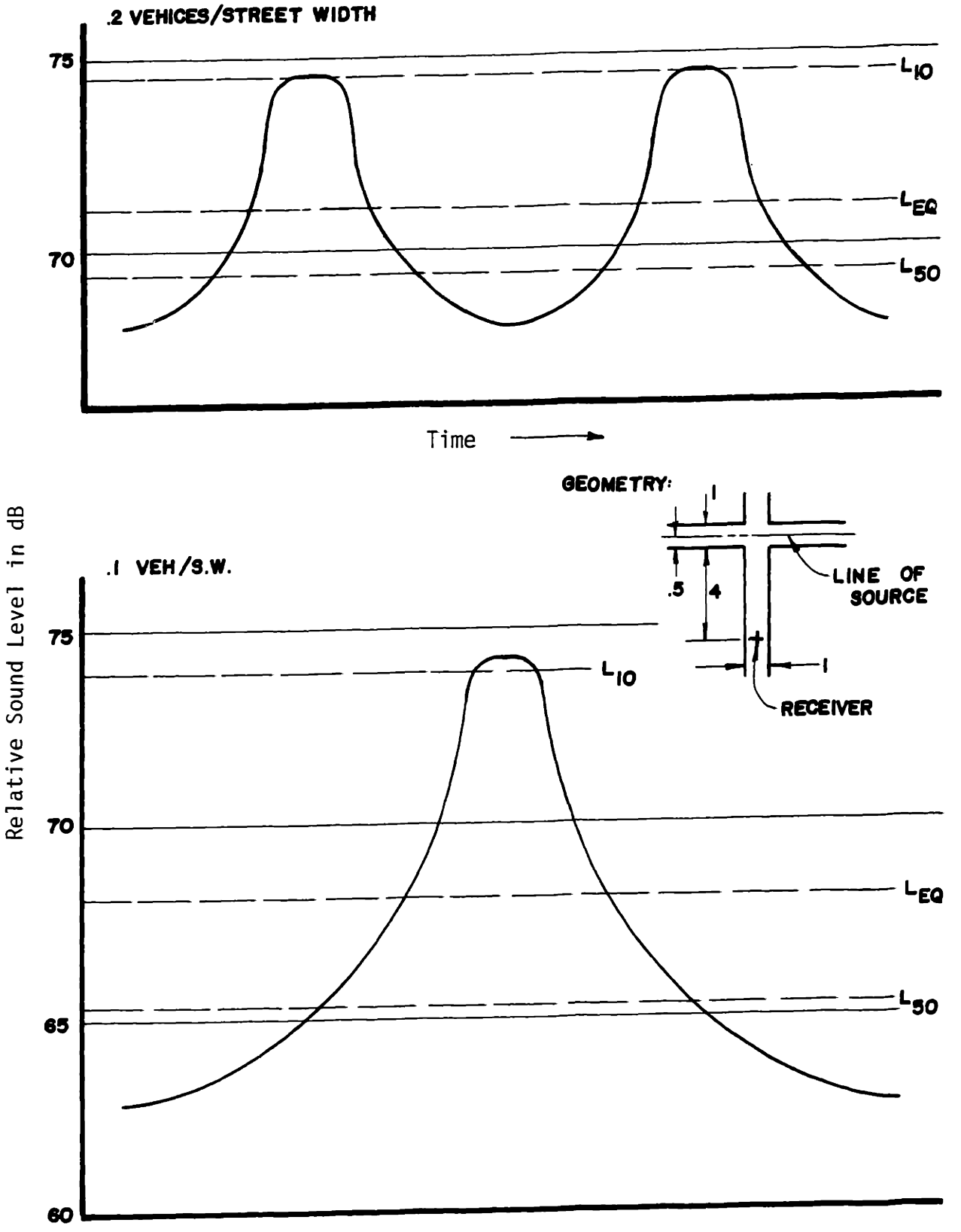

FIGURE 5.24: Temporal Level Fluctuation - Traffic Flow

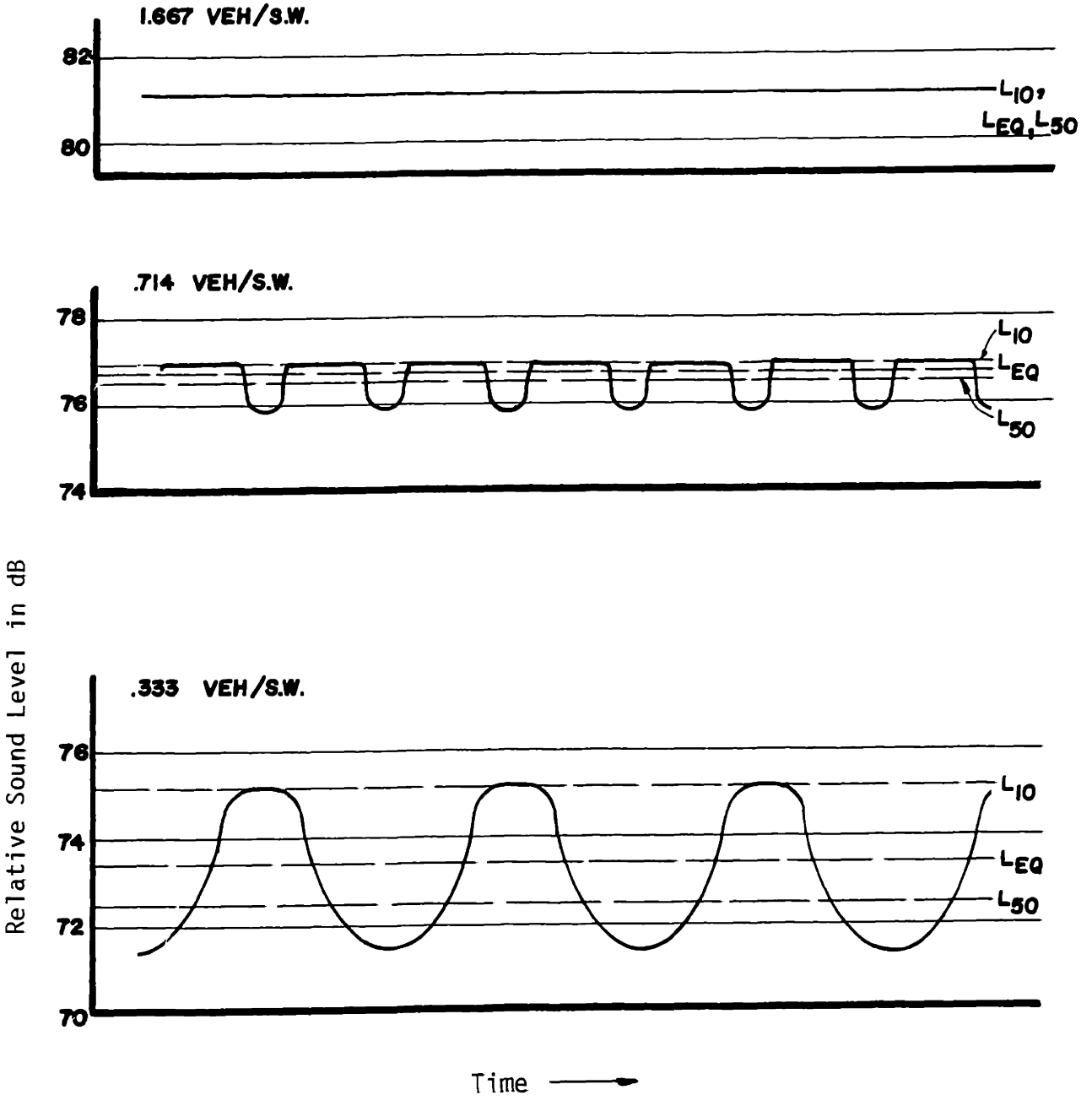

FIGURE 5.24: Temporal Level Fluctuation - Traffic Flow

values were chosen because of their lack of sensitivity to the assumptions discussed above. Supplied with the L_{50} data in the report is the value of traffic density during the test. This density corresponded to .5 vehicles per street width. The geometry of test was that of an open intersection with freely flowing traffic in the source street. Measurements of L_{50} up to 14 street widths from the traffic flow were made in the receiver street. As no average source strength was reported, the L_{10} value reported at curbside was used as this best approximated free field conditions. Using the methods outlined in Section 5.2.2, the normalized attenuations for receiver positions down the street were calculated. The corrections computed to simulate L_{50} were applied to the attenuations and L_{50} values were determined. The simulated L_{50}'s are presented in Figure 5.25 along with those reported by Delaney, Copeland and Payne. Within about a 2 dB margin, the two sets of results compare quite well.

5.5 Summary

In the preceding sections, two models of urban propagation have been developed which attempt to account for scattered reflection from building surfaces. In terms of predicting sound levels in urban areas, each model has strengths and weaknesses which should be remembered in their application. The first order or added absorption model of scattering has the advantage of being easy to apply for general prediction. It was found to be accurate in predicting sound levels when there is a direct line of sight between source and receiver.

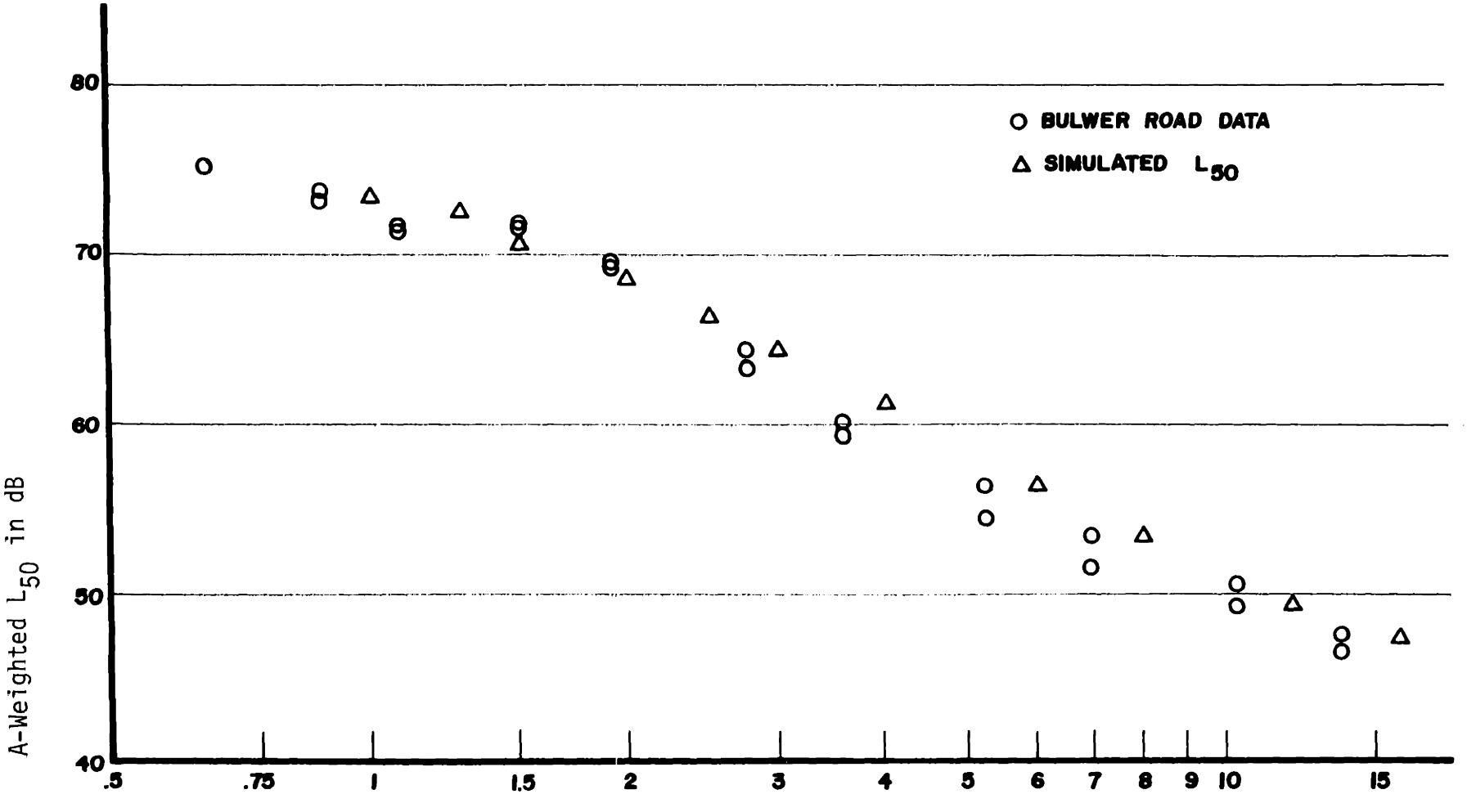

FIGURE 5.25: Simulation of Delany, Copeland and Payne -- Bulwer Road Data

However, when there is no line of sight, this model consistently underpredicts sound levels. The second order scattering model together with angularly dependent reflection ratio was shown to be an accurate propagation model for all situations. Its applicable to street propagation is, however, considerably more complicated than the first order model. Because of its accuracy, the second order model should generally be employed for sound level prediction. In cases where there is direct line of sight, however, the first order model is sufficiently accurate and simple to apply that its use may be chosen.

Imaging with the second order scattering model can in principle be applied to any given urban propagation problem. This is done using imaging theory as described in Section 2.2 and expressions of reflection ratio and scattered energy developed in Section 4.6 as are appropriate for the given geometry. As application of this propagation model is in general quite tedious, a number of propagation cases associated with the common urban grid pattern have been computerized. Results for variety of parameters for these cases were presented and discussed in Section 5.3. Additional values of point source pass-by attenuation are given in the Appendix. Although these special cases will not be applicable to all propagation problems, their utility goes beyond those cases of strict geometric similitude. From the simulation of the field data as described in Section 4.7, it is apparent that the effect of non-perpendicular intersections is negligible compared to the right-angled values. Further, in Section 5.3, it was observed that line source and often point source levels are

insensitive to intersection geometry and small openings in the propagation channel. With the knowledge of these insensitivities and with prudent interpolation, it is expected that the values presented in Section 5.3 and the Appendix may be extended with a minor loss of accuracy. In making such extensions, however, the predicted values should be bracketed as to accuracy by the cases which are available.

As discussed in Section 5.2, the urban propagation model can be applied to a variety of source types. These include simple point sources, line sources and traffic flows. For traffic flows of densities less than one vehicle per street width and for discrete source pass-bys, Equivalent Energy Level, L_{EQ}, was found to be a particularly convenient descriptor. Use of this statistic is also very convenient for superimposing contributions from more than one traffic flow.

In particular, situations as discussed in Section 5.4, corrections to the predicted level may be necessary. These included, when applicable, corrections for atmospheric absorption of sound, ground reflection for particular source specifications, and temporal sound variation for traffic flows. For traffic flows, corrections are necessary in order to predict the sound level statistics of L_{10} and L_{50} as produced solely by the geometrical considerations. Values for these statistics are given in the Appendix for those propagation cases described in Section 5.3. Corrections to the basic predicted levels are not necessary for temperature and wind gradients and diffraction.

REFERENCES

1. Shaw, E.A.G., and Olson, N., "Theory of Steady-State Urban Noise for an Ideal Homogeneous City, *Journal of the Acoustical Society of America,* Vol. 51, No. 6, Part 1, 1972, pp. 1781-1793.

2. Davies, H.G., and Lyon, R.H., "Noise Propagation in Cellular Urban and Industrial Spaces," *Journal of the Acoustical Society of America,* Vol. 54, No. 6, 1973, pp. 1565-1570.

3. Malchaire, J.B., and Horstman, S.W., "Urban Noise Model," *Journal of the Acoustical Society of America,* Vol. 56, No.6, 1974, pp. 1811-1814.

4. Schlatter, W.R., "Sound Power Measurement in a Semi-Confined Space," M.Sc. Thesis, Massachusetts Institute of Technology, Cambridge, Massachusetts, July, 1971.

5. Pande, L., "Model Study of Aircraft Noise Reverberation in a City Street," M.Sc. Thesis, Massachusetts Institute of Technology, Cambridge, Massachusetts, April, 1972.

6. Kinney, W.A., "Helicopter Noise Experiments in an Urban Environment," M.Sc. Thesis, Massachusetts Institute of Technology, Cambridge, Massachusetts, January, 1973.

7. Donavan, P.R., "Model Study of the Propagation of Sound from V/STOL Aircraft into Urban Environs," M.Sc. Thesis, Massachusetts Institute of Technology, Cambridge, Massachusetts, September, 1973.

8. Donavan, P.R., and Lyon, R.H., "Sound Propagation Near Ground Level in the Vicinity of Street Intersections," Proceedings of the Second Interagency Symposium on University Research in Transportation Noise, North Carolina State University, Raleigh, North Carolina, June 1974, pp. 491-504.

9. Lee, K., "Prediction of Propagation in a Network of Sound Channels with Application to Noise Transmission in City Streets, M.Sc. Thesis, Massachusetts Institute of Technology, Cambridge, Massachusetts, September 1974.

10. Holmes, D.G., "A Numerical Model of Sound Propagation in Urban Areas," Proceedings of the Second Interagency Symposium on University Research in Transportation Noise, North Carolina State University, Raleigh, North Carolina, June 1974, pp. 475-490.

11. Jones, R.C., "A Fifty Horsepower Siren," *Journal of the Acoustical Society of America,* Vol. 18, No. 2, October 1946, pp. 371-387.

12. Wiener, F.M., Malme, C.I., and Gogos, C.M., "Sound Propagation in Urban Areas," *Journal of the Acoustical Society of America,* Vol. 37, No. 4, April 1965, pp. 738-747.

13. Delaney, M.E., Copeland, W.C. and Payne, R.C., "Propagation of Traffic Noise in Typical Urban Situations, NPL Acoustics Report, No. AC 54 October 1971.

14. Deriugin, L.N., "The Reflection of a Plane Transverse - Polarized Wave from a Rectangular Comb," *Radio Engineering*, Vol. 15, No. 2, 1960, pp. 15-26.

15. Wagner, L.F., "Acoustic Reflection from Rough Surfaces," M.Sc. Thesis, Massachusetts Institute of Technology, Cambridge, Massachusetts, August 1974.

16. Sabersky, R.H., Acosta, A.J., and Hauptmann, E.G., *Fluid Flow*, The Macmillan Company, New York, 1971, pp. 193-194.

17. Morse, P.M., and Ingard, K.U., *Theoretical Acoustics,* McGraw-Hill Book Co., 1968, pp. 366-371, p. 312.

18. "The Use of Architectural Acoustical Materials Theory and Practice," Acoustical Materials Association, New York, New York, 1968, p. 33.

19. Lyon, R.H., *Lectures in Transportation Noise,* Grozier Publishing, Inc., 1973, pp. 164-165, p. 145.

20. Malkawa, Z., "Noise Reduction by Screens," *Applied Acoustics* Vol. 1, pp. 157-173, 1969.

21. Masiak, J.E., "Model Studies of Acoustic Barriers," M.Sc. Thesis, Massachusetts Institute of Technology, Cambridge, Massachusetts, September 1973.

22. DeJong, R.G., "A Model Study of the Effects of Wind on the Sound Attenuation of Barriers," M.Sc. Thesis, Massachusetts Institute of Technology, Cambridge, Massachusetts, May 1974.

23. Lyon. R.H., DeJong, R., Conn, R.G., and Schlaffer, F., "Acoustical Modeling System for Site Selection," *The Journal of the Acoustical Society of America,* Vol. 58, No. 2, August 1975, pp. 521-524.

24. Thompson, P.A., *Compressible-Fluid Dynamics,* McGraw-Hill Book Company, 1972, pp. 276-288.

25. Evans, C.B., Bass, H.E., and Sutherland, L.C., "Atmospheric Absorption of Sound: Theoretical Predictions," *Journal of the Acoustical Society of America,* Vol. 51, No. 5, (Part 2), May 1972, pp. 1565-1575.

26. Klinkoustein, R.E., "A Study of Acoustic Radiation from an Electrical Spark Discharge in Air," M.Sc. Thesis, Massachusetts Institute of Technology, Cambridge, Massachusetts, July 1974.

27. Shaw, E.A.G., "Noise Pollution - What Can Be Done?, *Physics Today*, Vol. 28, No. 1, January 1975, pp. 46-58.

28. Beranek, L.L., *Noise and Vibration Control,* McGraw Hill Book Company, 1971, pp. 169-173.

APPENDIX

Charts of Point Source Attenuation, L_{50}, and L_{10} Values for Traffic Flows

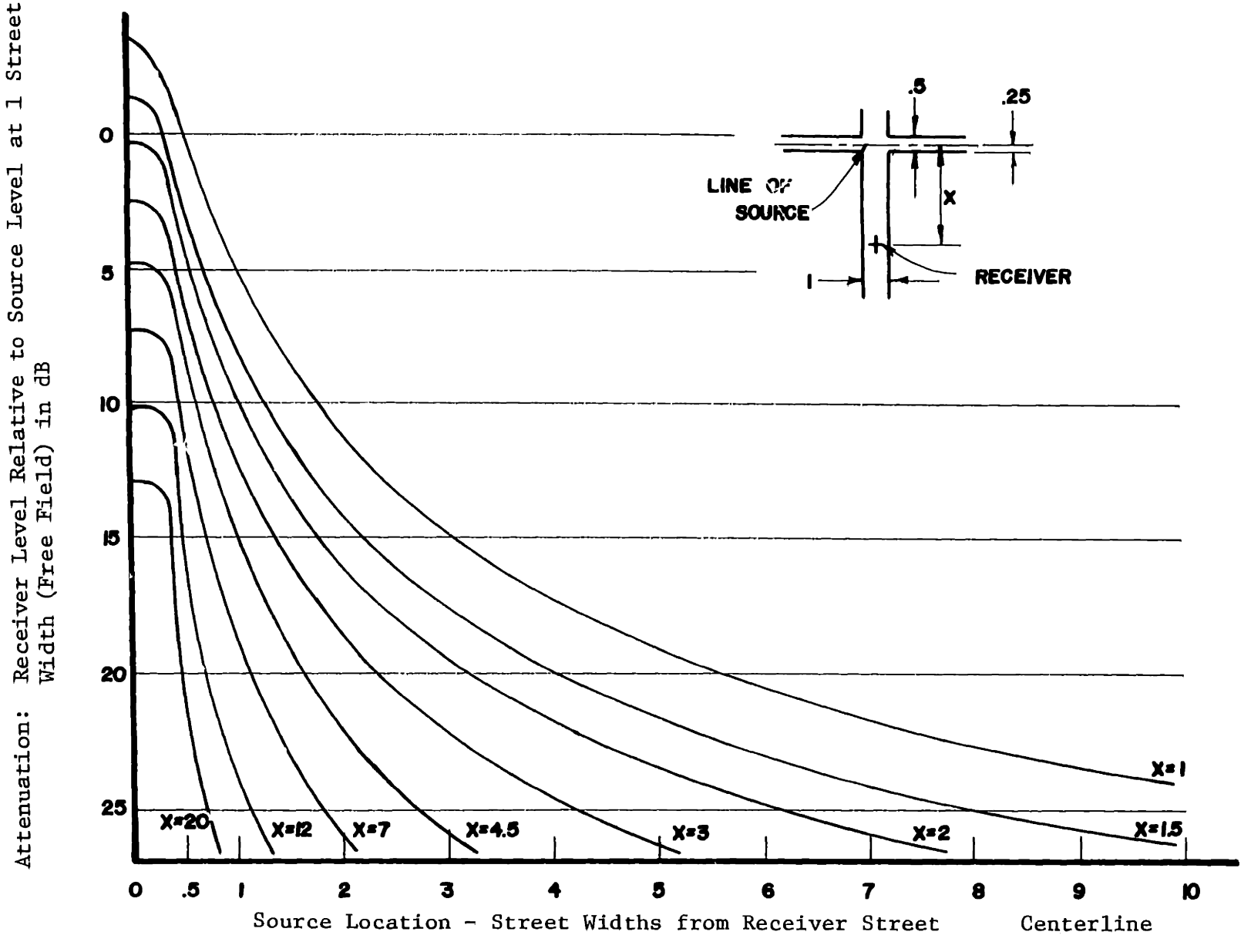

FIGURE A.1: Point Source Attenuation

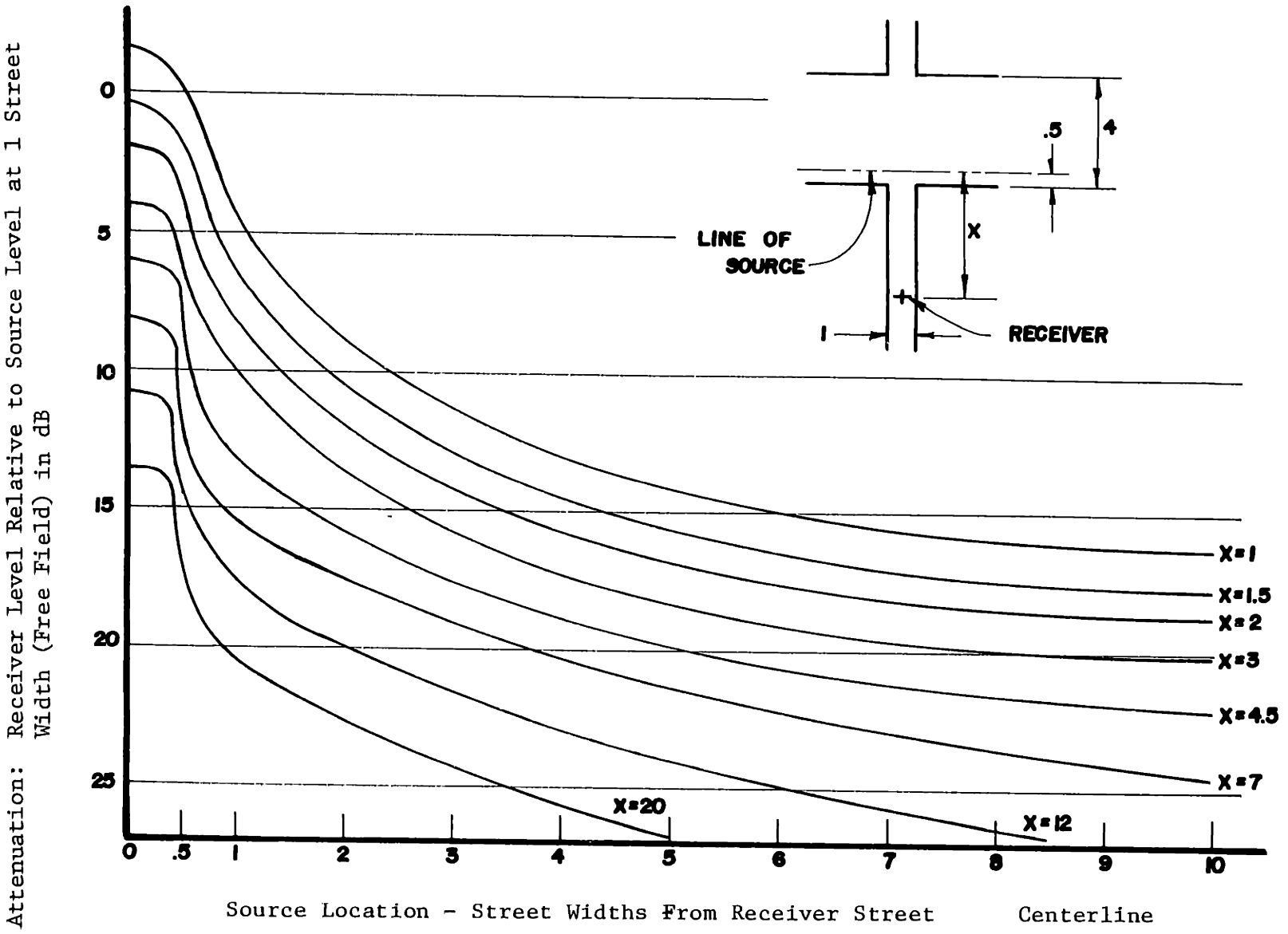

FIGURE A.2: Point Source Attenuation

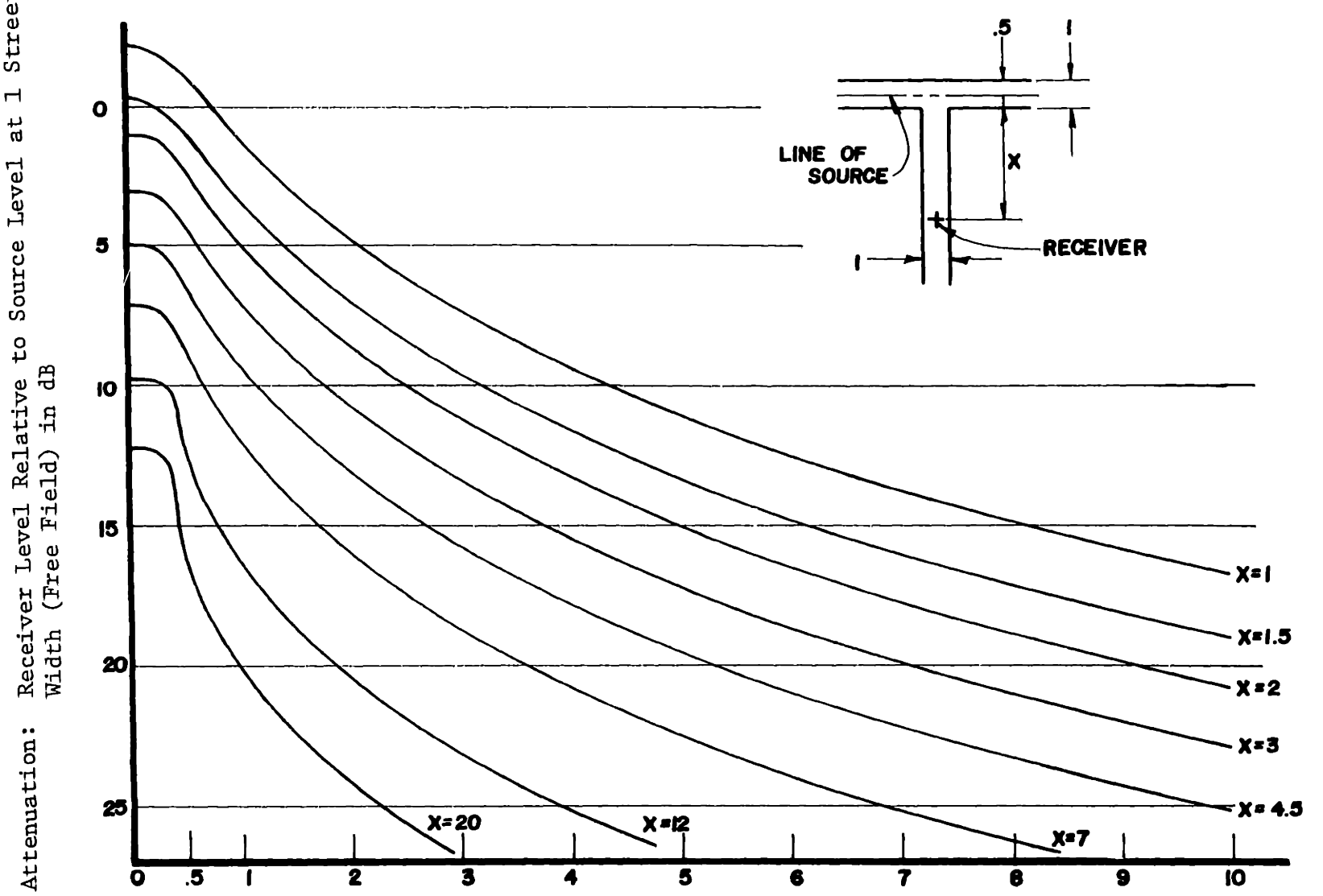

FIGURE A.3: Point Source Attenuation

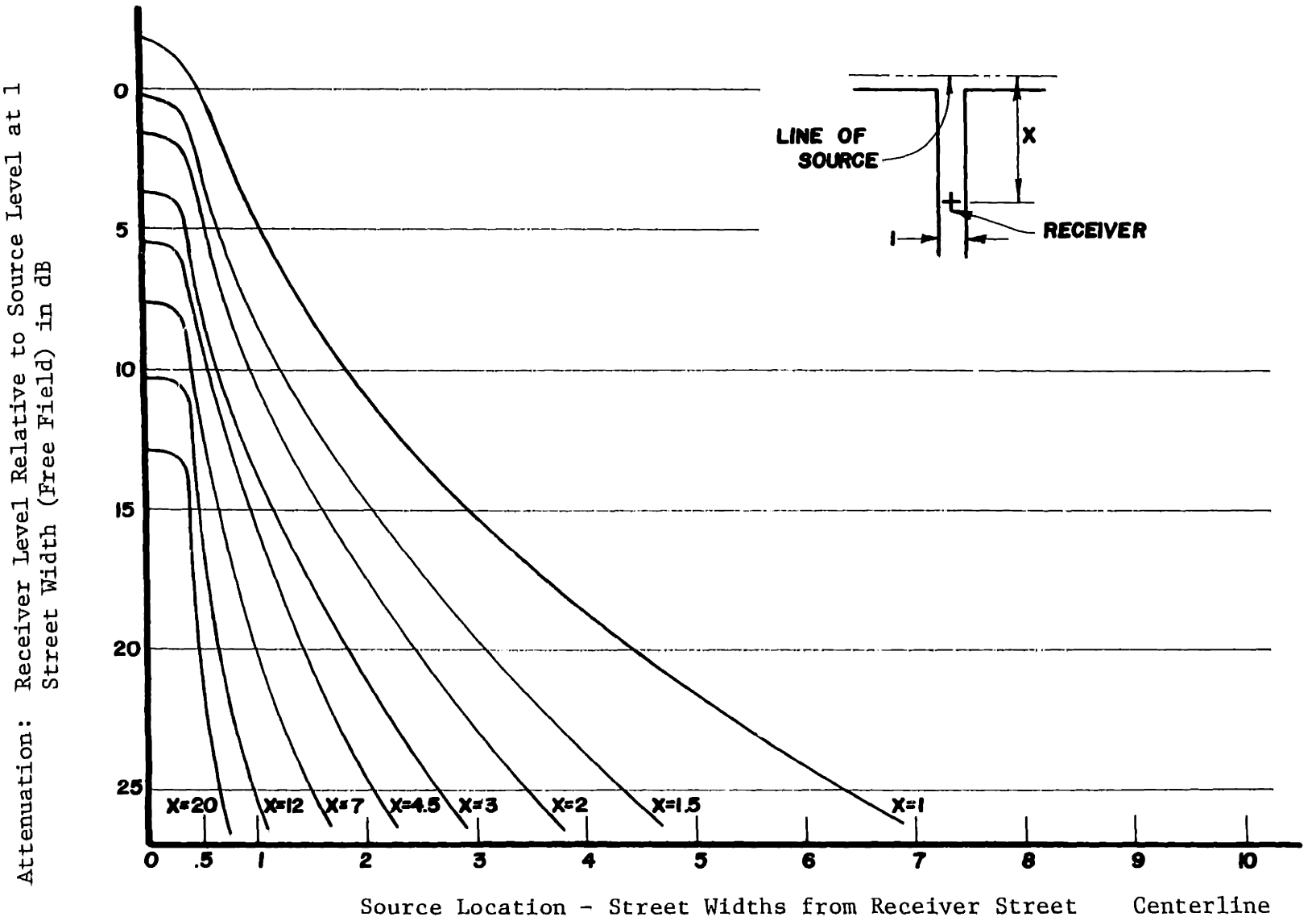

FIGURE A.4: Point Source Attenuation

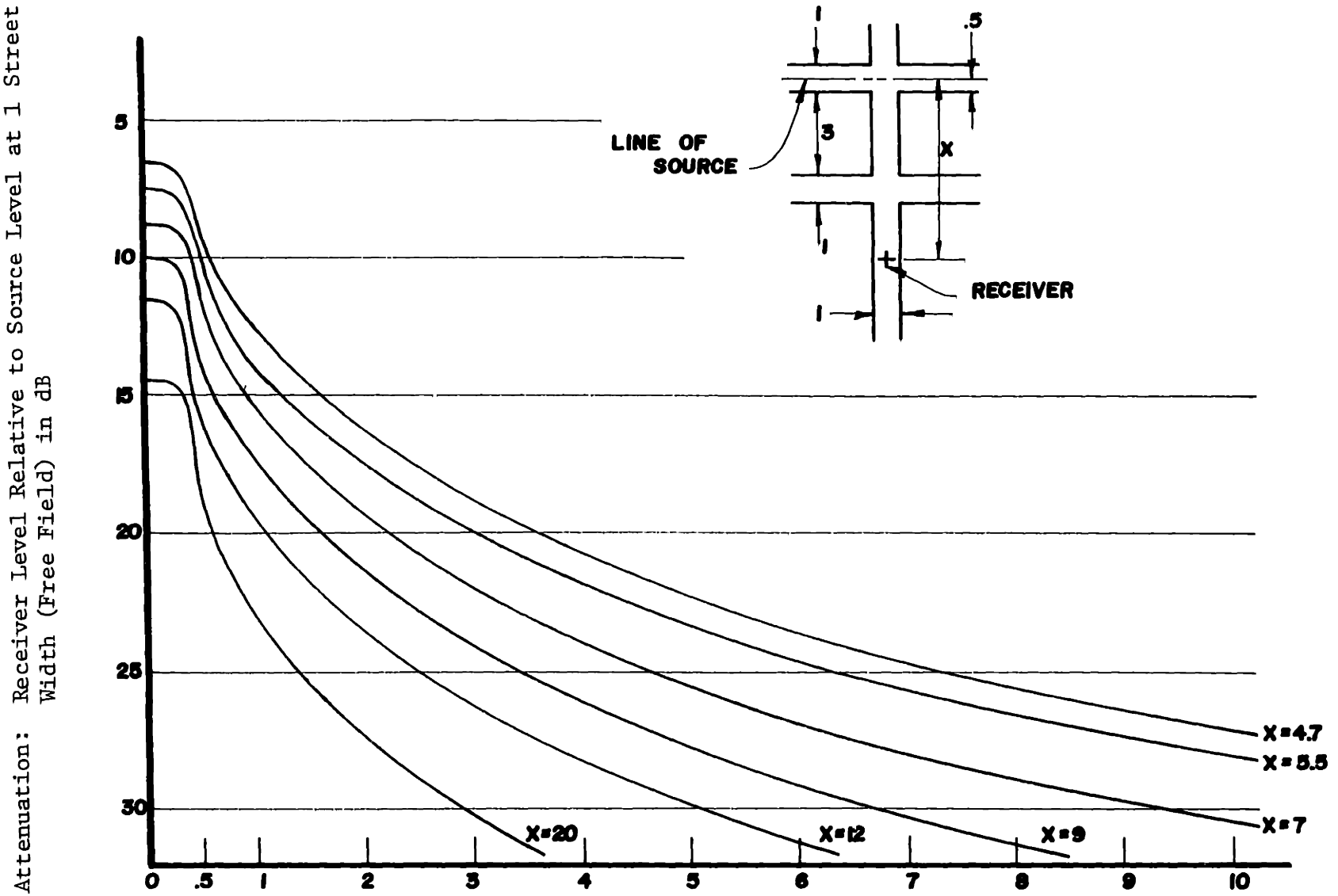

FIGURE A.5: Point Source Attenuation

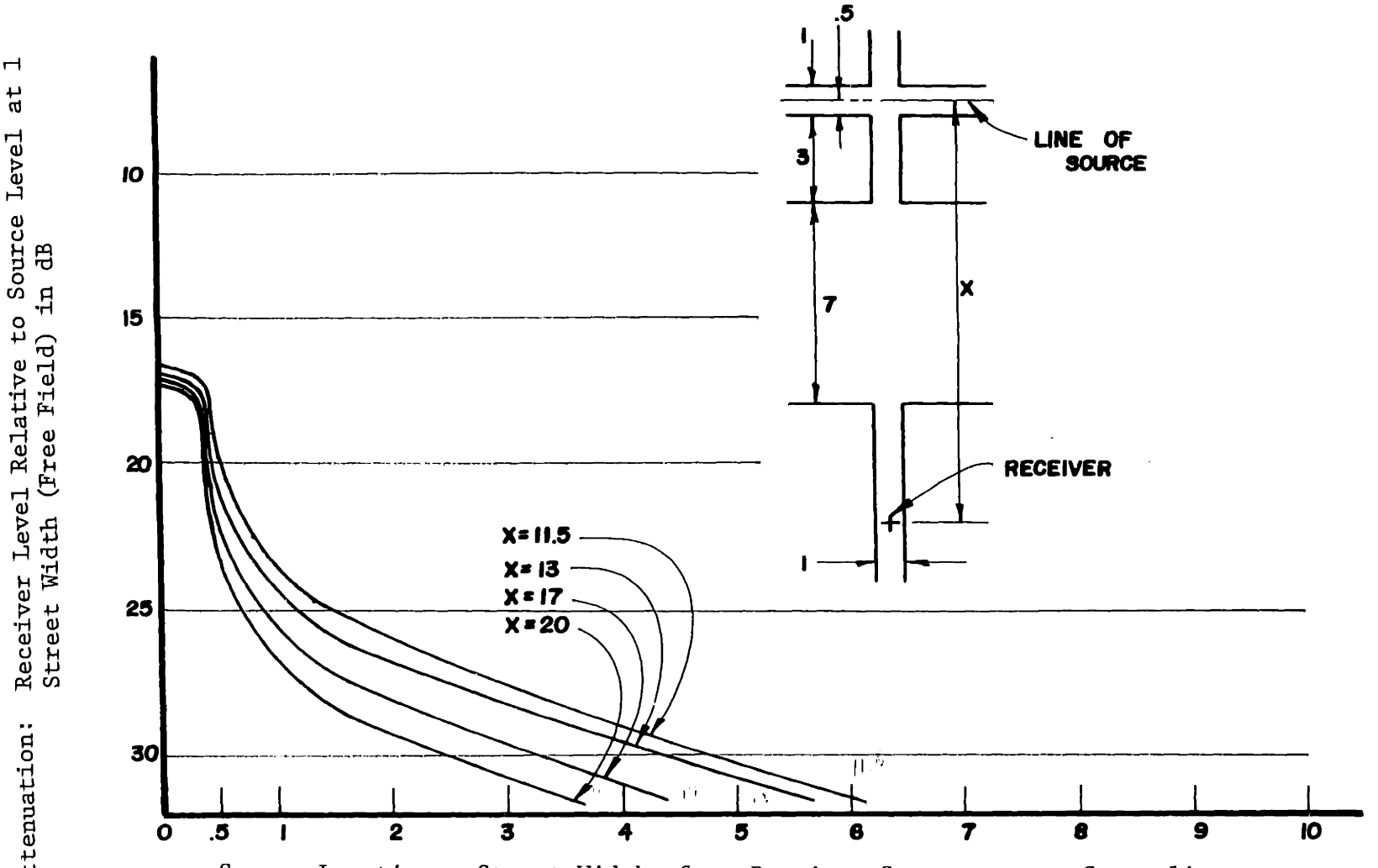

FIGURE A.6: Point Source Attenuation

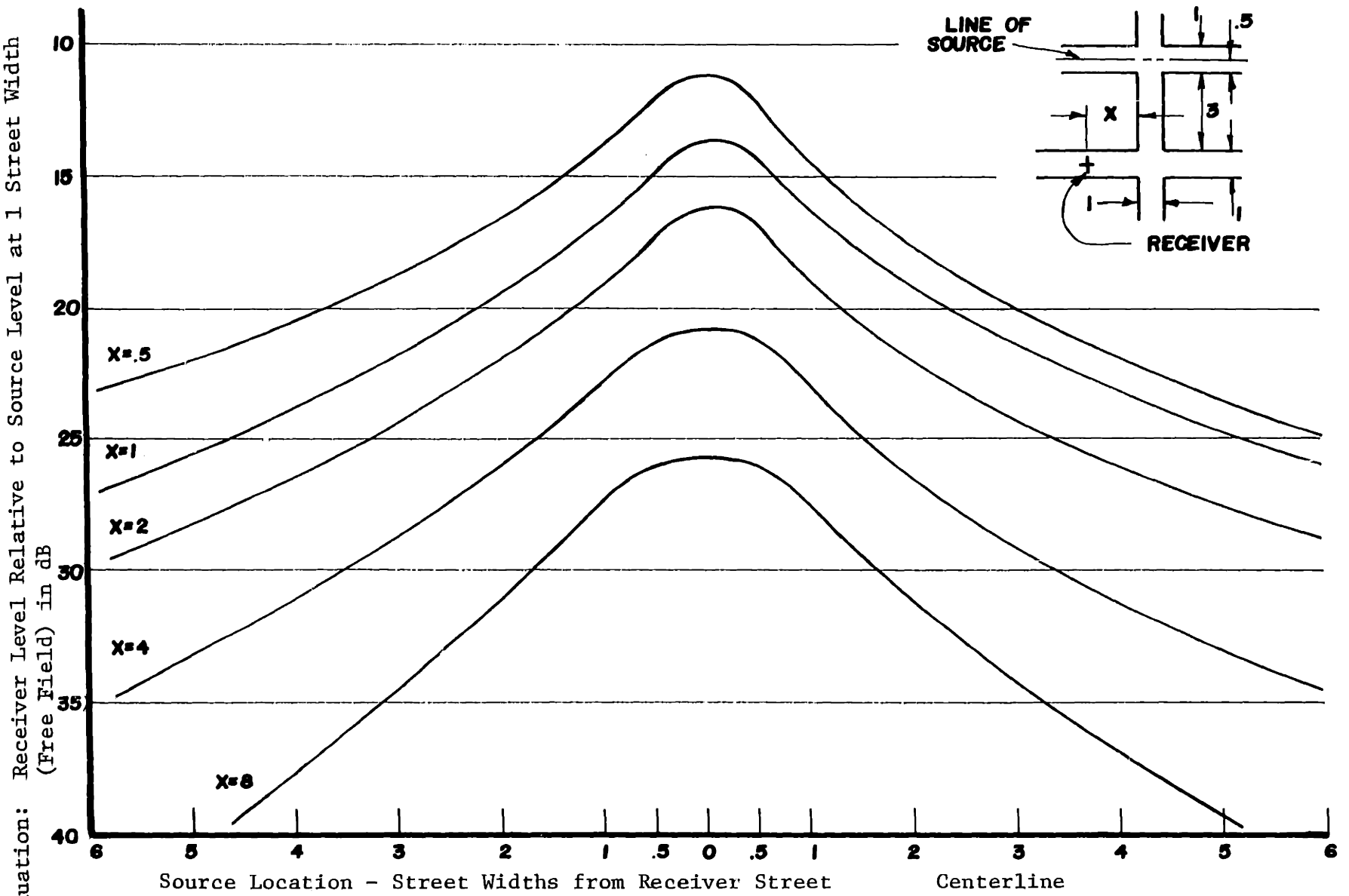

FIGURE A.7 Point Source Attenuation

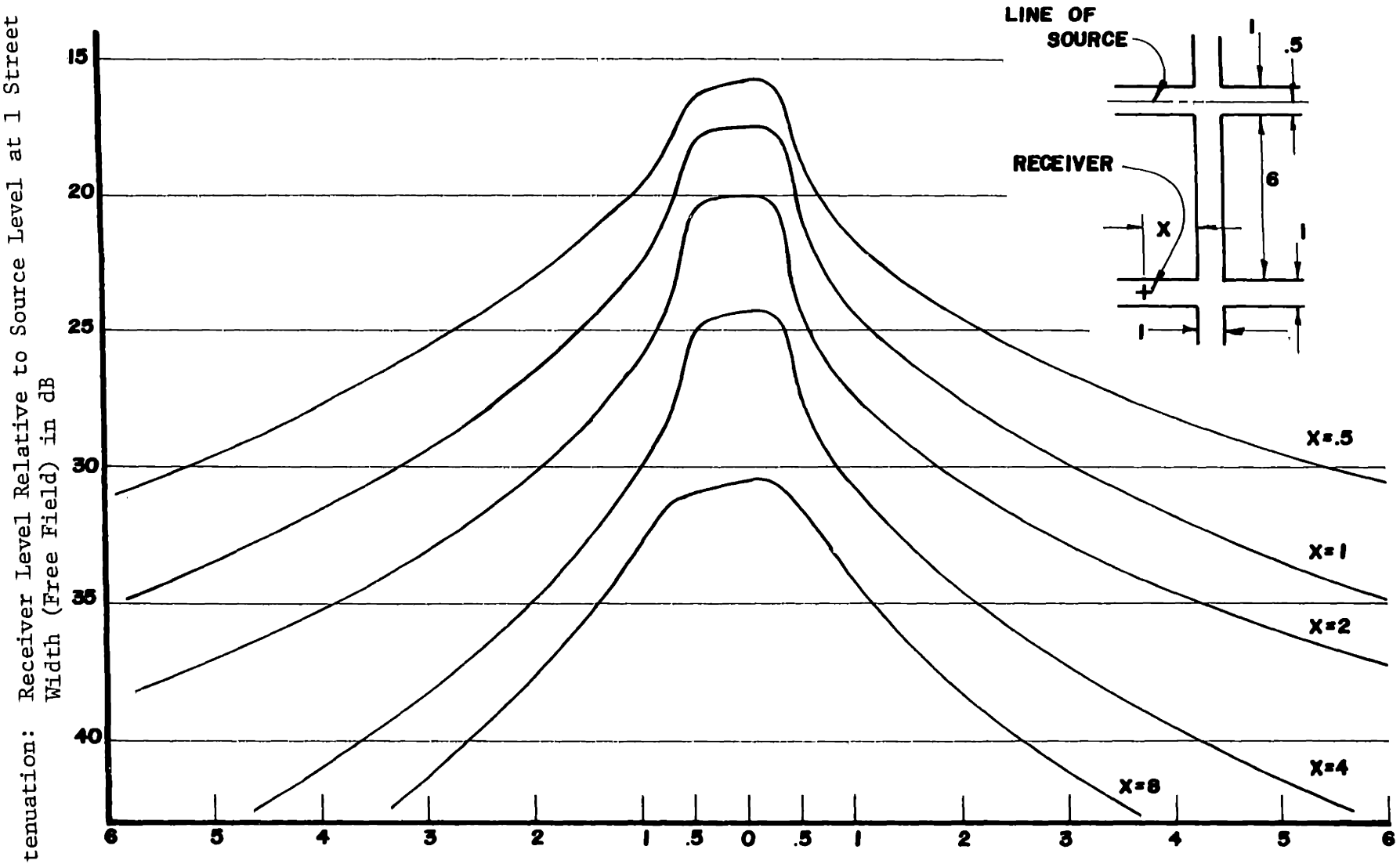

FIGURE A.8: Point Source Attenuation

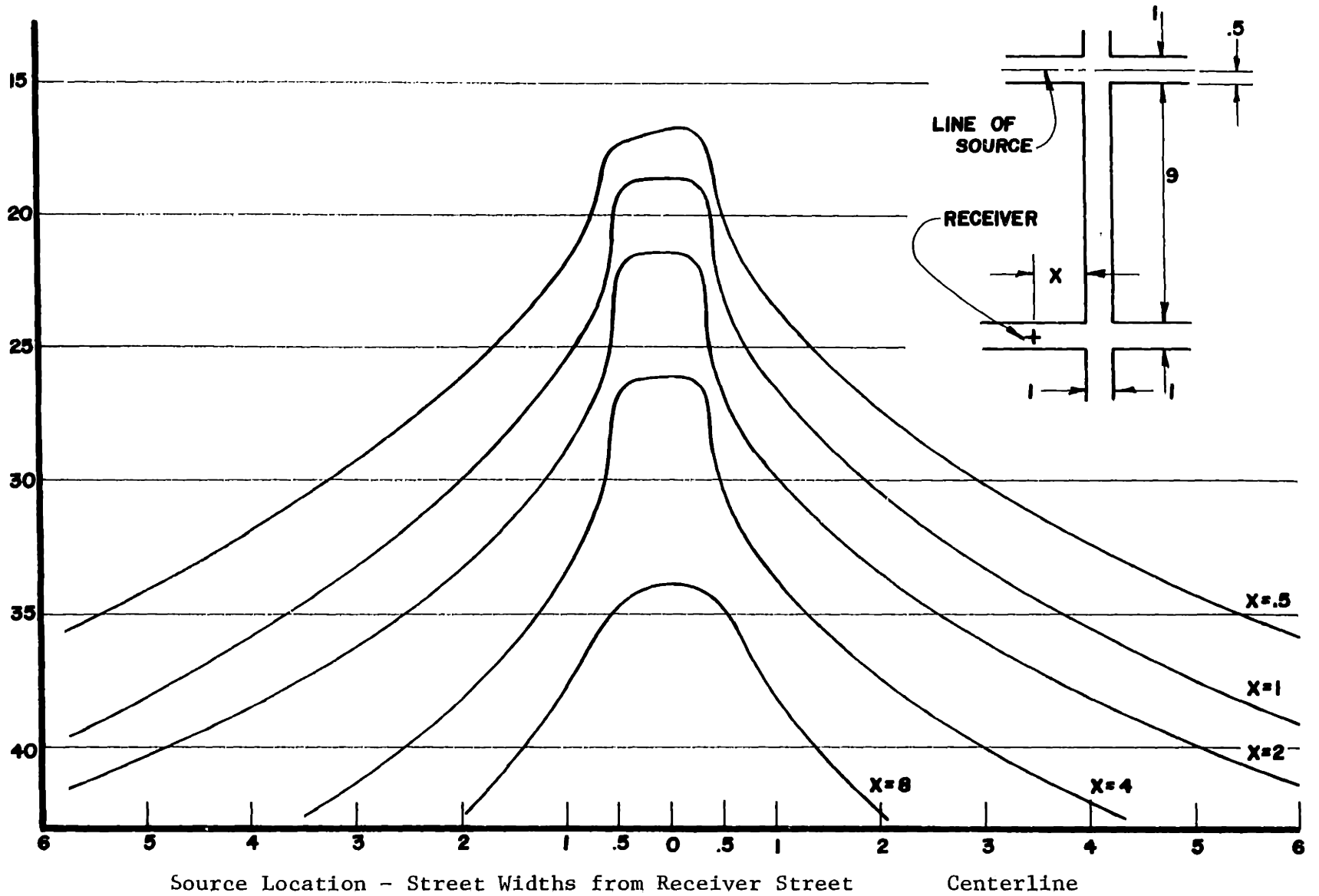

FIGURE A.9: Point Source Attenuation

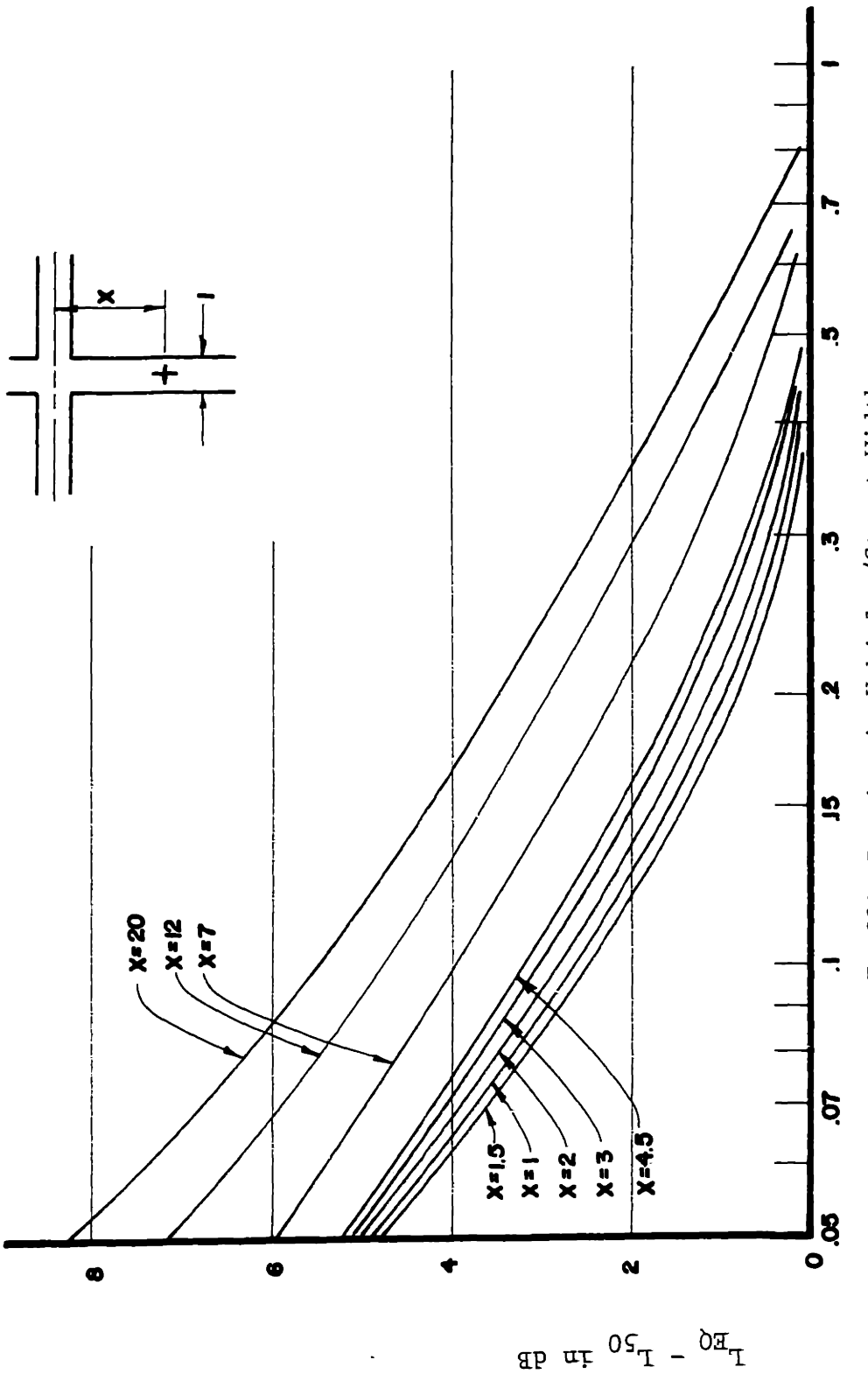

FIGURE A.10: L_{50} Values for Traffic Flow

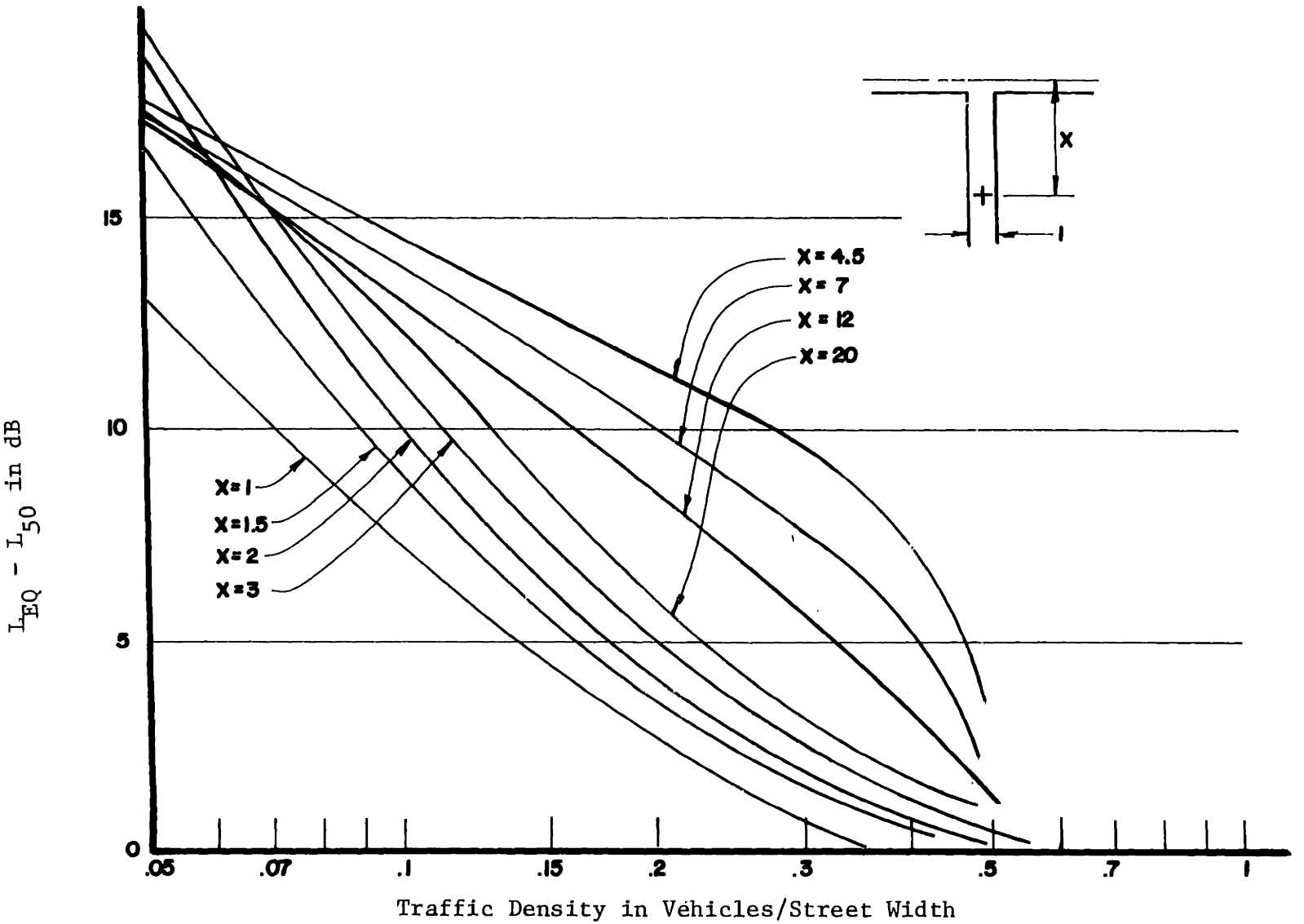

FIGURE A.11: L_{50} Values for Traffic Flow

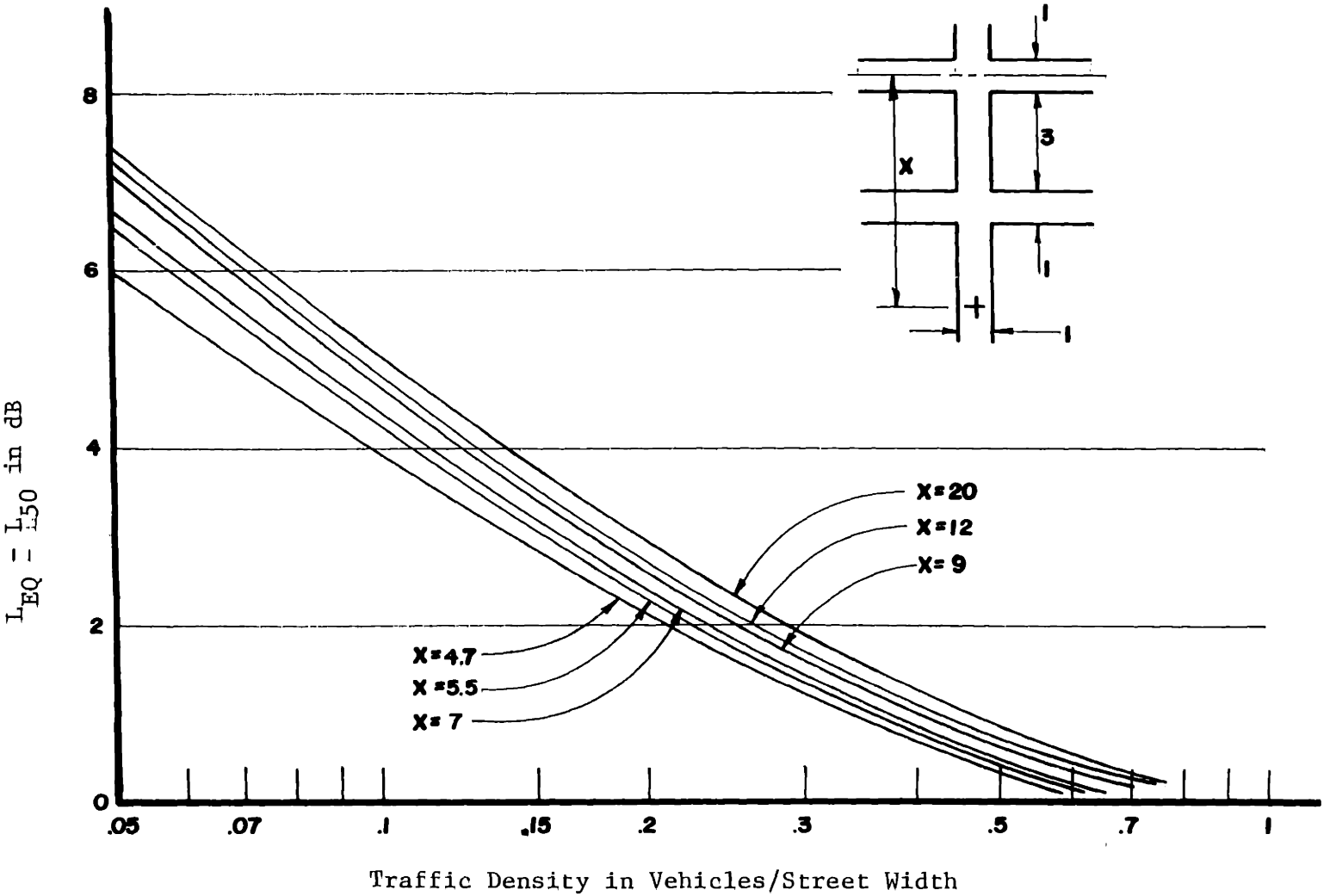

FIGURE A.12: L_{50} Values for Traffic Flow

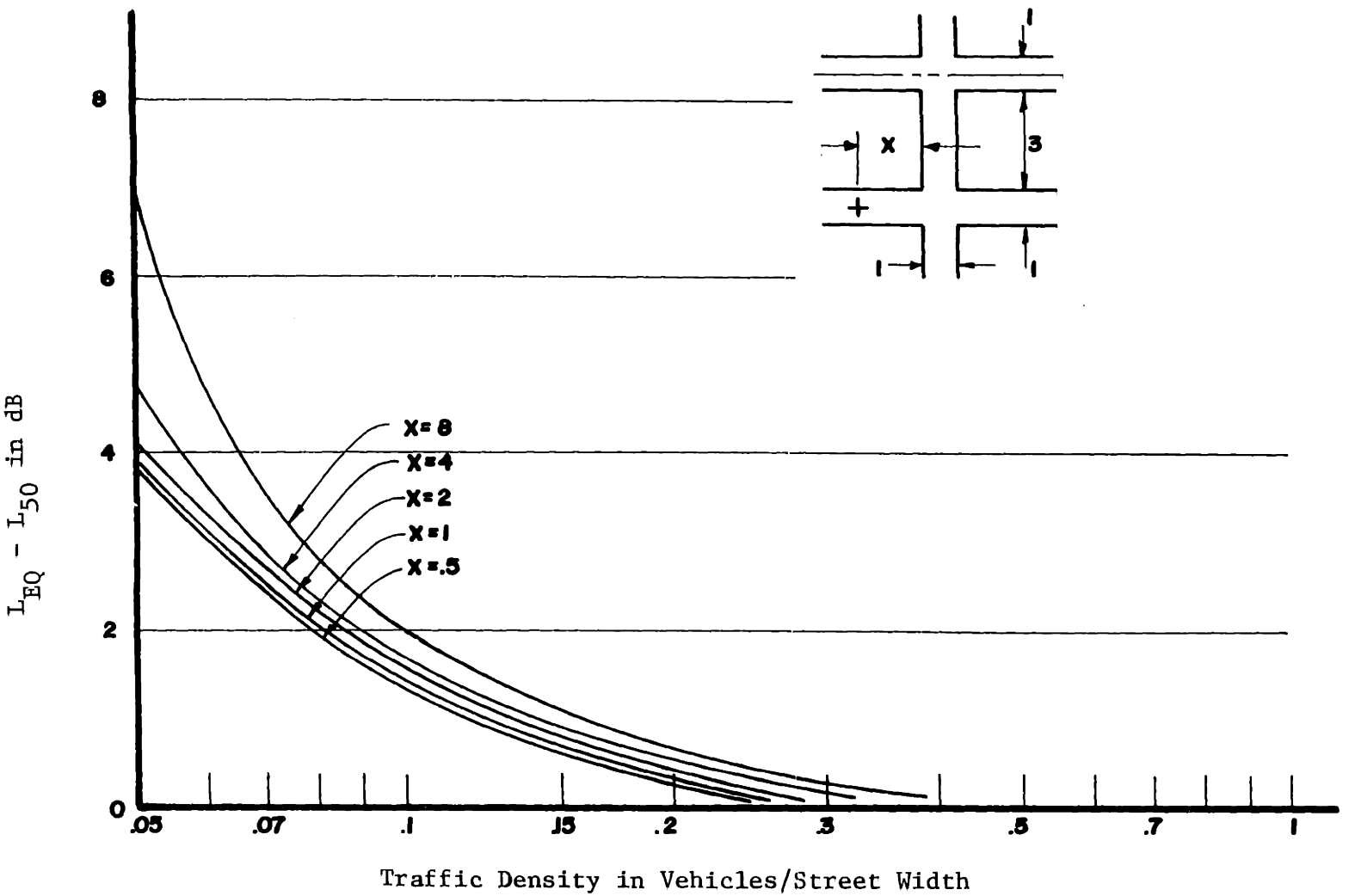

FIGURE A.13: L_{50} Values for Traffic Flow

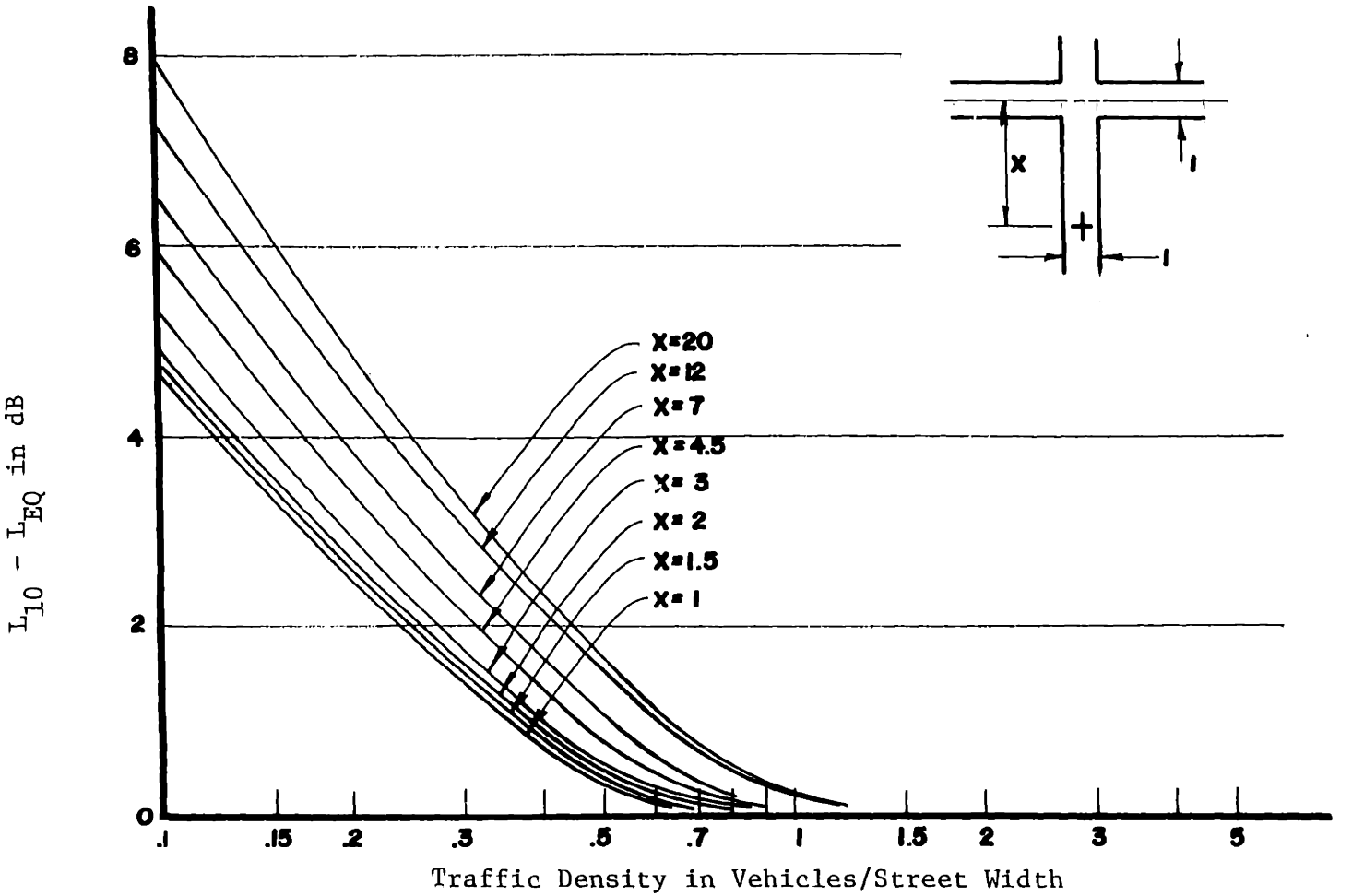

FIGURE A.14: L_{10} Values for Traffic Flow

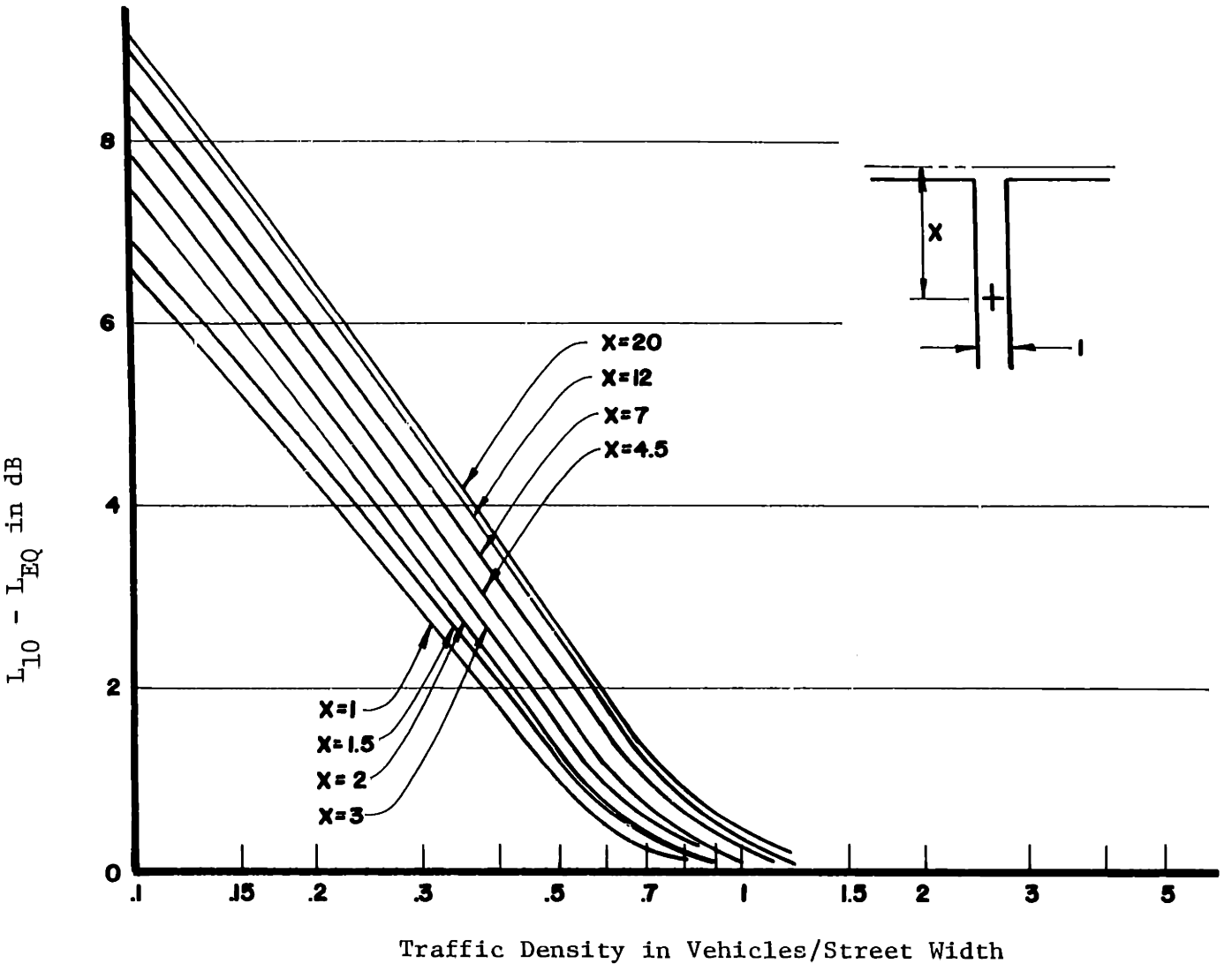

FIGURE A.15 L_{10} Values for Traffic Flow

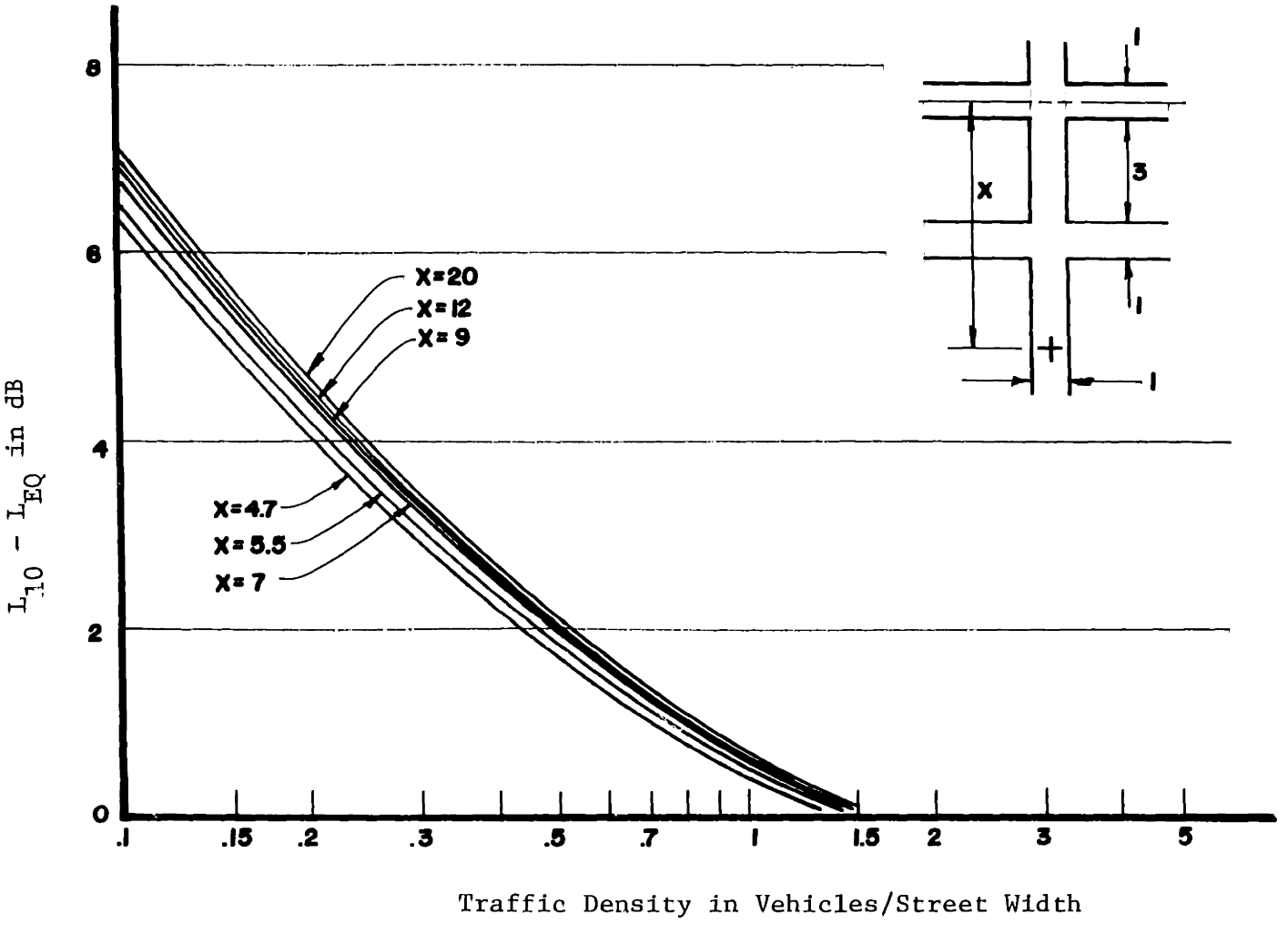

FIGURE A.16: L_{10} Values for Traffic Flow

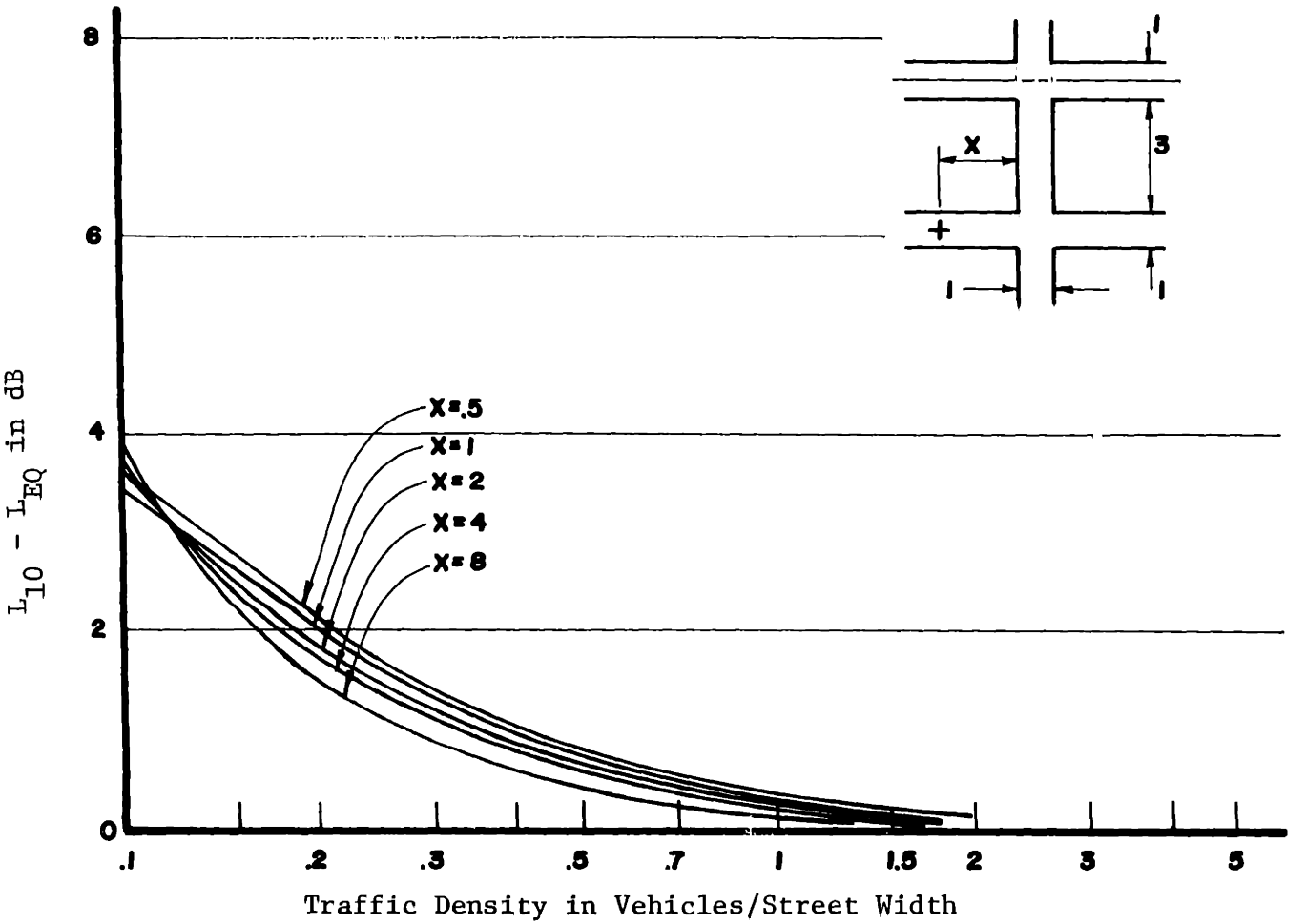

FIGURE A.17: L_{10} Values for Traffic Flow